Steel shear tab connections subjected to combined shear and axial forces

by

Alireza Mirzaei ©

The Department of Civil Engineering and Applied mechanics
McGill University

April 2014

A thesis submitted to the Faculty of Graduate and Postdoctoral Studies
in partial fulfillment of the requirements for the degree of

Doctor of Philosophy
in
Civil Engineering

Abstract

A common approach to connect steel beams to columns is to use single plate shear tabs. Numerous laboratory test programs of these connections subjected to vertical loading alone have been completed over the past 30 years. However, the effect of axial forces on the shear tab's performance has only recently been the subject of study. The presence of an axial force in the shear tab connection will typically result in the need for multiple vertical rows of bolts, which is not addressed in any Canadian design guide. The main objective of the research program described herein was to develop a design approach that could be used by the engineering community to address the effect of combined axial and shear force on a shear tab connection.

A series of four full-scale tests were performed on shear tab connections between a W610x140 beam and a W360 x 196 column, as well as a W310 x 60 beam and a W360 x 196 column. The shear tab, which was configured as a double bolt row connection, was subjected to a combined vertical (shear) force and axial tension along with the anticipated rotation of a typical beam-to-column joint. A matching specimen was then tested under shear and axial compression. The results from these tests and previous shear tabs tested under gravity load alone were used in the development of a finite element model that is capable of simulating the response of the connection under shear load; predict the ultimate resistance and the progression of failure. Previous finite element modelling of shear tabs lacked damage simulation capability, did not include the effect of weld tearing, and as such often overestimated the connection resistance. The models presented in this thesis featured special modelling techniques and were able to predict all types of failure modes such as bearing, net area fracture, shear yielding, flexural yielding, and weld tearing of the connections.

The FE models were then used to investigate the performance of shear tabs subjected to combined shear and axial force. Shear force–axial force interaction curves were generated for various levels of axial tension and compression force for twelve connections. A design approach was proposed which allows practicing engineers to include the effect of any axial force level in the design of a shear tab connection.

Résumé

L'utilisation d'une plaque de cisaillement seule est une approche courante pour relier les poutres en acier aux colonnes. Au cours des 30 dernières années, de nombreux programmes d'expériences en laboratoire ont porté sur ces assemblages soumis à une charge verticale seule. Cependant, l'effet des forces axiales sur la performance des plaques de cisaillement a récemment fait l'objet d'études. Typiquement, la présence d'une force axiale dans l'assemblage à plaque de cisaillement entraînera l'utilisation de plusieurs rangées verticales de boulons, ce qui n'est abordé dans aucun guide de conception canadien. Le principal objectif du programme de recherche décrit ici était de développer une approche de calcul qui puisse être utilisée par les ingénieurs pour prendre en compte l'effet combiné des forces axiale et de cisaillement dans une plaque de cisaillement.

Un ensemble de quatre essais grandeur nature ont été effectués sur des assemblages à plaque de cisaillement entre une poutre W610x140 et une colonne W360x196, ainsi qu'entre une poutre W310x60 et une colonne W360x196. La plaque de cisaillement, qui a été calculée comme pour un assemblage avec deux lignes de boulons, a été soumise à une force verticale (de cisaillement) combinée à une traction axiale ainsi qu'à la rotation attendue dans une liaison typique poutre-colonne. Le même type d'assemblage a été ensuite soumis au cisaillement et à la compression axiale. Les résultats de ces expériences et d'expériences antérieures, sur des plaques de cisaillement soumises seulement à une charge de gravité, ont été utilisés dans l'élaboration d'un modèle d'éléments finis (EF) capable de simuler la réponse de l'assemblage soumis à une charge de cisaillement, de prédire la résistance ultime et la progression de la rupture. Les modélisations de plaques de cisaillement par éléments finis réalisées jusqu'à présent ne simulaient pas l'endommagement, n'incluaient pas l'effet de la rupture de la soudure et, par conséquent, surestimaient souvent la résistance de l'assemblage. Les modèles présentés dans cette thèse utilisent des techniques de modélisation spéciales et sont en mesure de prédire tous les modes de rupture, tels que la rupture par pression diamétrale, la rupture de la section nette, la plastification par cisaillement, la plastification par flexion et la rupture de la soudure de l'assemblage.

Les modèles EF ont ensuite été utilisés pour évaluer la performance des plaques de cisaillement soumises à des forces de cisaillement et axiale combinées. Des courbes d'interaction force de cisaillement - force axiale ont été obtenues pour différentes amplitudes de forces de traction et de compression, et ce, pour douze assemblages. Une méthode de calcul a été proposée permettant aux ingénieurs d'inclure l'effet de n'importe quelle amplitude de force axiale, dans le calcul d'assemblage à plaque de cisaillement.

Acknowledgements

The performed research presented in this thesis would not be possible without the help of great people and organizations that I owe a depth of gratitude. I would like to express my deepest appreciation to all those who provided me the possibility to complete this research.

Firstly, I would like to thank my dear supervisor, Professor Colin A. Rogers. You have been a tremendous mentor and friend for me and I would like to thank you for encouraging my research and for allowing me to grow as a research scientist and experienced engineer. Your advice and guidance throughout the research has been priceless. It has been a privilege working under your supervision. I would also like to thank my co-supervisor Professor Robert Tremblay of École Polytechnique de Montréal who has also provided us his valuable knowledge and experience that helped us overcome roadblocks during the research.

I would like to thank Marco D'Aronco from DPHV and especially students Nathan Goldstein Apt and Farbod Pakpour, for assistance in executing the laboratory work. Thanks for spending your summer working by my side at McGill's Jamieson Structures Laboratory. I would also like to thank Jennifer Marshall for her help in the development of the FE modeling techniques. Many thanks to Dr. Bill Cook along with the laboratory technicians Marek Przykorski, John Bartczak, Ron Sheppard, and Gerard Bechard for their help with the laboratory equipment. I have learned to safely use so many useful tools and I owe it to you.

Special thanks to Denis D'Aronco, Martin Frappier, and Marco D'Aronco from DPHV for providing me with their extensive knowledge in shear tab connections. Their help in the design and detailing phase of the laboratory test setup is highly appreciated. I would like to also thank Talia Paschini from ADF for managing the preparation of the test components for laboratory testing. Funding for this project was kindly provided by ADF Group Inc., DPHV and the Natural Sciences and Engineering Research Council of Canada which made this research possible.

I would like to express my great appreciation to my parents, Hossein Mirzaei and Marhamat Jahanpour, whom I'm eternally grateful for their love and support throughout my studies. Last, but certainly not least, a special thanks goes to my wife Shohreh Asadi, for her tireless love, support, motivation, patience and understanding throughout this process; and the sacrifice of all the moments being apart which allowed me to complete this project.

Jamieson Structures Laboratory at McGill University, Summer 2012

Table of Contents

List of Figures

List of Tables

Chapter 1

Introduction

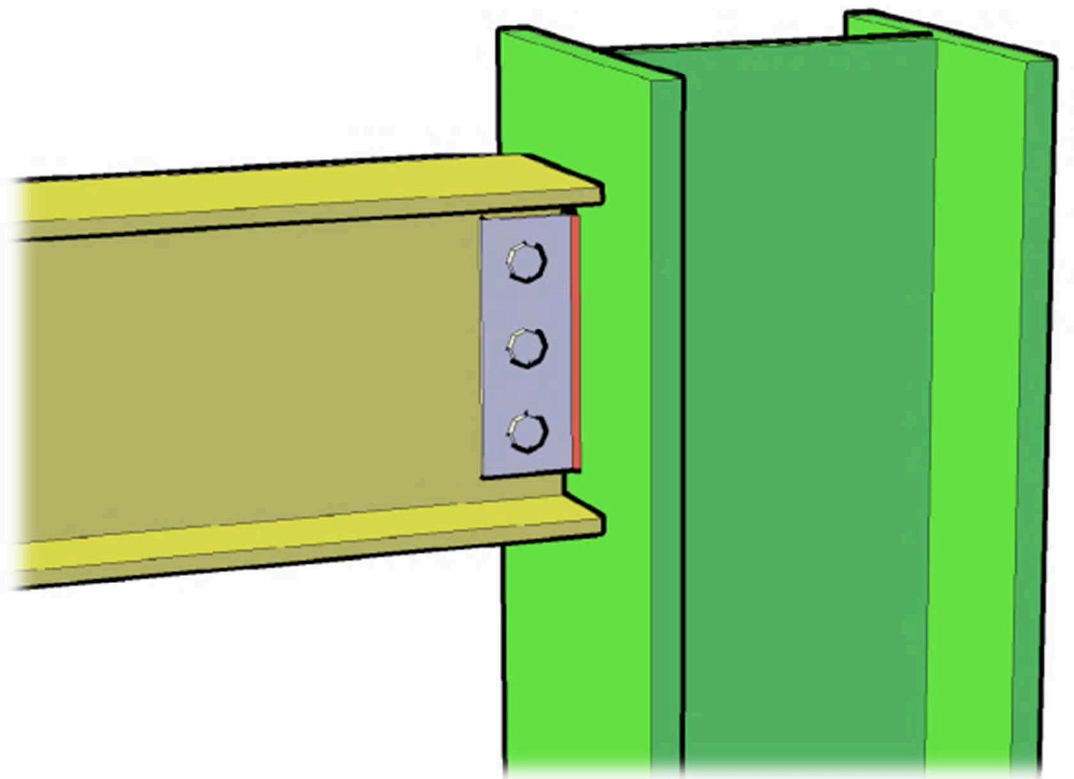

1. Chapter 1- Introduction

1.1. Shear tab connections

Single steel plate web connections, also known as shear tabs, are one of the most popular and common simple connections used in the steel construction industry. Shear tabs are used due to their cost efficiency, ease of fabrication and rapid erection capabilities. The connecting plate is welded horizontally to the supporting member in the fabrication shop, while the connection between the beam and the steel plate is typically achieved with the use of bolts. Holes are either punched or drilled at the fabrication shop and the bolts are installed during the erection process. The main application of shear tabs is to connect main girder beams to columns (Figure 1.1-A) or secondary beams to main girders (Figure 1.1-B). If the shear tab is used to connect a beam to a column, there are two possible support conditions which affect the performance of the connection: The first is a rigid support condition which is typically formed when a beam is connected to the flange of a wide flange column in such a way that the shear tab is aligned with the web of the column (Figure 1.1-A). The other type of support condition is a flexible support which allows more rotational capabilities to the connection. A shear tab that is welded to the web of a wide flange column (Figure 1.2-A) or a shear tab connecting a beam to a girder (Figure 1.1-B) are common examples of this type of support condition. The reason for coping the top of the connecting beam in a beam to girder connection (Figure 1.1-B) is to acquire the same elevation on top of the flanges resulting in a flat surface for easier floor construction.

(A)

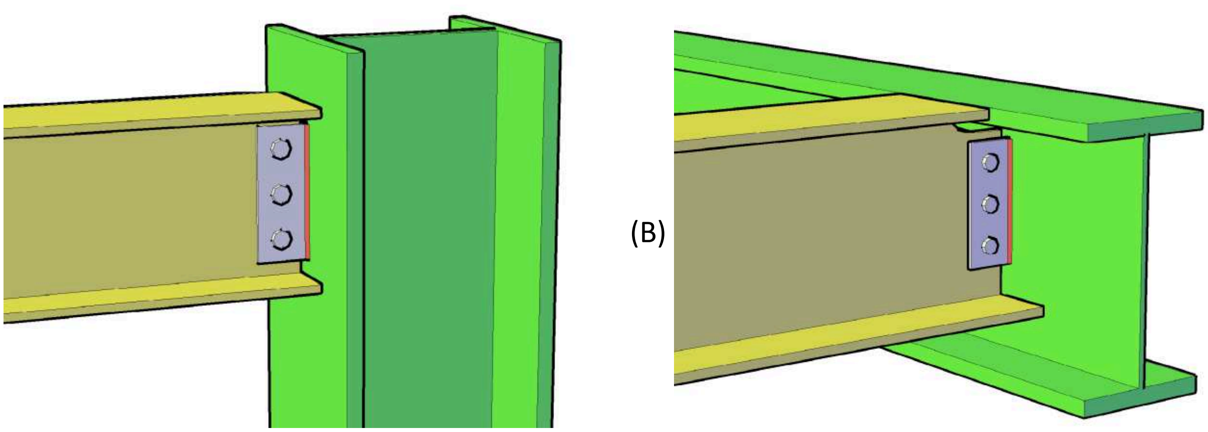

(B)

Figure 1.1-(A) Beam to column shear tab connection, (B) Beam to girder connection

The connections shown in Figure 1.1 are known as standard shear tabs in which the eccentricity of the bolt line has a specified small distance (typically 75mm) to the weld line. Another family of shear tabs also exists, known as extended shear tabs (Figure 1.2). These connections have a higher eccentricity compared to standard shear tabs. The extension eliminates the requirement of beam coping in beam to girder connections and provides easier erection for beams that are connected to the web of columns. Although the extension may benefit the construction process, it also creates a higher moment in the connection resulting in greater stresses in the weld interface and influences the plastic deformation of the shear tab itself; therefore, it must be designed with an appropriate method. Shear tabs can be connected by using a single or multiple vertical rows of bolts allowing for a greater distribution of stresses amongst the fasteners. This is a common method to increase a shear tab's resistance to carrying axial loads in addition to vertical loads. The shear tabs investigated in this thesis are single and double vertical row non-extended shear tabs varying in size and number of bolts.

(A) (B)

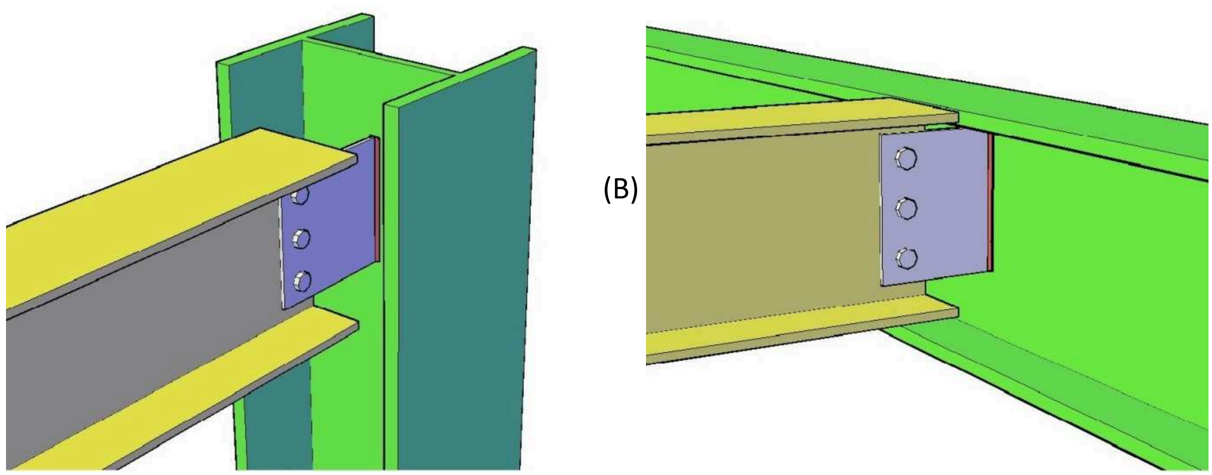

Figure 1.2-(A) Beam to column extended shear tab connection, (B) Beam to girder extended shear tab connection

In terms of structural response, shear tabs are classified as simple connections due to their high rotational capabilities. According to the AISC Manual of Steel Construction-LRFD design (2000), shear tabs are classified as shear connections. Shear connections are defined by Salmon and Johnson (1996) and Astaneh (1989) to be connections that have a moment capacity less than 20% of the connecting beams plastic moment capacity. Figure 1.3 shows the response moment-rotation curve for different types of connections by Astaneh (2005). Although shear tabs are classified as simple connections, they still transfer a small amount of moment. A web connection by an angle could result in a more flexible connection than a shear tab, but due to simplicity of fabrication and erection, shear tabs are more commonly used instead.

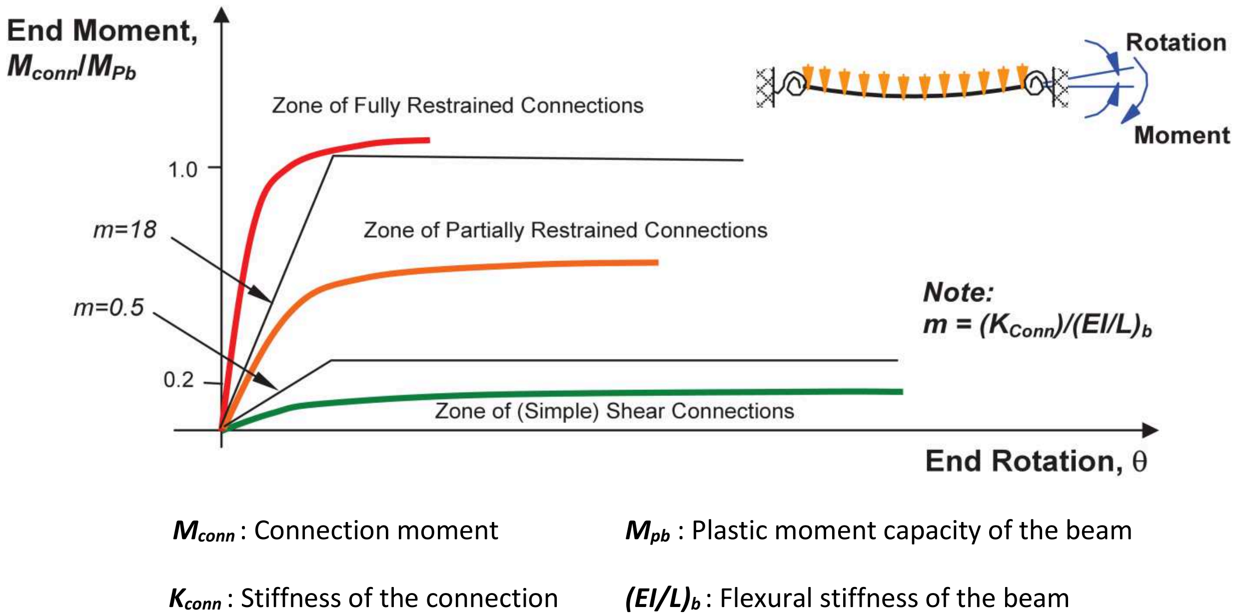

Figure 1.3-Moment-rotation curve for different types of connections, Astaneh (2005)

1.2. Possible sources of axial loads

Seismic loads: One of the most important phenomena that is capable of developing axial forces in beams and finally in connections is earthquake loads. Consider the braced frame in Fig 1.4 as an example, when an earthquake acts on the frame the inertia force generated in the mass is distributed between the nodes. For example the lateral load on the top floor is distributed between point A, B, C, and D. Since the braced bay restrains nodes B and C from movement the force acting on Point A will cause a compression force in Beam AB. On the other hand the force acting on point D will cause a tension force to develop in beam CD. Furthermore, the compression capacity of steel braces is lower than the tensile capacity due to buckling. Since earthquake loads are cyclic it is possible that the braces will buckle. The joint that is connected to the buckled brace will no longer help effectively (some post buckling resistance may exist but much lower than the tensile resistance of the brace) in transferring the axial load created by the earthquake and the force will be transferred from beam AB into Beam BC. The axial forces developed in the beams will once again have to be transferred by the connections.

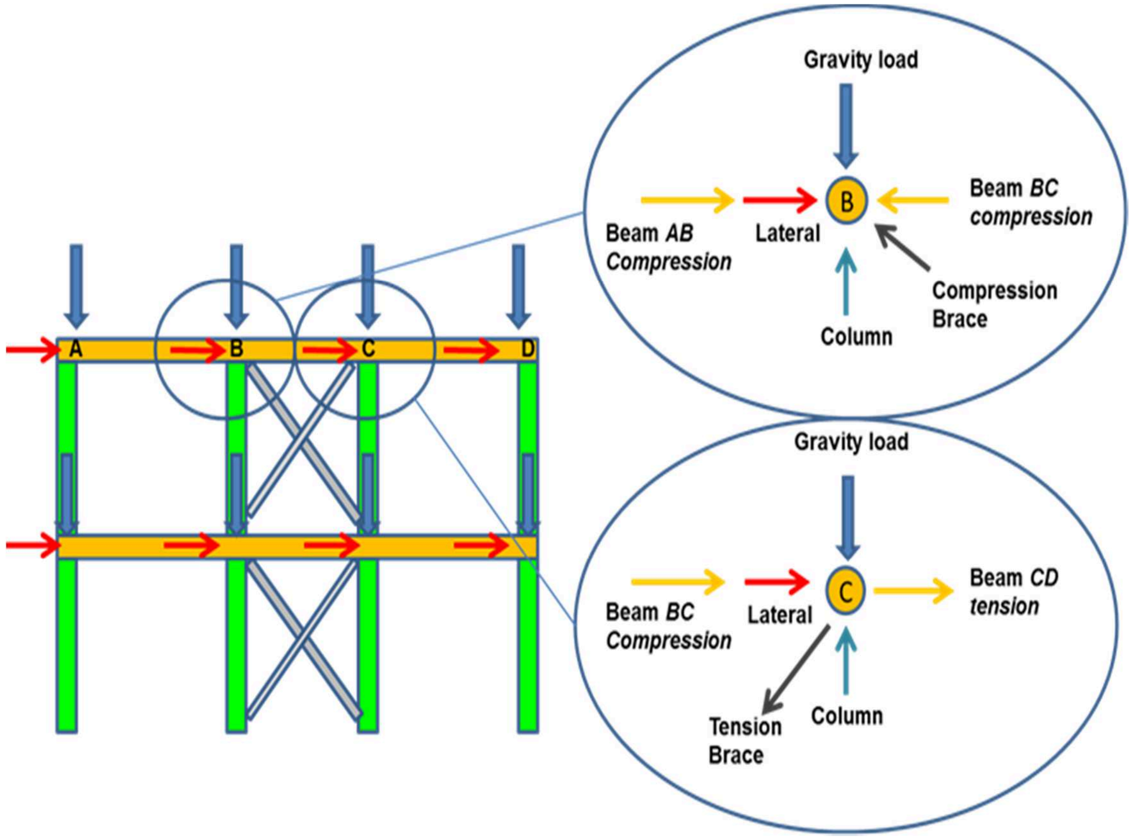

Figure 1.4-Axial forces developed in beams by lateral loads

Wind loads: In the case where wind load is transferred from the cladding to the structural frame and finally to the lateral load resisting system the shear tabs may experience axial forces. In order for the wind force to reach the lateral load resisting system it must pass through beams that will develop high axial forces; hence the connection from the beam to column must also be designed for these forces.

Bracing element: Axial loads can be developed in the connection of a bracing element which supports a main member in a structure. For example a beam which is connected to the mid-height of a column that is subjected to high axial load can act as a bracing member. In order to change the buckling mode of that column, the beam has to transfer force from the column into itself through the connection and that will develop axial force in the connection.

Blast and impact: Robustness of structures has become one of the main subjects that engineers must take into consideration in the design of a building. For example in the case of a loss of a column due to explosion or impact the structure should not entirely collapse due to the catenary action that would develop in the floor and roof structure. This would cause high axial forces to develop in the beams above the damaged column; these forces would have to be transferred by the connections (Figure 1.5). Due to this action, connections can experience rotations up to 0.2 rads. Note, the deformation and loading demand placed on a shear tab connection in this situation was not considered as part of the research described herein.

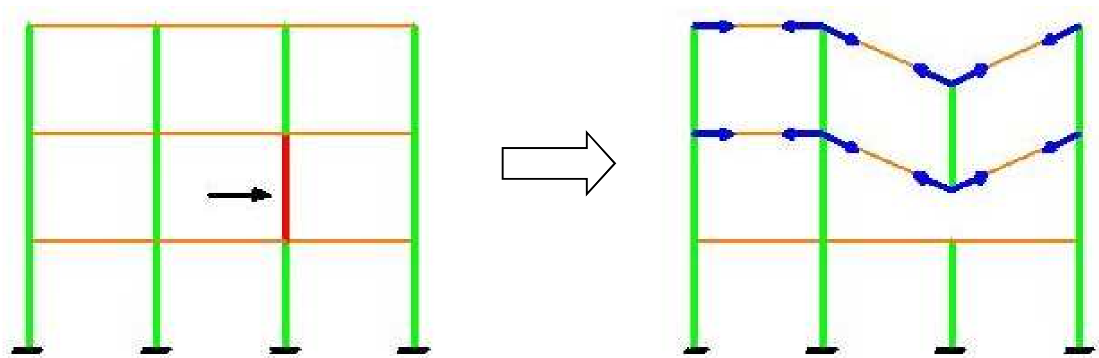

Figure 1.5-Axial forces developed in beams and connections due to the loss of a column

Other sources: Special structural member orientations may also lead to axial load in beams like a stair beam with slope connected to a beam in the same direction. During the erection of a steel frame, columns might have out-of-straightness and in order to connect the beams to the column it may be required to pull the column to straighten it enough for the connections to be made. Axial forces will be created in the beams, and the connecting shear plates, during this process.

1.3. Statement of problem and the global research project

The current design procedure used for shear tabs in Canada (CISC, 2010) is based on the research carried out by Astaneh (1989) and Astaneh et al. (1989); it has not been further developed. This approach is only applicable to shear tabs with one vertical row of 2 to 7 bolts connected to a rigid support (e.g. the flange of a W section column) or a flexible support (e.g. the web of a column or a girder) by using E49 fillet welds and A325 bolts. The current Canadian approach does not cover the usage of multiple vertical rows of bolts or the use of configurations with more than 7 bolts per vertical row of bolts. The size and thickness of the shear tab is further limited due to design restrictions. The existing design approach also does not address the application of combined shear and axial forces on the connection, which leads to the necessity of research on this specific subject.

The global research project involves the development of shear tab design and detailing provisions to be used in Canada and is carried out by a team of researchers and students. It comprises full-scale laboratory testing and finite element (FE) modeling. The advantage of using finite element simulation is that the load level and connection configuration can easily be changed and more cases can be investigated in less time and with less cost compared to full-scale testing. One of the global research project's intentions is to evaluate the behaviour of shear tabs that are subjected to axial forces in combination with shear force, which is also the main focus of this thesis. The remaining goals of the global research program which are to be carried out by other co-researchers are:

- Evaluating standard shear tabs designed based on the current procedure (single vertical row up to 7 bolts with specified dimension and eccentricity limitations, weld sizes, bolt type and steel grade.)
- Investigating configurations which are not covered by the current design procedure including the use of more than 7 bolts in a row, multiple vertical rows of bolts (two & three), shear tabs that exceed the dimensions described in past test results which can be used to connect large W beams, and the use of 350 MPa steel.
- Assessing partial and fully welded shear tabs in the case of misalignment between the holes on the beam web and shear tab.
- Investigating extended shear tabs which are subjected to high eccentricity due to the distance from the supporting element (column or beam girder).
- Examining shear tabs connecting coped beam webs with stiffeners and doubler plates.

1.4. Objectives

The primary objective of the research program described herein was to develop a design approach that could be used by the engineering community to address the effect of combined axial and shear force on a shear tab connection. This main goal was accomplished by achieving the sub-objectives described below:

1. Develop finite element models that are capable of simulating shear tab connection tests subjected to vertical loading performed by Marosi (2011).
2. Perform a series of full-scale laboratory tests of shear tabs subjected to combined axial plus shear forces in order to observe the behaviour of the connections and to calibrate the finite element models.
3. Investigate the behaviour of shear tab connections subjected to combined shear and axial tension forces as well as combined shear and axial compression forces by means of finite element modeling.
4. Propose a design approach for shear tabs subjected to combined shear and axial forces (at rotation levels lower than 0.1 rads) based on the findings of the test and finite element studies.

1.5. Scope

Objective 1 was achieved with the replication of six laboratory shear tab tests conducted by Marosi (2011) by using FE simulation. The connections simulated were shear tabs specimens connecting W310, W610 and W920 beams with one & two vertical rows of bolts. The software ABAQUS (Simulia, 2011) was relied on for the FE modeling due largely to its advanced nonlinear simulation capabilities. These models were used to verify the capability of ABAQUS to closely match the shear tabs' behaviour with the tests conducted by Marosi, providing confidence in their potential use for the evaluation of other loading scenarios. The loading protocol used was based the suggested protocol for beams subjected to gravity loads by Astaneh et al. (2002), where the highest recorded rotation of the specimens was 0.1 rads. To obtain a more accurate FE simulation of the shear tab connections, material properties were obtained by performing coupon tests on specimens cut from the plates and beams used for the connection testing. The coupons were then modeled in ABAQUS to develop a material database which was subsequently used for the FE simulation models of the test shear tab connections. Final improvements such as material calibration and damage property modifications were included in the models.

Objective 2 was achieved by performing four full-scale laboratory tests of shear tabs subjected to combined shear plus axial force. Due to the complexity and expense of these tests only two shear tab specimens connected by two vertical rows of bolts were tested; The tests were performed on a 456x178x16 mm shear tab connection between a W610x140 beam and a W360 x 196 column, as well as a 225x165x10 mm shear tab connection between a W310 x 60 beam and a W360 x 196 column, configured as a double vertical row bolted connection. A test setup with an axial load application system was designed, drafted, fabricated and installed in the laboratory. Each specimen was individually tested for combined shear plus tension and combined shear plus compression force. The results from these tests were used to identify the connections' behaviour under combined forces and to calibrate and improve upon the FE models simulating the connections under various levels of axial force.

Objective 3 was achieved by using the developed FE models replicating Marosi's (2011) tests to investigate the performance of the same shear tab specimens subjected to combined effects of shear and axial force. From the fact that applying axial load to a test specimen during a full-scale lab test that is undertaking shear force and some moment at the same time is extremely difficult and expensive, FE simulation was found very useful to be utilized for this stage of the research. Different levels of axial force in forms of tension and compression were applied to the FE models and a parametric study was performed. The output of this part of the study was shear vs. axial force interaction curves for each shear tab specimen and shear force vs. shear tab displacement for different levels of axial force applied on each specimen.

Objective 4 was accomplished by establishing a relation between the change in the shear resistance of the shear tab specimens due to the presence of tension and compression axial force. The results obtained from FE simulation and laboratory testing was analysed and a design approach was suggested.

The overall objective of developing a recommended design method for combined axial and shear forces was achieved by proposing an interaction equation based on the overall results such that practicing engineers could design shear tab connections that are expected to be subjected to combined shear and axial forces. The design approach requires modification of the ultimate shear resistance of the shear tab connection based on the level of axial force, either in tension or compression.

1.6. Original Contributions

Since the current Canadian design approach used for shear tabs is based on a research project limited to connections with a single vertical row of bolts that was carried out in 1989 by Astaneh et al., it does not cover the more sophisticated and complex connections and potential loading used in structures today. For example the Bow building in Calgary which requires connections much larger and stronger than the shear tabs described in the CISC Handbook of Steel Construction (2010), as well as shear tabs that must carry both vertical and axial loads. The research contributes to an improvement of the design procedures for shear tabs that will enable engineers to design these connections accounting for situations where combined axial and shear forces are present, a loading situation for which no design guidance is currently available. With the completion of the research, recommendations will be made to the Canadian Institute of Steel Construction to revise their current design approach leading to improvements in the level of performance of this type of connection, which will ultimately benefit the steel industry, the engineering design community, the building owners, and the safety of occupants.

1.7. Outline

Chapter 2 discuses a summary of the past research carried out on shear tab connections. The literature review focuses on research that had the most significant contribution to existing shear tab design approaches.

Chapter 3 explains the methodology used, research plan, and different phases of the research program. Available test data performed by the co-researchers is also presented.

Chapter 4 presents the finite element modeling stage of the research program. The finite element model features, simulation techniques and obtained results are provided. Material data preparation, lab testing of coupons, coupon FE simulation and processing is also discussed.

Chapter 5 provides a description of the full-scale laboratory testing performed on shear tabs subjected to combined shear plus axial forces. The setup, instrumentation and final findings of the tests are discussed in detail.

Chapter 6 presents the results obtained from the finite element modeling of the same shear tab connection models developed in Chapter 4, with the addition of different levels of axial force. The effect of axial load on the connections' behaviour by using FE simulation is presented.

Chapter 7 summarizes the results obtained from full-scale laboratory testing, FE simulation and the results obtained by the co researchers; and contains a recommendation for a shear tab design approach that includes the effect of axial load.

Chapter 8 presents the final conclusions and future recommendations for further research.

Chapter 2

Literature review

2. Chapter 2- Literature review

2.1. Overview

The material covered in this Chapter is categorized into three main groups: Past research on shear tab connections subjected to gravity loads, finite element modeling of shear tab connections, and research on shear tabs subjected to combined shear and axial forces. A brief outline of the most relevant existing research that shaped the scope of this thesis is presented. Following the literature review, the current design approaches used for shear tabs in North America are discussed.

2.2. Past research on shear tab connections subjected to gravity loads

Due to the high demand and complicated non-linear behaviour of single plate connections (shear tabs) numerous research projects have been performed. The reviewed literature provided a better understanding of the subject and helped identify areas that required further improvements. A brief outline of the most relevant research is presented.

In 1968, Lipson (1968) at the University of British Columbia presented a report on the performance of three different types of simple connections. One which was the single welded-bolted plate, now commonly referred to as a shear tab. His main goal was to evaluate the feasibility of angles and shear tabs. The research investigated thin shear tabs (t=6mm) connected by using a single vertical row of bolts (two to six ¾ inch ASTM A325 bolts). A series of 12 full-scale tests called the P-series were related to shear tab specimens. Three testing protocols were used: pure moment, moment-shear with no rotation and moment-shear with rotation. The test setup used for two test methods is shown in Figure 2.1. The rotation in the moment-shear tests was controlled by the extension of two hydraulic jacks (with 50 mm stroke) close to the tip of the beam supported by an end frame.

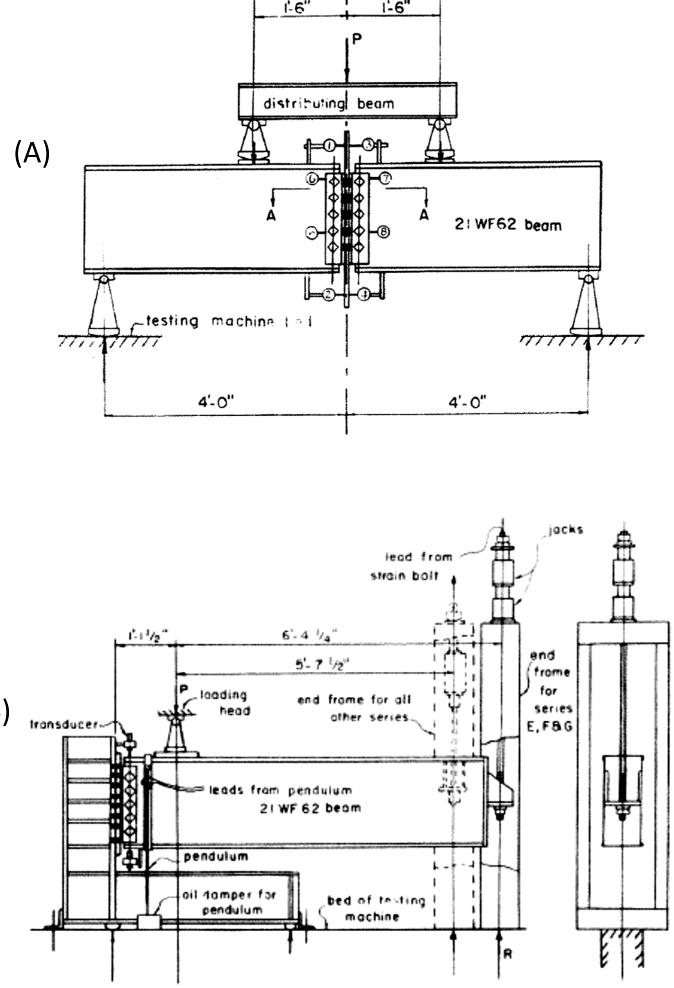

Figure 2.1-(A) Pure moment test setup, (B) Moment-shear test setup (Lipson, 1968)

Figure 2.2 shows the response of the shear tabs specimens tested by Lipson. Figure 2.2-A shows the moment-rotation relation of the shear tab specimens tested under pure bending. As it can be seen in the figure, for each test a pair of data is available since two shear tabs were tested in the pure bending test setup. The reason for the differences in the behaviour of the same shear tabs specimens tested in one operation is specified to be the clearances around the bolts when the joints were made up. As the number of the connecting bolts increase, the moment that the shears tab resists increases with a decrease in rotational ductility. The shear tabs tested experienced an ultimate rotation between 0.022 and 0.06 radians; however the testing was limited to the capacity and stroke of the hydraulic jacks and the two and three bolted specimens might have experienced higher rotations under pure bending. Figure 2.2-B represents the shear force-vertical deflection response curve of the shear tab specimens tested by the moment-shear testing method. All the specimens experienced a similar behaviour and some non-linearity at very small displacements.

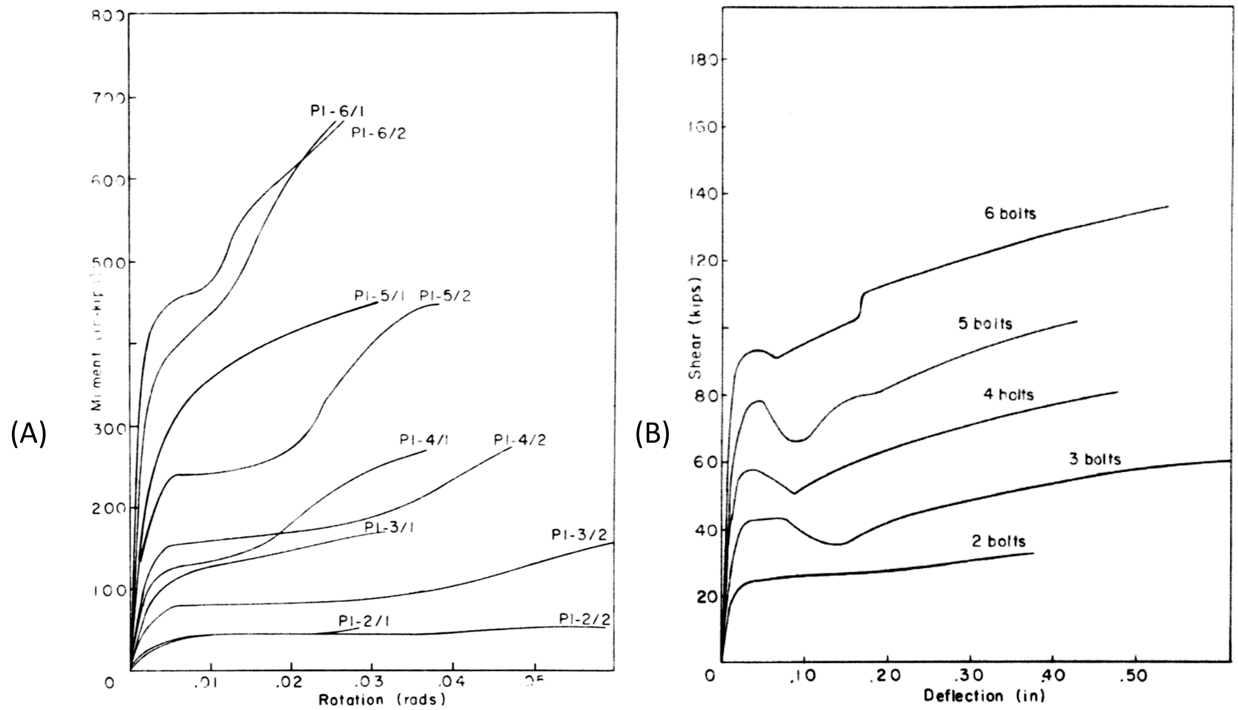

Figure 2.2-(A) Response curves obtained from the pure moment tests, (B) Response curves plotted based on the moment-shear tests (Lipson, 1968)

Lipson confirmed that the centre of rotation was situated close to the centre of the bolt group, and not more than 20 mm (0.8”) from the centre in the direction of the compression edge of the shear tab. Another important finding was that for all the welded-bolted connections that he tested, slip occurred at a rotation less than 0.04 radians. Lipson recommended not using shear tabs in beam framing because they experience end rotations higher than 0.04 radians for most working loads.

Richard et al. (1980) aimed to determine the amount of moment generated in single plate connections by using the beam-line methodology (Figure 2.3). Based on the theory, a beam line is created on a moment-rotation curve graph. The start point of the beam line is the highest possible moment (fixed end moment of a simple beam) on the vertical axis and the end point is the highest value of possible rotation (completely free end rotation of a simple beam) on the horizontal axis. The intersection of the beam line with the moment-rotation curve which is determined by using laboratory tests and finite element analysis gives a good approximation of a connection's moment. Richard et al. also noticed that the thinner plate (beams web or shear tab) will govern the load-deformation relationship and the ductility and strength will mainly be based on the characteristics of the thinner element.

For a Simple beam with uniformly distributed load:

$$M_{fixed} = \frac{ql^2}{12} \qquad \phi_{free\ end} = \frac{ql^3}{24EI}$$

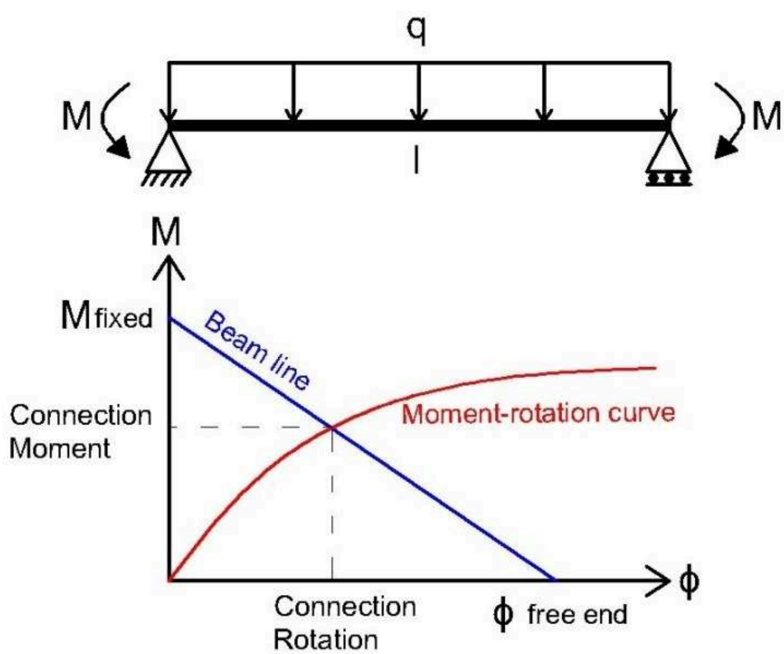

Figure 2.3-Beam line method (Richard et al, 1980)

Astaneh (1989) believed that using the classic beam line method was not sufficient to predict the true behaviour of the connection because it was based on a complete elastic response. The inelastic beam line concept (Figure 2.4) was introduced which predicts a response very close to the true behaviour of the connection.

Astaneh et al. (1989) provided a design approach for proportioning and rating shear tabs based on an experimental program. This study comprised of shear tab tests using a single vertical row of up to 7 bolts. One of their main assumptions was that axial forces were not applied to the connection.

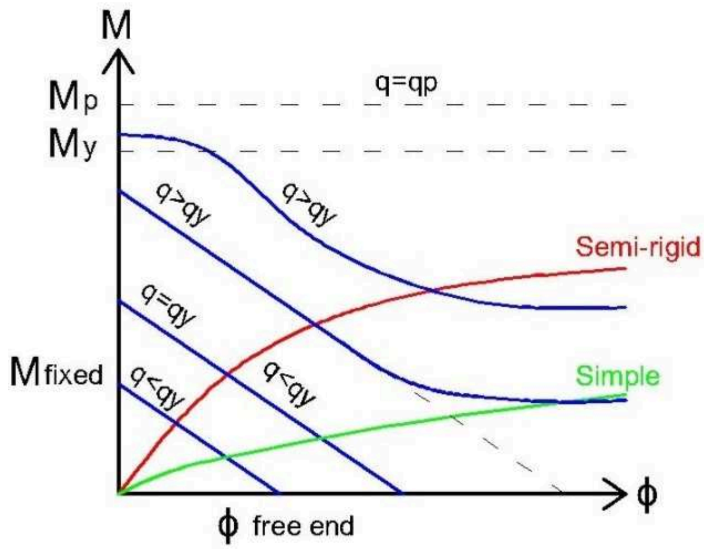

Figure 2.4- Modified inelastic beam line theory (Astaneh, 1989)

In 1993, Astaneh et al. (1993) developed and presented a strength based design guideline for shear tabs which was used in the American Institute of Steel Construction (AISC) manual (1989, 1992) at that time. Six strength limits states were introduced and formulated for the shear tabs. The limits states ordered by desirability (higher ductility to brittle failure modes) were: plate yielding, bearing failure of bolt holes, fracture of the net section of the plate, fracture of the edge distance of the plate, bolt fracture and weld fracture. The proposed design approach was compatible with ASTM A325 and A490 bolts. Both Snug tight and slip critical bolts with a 76 mm vertical spacing between the bolts were allowed in the design method. The distance between the bolt line with the weld line was limited to 64-76 mm. A distance bigger than 76 mm was not recommended due to the possibility of local buckling at the bottom portion of the shear tab. For the connecting weld design, it was recommended to design the welds with enough resistance to allow the plate to undergo plastic yielding before failure. To ensure that this mechanism would occur, the weld size D was required to be greater than 0.75 t, where t is the thickness of the shear tab. A series of tests was performed on connections designed with this approach; the results showed sufficient ductility of the shear tab and a maximum rotation of 0.026 to 0.054 radians at the maximum shear force level. The number of bolts had a major influence on the rotational ductility; the higher the number of bolts, the lower the rotational ductility that could be achieved.

In a subsequent paper Astaneh et al. (2002) presented an investigation of the behaviour of shear tabs under gravity loads in combination with cyclic lateral loads. The effect of a concrete slab on the behaviour of the shear tab connections under cyclic loading was also studied. Ten cyclic tests were performed with typically used shear tabs, different types of concrete and composite connectivity. The total moment capacity of the connection and the contribution of the concrete slab to the moment capacity were evaluated. After about 0.04 radians of drift, the composite action was lost and the presence of the floor slab exhibited a 30 to 60 percent increase in the resistance of the beams plastic moment capacity. The hierarchy shown in Figure 2.5 also applied to the behaviour of the shear tab specimens subjected to combined gravity and cyclic loading. Overall the shear tabs experienced yielding and slip at low levels of drift, followed at large levels of drift by ductile performance.

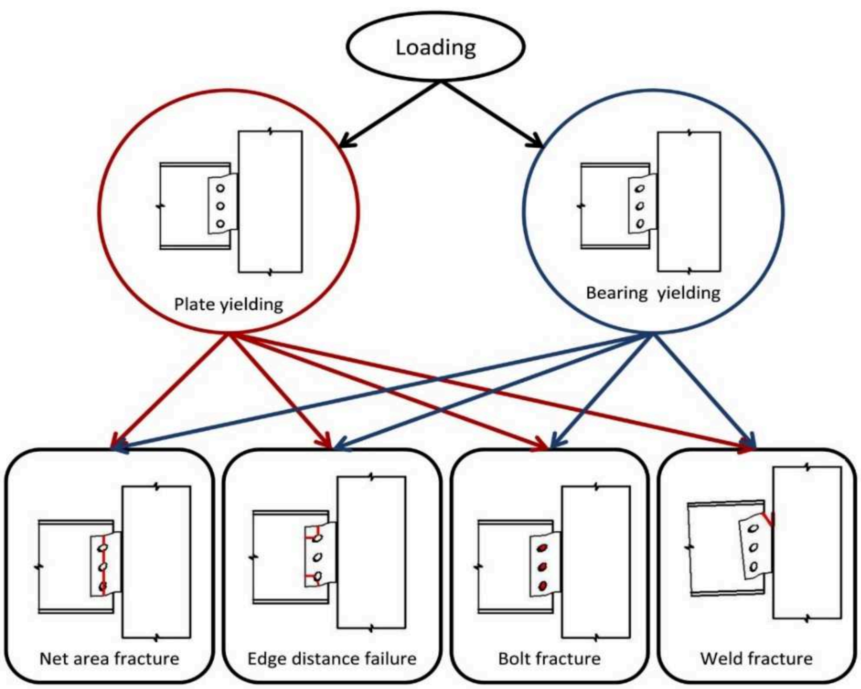

Figure 2.5- Shear tab failure mode hierarchy (Astaneh et al., 2002)

Sherman and Ghorbanpoor (2002) developed a design approach for extended shear tabs. This research was based on 31 full-scale tests to evaluate the behaviour of stiffened and unstiffened extended shear tabs that were used to connect beams to girders or to the web of a wide flange column (Figure 2.6). In terms of eccentricity, the bolt line was recommended to be 64-89 mm away from the tips of the supporting members flange. The possibility of additional limit states that could occur such as twisting or failure in the web of the supporting member due to high eccentricity between the bolt and the weld line was also investigated. The important parameters that were studied based on the test results were span to depth ratio of the supported beam, width to thickness ratio of the supporting member's web, number of bolts used, dimensions of the shear tab, type of bolt holes, and lateral support of the connecting beam. A new limit state was identified for unstiffened extended shear tabs based on a yield line mechanism observed in the web of the supporting column; however it was ruled out in the design procedure by recommending the utilization of stiffened extended shear tabs in this case scenario. The proposed design procedure became a modification of the AISC criteria used for shear tab design at that time and supported shear tabs connected by 2 to 10 bolts in a single vertical column.

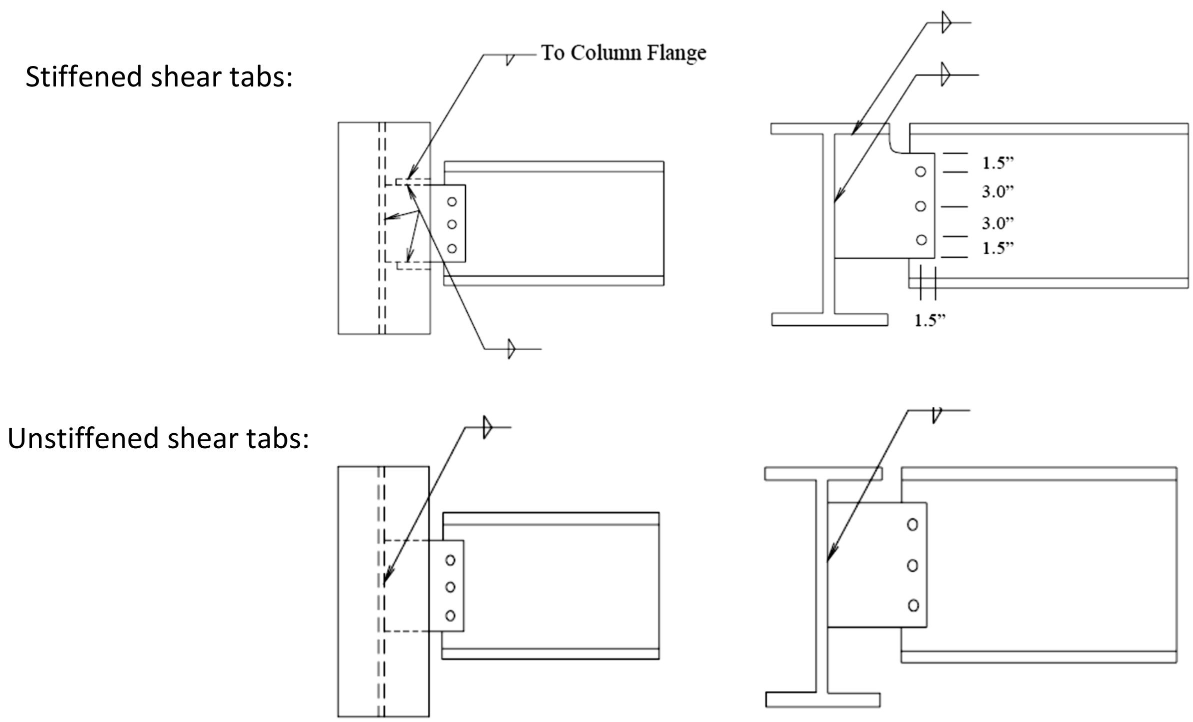

Figure 2.6- Extended shear tab configurations tested by Sherman and Ghorbanpoor (2002)

Crocker and Chambers (2004) performed a series of full scale tests on 10 mm thick shear tab connections connected by three, four and six 19mm (3/4 inches) ASTM A325 bolts in a single vertical row configuration. The specimens were tested for rotations up to 0.06 radians. Their main objective was to determine the maximum deformation demand placed on the bolts. The bolts used in their study included the threads in the shear plane. Only the six bolted configuration experienced a bolt shear failure at a rotation of 0.04 rads. The other two specimens were able to carry the moment up to a rotation of 0.06 rads and did not fail. The location of the neutral axis after bearing at high rotations was also investigated and its effect on the capacity of the shear tab was determined and finally equations were presented to estimate the rotation capacity of the common size shear tab connections.

Creech (2005) performed a series of 10 full-scale tests on shear tabs connected to flexible and rigid supports to investigate the procedure used to predict the connection resistance as described in the AISC LRFD manual 3rd edition (AISC, 2003). The test setup (Figure 2.7) was different compared to those used by past researchers. Creech tested a full span simple beam which was connected on one side to a connection column and a roller support was used on the other end. The load was applied at two points as it was a pure moment test setup. Lateral braces were installed to fully restrain the test beam from lateral torsional buckling. A similar setup was used for flexible supports by replacing the connection column with a support girder.

The predicted limit states were compared to design procedures from different countries. It was found that Astaneh's equations used in the AISC LRFD Specification 3rd edition (AISC, 2003) estimated the closest ultimate capacity of the connection. The steel plate and the connection bolts were the two main components that Creech focused on. Eight out of ten tests failed with the rupture of the connection bolts. Based on Creech's findings, the bolt eccentricity can be ignored for connections connected by more than 3 bolts and the shear tab could be designed for pure shear strength.

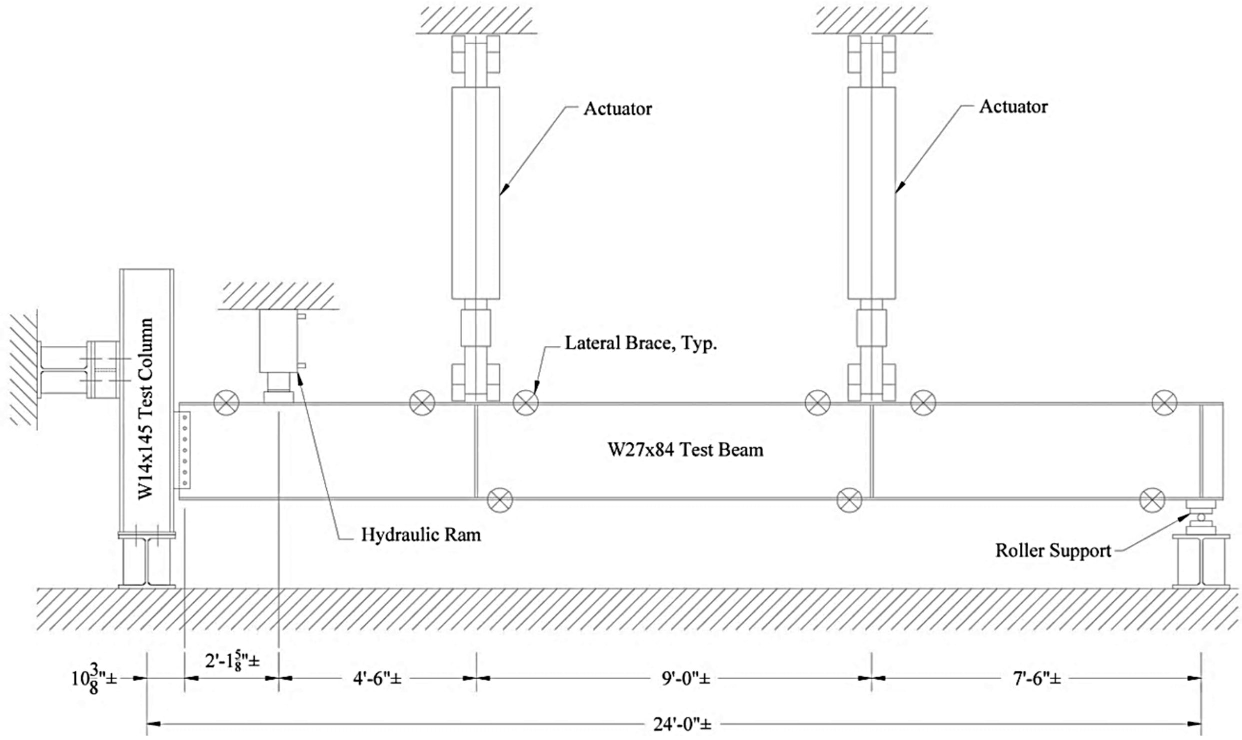

Figure 2.7-Typical rigid support test setup used by Creech (2005)

Goodrich (2005) investigated the performance of a series of extended shear tabs by experimental and numerical testing. The experimental work was used to verify his finite element modeling simulations and to help attain a better understanding of the extended shear tab specimen's behaviour. A series of six tests on three shear tabs was conducted. The test setup was designed in such a way to simulate a 9144 mm simply supported W27x84 beam with a uniformly distributed load. The load was applied as a point load at a specified location to produce a reaction force equivalent to the reaction force produced by the uniformly distributed load at the connection. The shear tabs were designed based on the AISC LRFD manual 3rd edition (AISC, 2003) and by using the approach developed by Sherman and Ghorbanpoor (2002). All the connections failed by yielding and buckling of the plate. His results showed the necessity for further developments in extended shear tab design procedure at that time. Based on Goodrich's laboratory test results, the extended shear tabs with the continuity plates could support over two times the force they were designed for with a safety factor of 2.3 to 3.7. Finally Goodrich (2005) proposed a design approach for the extended shear tabs that he had studied.

Metzger (2006) examined shear tabs that were designed based on the new approach described in the AISC 13th edition Steel Construction Manual (AISC, 2005). Her research was based on 8 full-scale tests on shear tabs connected on only rigid supports. The setup used was identical to that of Creech. Four of the tests were focused on shear tabs classified as conventional configurations and the remaining four were specimens designed based on the new extended configuration approach. A target rotation of 0.03 radians at the plastic moment capacity of the beam was used for the loading protocol. Metzger concluded that the strength limit states used for predicting the resistance of the shear tabs for both configurations (conventional and extended) still were conservative, however the predicted values were more accurate compared to the 3rd edition AISC LRFD Manual (AISC, 2003). The shear tabs designed based on the conventional method were overestimated by 27-38% (based on design strength) while the extended shear tab specimens showed an overestimation of 35-48%. Bolt shear and weld rupture was identified as the failure mode of four of her tests and the remaining tests experienced the failure of the test beam prior to the connection.

The integrity of shear tab connections in case of a simulated column removal scenario was investigated by Weigand and Berman (2014). A series of gravity systems were generated to cover a range of configurations that were typically used in the design industry practice. The span lengths investigated varied from 7.32 m to 15.2 m and two types of concrete slabs (normal and light weight) with metal decks were assumed. The designed primary and infill beams ranged from ASTM W18 × 35 and W16 ×26 sections for shorter spans to W24 × 104 and ASTM W21 × 44 for longer spans. Laboratory testing was conducted for 13 shear tab sub assemblage specimens (column stud, shear tab, beam and structural bolts) and connection parameters such as number of bolts, bolt diameter, bolt grade, plate thickness, edge distance, and type of holes(STD and SSLT) were investigated. The tested connections mainly failed by subsequent bolt shearing and tear-out of the plate edge distance. Using SSLT holes increased the maximum vertical load capacity and ductility of the connections. The results showed that the shear tabs alone (without the steel deck and concrete slab) were able to sustain approximately 15-25% of the LRFD specified design shear strength under the column removal scenario.

2.3. Past research on finite element modeling of shear tab connections

In this section, research conducted on shear tabs by using finite element simulation is discussed. The objectives, modeling, simulation techniques used, and findings of recent researchers are presented.

Ashakul (2004) performed an advanced finite element analysis of single plate connections by using ABAQUS (2011a, b). He investigated the behaviour of single and double row shear tabs and attempted to simulate laboratory tests conducted by Astaneh et al. (1989) and Sarkar (1992). He used the developed FE models for further investigations on major parameters that play an important role in the design of shear tabs. The parameters that he investigated were: the a-distance which was defined to be the distance between the weld and bolt line, material of the plate, plate thickness, and the connection's position relative to the neutral axis of the connecting beam. The strategy he used was to first create eight FE models that replicated test data from Astaneh et al. (1989) and Sarkar (1992). Two additional models were created to examine the effect of the test beams' size and length; and two other models were built to investigate the effects of loading type and bolt strength on the connections' behaviour. A total of 12 FE models were built for the first step of his research. A summary of his simulation results is presented in Table 2.1.

Table 2.1- Summary of the FE simulation results by Ashakul (2004)

Model	Bolts in Simulation	Bolts in Test	Simulation Prediction (kips)	Test Results (kips)	Ratio of Prediction/Exp	Source
1	3-A325X	3-A325N	85.5	84, 94	1.02, 0.91	Astaneh et al. (1988)
2	5-A325X	5-A325N	131.6	137	0.96	
3	7-A325X	7-A325N	189.6	160	1.19	
4	3-A490X	3-A490N	84.7	79 (W)	1.07	
5	5-A490X	5-A490N	158.3	130	1.22	
6	2-A325X	2-A325N	57.7	51.8, 60.8 (W)	1.11, 0.95	Sarkar (1992)
7	4-A325X	4-A325N	109.1	81.6, 84.6	1.34, 1.29	
8	6-A325X	6-A325N	128.8	102, 109	1.26, 1.18	
9	5-A325X	5-A325N	140.3	137	1.02	Astaneh et al. (1988)
10	7-A325X	7-A325N	197.0	160	1.23	
11	4-A325N	4-A325N	83.0	81.6, 84.6	1.02, 0.98	Sarkar (1992)
12	6-A325N	6-A325N	104.1	102, 109	1.02, 0.96	

Note: The failure mode is bolt shear rupture unless indicated otherwise
W = Weld rupture

As can be seen from Table 2.1, the FE models were able to predict the ultimate shear resistance of the connections with a fair accuracy; however most of the FE models overestimated the resistance, which in some tests by over 20%. Ashakul (2004) believed that models 3, 5 and 10 should be modified to account for the bolt threads being in the shear plane. If the results obtained from these models were to be reduced by 20 %, they would be very close to Astaneh et al. (1989) and Sarkar's (1992) measured resistances. Thirteen other FE models were created to investigate the effect of the a-distance and plate material on the shear strength of the bolt group, 6 models to investigate the effect of plate thickness, and finally 11 models to study the performance of a double row bolted shear tab. A total of 42 simulation models were built.

The FE modeling technique that Ashakul (2004) used was based on the half span of the test beam with the shear tab and the bolts. A shear release boundary condition was used at the end of the test beam and the beam was restrained laterally along its entire length to prevent lateral-torsional bucking. The beam was also restrained in the axial axis of the test beam. The assembly of the model was built of the steel plate, bolt and test beam. Each component was meshed individually (Figure 2.8) and interactions were defined between the parts. Two mesh densities were attempted, a fine mesh and a very fine mesh. In order to have a smooth contact between the bolts and their holes the very fine mesh configuration was selected even though it consumed 5 times more computing time. The 2 mm gap between the bolt and the hole was also included in the FE models. The welds were restrained at the location where they were connected to the column. A wide range of element types was used in his research. The second order reduced integrated element (C3D20R) was used at locations subjected to high stress concentrations such as the body of the plate, welds and the portion of the test beams web that contained the holes. First order C3D8 cubic elements were utilized at locations of less interest such as the beam flanges, part of the beams web under the holes and a region with a courser mesh density close to the bolt line on the beam web. Due to geometry conditions, the second order prism element (C3D15) element was used at some locations such as the body of the bolts to satisfy geometry confinement. Finally the first order incompatible element (C3D8I) was used at the remaining portion of the beam (course mesh as shown in Figure 2.8) to simulate the beams bending and shear deformations.

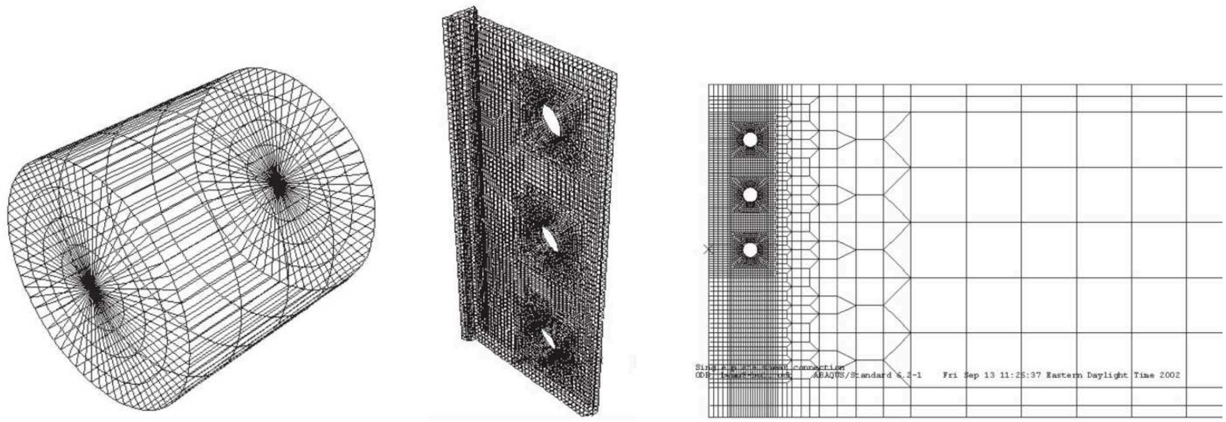

Figure 2.8- Bolt, shear tab and beam mesh design used by Ashakul (2004)

One major issue rose with the simulation of the gap between the bolt and the holes. At the initial stage of the analysis contact was not completely established which led to numerical instability, to resolve this issue Ashakul (2004) employed a special gap element in ABAQUS (2011a, b) to fill the void between the bolts and the holes. Figure 2.9 demonstrates the installation of the gap elements around the bolts. The only problem with the gap elements was that it required a very fine mesh around the bolt and since the element type of the gap elements was a wedge type element, the angles were very small with a poor aspect ratio, but overall the results showed that they performed very well.

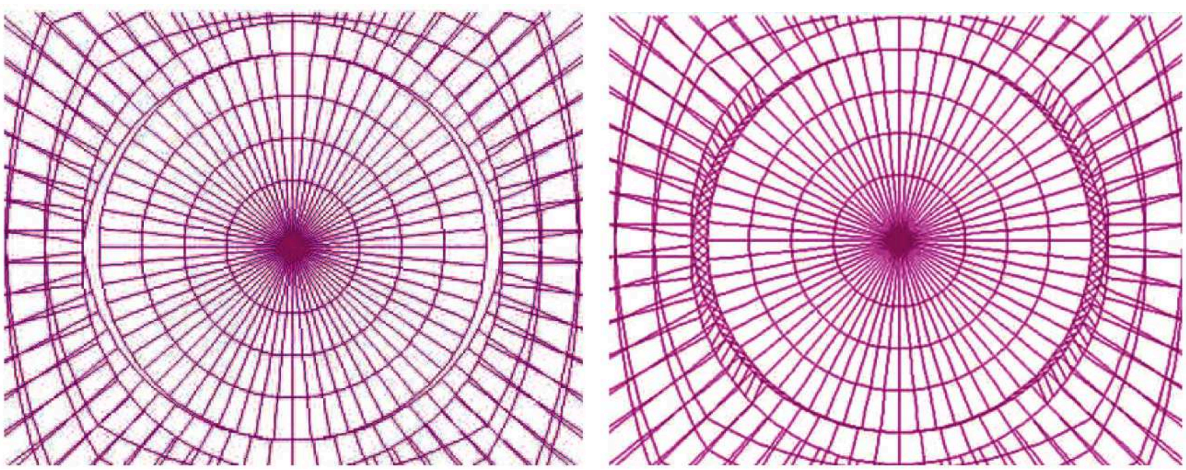

Figure 2.9- (A) Bolt position without gap elements, (B) with gap elements Ashakul (2004)

To simulate bearing in the FE models, a hard contact interaction was used for the normal behaviour between the bolts and the inner surface of the holes on the steel plate and beam web. For the tangential direction interaction, the SMALL SLIDING feature in ABAQUS (2011a, b) was used for defining the contact. SMALL SLIDING was recommended when nonlinear geometry effects were included in the simulation.

An elastic perfectly plastic plus strain hardening stress-strain relation was used for the plate and the test beam material (Figure 2.10), while an elastic perfectly plastic relation was used for the welds and the bolts. Two types of loading were used for the simulation; initially a uniformly distributed load which was applied on the top flange of the beam throughout its length, secondly, concentrated forces were applied on the top flange at the same location where the force was applied in the lab tests. At these locations the web of the beam was stiffened to prevent yielding or crippling of the beam's web.

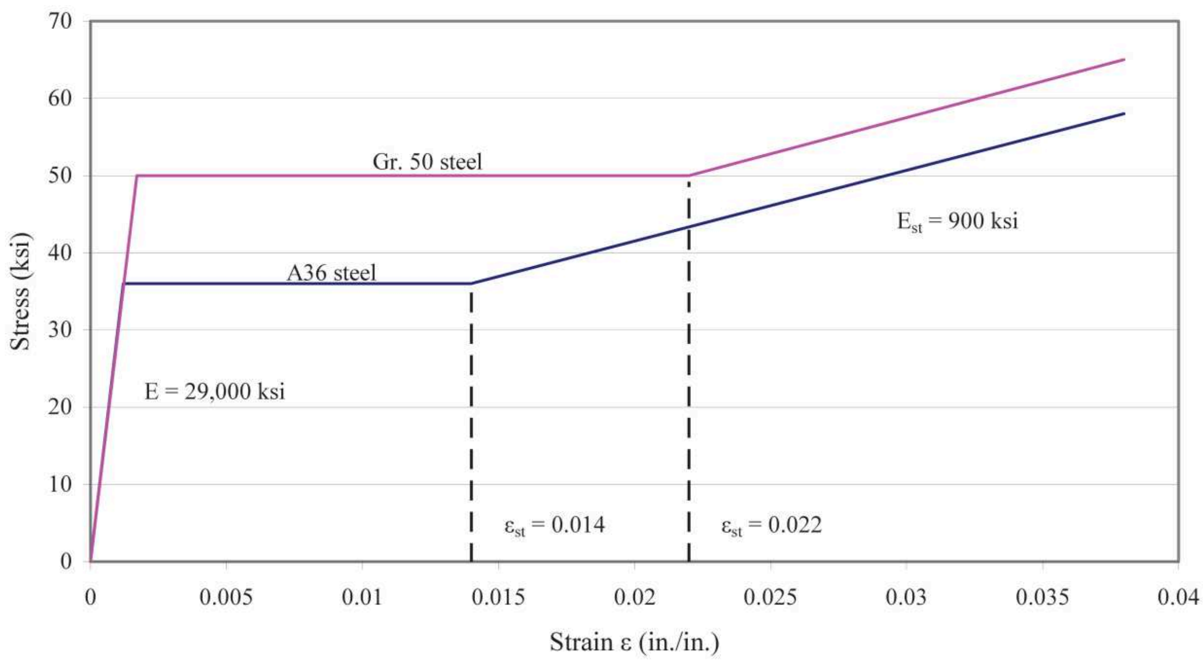

Figure 2.10- Material property input used by Ashakul (2004)

Several important findings of Ashakul (2004) are outlined:

- The bolt shear rupture strength was not a function of the a-distance
- Connections that did not satisfy the ductility criteria used for plates (material and thickness), led to high horizontal forces in the bolts that reduced the shear strength of a bolt group. These forces created an additional moment that must be considered in design.
- In double row bolted shear tabs, if a thick plate was used force redistribution between the two bolt rows did not function and the outer row (from the support) took most of the stresses while the inner row resisted very small forces.
- The shear stress distribution was not constant throughout the cross section of the steel plate when strain hardening occurred.

Goodrich (2005) performed a numerical and experimental study on extended shear tabs. His objectives were to investigate the effect of using continuity plates on the performance of extended shear tab connections and to evaluate the safety of reduced eccentricity due to the presence of continuity plates in design. The effect of the connection on the column support was not examined in his study. Goodrich developed a series of finite element models by using ANSYS (1996) in order to replicate the full scale testing that he had performed.

A basic FE model was used compared to that which was developed by Ashakul (2004). His model comprised the shear tab with the continuity plates; all made of one single part, and did not include the bolts or contacts. The meshing of his model was composed of only 10 node tetrahedral elements (Figure 2.11-A). Approximately 10000 elements were used in the mesh and the running time never exceeded one minute due to the simplicity of the model. Load was applied as a surface pressure at the bottom of the inner surface of the holes on the shear tab. The continuity plates and the shear tab were restrained at the location where they were welded on the supporting member. For the material properties, coupons were not extracted and the material response was based on mill reports of the steel manufacturer. Other simulation schemes such as modelling the test beam, column, bolts with contact and interactions were attempted but did not yield proper results. Stresses, strains, reaction forces and displacements were used for comparison with the results obtained from laboratory testing. Figure 2.11-B represents the Von misses stress distribution of model 2B developed by Goodrich (2005). Finally He stated that the modeling procedure used was very approximate and needed further improvements, especially by using a more accurate material property for the simulations.

(A)

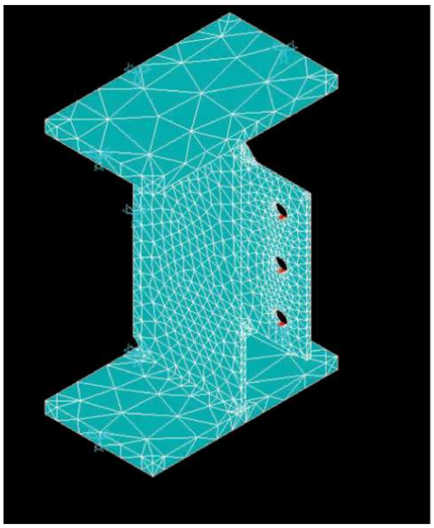

(B)

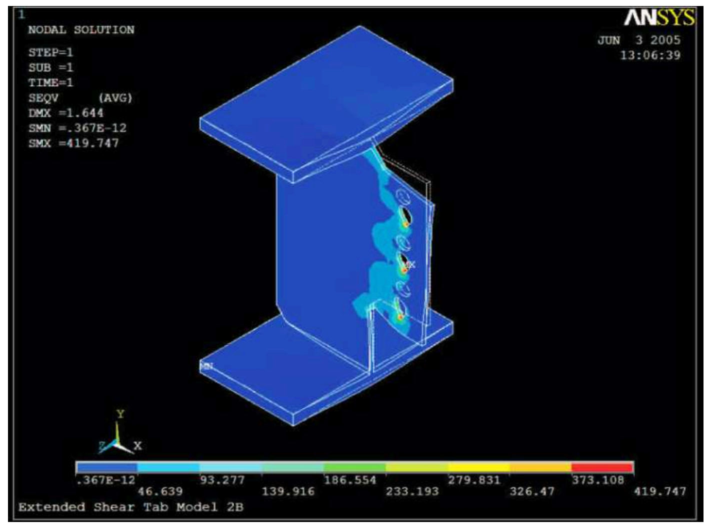

Figure 2.11- (A) Mesh design assembly, (B) Von mises stress distribution, Goodrich (2005)

Rahman et al. (2007) developed 3D finite element models in order to simulate and further investigate the experimental work on extended shear tab connections carried out by Sherman and Ghorbanpour (2002). Their primary objective was to develop a finite element model that was capable of simulating the nonlinear behaviour of non-stiffened extended shear tabs to prevent the necessity of performing further experimental work which was expensive and time consuming. Investigation on the effect of a deeper connection beam, compared to those tested by Sherman and Ghorbanpour (2002), on the connection behaviour was also in his scope of study. For this purpose in addition to a three bolted model, a five bolted model was constructed. ANSYS (2000) was selected as the finite element package for analysis. The technique that he used was to model the complete assembly built of the shear tab, test beam, supporting column and bolts. All parts were modeled and interactions between the components were defined. Figure 2.12 illustrates the constructed assembly with the mesh design used. Eight node brick elements were mainly used to mesh most of the components (beam, shear tab and supporting members) except for the bolts where ten node tetrahedral elements were used.

(A) (B)

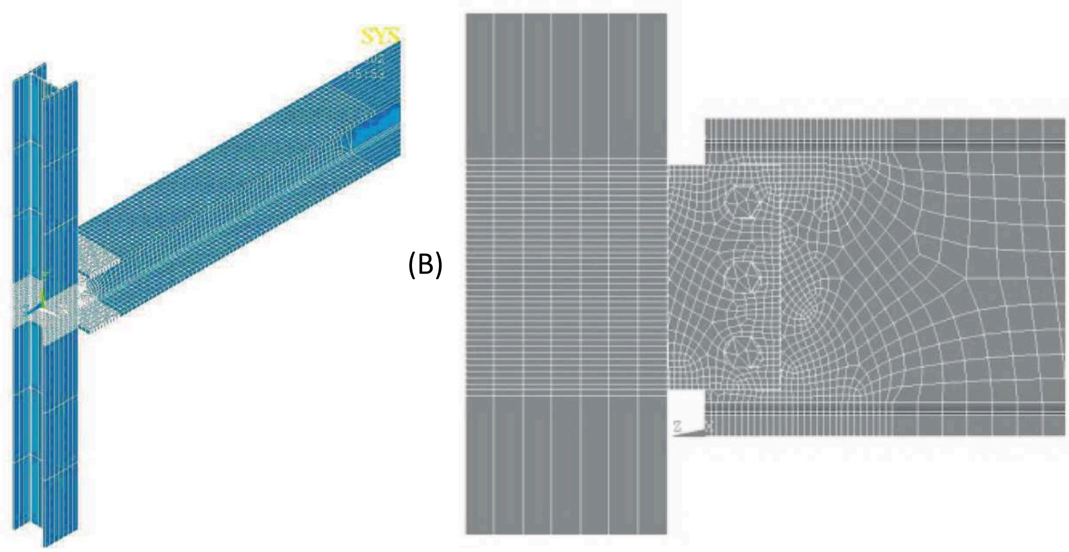

Figure 2.12-(A) Connection assembly, (B) Mesh design, Rahman et al. (2007)

Pre-tension force was used for the bolts since this is how they were installed in the physical tests by Sherman and Ghorbanpour (2002). Rahman et al. suggested a pre-tension force of 30 kips for fully tight and 18 kips for snug tight bolts. Friction was also included, using a coefficient of 0.3, in the contact interactions between the components. ASTM grade 36 material was used for the steel plate, ASTM A325-X for the bolts and ASTM grade 50 steel for the structural members. The input stress-strain curves used for the input were based on experiments for each material. The column was supported by a vertical wall during the laboratory tests therefore the nodes at the same location were restrained in the FE models. Based on the experimental results weld fracture was not a failure mode in the conducted tests therefore the weld was modeled continuous with the shear tab and the column. The loading protocol was the same as the one used for the laboratory testing. The main parameters that Rahman et al. (2007) focused on in this study were: vertical displacement of the shear tab along the bolt line, shear load eccentricity relative to the bolt line, twisting of the shear tab, nonlinear behaviour and failure modes. Figure 2.13 contains an illustration of the final deformed shape obtained from FE simulation with the 5 bolted extended shear tab test result. As can be seen from the figure, the shear tab experienced a twist failure mode. FE models developed by Rahman et al. (2007) proved to be very reliable and useful for further studies. Shear force-deflection curves obtained from FE simulation were within an average deviation of 12% from the experimental results. The failure modes observed in the FE models also matched the same failure modes that occurred during the full-scale laboratory tests.

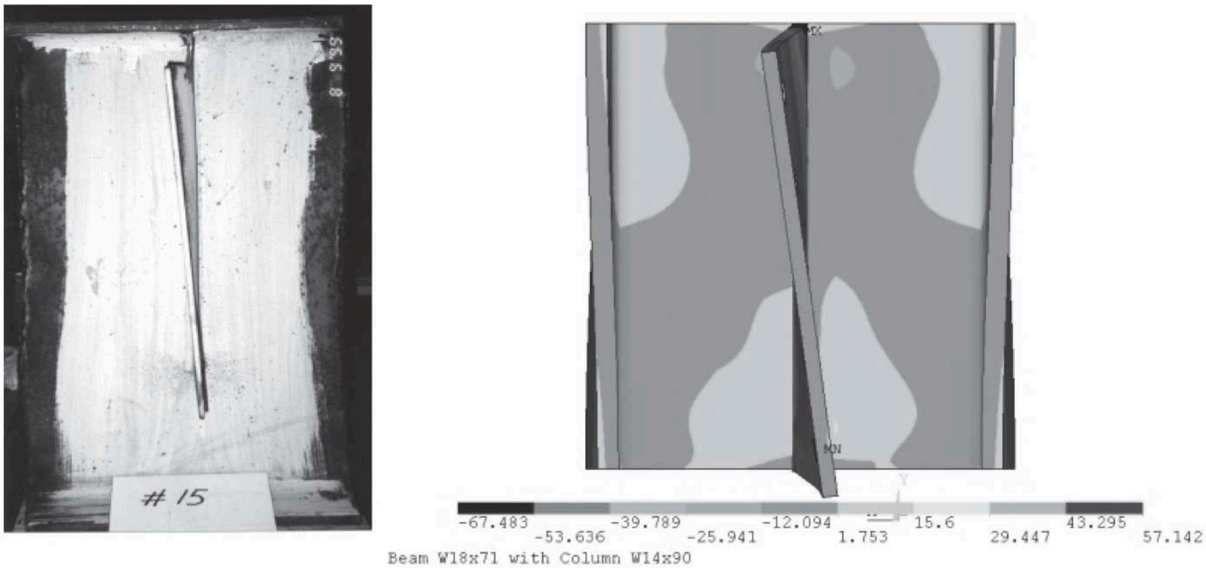

Figure 2.13- Experimental vs. FE model final deformed shape, Rahman et al. (2007)

Daneshvar and Driver (2011) attempted to replicate the experimental work on shear tabs subjected to combined moment, shear and axial force by Thomson (2009) (see Section 2.4). ABAQUS was used to model 9 tests from Thomson. The FE model used consisted of a column in the centre with the shear tabs attached to it, and two adjacent test beams which were connected to the central column by bolts. True pins were simulated at the other ends of the test beams. The testing procedure was identical to Thompson's protocols. An imposed displacement was assigned to the central column while the connection behaviour and developed forces were monitored.

Figure 2.15-A shows the assembly of the FE model prior to simulation while Figure 2.15-B shows the final deformed shape of the test specimens. ASTM A325 bolts, ASTM A36 steel for the shear tab, and ASTM A992 grade steel was used for the rest of the components in the model. Out-of-plane displacements were also restrained to provide lateral support for the test beam. First order reduced integration elements were used for the entire meshing. The connections experienced a rotation over 0.1 radians which was higher than the suggested accumulated gravity and seismic rotation of 0.08 radian recommended by Astaneh (2005). The specimens showed

high ductility capabilities due to bearing around the holes in the steel plate. The FE models provided an acceptable response compared to the test results. Daneshvar and Driver concluded that nonlinearity definitions were the most challenging part of the simulation, external restraint can considerably influence the behaviour of the shear tabs under catenary action, and finally the response curves developed could be used as an input for models that simulate a full building collapse.

(A)

(B)

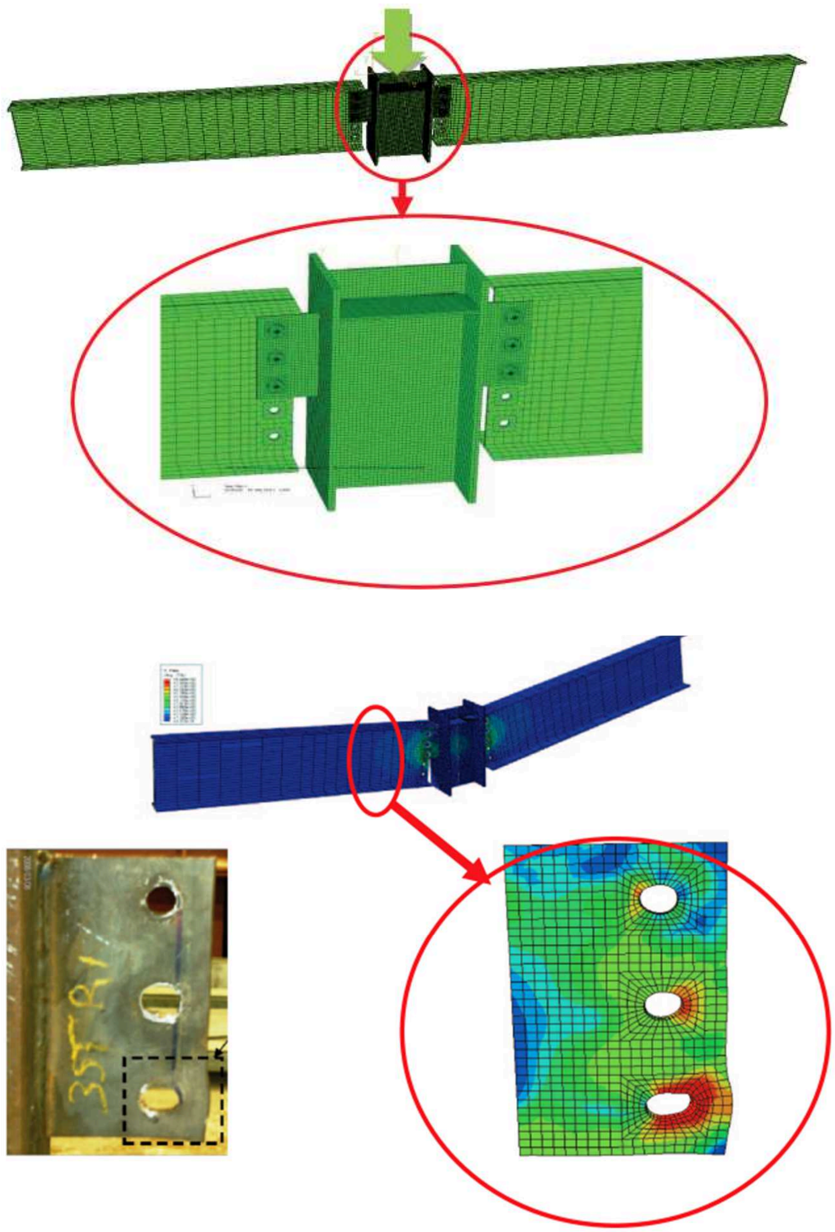

Figure 2.14- (A) FE model assembly prior to testing, (B) Final deformed shape with the Von-Mises stress distribution of the assembly and shear tab, Daneshvar and Driver (2011)

Schroeder (2012) performed a numerical study to determine moment-rotation curves of theoretical shear tab connections by using ABAQUS (Simulia, 2011a). He believed that the idealization of assuming that shear tabs resist no moment is not correct when calculating the lateral stiffness of a steel frame. Schroeder also mentions that if the rotational stiffness of shear tabs were added to the lateral load resisting system, the building response to seismic loads can be improved resulting in lower storey drifts. Experimental work performed by other researchers such as Larson (1996), Liu and Astaneh (2002) and Crocker and Chambers (2004) were simulated.

The model that Schroeder (2012) developed was built of an assembly of a test beam, shear tab, support column and bolts including contact interactions. C3D8R elements that were 8-noded reduced integration brick elements with hour glass control were used in mesh design. The material properties were based on data from the corresponding experimental tests. For experiments that did not specify complete material data, A992 grade 50 steel was used for the components. The loading was applied as a tip displacement boundary condition to the model and the beam rotated up to 0.1 radians. Figure 2.15 shows the deformed shape of the connection and bolt obtained from the FE simulation of Crocker and Chambers (2004) tests.

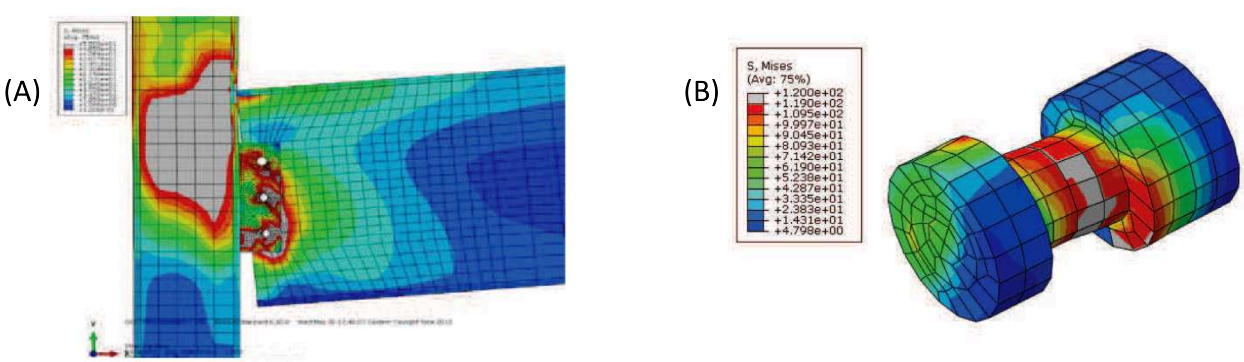

Figure 2.15- (A) Von–mises stress distribution in the connection, (B) Bolt deformed shape, Schroeder (2012)

Schroeder (2012) concluded that his models were able to simulate the experimental work from the other researchers with acceptable accuracy and predict the initial stiffness of the connections within a margin of 2-12%. If the shear tabs were counted as partially restrained connections, the inter-storey drift of a building could be reduced by 22% compared to a case where the shear tabs are assumed to be ideal pin connections.

Yim and Krauthammer (2012) developed a series of finite element models to replicate the experimental work carried out by Crocker and Chambers (2004). Once validated , the models were then used to develop a mechanical model representing shear tab connection behaviour under monotonic, cyclic and blast loading. Details of the FE modeling were not presented, however the mesh design used for the FE simulation can be seen in Figure 2.16. The suggested mechanical models presented for the shear tab connections behaviour was in terms of a nonlinear M–θ relationship for monotonic loading, M– θ hysteresis loop for cyclic behaviour, and M–I diagram for a blast-rate loading scenario.

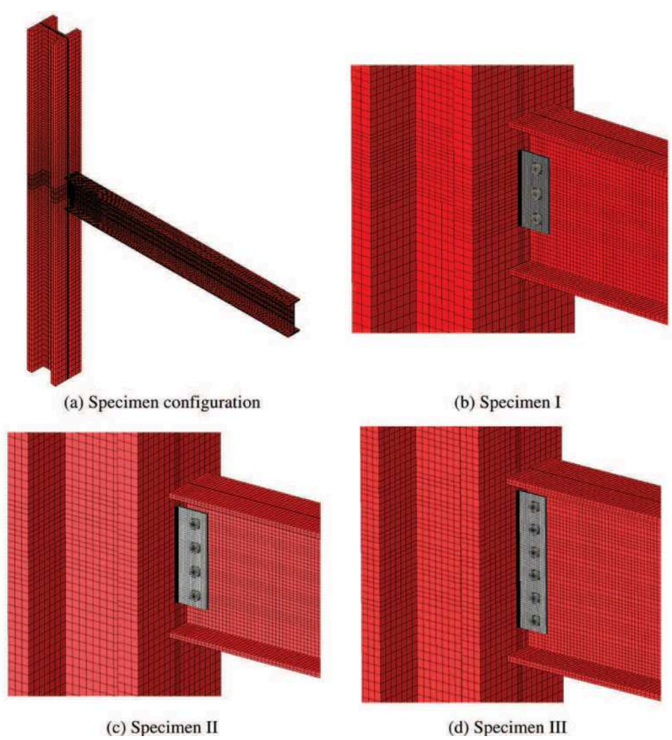

Figure 2.16-Mesh design used for FE simulation by Yim and Krauthammer (2012)

2.4. Past research on shear tabs subjected to combined shear and axial forces

A limited number of publications of past research are available on shear tabs subjected to combined shear and axial forces. The subject has become a more active field of study in recent years; however few shear tab specimens have been tested for the interaction of shear and axial forces. The configurations tested were very limited in size, material, loading scenario, axial force type (compression or tension), extension of the shear tab, and rows of bolts used. A summary of the most recent related literature is presented:

Guravich and Dawe (2006) investigated the performance of simple shear connections under the effect of combined shear, moment and tension force. The research was carried out by performing 108 full-scale lab tests on header angle, knife angle, single angle and shear tab connections. Eleven tests were performed on a single row 3 bolt standard shear tab specimens. The reason for this specific specimen selection was that it was commonly used in construction. 3/4 inch ASTM A325 bolts were used and tightened to be snug tight. The thickness of the shear tab specimens were 7.9 mm and the weld size was one size larger than the minimum size required for a 7.9mm thick plate to improve the tension resistance of the connection. The test setup used by Guravich and Dawe (2006) is illustrated in Figure 2.17.

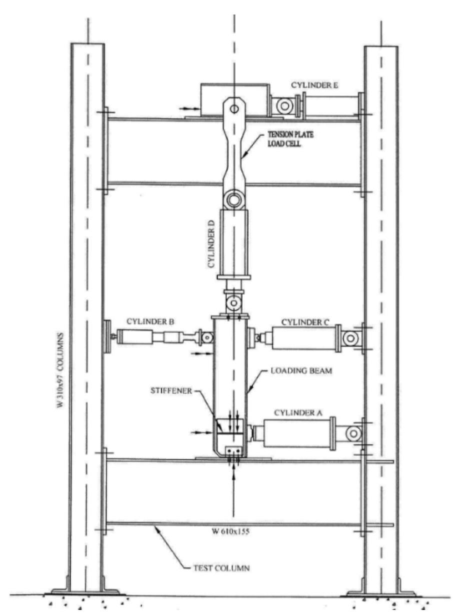

Figure 2.17- Test setup used by Guravich and Dawe (2006)

The setup was built of two vertical W310x97 columns which were connected to the base and linked together by two horizontal wide flange beams. The lower beam was a W610x155 wide flange section which acted as a rigid support column for the specimens and was selected to minimize additional rotations. The top beam was used as a support for the cylinder that applied the tension force. Five hydraulic cylinders were used. Cylinder A applied the main shear force to the connection, cylinders B and C controlled the rotation of the connection, cylinder D applied the tension force and finally cylinder E controlled the position of cylinder D to keep the force perpendicular to the beams cross section. The shear tab specimens were welded on a steel plate and the plate was bolted on the lower beam. The testing procedure was to first rotate the test beam to 0.03 radians and simultaneously apply the shear force from zero to the desired value. The shear load level was either 50% or 100% of the factored bolt shear capacity. In the next step the axial tension was applied to the test beam with a magnitude of 50% and 100% of the design ultimate shear resistance of the connection while the shear and rotation remained constant throughout the testing. The first two shear tab specimens experienced out of plane buckling under only shear load which resulted in twist of the test beam. To resolve this issue, for the next series of tests a lateral support system was designed and utilized in the test setup. Table 2.2 shows a summary of the tests conducted by Guravich and Dawe (2006) on shear tabs.

Table 2.2- Summary of the test results for shear tab specimens by Guravich et al. (2006)

Specimen	F_y (MPa)	F_u (MPa)	V_{test} (kN)	T_{ult} (kN)	Failure mode[a]	V_{res} (kN)	B_p (kN)	V_{res}/B_p
T308-1	260	321	380	0	H	380	—	—
T308-2	260	321	337	0	H	337	—	—
T308-4	260	321	89	384	G	394	402	0.98
T308-5	260	321	104	370	G	384	411	0.94
T308-9	260	321	102	382	G	395	414	0.96
T308-8	260	321	213	321	G	385	403	0.96
T308-10	260	321	253	310	G	400	401	1.00
T308-11	260	321	245	284	G	375	401	0.94
T308-6	260	321	0	360	G	360	401	0.90
T308-7	260	321	0	374	G	374	412	0.91
T308-12	260	321	0	386	G	386	412	0.94
Avg.								0.94
COV								0.03

Note: —, buckled prematurely.
[a]G, shear fracture through tab plate; H, plate buckling

V_{test}: Applied shear load, T_{ult}: ultimate tension load, V_{res}: Resultant shear force

B_p: Bearing resistance of shear tabs (CSAS16-94) (CSA 1994)

As can be seen from Table 2.2, tests T308-1 and T308-2 failed under only shear force with a plate buckling failure mode while all other specimens failed by a steel plate shear fracture mode. Based on the average V_{res}/B_p ratio of 0.94 obtained from the tests, B_p which is the bearing resistance of the steel plate was found to be a suitable limit state to predict the ultimate resistance of the connection under combined shear and tension.

The effect of axial, shear and moment interaction on shear tab behaviour in the case of a column failure was investigated by Thompson (2009). He evaluated the performance of shear tabs that were designed based on the AISC 13th Edition manual (AISC, 2005) by conducting 9 full-scale tests. The typical test setup configuration used by Thompson is shown in Figure 2.18. An interior column which supported two identical shear tabs and test beams was positioned over a hydraulic cylinder. The other ends of the test beams were connected by true pin connections to a supporting frame. In order to simulate the catenary action in case of a column failure, the column was lowered and the forces were monitored. The tests did not include the effect of a concrete slab on the connection. The main goal of this testing procedure was to induce tensile forces in the shear tabs, and produce rotations exceeding 0.03 radians which was the design standard rotation at that time. In addition the robustness of the connection and its ability to resist the catenary state was investigated.

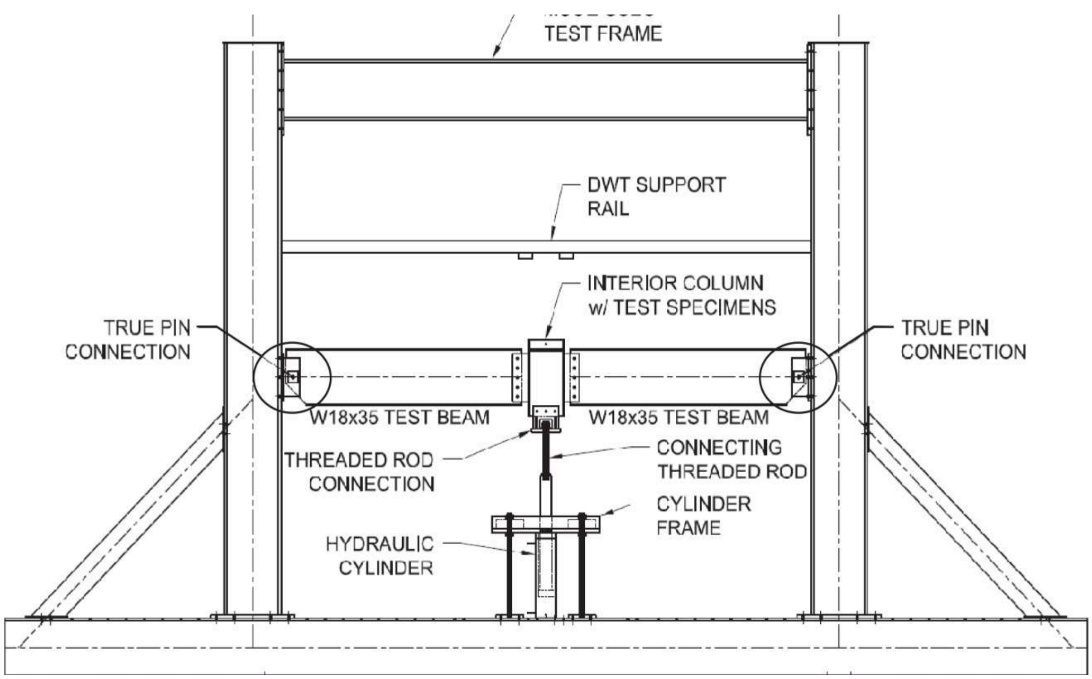

Figure 2.18- Typical test setup used by Thompson (2009)

Based on the configurations of his tests, three limit states mainly controlled the ultimate capacity of the connections; bolt shear, localized net section tensile rupture and localized block shear rupture were observed at the bottom bolt location. Thompson's (2009) overall results showed that the shear tabs which he tested had the ability to resist the developed unexpected forces due to progressive collapse of a column.

Oosterhof and Driver (2011) assessed the capacity, ductility and failure modes of different types of simple connections under combined moment, shear and axial forces by conducting 45 full-scale laboratory tests. The shear tab was one of the connection types that were investigated. Unlike the test setup used by Thompson (2009) which required testing two shear tab specimens plus two test beams in one testing operation, the test setup used by Oosterhof and Driver (2011) only required a single connection installed on a W250x89 test column and one test beam (Figure 2.19). The setup was capable of applying any combination of moment, shear and axial force to the specimens. This was possible with the aid of three hydraulic actuators. Actuators 1 and 2 generated the moment and shear while actuator 3 applied the axial force to the connection. The plates used to fabricate the connections were made of CSA G40.21-04 (1998) Grade 300W steel and grade 350W steel test beams and columns were used. The two shear tab specimens tested were: (a) 230x110x6.4 mm shear tab connected by three 3/4 inch ASTM A325 bolts to a W310x143 test beam (b) 390x110x9.5 mm shear tab connected by five 7/8 inch ASTM A325 bolts to a W530x165 test beam.

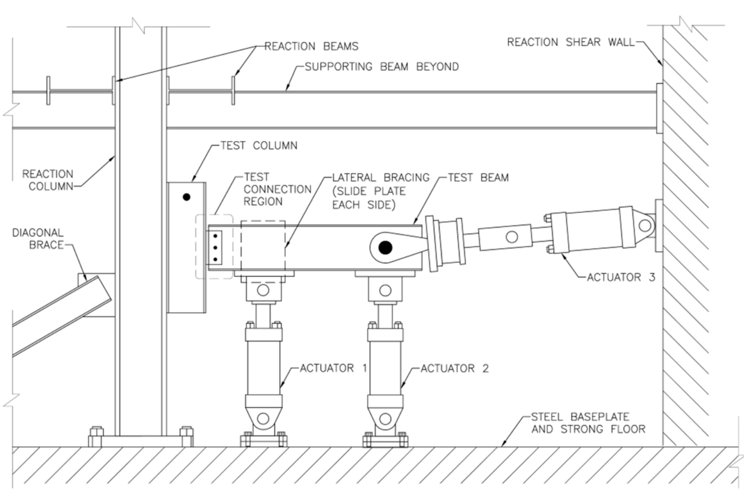

Figure 2.19- Typical test setup used by Oosterhof and Driver (2011)

A loading protocol simulating a column removal scenario was outlined and used for the testing procedure. The response of the specimens was studied by plotting vertical, horizontal forces and moments versus the test beams' rotation. The span length assumed for the 9 shear tab tests was 8m with a uniform distributed load applied. A high rotational stiffness of the connection was experienced at low rotations. Once the moment reached its peak level, the catenary action initiated axial stresses in the connection followed by the reduction of the moment from the peak to zero. The horizontal force reached its peak just before the initiation of a crack near the lower bolt on the shear tab as shown in Figure 2.20 and started to decrease stepwise as damage occurred around the remaining bolts. The plate experienced excessive yielding around the bolts providing ductility of the connection to reach rotation levels of 0.08 to 0.13 radians before the bolt tear-out failure at the lowest bolt. No contact of a test beam's flange with the test column was observed.

Oosterhof and Driver (2011) concluded that the bolt tear-out was the governing failure mode for the tested shear tabs and the test setup used was proved to be a practical approach for evaluating connections in a column failure scenario. The shear tabs showed acceptable strength and ductility to develop catenary forces.

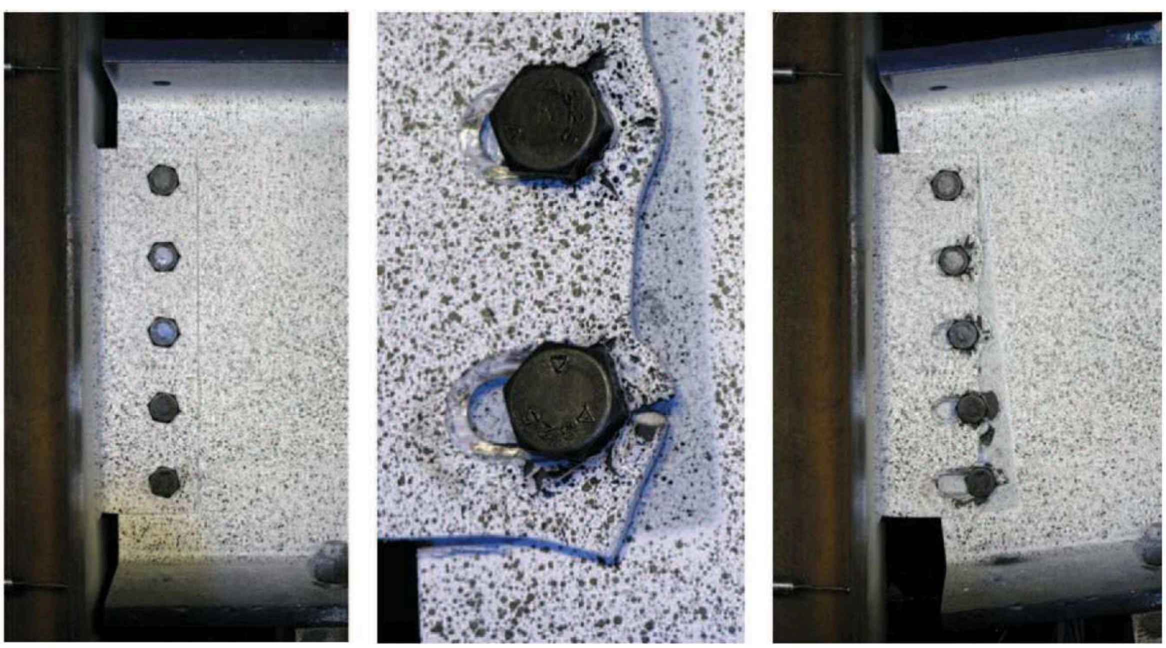

Figure 2.20- Specimen prior to testing and failure by Oosterhof and Driver (2011)

2.5. Current shear tab design approaches used in North America:

2.5.1. Canadian approach (CISC Handbook, 2010)

The current design procedure used for shear tabs in the CISC Handbook of Steel Construction (2010) is based on the research carried out by Astaneh et al. (1989); it has not been further developed. Table 3-41 in the Handbook presents the factored resistances of shear tabs with one vertical row of 2 to 7 bolts connected to rigid supports (such as the flange of a W section column) or flexible supports (e.g. the web of a column or a girder) by using E49 fillet welds and ½”, ¾”, 20 mm and 22 mm A325 bolts. The methodology behind the values listed in the table is as follows: determine the effective eccentricity for the bolt group based on Astaneh et al’s (1989) research, find the single plane shear resistances of the bolts used, determine the thickness for the shear tab, and choose the weld size to fully develop the shear tab. The current Canadian approach does not cover the usage of multiple vertical rows of bolts or the use of more than 7 bolts per row. The size and thickness of the shear tab is also limited due to restrictions largely based on the original scope of test specimens. It also does not address the application of axial forces on the connection.

2.5.2. AISC approach (AISC Steel Construction Manual 13th edition, 2005)

The AISC Manual of Steel Construction (2005) contains two approaches for designing shear tabs:

The conventional method (simple approach) is applicable to the shear tab configurations similar to those covered in the Canadian approach. The limitations of this method are listed below:

- The usage of a single vertical row of 2 to 12 bolts.
- Distance from the bolt line to the weld line (a) should be less than 3.5 inches.
- The usage of standard or short slotted holes.
- The horizontal edge distance (L_{eh} as shown in Figure 2.21) should be equal or greater than two times the diameter of the bolt for both the plate and the web of the beam.
- L_{ev} (The vertical edge distance) must satisfy the requirements of Table J3.4 of the AISC Specification (AISC, 2005).

- The plate or the beam web's thickness must be equal or less than half the diameter of the bolt plus 1/16 inch.

If the connection does not satisfy the requirements, it should be designed based on the method for extended shear tabs.

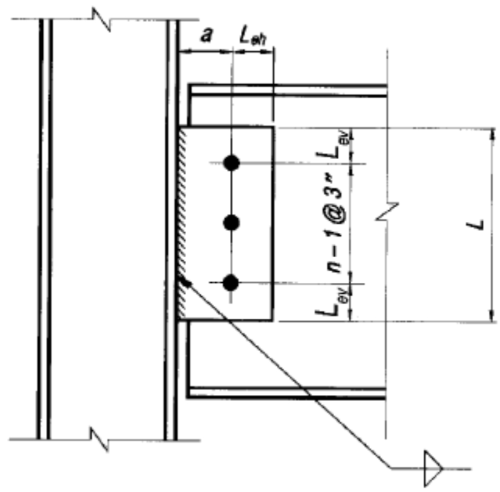

Figure 2.21- Shear tab connection (AISC, 2005)

The design procedure for conventional shear tabs consists of checking the connection for different limit states. This can be performed by using the equations summarized in Table 2.2; however, spacing and edge distance checks as well as ductility requirements should be also taken into consideration. A summary of the main equations used to calculate the connections resistance is presented. The resistance from each limit state must be calculated and the lowest value should be higher than the factored shear force applied to the connection.

An alternative approach is to use Table 10-9 from the AISC manual (2005), which provides tabulated plate and bolt resistances based on the limit states of bolt shear, bolt bearing, shear yielding and rupture of plate, and weld tearing. All tables are based on the 'a' distance (distance between bolt line and weld line) of 3 inches and can be conservatively used for 'a' values between 2.5 and 3 inches. The tables are valid for laterally supported beams, snug tight or pretensioned bolts and for supporting members of any grade of steel.

Table 2.3- Summary of the AISC limit state design equations used in the conventional design approach (AISC, 2005)

Limit state	*Equation*	*Reference*
Bolt shear rupture (single bolt)	$R=\phi F_{nv} A_b$	EQ J3-1
Block shear rupture of plate	$R=\phi U_{bs} F_u A_{nt} + \min(0.6\phi F_u A_{nv}, 0.6\phi F_y A_{gv})$	EQ J4-5
Bearing resistance (single bolt)	$R= 1.2\ \phi\ L_c\ t\ F_u \leq 2.4\ \phi\ d\ t\ F_u$ [1]	EQ J3-6a
	$R= 1.5\ \phi\ L_c\ t\ F_u \leq 3.0\ \phi\ d\ t\ F_u$ [2]	EQ J3-6b
Shear yielding of plate	$R = 0.6\ \phi\ F_y A_{gv}$	EQ J4-3
Shear rupture of plate	$R = 0.6\ \phi\ F_u A_{nv}$	EQ J4-4
Base metal rupture	$R = 0.6\ \phi\ F_u A_{nw}$	EQ J4-4
Weld shear rupture	$R=0.6\ \phi\ F_{EXX}\ (1+0.5 \sin \theta \wedge 1.5\ )0.707\ A_w$	EQ J2-4

Notes:

1- To be used when deformations at the bolt hole at service load is a design consideration.
2- To be used when bolt hole deformation at service load is not a design consideration.
3- The ϕ factor for LRFD design is 0.75 for all limit states except for shear yielding of plate where a ϕ factor of 1 should be used instead.
4- For determining the connection's bearing resistance and bolt shear resistance, the sum of the resistances of the individual bolts should be used.

A_b : Nominal body area of bolt

F_{nv} : Shear stress from table J3.2 of AISC Specification (AISC, 2005)

F_u : Minimum ultimate strength of the connected material

F_y : Minimum yielding stress of the connected material

t : Thickness of the connected material

d : Nominal bolt diameter

A_{gv} : gross area subjected to shear

A_{nv} : Net area subjected to shear

A_w : Effective area of weld (0.707 x depth x length)

A_{nw} : Net area of weld subjected to shear (depth x length)

A_{nt} : Net area subjected to tension

U_{bs} : If tension stress is uniform $U_{bs}=1$, if non-uniform 0.5 should be used

θ :Angle of loading with the weld axis in degrees

F_{EXX} : Electrode classification number

L_c : Clear distance in the direction of force between edge of hole to the edge of an adjacent hole or the edge of the member

The extended configuration design procedure (general approach) can be used for any number of bolts and vertical rows of bolts with any distance from the bolt line to the weld line, as long as the hole and edge spacing satisfy the AISC J3.2 and J3.4 requirements (AISC,2005). This method is usually used for extended shear tabs (Figure 2.22) and shear tabs with multiple vertical rows of bolts. This approach was introduced by Muir and Hewitt (2009) and has been accepted by the AISC Committee and was adopted in Manuals and Textbooks. The background and development of this method is explained in detail in Muir and Hewitt's (2009) paper. The extended approach has been evaluated by the work of researchers such as Creech (2005) and Metzger (2006) and has been proven to give conservative estimates of the connection resistance.

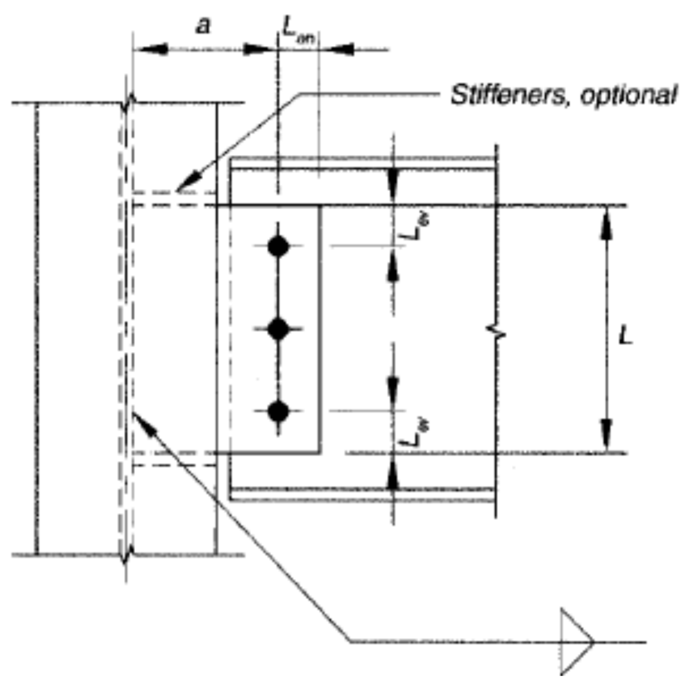

Figure 2.22- Extended shear tab connection (AISC, 2005)

The design procedure is to:

1) Determine the bolt group required for bearing and bolt shear based on the a distance which is specified as the distance of the first row of bolts to the support or other distances if justified by using rotational analysis similar to the work of Sherman and Ghorbanpour (2002). By utilizing the design aid tables in Chapter 7 of the AISC manual (2005), the effective number of bolts can be found and the ultimate shear resistance based on bolt shear and bearing can be determined.

2) Determine the maximum plate thickness of the shear tab such that its moment strength does not exceed the moment strength of the bolt group in shear. This ductility check can be achieved by using Equation 2.1.

$$t_{max} = \frac{6\, M_{max}}{F_y\, d^2} \quad , \; M_{max} = 1.25 F_v\, A_b \qquad \text{Equation 2.1}$$

where

A_b : Nominal body area of bolt

F_v : Shear strength of single bolt from Table J3.2 of AISC Specification (AISC, 2005)

F_y : Plate yield stress

C' : Coefficient for moment-only case from Chapter 7 of AISC manual (2005)

t :Thickness of the connected material

d : Plate thickness

This thickness criterion can be neglected for two cases:

a) If the plate or beam web thickness is less than half the bolt diameter plus 1/16 inch and both satisfy $L_{eh} \geq 2\, d_b$. This is applicable to only single vertical row bolted shear tabs.

b) For shear tabs with two vertical rows of bolts; if the plate and the beam web thickness are less than half the bolt diameter plus 1/16 inch and both satisfy $L_{eh} \geq 2\, d_b$.

3) Check shear yielding, shear rupture and block shear rupture of the steel plate by utilizing the same corresponding equations presented in Table 2.2.

4) Check flexural resistance of the plate including the Von-Mises shear reduction by using equation 2.2 :

$$\phi\, M_n = 0.9\, F_{cr}\, Z \qquad , \quad F_{cr} = \sqrt{{F_y}^2 - 3{f_v}^2} \qquad \text{Equation 2.2}$$

where

ϕM_n : Flexural yielding strength of the steel plate

F_{cr} : Critical stress

F_y : Yield stress of the steel plate material

f_v : Shear stress in the steel plate

Z : Plastic section modulus of the steel plate

5) Check buckling of the steel plate by using the following equation :

$$f_{bp} \le F_{cr} \quad , \; F_{cr} = \phi\, F_y\, Q \quad , \; \phi = 0.9 \qquad \text{Equation 2.3}$$

$$\lambda = \frac{h_0\sqrt{F_y}}{10t_w\sqrt{475 + 280\left(\frac{h_0}{c}\right)^2}} \qquad f_{bp} = \frac{V\,a}{Z}$$

$$Q = 1 \qquad for \quad \lambda \le 0.7$$

$$Q = (1.34 - 0.486\lambda) \qquad for \quad 0.7 < \lambda \le 1.41$$

$$Q = \left(\frac{1.30}{\lambda^2}\right) \qquad for \quad \lambda > 1.41$$

where

F_{cr} : Critical stress, ksi

F_y : Yield stress of the steel plate material, ksi

f_{bp} : Bending stress in the steel plate material, ksi

h_0 : Depth of the plate, in.

c : Length of the plate parallel to the compressive force , in.

t_w : Thickness of the steel plate ,in.

Z : Plastic section modulus of the steel plate, in. ^3

V : Shear force in the connection, kips

a : Distance between bolt line and weld line ,in.

6) Ensure the connecting beam is braced at points of support.

2.5.3. AISC approach (AISC Steel Construction Manual 14th edition , 2011)

The design procedure introduced in the 14th edition of the AISC Manual (AISC, 2011) is very similar to the 13th edition of the Manual (AISC,2005) with a few differences such as revised eccentricities and further limitations on the plate thickness to allow the use of a deeper beam by using standard holes.

The nominal bolt shear resistances listed in Table J3.2 of the AISC 2010 Specification (AISC,2010) accounted for a 20 % reduction of the theoretical values to take into account uneven stress distribution among the bolts in end-loaded connections such as bolted lap slices. This reduction also provided an additional factor of safety for the connections that were designed using the AISC Specification. The design approach provided in the AISC 13th edition Manual relied on the reduction of the bolt shear strength values to justify neglecting eccentricity in the bolt group. A recent research project on the development of the shear tab design method for the 14th edition Manual by Muir and Thornton (2011) shows that neglecting the eccentricity is no longer appropriate by the fact that the bolt strengths have been increased in the 2010 AISC Specification. Therefore when calculating the bolt shear strength, the 20% reduction is no longer required.

2.6. Summary

The reviewed literature provided a better understanding of the behaviour of shear tab connections and highlighted the work of major contributors to current design approaches. Various test setups used by the past researchers and the finite element simulation techniques were used as a basis for the FE modeling phase and full-scale laboratory test setup in this research program. However, limitations and areas of shear tab design and behaviour that require further investigation were also identified:

- Most of the work done was carried on shear tabs that were connected by a single vertical row of bolts and the usage of multiple rows of bolts was not investigated.

- Most of the past research lacked the usage of grade 350W steel in the fabrication of the test specimens therefore the performance of shear tabs fabricated with grade 350W steel under combined loading is unknown and requires further research.

- Weld fracture plays an important role in the overall performance of shear tab connections, especially under extreme loading conditions. No past finite element modeling research included the weld tearing in their FE simulation or damage simulation in general. This highlighted the need for more sophisticated FE modeling to include these aspects.

- Based on the reviewed literature, no design approach has yet been codified for shear tabs under combined axial and shear forces and most of the research was the evaluation of the connections performance under combined axial and shear forces.

- More recent research programs mainly focused on connections that were influenced by the forces created by a column collapse which caused extreme rotations in the connections; shear tabs that are used in typical building frames (such as connections connecting a beam in a braced bay of a steel frame) were not studied.

Chapter 3

Research methodology and available test data

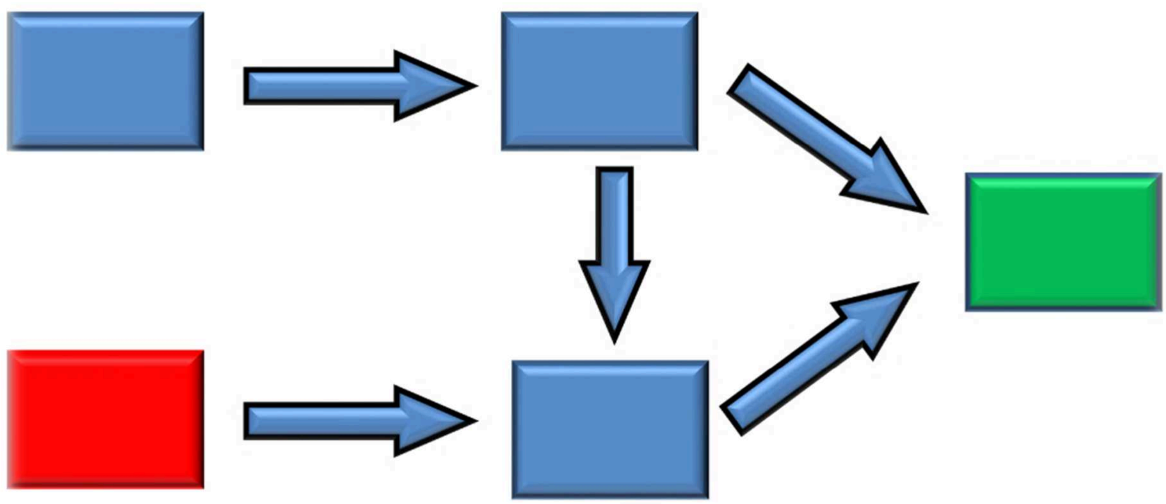

3. Chapter 3-Research methodology and available test data

In this chapter the research plan including the research roadmap is discussed followed by a brief review of the available test data and conclusions from co-researcher Marosi (2011).

3.1. Research plan

The overall research roadmap is presented in Figure 3.1. The research consisted of 5 main phases and was carried out by finite element simulation and full-scale laboratory testing:

Phase 1- FE training and material data base preparation

Training to use the finite element package (ABAQUS) was the initial step of the research program. Simple models such as 2D beams, trusses, and frames were created and verified with hand calculations. At a later stage more sophisticated models such as 3D solid models exposed to surface loads and boundary condition displacement applications were produced. The training was performed by using simple elastic or bilinear–plastic material behaviour with no strain hardening feature. In order to have a good non-linear finite element simulation, a very accurate material property was required. For this purpose coupons were extracted from the full-scale test components and then tested; this work has been performed by the co-researchers. The results from the coupon tests were based on engineering stress-strain curves. Since the finite element software required a true stress-strain curve as a material input it was necessary to model the coupons in ABAQUS. The coupons were modeled to develop an input curve in order to obtain a response similar to the coupon test results. This phase was completed with the production and organization of the material database which was used to achieve a realistic FE simulation.

Phase 2-Preliminary FE modeling

With the preparation of the material database a preliminary finite element model was created to simulate six of the tests conducted by co-researcher Marosi (2011). The 6 configurations were selected such that different types of shear tabs with different sizes, number of vertical bolt rows and bolts were covered. The data exported from the performed tests and the Phase 1 material database were used to calibrate the preliminary models to give a response (such as force vs. displacement or rotation curve), similar to laboratory tests. Any necessary changes to the finite element model such as modeling scheme, element selection, load application, mesh design, etc., were executed during this phase to improve the FE simulation resulting in a reliable FE model.

Phase 3 – Full-scale laboratory testing

In order to enhance and further calibrate the FE models used for investigating the performance of shear tabs subjected to combined shear and axial forces (utilized in Phase 4), full-scale experimental work was performed. From the fact that applying axial load to a test specimen that is undertaking shear force and moment at the same time is extremely difficult and expensive, only two configurations were tested in this phase. The specimens were planned to be separately subjected to compression and tension axial force in combination with shear force and moments.

Phase 4- Combined loading FE modeling

To investigate the effect of axial loads on shear tab connections, different levels of axial load (compression and tension separately) were applied to the final 6 models prepared in Phase 2. By using finite element simulation various cases with different levels of axial loads were easily inspected and analyzed. For each case the stress distribution pattern, strain concentration points, deformed shape and other useful data was recorded to later help in understanding the effects of axial force on the behaviour of shear tab connections. The final output of this phase of the research, was interaction curves of axial load vs. shear force for the specimens from Phase 2. The reliability of the results at this stage was confirmed with the conducted full-scale laboratory testing of Phase 3.

Phase 5- Design approach

The final stage of the research consisted of applying final modifications to the FE models, gathering and processing all the data obtained from finite element simulation and laboratory testing, studying the behaviour of the shear tabs subjected to combined axial and shear forces and ultimately providing an approach for design purposes. Response curves such as force vs. displacement curves, moment vs. rotation curves, shear force vs. axial force interaction plots, other useful plots, and comparison tables were prepared. The effect of compression and tension on the connection behaviour was investigated separately. Based on the findings, a design guideline was prepared and included in this thesis which can be used by practicing engineers to consider the effects of axial forces in the design of shear tab connections.

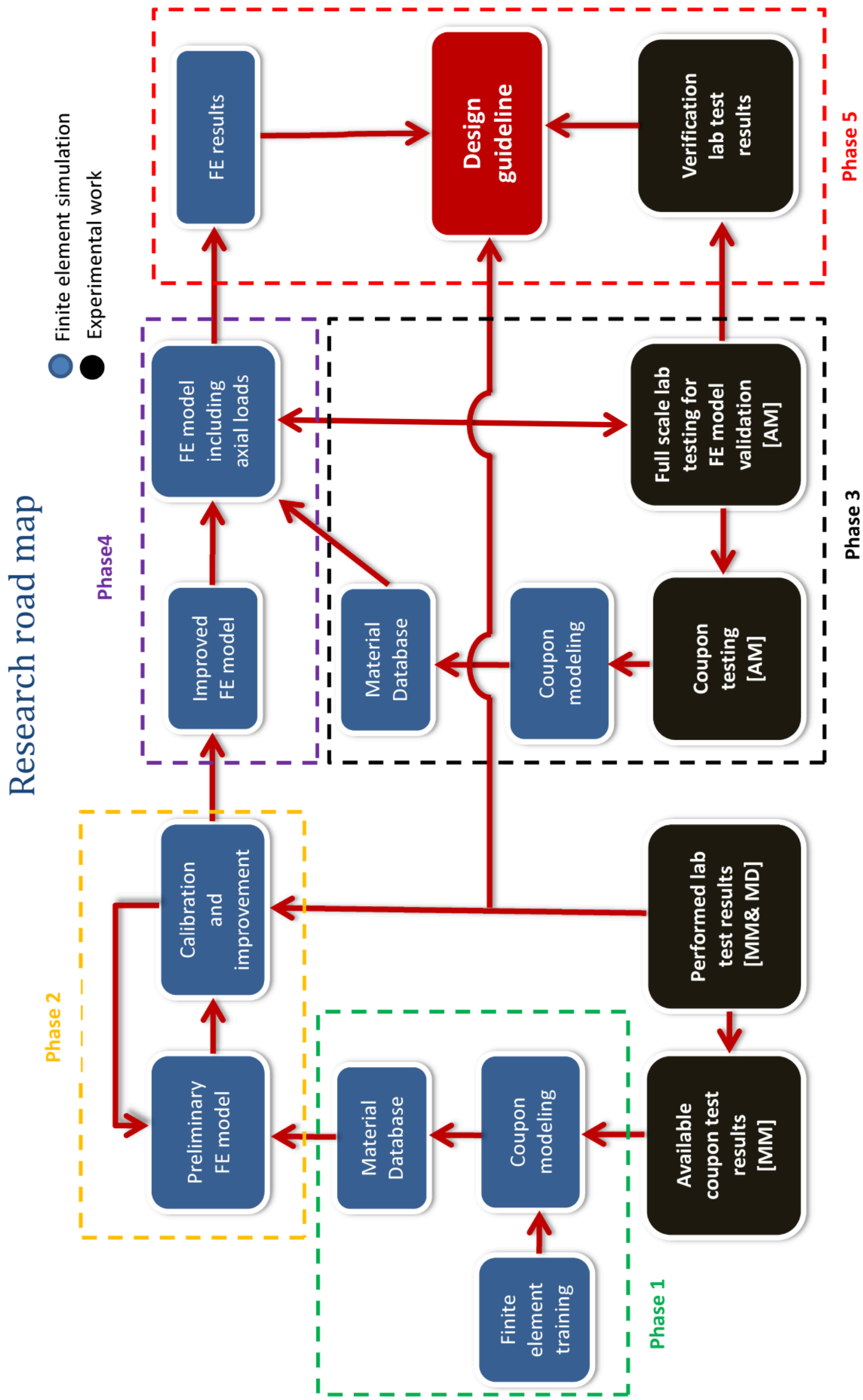

Figure 3.1- Research roadmap

3.2. Available test data

A series of 16 full-scale laboratory tests was carried out at McGill University by Marosi (2011) on "standard" and "non-standard" shear tab connections subjected to gravity loads. Six of the test specimens were bolted shear tabs while ten additional test specimens were used to evaluate the performance of retrofit welded shear tab connections. Data collected from the tests were used to calibrate the FE models capable of simulating the test procedure and predicting the performance and ultimate shear resistance of the same tested shear tab connections. The shear tab test configuration used by Marosi with its functionality schematic is illustrated in Figure 3.2.

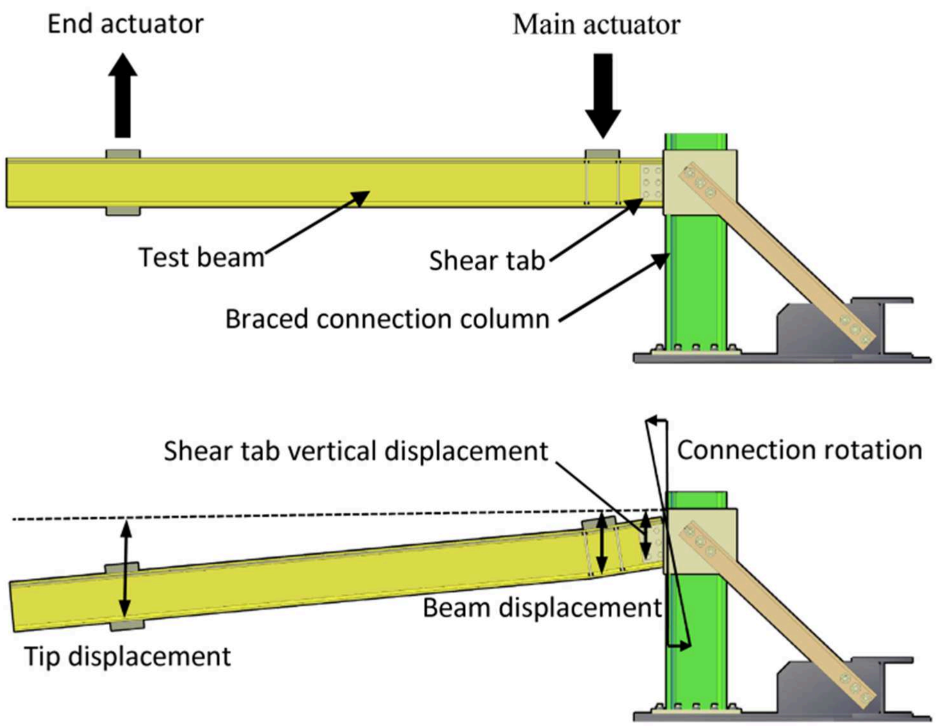

Figure 3.2- General schematic of the shear tab connection test functionality

The shear tabs were shop welded to a W360x196 ASTM A992 Grade 50 (F_y = 345 MPa) column which was secured to the strong floor, minimizing column movement and rotation. The shear tabs, ASTM A572 Grade 50 (F_y = 345 MPa) hot rolled plate, were fillet welded on both sides using a flux-cored arc welding (FCAW-G) process along with an additional shielding gas (CO_2) and an E71T (480 MPa) electrode. An ASTM A992 Grade 50 (F_y = 345 MPa) test beam, varying in size and length for each test configuration (Table 3.1), was used to transfer the forces from the actuators to the connection. A 12MN actuator was responsible to create the main shear force in the connection. To eliminate friction and permit free rotation between the actuator head and the test beam's top flange a half steel cylinder, steel plate and roller system was used. The end of the beam was attached to a 269KN actuator which limited the vertical displacement in order to control the rotation of the connection. ASTM A325 snug tight bolts, placed at a 75 mm spacing both vertically and horizontally (when applicable), were used to connect the shear tab to the test beam. A lateral bracing system was used which simultaneously allowed the test beam to displace vertically (Figure 3.2) without lateral movement. A target rotation of 0.02 rad for the W310 and 0.015 rad for the W610 and W920 beam connections at the predicted ultimate shear resistance was used for the loading protocol. A displacement based loading approach was used in which the relative displacement rate of the two actuators was controlled to attain the target rotation.

Table 3.1- Bolted shear tab specimens tested by Marosi (2011)

Test designation.	*Shear tab size (mm)*	*Beam size*	*Bolts size (mm, inches)*	*Row and number of bolts*	*Fillet weld size (mm)*
M1	228x89x6	W310 x 60	19, 3/4",	1x3	6
M2	228x165x10	W310 x 60	19, 3/4"	2x3	6
M7	456x102x8	W610 x 140	22 , 7/8"	1x6	6
M8	456x178x16	W610 x 140	22 , 7/8"	2x6	10
M13	760x102x10	W920 x 223	25 , 1"	1x10	6
M15	760x178x22	W920 x 223	25 , 1"	2x10	14

A range of instrumentation was used to measure vertical, horizontal and rotational movements of the shear tab, test beam and column. To monitor the change in strain throughout the steel plate, strain gauges were installed on the shear tabs. The connection shear force was determined based on the data from load cells attached to the actuators. Table 3.1 contains a summary of the six test configurations that were modeled in ABAQUS which is explained in detail in Chapter 4 of this thesis.

A summary of the bolted shear tab tests conducted by Marosi (2011) is shown in Table 3.2. As can be seen from the table, the test specimens exhibited higher resistances compared to the predicted calculated values. If design resistance factors were to be used, the measured/predicted ratio values would have been even higher than the values shown in the table. These results indicate that the design approach used gives very conservative predictions and requires further development.

Table 3.2- Experimental results compared to predicted values, Marosi (2011).

Test designation	*Measured test result (kN)*	*Predicted resistance (kN)*	*Measured / predicted ratio*	*Predicted resistance (kN)*	*Measured / predicted ratio*
		Nominal material properties		*Actual material properties*	
M1	363	257	1.41	297	1.22
M2	513	405	1.27	424	1.21
M7	961	676	1.42	737	1.30
M8	1734	1334	1.30	1476	1.18
M13	1762	1323	1.33	1531	1.15
M15	3489	2887	1.21	3515	0.99

Note:

-The resistances were calculated based on the modified AISC method presented by Marosi (2011)

-Nominal refers to the minimum material strength specified for the components.

-Actual refers to material properties obtained from testing coupons extracted from the components.

-A resistance factor of 1 was used for calculating the resistances

Additional information on the testing and shear tab design procedure can be found in the work of Marosi (2011).

Chapter 4

Finite element modeling

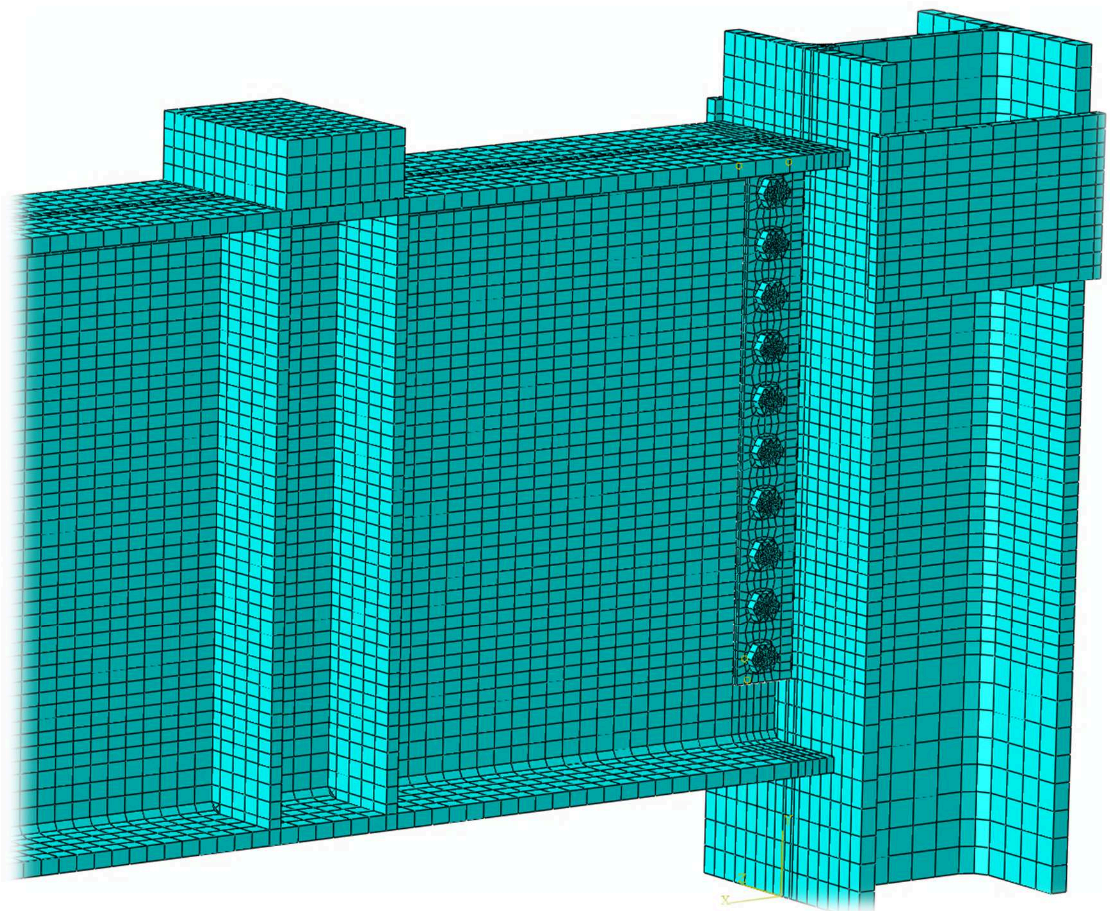

4. Chapter 4- Finite element modeling

The major portion of the research presented herein involved finite element (FE) simulation. This chapter covers the methodology behind the FE modeling procedure, material processing and the FE simulation results of replicating the 6 full-scale lab tests conducted by co-researcher Marosi (2011). The results from these tests were used in the development of a finite element model that was capable of simulating the response of the connection under load, predicting the ultimate resistance and following the progression of failure. The intent was to use the model for the evaluation of shear tabs under combined axial and shear forces, which is discussed in Chapter 6.

4.1. Modeling process in ABAQUS

ABAQUS (Simulia, 2011a, b, c) was selected to carry out the finite element investigations of the research. The global modeling approach was to first generate the geometry, design the mesh, input material properties, define boundary conditions, apply the loading, analyse the model and finally post process the results. The modeling procedure used in the software is explained via the flowchart shown in Figure 4.1.

The first step of the modeling was to create the geometry of the components which could have been done by either using the drawing tools embedded in the software or by importing geometry data from an external source. The geometry of all components was drawn in AutoCAD 2011 (Autodesk, 2010) and was then exported into a 3D geometry SAT file. To simplify the later assembly step, the geometry of each component was situated at its assembly position in AutoCAD 2011. The SAT file was then imported into ABAQUS and an individual deformable 3D part was generated for each component. These parts were then partitioned, seeded to control the number of elements and eventually based on the selected elements and meshing algorithm, the mesh design was completed.

A solid homogenous section was used for all the components and the corresponding material properties were based on processed coupon test results described in Section 4.2. Section assignments in ABAQUS provide the ability for users to assign different material behaviour in different regions of a single part. As an example the material behaviour used for the test beam flanges was not the same as the material used for the web; therefore a section based on the flange's material behaviour was assigned to the flanges, likewise an additional section representing the web's material behaviour was used for the web of the test beam.

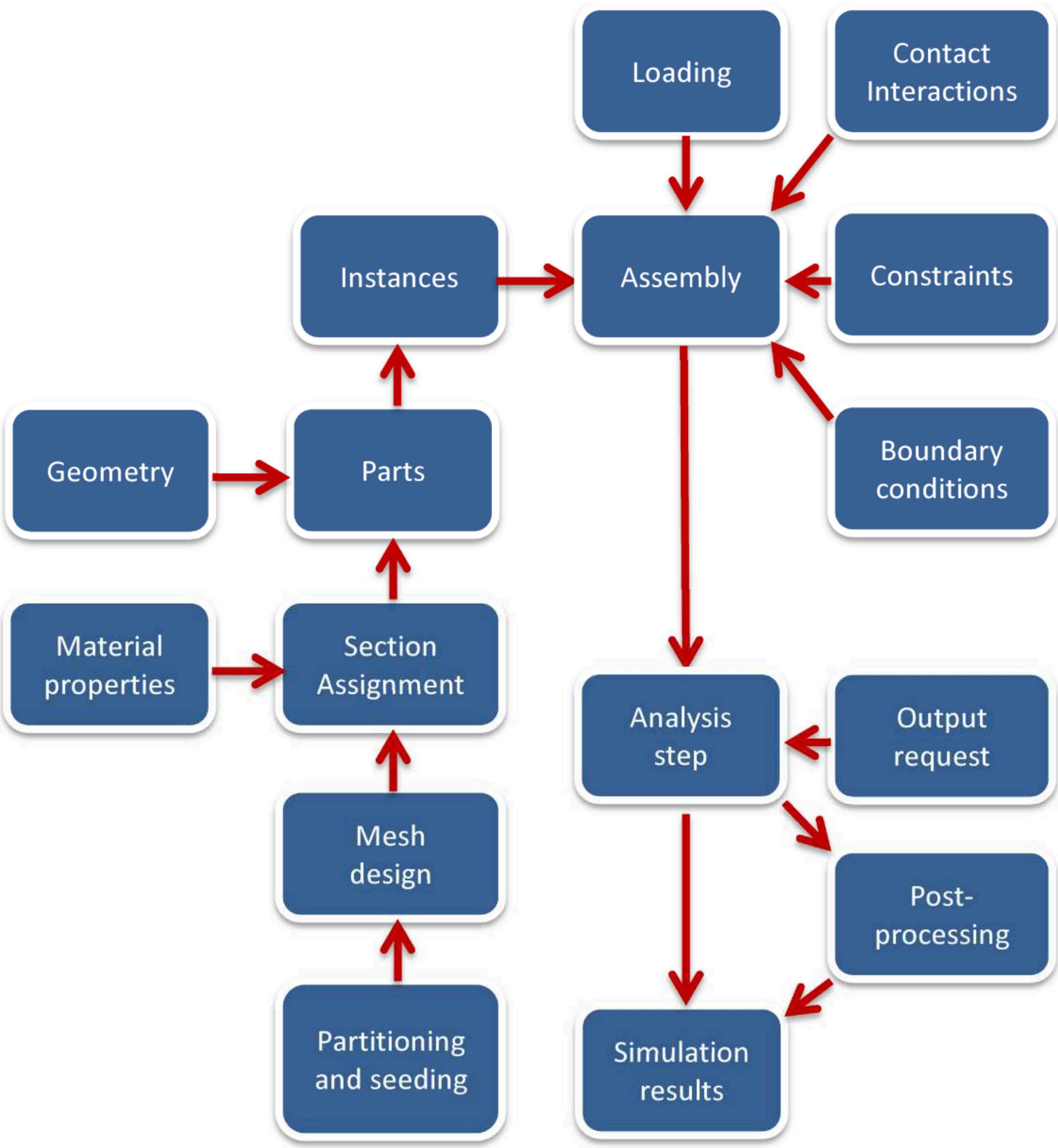

Figure 4.1-Modelling process in ABAQUS

Instances are representations of parts used to assign interaction properties such as contact, constraints, boundary conditions and loads acting on or interacting between components in an assembly. If a connection consisted of three bolts, one bolt part was created for mesh design and three instances of the bolt part were built for each individual bolt represented in the assembly.

A general static analysis (an analysis where inertia effects are neglected) was used as the main analysis step in the simulation. “NLGEOM” was switched on to include the effects of geometric non-linearity in the analysis step. The default direct sparse solver was used as the equation solver and the non-linear equilibrium equations were solved by the “FULL NEWTON” solution technique. The total running time was assumed to be 1 second, therefore the time data from the experimental work was normalized to 1. The initial and minimum time step used was 0.001 and 1E-10; the maximum time step used was dependent on the number of requested time steps but never exceeded 0.2. Prior to analysis, data of interest such as displacements, forces, stresses, damage initiation indexes and other useful data were requested at nodes, surfaces or at elements of interest in the assembly.

The visualization module of the software generated useful graphics and was used to identify the stress and strain patterns as well as the damage progression on the deformed shape of the specimens. Animations were also produced based on the deformed shape snapshots taken at each time step to be compared with the videos created by the experimental work. Two options existed for exporting the results; first was directly exporting the data and processing it in another application such as Microsoft Excel or the other option which was used in the modeling was to post-process the data in ABAQUS and then export the final desired information. The post processing module was found to be very useful since it had a variety of mathematical and statistical commands embedded.

4.2. Material properties

In order to obtain an accurate FE simulation, material properties were determined by performing ASTM A370 coupon tests on specimens cut from the plates and beams used for the connection tests. Four coupons were extracted from the flanges and three from the web of each beam, while three coupons were obtained from each plate type used for the shear tabs. Two series of coupons were tested, simulated and processed: Series A were extracted from the components of the 6 full-scale shear tab tests subjected to vertical loads conducted by Marosi (2011). Series B were coupons extracted from the test components of shear tab tests subjected to combined shear and axial forces (described in Chapter 5). Tests were not conducted for the bolt material property; the nominal properties (F_y=636 MPa , F_u=827 MPa, Elongation=0.14) were converted into true stress and strain input because shear failure of the bolts was not observed. For the fillet welds, the same elastic and plastic data from the corresponding shear tab specimen were used, but with different damage parameters that were calibrated with the shear tab test data. This strategy was justified based on the FE models that did not experience weld tearing. A summary of the coupon modelling in addition to material data processing is presented herein.

4.2.1. Material data processing

The raw coupon test data provided the force measurements from the load cell embedded in the MTS actuator, displacement of the actuator head, relative displacement of an extensometer installed between two points with a gauge of 200 mm on the coupon specimen, and strain measurements by two strain gauges glued on the centre of the coupon (on two faces) at each recorded time step. Strain gauges were able to measure the change in strain at a specific location on the coupon, both elastic and plastic deformations, which were then followed by their failure after reaching approximately 10000με-15000με. The engineering stress was calculated by dividing the force by the initial cross section of the coupon specimen which was measured prior to testing. Due to the possibility of slip in the grips of the machine that was used to test the coupons, the engineering strain after yielding was measured by dividing the relative displacement of the extensometer by 200mm. Five main mechanical properties of the coupons were determined from the processed data and plots: The modulus of elasticity (E), the yield stress (F_y), the ultimate stress (F_u), the strain prior to strain hardening (ε_{sh}) and finally the strain at the ultimate stress level (ε_u). The strain at the yield stress (ε_y) was calculated by dividing F_y by E. The method used to determine each mechanical property is explained below:

Two strain gauges were used at the center of the coupon specimens (two sides). The readings (engineering stress-strain data) from the strain gauges were used to determine the module of elasticity (E). The final value of E representing the material behaviour was calculated from taking the average of the two E values. The yield stress (F_y) was found by intersecting a 0.2% yield offset line with the stress-strain curve of the corresponding coupon specimen as shown in Figure 4.2-A. The strain prior to strain hardening (ε_{sh}) was selected visually from the stress strain plots (Figure 4.2-B). The maximum stress in the tabular data was selected to be F_u and the corresponding strain was selected to be ε_u.

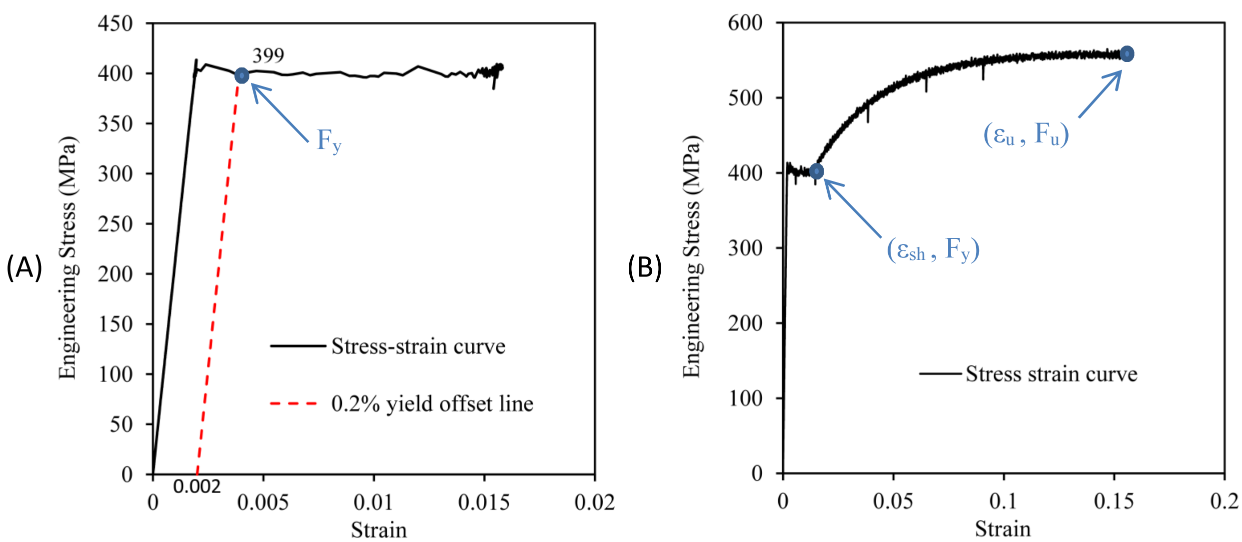

Figure 4.2-(A) Determination of F_y by using the 0.2% yield offset line, (B) Determination of ε_{sh} by using the stress-strain plot generated from coupon testing data

Coupons from series A were already processed and presented by Marosi (2011), but due to the important role of material behaviour in FE simulation, the coupon data was reprocessed for consistency. Table 4.1 shows a summary of the mechanical properties of the steel used to fabricate the shear tabs used in Marosi's (2011) tests. In a similar manner this process was carried out for all coupons extracted from the test beams' flanges and webs. Coupons from series B were also processed by using the same methodology. The material data used for the beams flanges, webs and data related to series B coupons can be found in Appendix A.

Table 4.1-Steel mechanical properties extracted from shear tabs (Series A coupons)

Coupon designation	*Test used*	*E (MPa)*	F_y *(MPa)*	F_u *(MPa)*	ε_y	ε_{sh}	ε_u
6A	M1	207593	415	486	0.0019	0.031	0.153
7A	M7	206171	386	515	0.0018	0.015	0.15
8A	M2,M13	210822	382	526	0.0018	0.014	0.146
9A	M8	205840	387	543	0.0018	0.017	0.145
10A	M15	204727	401	565	0.0019	0.014	0.146

4.2.2. Coupon simulation

The mechanical properties obtained from the coupon tests were available in terms of engineering stress-strain curves; however, since the FE package required true stress-strain curves as an input the coupon tests were modelled in ABAQUS such that the material models could been accurately calibrated with the test information. The development of the ABAQUS input model is presented below:

ABAQUS requires the definition of elastic material behaviour, i.e. the modulus of elasticity and Poisson's ratio. The data representing plasticity with isotropic hardening was entered as a tabular input based on plastic strain and stress. The plastic input was derived for two regions, the perfectly plastic and the strain hardening region. Engineering stress and strain data after the initiation of strain hardening were converted into true stresses and strains by means of Equations 4.1 and 4.2. In the perfectly plastic region, the first point was not converted into true stress and a line was used to connect the initial yield point to the first strain hardening true stress point which resulted in a perfectly flat yield plateau in the simulation response. The curve used for the strain hardening region constructed by true stress and strain values was generated by using Equation 4.3 presented by St-Onge (2012). Based on the results obtained from his research, an initial calibration factor of 23 was selected to be used for A, and calibration factor B was set as 1.

The produced data was used in the FE models of the coupons and the testing procedure was simulated. Subsequently, the response curve of the simulation was matched with the experimental data. If the response curve of the simulation matched the test data, as shown in Figure 4.3, the produced input curve was defined as the material input for the corresponding coupon representing the material behaviour of the component which it was extracted from. If a mismatch existed, the calibration factors where changed based on a trial and error sequence and iterations were performed up to a point where a fit was achieved. This process was performed for all the coupons from series A and B.

$$\varepsilon_t = \ln(1 + \varepsilon_E) \qquad \text{Equation 4.1}$$

$$\sigma_t = \sigma_E(1 + \varepsilon_E) \qquad \text{Equation 4.2}$$

where,

ε_t = True strain, σ_t = True stress, ε_E = Engineering strain, σ_E = Engineering stress

$$\sigma(\varepsilon) = F_y \left[1 + \left[\left[\left(\frac{F_u}{F_y}\right) - 1\right] * \left[1 - B(1 - r) * \exp\left(A * (\varepsilon - \varepsilon_{sh})\right)\right]\right]\right] \qquad \text{Equation 4.3}$$

where,

$$r = \frac{(\varepsilon - \varepsilon_{sh})}{(\varepsilon_u - \varepsilon_{sh})}$$

ε_y = strain at yielding stress

ε_{sh} = strain prior to strain hardening

ε = strain between ε_y and ε_{sh}

ε_u = strain at ultimate stress

A = Calibration factor influencing the rate of hardening (curvature of the strain hardening curve)

B = Calibration factor influencing the first point on the strain hardening curve

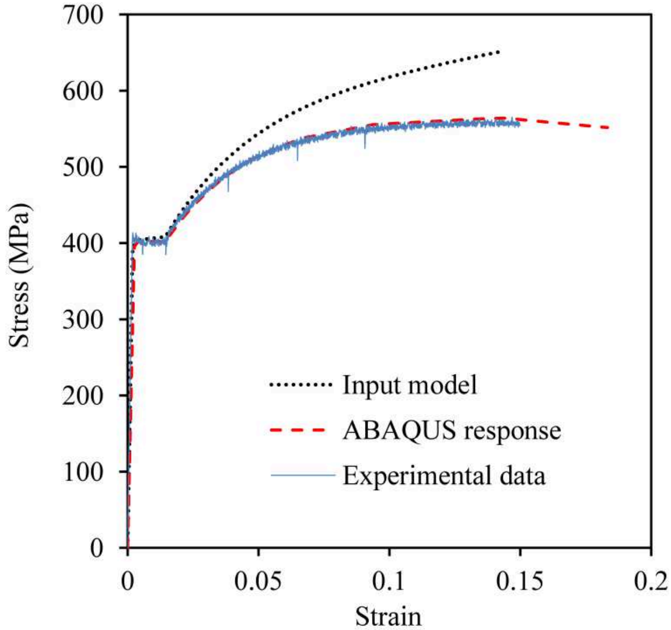

Figure 4.3-Material input model used for coupon simulation

Each coupon was modelled as one individual 3D deformable homogenous solid part. Large non-linear geometry effects were included in the analysis. The mesh was built by using first-order brick elements (C3D8) with full integration and by using a maximum global seed size of 3mm. (Figure 4.4) .Reduced integrated elements were not utilized due to the unstable state they created at the time step prior to necking.

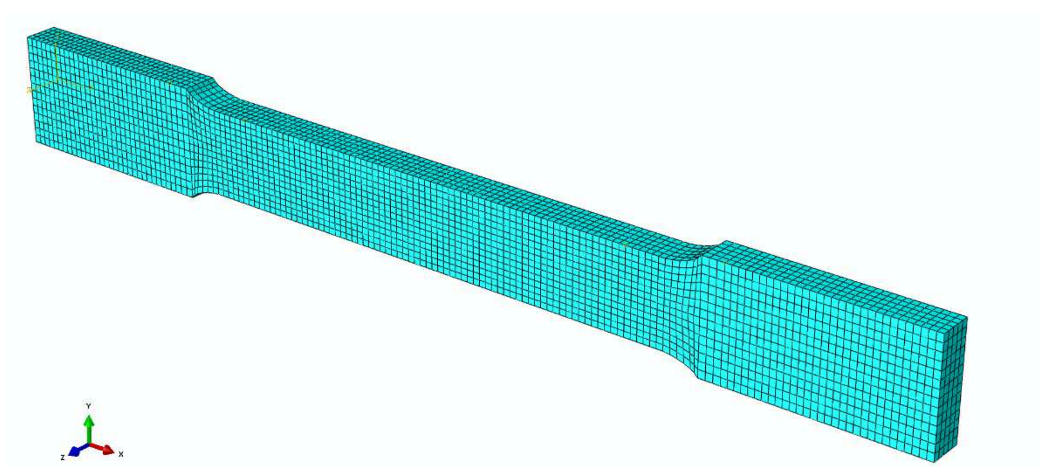

Figure 4.4-Mesh design used in coupon test simulation

Second-order elements were also tested and showed very good performance in capturing the stresses and strains in normal density meshes (global seed of 10 mm and over); however, if used in a very high dense mesh assembly, they caused high numerical instability at the time step when necking initiates. To reduce the chance of mesh quality requirement influencing the response of the coupon models, a high mesh density with an average aspect ratio of 1.2-1.5 with a worst aspect ratio of 1.6-2 was used in the mesh design (Figure 4.4).

Several important partitions were created to divide the coupon "instance" into sub regions of interest. The first partitions separated the region were the coupon was clamped in the grips during laboratory testing. On one end of the coupon, the clamped surfaces on both sides were completely restrained from any translation and rotational movements; on the other end an imposed displacement boundary condition was applied to the surfaces representing the grip on the actuator head (Figure 4.5). The second partitions were created at the locations where the extensometer was installed during testing. This technique enforced the mesh module to create a node at these locations (Node 1 and 2) so that data such as displacements could be requested to be available at the end of the simulation. The strain in the simulation output was measured exactly the same way it was measured during the testing. The relative displacement of nodes 1 and 2 at each time step was divided by 200 mm resulting in engineering strain history.

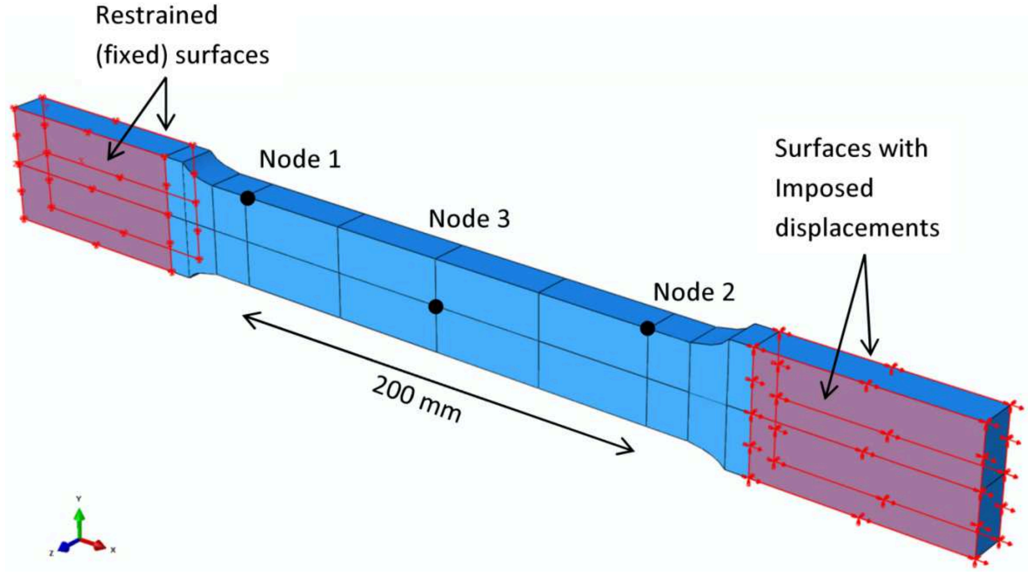

Figure 4.5- Partitions and boundary conditions applied to the coupon specimens

The engineering stress was achieved by requesting the reaction force in all the nodes of the surfaces that were restrained. The post processing module of the software was used to take the summation of all the reaction forces at the requested nodes as a function of time and dividing it by the initial cross sectional area of the coupon to obtain the history of engineering stress. The third most important partitions were those that cut through the centroid of the coupon's geometry. These partitions ensured the symmetry of the coupon in all directions and helped the necking to occur at the centre of the coupon; however, the location where necking occurs depends on other factors such as the imposed displacement value, the maximum time step, element type and mesh design. By establishing this technique, the location of necking was successfully controlled to occur at the centre of all the coupons modelled (Figure 4.6). The other benefit of these partitions was that a node was generated at the centre of mass and at locations where strain gauges were installed during lab testing (Node 3). This allowed the exportation of valuable data such as stresses, strains, triaxiality and damage related data at these locations.

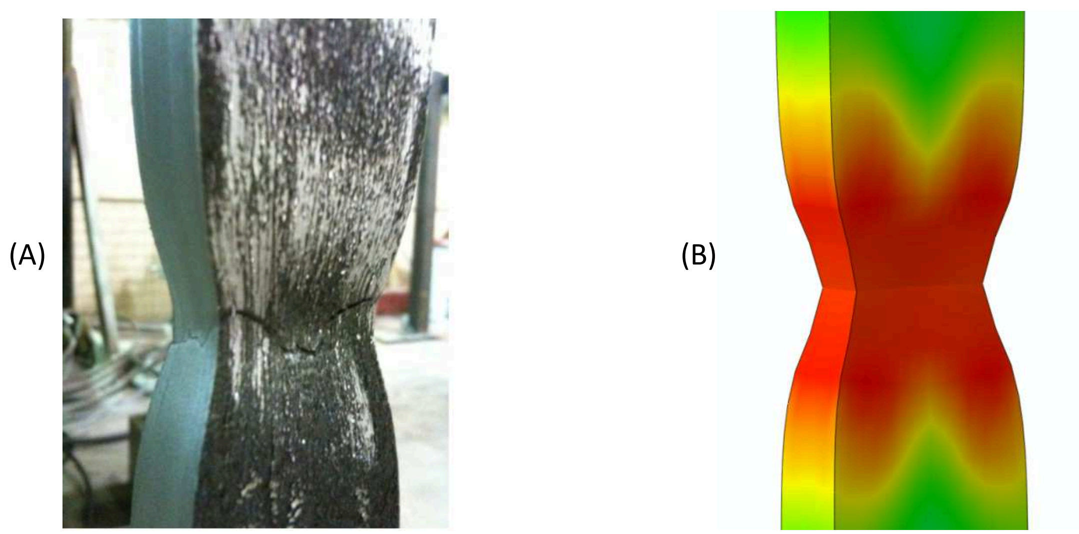

Figure 4.6- (A) Laboratory coupon test specimen at fracture, (B) Coupon FE model result

4.2.3. Damage simulation

The results from testing showed that the performance of the shear tabs was dependent on the ductility of the steel plate and the strength of the connecting weld. In tests where the weld started to tear, the shear tab continued to carry shear force until a point at which either cracks developed in the plate itself between the bolt holes or the weld was excessively fractured (Marosi 2011).

For shear tabs in which the ultimate resistance was governed mainly by net area plate fracture with no tearing in the welds, the FE models without damage simulation could still approximate the ultimate shear resistance with reasonable accuracy. In contrast, for shear tabs that experienced weld tearing, the FE model without damage simulation overestimated the shear resistance and stiffness of the connection. Based on this initial observation a damage model was deemed essential for shear tab FE simulation since the failure mode is not necessarily known a priori.

The material damage simulation model is illustrated in Figure 4.7. At the onset of loading the material behaves elastically until it reaches point 1 (yielding point). Subsequently, the material experiences plastic deformation until it reaches point 2 at the ultimate stress level. At this point the damage parameter (D) is incorporated in the analysis. A ductile damage for metals initiation criterion was utilized, which is a function of triaxiality, fracture strain and strain rate. Determination of the damage parameters requires accurate measurement of the fractured coupons and recorded data of the post-ultimate behaviour; therefore, for simplicity it was assumed for different levels of triaxiality that the fracture strain is 0.21 at a strain rate of 0.01.This fracture strain was selected based on research conducted by Arasaratnam et al. (2011). His research led to a five stage true stress-strain model for A992 and 350W steel grades that was developed for modeling purposes. The damage initiation criterion controls when damage initiates and has no effect on the material unless equipped with damage evolution capability. Damage evolution controls the stiffness degradation parameter (D) by using an energy approach which is based on the fracture energy required for failure. Beyond point 2, through to point 3, the D parameter increases, leading to stiffness degradation (softening) of the material. At point 4, D=1 which means the stiffness is absent, and as such the material cannot develop any stress. Generally steel never reaches point 4, therefore another parameter called the maximum stiffness degradation is used to determine where the material fails; it can be determined based on the post ultimate coupon test information. In cases where the data was not available a maximum stiffness degradation of 0.5 was used. Once D reaches its specified limit, an option exists to remove the degraded elements from the global stiffness matrix or to keep them in the system although having a degraded stiffness. Element removal results in a modification to the global system stiffness and gives the ability to redistribute stresses in the connection to compensate for the loss of stiffness, at weld fractures for example (Simulia, 2011b).

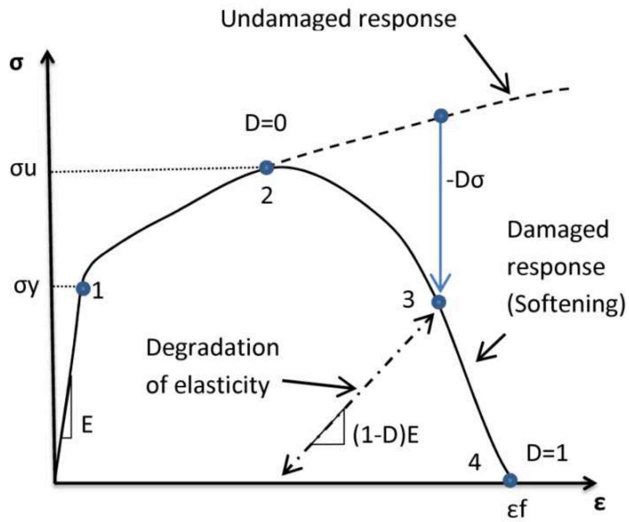

Figure 4.7- Schematic representation of the material damage model (Simulia, 2011b)

As an example, Figure 4.8 shows the effect of the damage model in the simulation of a coupon extracted from the shear tab specimen used in Test M2. The colour contour indicates the level of Von-Mises stress in the coupon specimen. As it can be seen from the Figure residual stresses still exist after fracture around the necking region and close to the grip. Figure 4.9 shows the corresponding stress-strain curve.

Coupon excluding
damage simulation

Coupon including
damage simulation

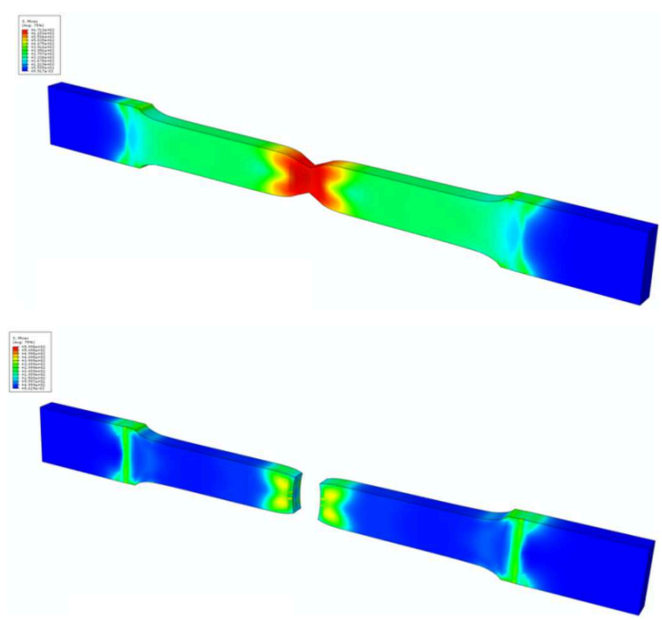

Figure 4.8-Comparison of Mises stress in a coupon simulation including and excluding damage

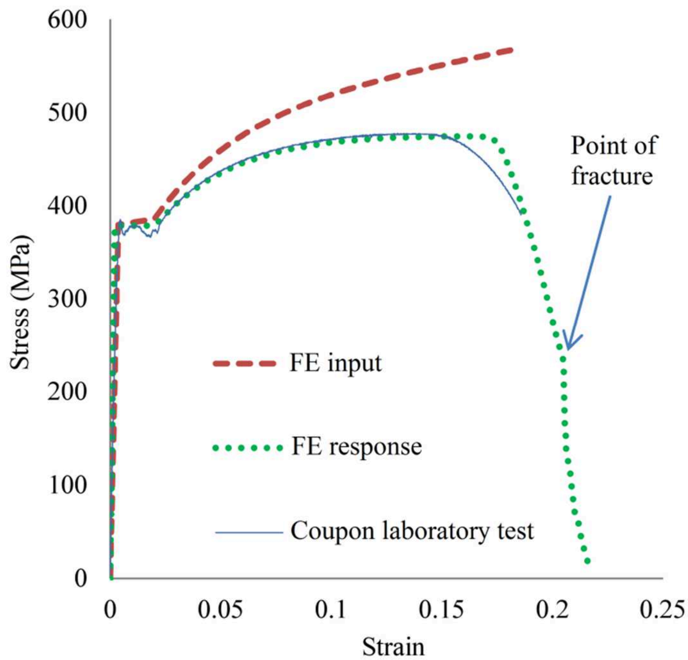

Figure 4.9- Stress-strain curve of coupon (damage included)

4.3. FE modeling of shear tabs subjected to only vertical forces

This Section covers the development and features of the finite element models built to simulate the experimental work performed by Marosi (2011). This includes a comparison of the results obtained from FE simulation with laboratory testing data.

4.3.1. General simulation strategy

A 3D solid finite element model comprising a beam with stiffeners, stub column with side plates, shear tab, bolts, washers, welds and load blocks representing the actuators was used for the simulation (Figure 4.10). Angle braces connecting the side plates of the stub column were also included in the model, but were removed later due to the high rigidity of the stub column and small column horizontal movement readings from the test data (around 1-3mm). The lateral brace mechanisms used in the full-scale testing were simulated by applying a boundary condition to the beam flanges to prevent lateral displacements but allow for other degrees of freedom to displace and rotate. The base support structure was not modelled; instead the base of the column was restrained by using a fixed boundary condition. The load was generated by the displacement of the two load blocks that were in contact with the test beam's flanges. The connecting bolts transferred the forces from the web of the test beam to the shear tab specimen by contact; subsequently the force was transmitted through the shear tab, through the connecting weld, into the stub column and finally transmitted to the base. A complex load path was used for the simulation therefore special attention and investigations were required to gain confidence in the performance of the models.

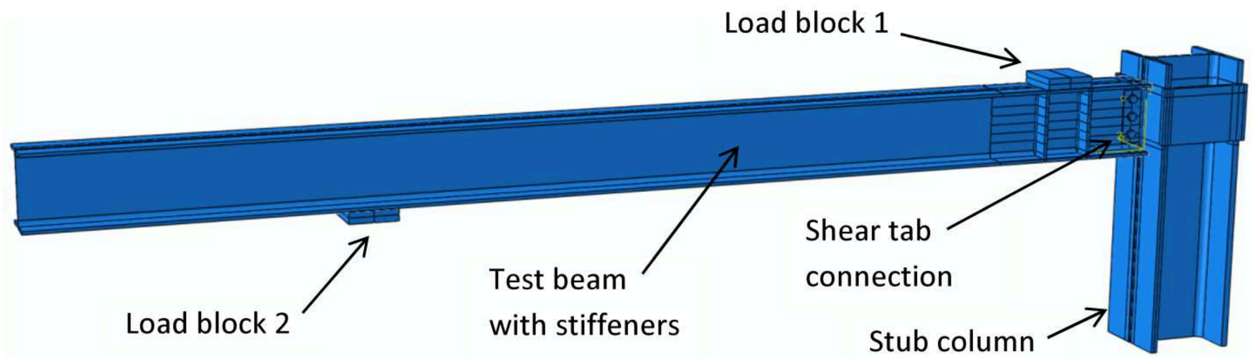

Figure 4.10- Part assembly of Test M1 FE model

4.3.2. Element library

A wide range of element types was utilized in the research. All elements belonged to the 3D solid family; however they were of different formulation, order, integration method, and degrees of freedom. Table 4.2 presents the specifications of the eight hexahedral and wedge elements that were used in the research and Figure 4.11 presents the corresponding nomenclature. The full integration elements are capable of capturing more severe pitches at locations with high stress concentrations such as regions around holes, and showed better performance when steel began to neck under tension; however they require massive computational power. Reduced integration elements could be a substitute for the fully integrated elements to decrease the analysis running time but must be used with caution since they are sensitive to the phenomena called "hour glassing" especially in first order elements. First order reduced integration elements (C3D8R) have only one integration point and when subjected to bending, the stress at the single integration point will be zero resulting in an element with no stiffness. To resolve this issue, ABAQUS is equipped with an hour glass control that generates some artificial hourglass stiffness and will perform more effective if the number of elements increase.

Fully integrated linear solid elements suffer from a numerical problem called "shear locking". Shear locking occurs when the elements are very stiff in bending and they cannot produce the required curvature obtained in an idealized bending scenario. The C3D8I element is an 8-noded brick incompatible mode element which features a special formulation that resolves "shear locking" in meshes with a low number of elements along the length and subjected to bending. Fully integrated second order solid elements such as the fully integrated 20-node brick element (C3D20) do not suffer from shear locking. The reason for this capability is that they have a centre node on the edges that helps them to create curvature on the edge lines therefore they are very suitable in modelling bending effects. The second order reduced integration elements (C3D20R) have more than one integration point therefore were not very sensitive to hour glassing. Geometry condition in the mesh design was the most important factor in selecting the element shape therefore the element selection criteria and final selections are discussed in Section 4.3.5.

Table 4.2-Element library and corresponding figures (Simulia, 2011c)

Element code	*Shape*	*Order*	*Nodes*	*Integration points*	*Figure*
C3D8	Hexahedral	Linear	8	8	4.11-A
C3D8R	Hexahedral	Linear	8	1	4.11-A
C3D8I	Hexahedral	Linear	8	8	4.11-A
C3D20	Hexahedral	Quadratic	20	27	4.11-B
C3D20R	Hexahedral	Quadratic	20	8	4.11-B
C3D6	Wedge	Linear	6	2	4.11-C
C3D15	Wedge	Quadratic	15	9	4.11-D

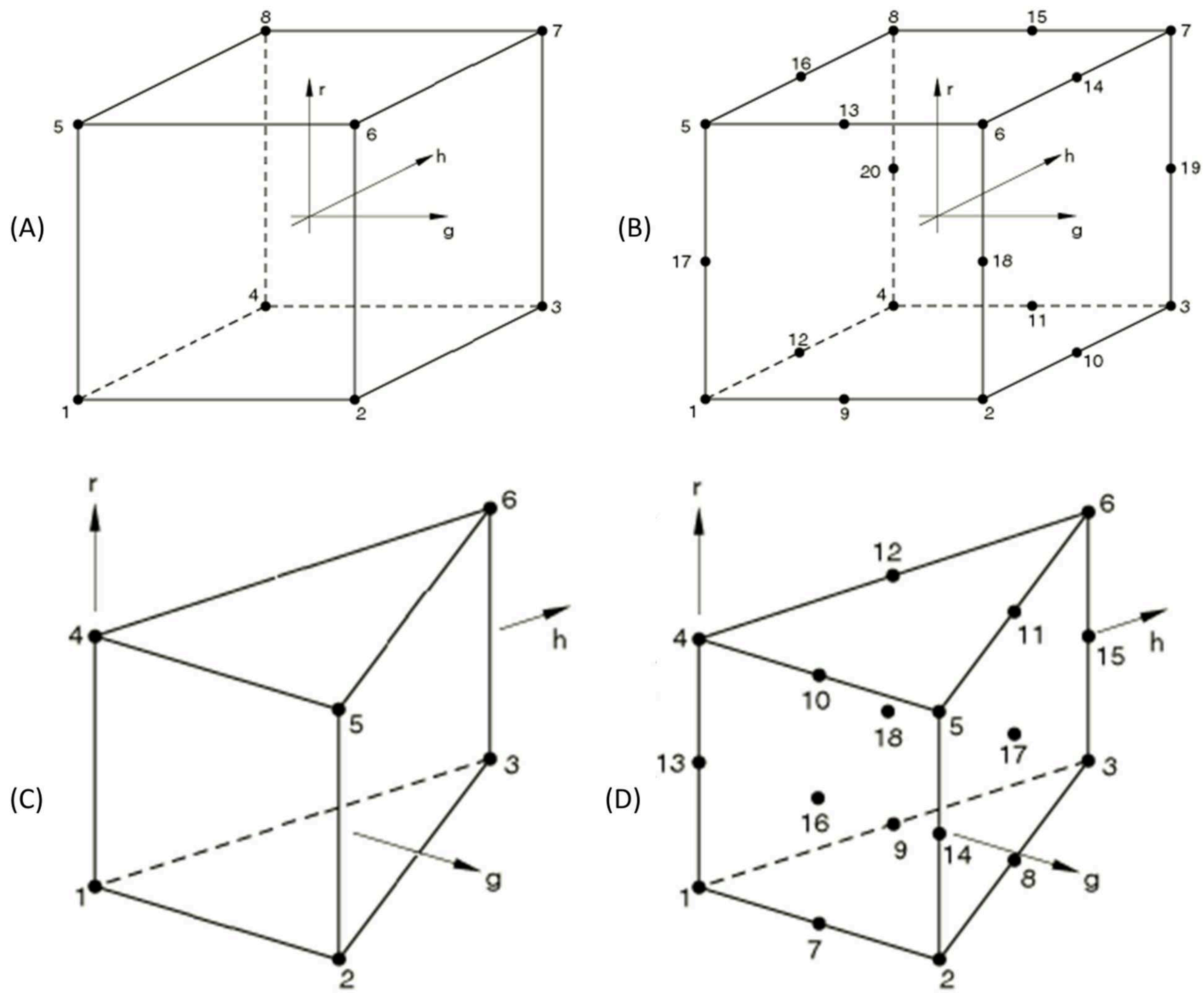

Figure 4.11- Element node labeling for elements described in Table 4.2, (Simulia, 2011c)

4.3.3. Separation of the test beam

One major innovation towards computational efficiency was the separation of the test beam FE model into two segments. The first segment, referred as the "test beam", was subjected to high plastic deformations, whereas the "test beam extension" (second segment) experienced pure elastic behaviour and was responsible to transfer the curvature created by the end actuator to the connection. Thus using a higher mesh density with higher order elements in the test beam segment and equipping the extension segment with a courser mesh involving lower order elements benefited the simulation results and running time. The region of the test beam that was subjected to extreme shear yielding was mainly between the main actuator and the connection. The first 700 mm of the W310 x 60 beam, 800mm of the W610 x 140 and 1400 mm of the W920x223 was selected as the length of the main test beam segment. This selection was based on an initial FE study to locate the regions that were expected to undergo plastic yielding. The length of the test beams included an additional extension to ensure elastic behaviour at the separation interface. The remaining lengths of the test beams used by Marosi (2011) were defined as the extension beam. The extension beam lengths were 4024mm for tests M1 and M2, 7100mm for tests M7 and M8, and 6980 mm for tests M13 and M15.

In a classic FE model it is possible to change from a high density mesh region to a lower density region on a single part by manually designing the elements near the interface similar to the beam modelled by Ahkul (2004); but overall, the process is time consuming and requires special attention to keep the mesh quality acceptable. Another approach is to create the mesh at the interface with a disorganized mesh pattern resulting in elements with various aspect ratio and sizes that could increase the chance of errors in numerical calculations. This approach can be observed in the FE models developed by Rahman et al. (2007). Both methods had the capability to change the mesh density with only one type of element being assigned to the part. The major benefit of the applied separation technique was that it gave the ability to the user to have independent partitioning, mesh density, element type, global seed size and even contact interactions on both segments. The two segments were then connected to each other by a tie constraint. A surface to surface tie requires the selection of a master and slave surface. Generally the test beam segment required a higher mesh density therefore the slave surface was selected to be on the test beam segment while the master surface was assigned to be the extension segment.

The performance and accuracy of the technique was validated through various investigations on a simplified test beam FE model with no hole and stiffeners (Figure 4.12).The two segments were built and tied together with a tie constraint. The end of the test beam segment was fixed and an imposed displacement of 50 mm was applied by a load block at a distance of 3.5 m from the support. This model was not only used to validate the separation, but was also used to help decide on the following modelling considerations:

- Element selection
- Number of layers of element in the flange and web
- Mesh size sensitivity and mesh quality
- Computational efficiency (running time)
- Load application type (displacement or force control)

Twenty nine different cases were investigated by changing variables and mesh designs for the model shown in Figure 4.12. Due to consistency only six cases are presented in Table 4.3 with the corresponding beam models shown in Figure 4.13. All the presented cases were analysed by a displacement control load application. Based on laboratory test observations from Marosi (2011) and initial FE model simulations it was proved that the beam remains elastic at the separation region therefore for this investigation elastic material behaviour with no plasticity was used for the material input.

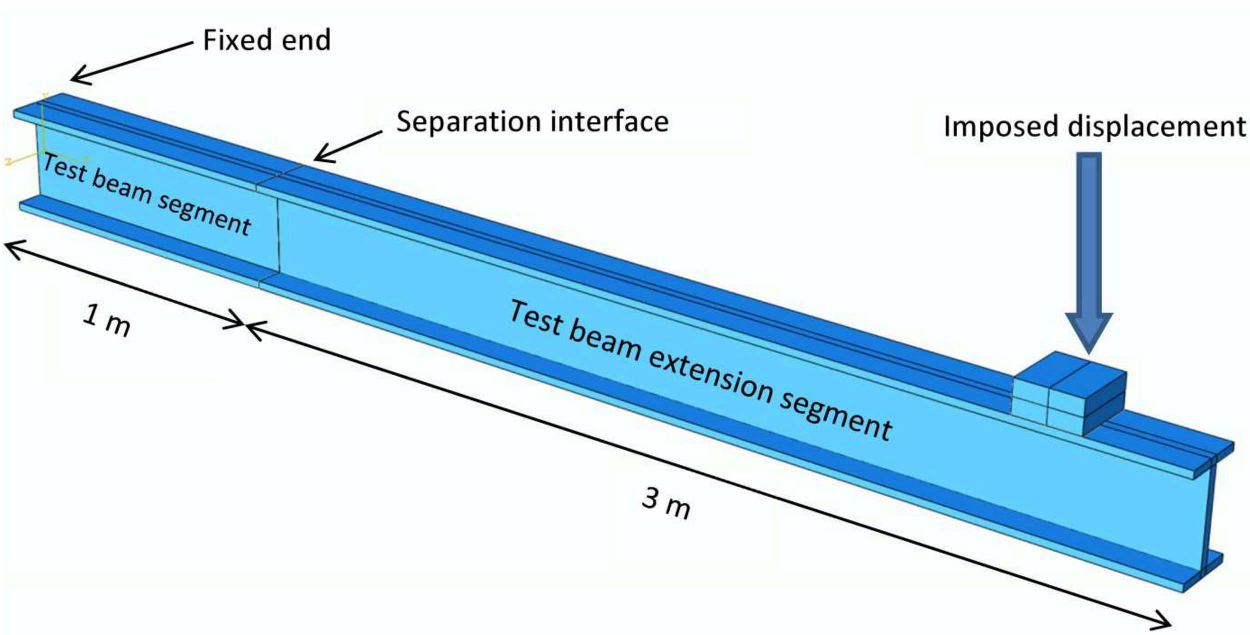

Figure 4.12-Test beam separation representation

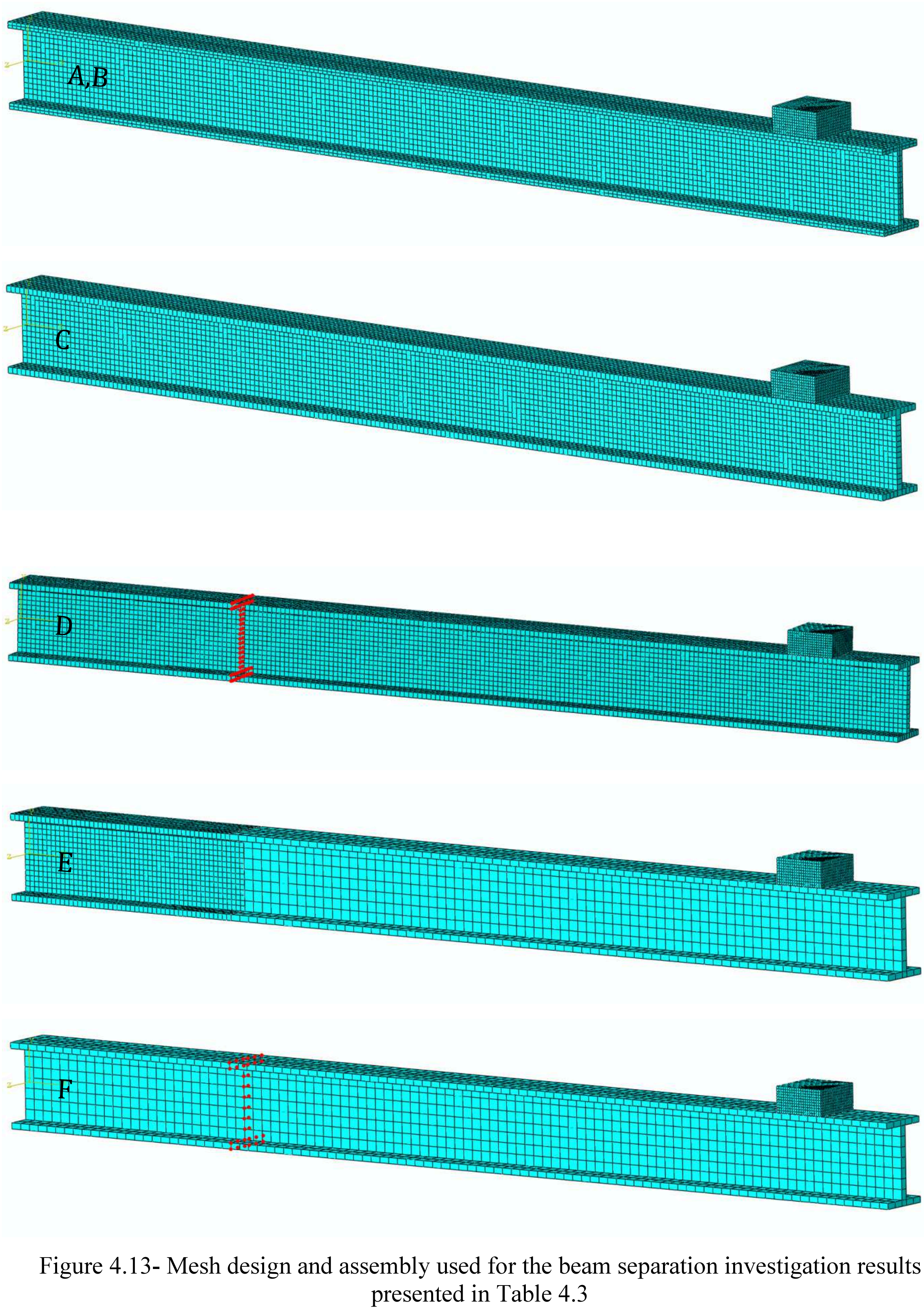

Figure 4.13- Mesh design and assembly used for the beam separation investigation results presented in Table 4.3

Table 4.3-Beam separation investigation results

Case ID	*A*	*B*	*C*	*D*	*E*	*F*
Continuity	Single segment	Single segment	Single segment	Tied segments	Tied segments	Tied segments
Total number of elements	17600	17600	10400	10400	5875	1400
Maximum seed size of main beam (mm)	20	20	20	20	20	40
Maximum seed size of extension beam (mm)	20	20	20	20	40	40
Main beam element type	C3D20	C3D8	C3D8	C3D8	C3D8	C3D8
Layers of element used in flange	2	2	1	1	1	1
Extension beam element type	C3D20	C3D8	C3D8	C3D8	C3D8	C3D8
Layers of element used in web	2	2	1	1	1	1
Total CPU time (s)	1795.2	320	194	189.6	140.5	125.8
Physical time (s)	290	66	41	40	30	27
Average CPU load per thread (%)	77.38%	60.61%	59.15%	59.25%	58.54%	58.24%
Shear force at support (kN)	169.23	169.35	169.30	169.30	169.40	169.70
Moment at support (kN-m)	608.70	609.10	608.80	608.80	609.30	610.30
Shear force change* (%)	0.00%	-0.08%	-0.04%	-0.04%	-0.10%	-0.28%
Moment change* (%)	0.00%	-0.07%	-0.02%	-0.02%	-0.10%	-0.26%

The cantilever model in Cases A, B and C was modelled as one single part, and cases D, E and F were based on the same cantilever but made of two segments that were tied. The physical time, also referred as wall clock time, is the same time measured by an ordinary clock. A parallel processing method by using 4 physical cores and 8 threads was used for the job execution. The total CPU time is the summation of all the elapsed durations it took for each thread to complete the calculation operations including input and output. The average CPU load is calculated by dividing the total CPU time by the number of threads used, divided by the physical time. This parameter is a very useful index indicating the amount of load that the model puts on the system and how efficient the parallelization is in reducing the analysis running time. Based on the results using C3D20 elements consumed 77.38% of the CPU power while the C3D8 elements consumed about 60% of the CPU capacity. The change in stiffness and the performance of each case was evaluated by the change in shear force and moment reaction at the support in comparison with case A. Investigation B showed that by replacing the second order elements with linear elements a 0.08% increase in the stiffness of the beam was resulted. The number of element layers in the web and flange was reduced from 2 to 1 in Case C causing a 0.04% increase in stiffness. Case D had the same specifications of case C but was built of two tied pieces instead on one part. Interestingly the results were the same as case C and the model ran 1 second faster with a very slight increase of load on the CPU. The global seed size and mesh density was changed on both segments to examine the capability of having a finer mesh on the test beam segment and a courser mesh on the extension part (Case E). Still the change of stiffness was negligible. Case F was targeted to determine the maximum global seed size used for meshing that ended in acceptable results.

4.3.4. Partitioning and mesh design

The initial step of the mesh design procedure was partitioning each individual imported part. ABAQUS could not recognize complex geometry shapes; therefore it required the user to separate them into regions built of simple geometry forms similar to cube or wedge shapes. The general “structural meshing” technique employed predefined mesh topologies for regularly shaped regions and first or second order hexahedral cubic elements to create the mesh. As an example Figure 4.14-A demonstrates the partitions made on the test beam part. The major portion of the test beam's mesh (shown in green) was done by using the structural meshing technique. Due to geometric conditions some regions still couldn't be meshed by using the structural meshing feature; consequently a second meshing approach called "swept meshing" was utilized. The algorithm replicated one element layer at a time along a sweep path to build up the mesh. (Simulia, 2011a). This technique was essential in building geometries that involved curvature such as the curve between the flange and the web of the beam as shown in yellow in Figure 4.14-A, the curve between the flange and the web of the column, bolts, and mainly regions that were built of wedge elements. Various partitioning possibilities were investigated and the scheme resulting in a more organized element distribution that satisfied element quality requirements was selected as the final partitioning pattern. Figure 4.14-B illustrates the final mesh design used for the test beam segment.

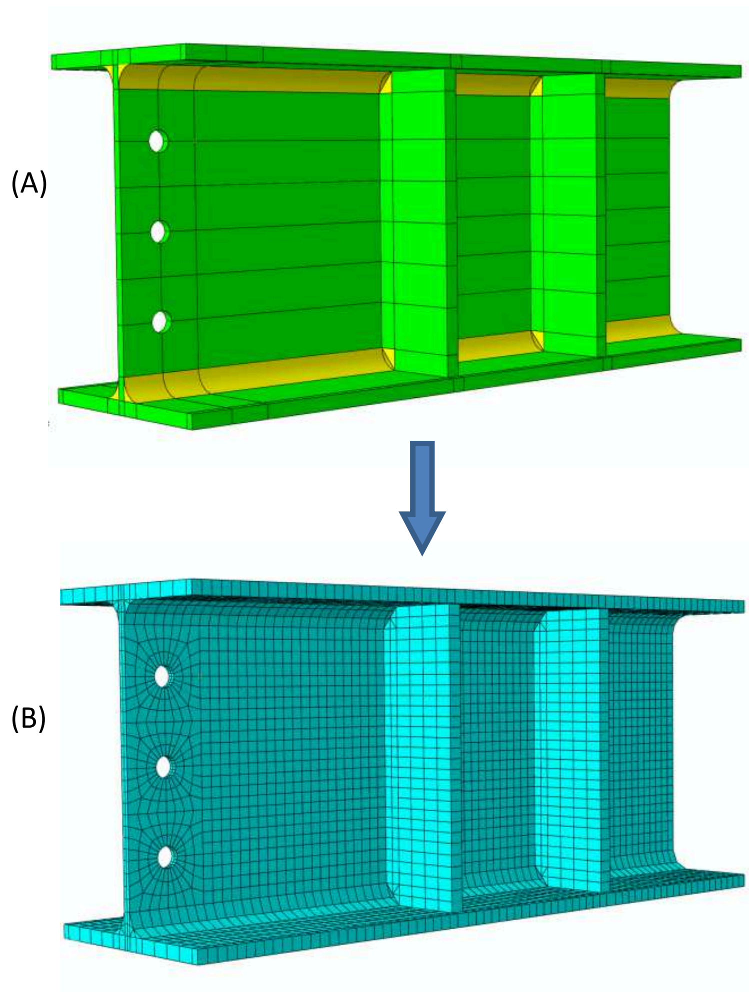

Figure 4.14- (A) Partition cuts used in the test beam's mesh design, (B) Test beam's final mesh

The subsequent application of the partitions was to separate regions that were used in contact interaction definitions, constraint surfaces, boundary conditions, and load applications. Finally the partitions provided the capability of generating nodes at locations of interest such as locations that instrumentation was installed during experimental testing which was useful for comparing the results obtained from the simulation with the lab test data. The software accomplished this goal by constructing element boundaries on the partition lines hence by intersecting two partition cuts, a desired node of interest was forced to be included in the mesh design. Overall the partitioning was an essential step in mesh design which significantly influenced the mesh quality of the model parts.

4.3.5. Element selection

Geometry condition was the first important factor in selecting the element shape. The order and type of element utilized in the FE models varied throughout the research. In the preliminary FE models developed in phase 2 of the research program; the shear tab, bolts, test beam segment were built of second order elements and first order elements were utilized in the extension beam, column and load blocks. The second order elements showed excellent performance in capturing deformations especially around the holes but the overall deformed shape did not match the experimental results in shear tabs that experienced weld tearing. With the inclusion of damage and major improvements in Phase 3, the strategy for element selection changed and all elements were replaced with fully integrated first order elements with a higher mesh density. CD3D8 elements were used for the structural mesh zones and C3D6 wedge elements built up the swept mesh regions and finally C3D8I elements were used for the beam extension segment. Second order elements due to their high number of integration points and higher flexibility compared to linear elements, were not likely to be damaged easily and created numerical problems, consequently the software was not able to run the entire simulation when damage initiated. The reason was that the damage model monitors stresses and strains at all integration points therefore the damage initiation criteria would have to be satisfied at all integration points before the damage evolved. With the higher number of integration points, the more complicated the iterations were for the software to achieve convergence.

4.3.6. Seeding and mesh quality

The density of the mesh was controlled through seeding which limited the biggest dimension of the elements used to construct the mesh. The maximum global seed size used was 15mm for the bolts and load block, 25mm for the test beam, 40 mm for the connection column and the beam's extension part, and finally 10mm for the shear tab. However these were the maximum seed sizes and the dimensions of the elements were smaller than these values in different models. Edge seeding was also utilized to manually control the number of elements in different regions of the parts in order to obtain an effective mesh design .This was achieved by decreasing the number of elements in regions of less interest such as stiffeners and using more elements in areas subjected to higher stresses. A minimum of 12 elements per circle was used for assembling the elements around the holes or in the body of the bolts. Models sensitive to net cracks were built by using up to 26 elements per circle. The reason that the same number of elements couldn't be used for all cases was that by increasing the number of elements in a circle, the internal angle of the surrounding elements also decreased leading to dissatisfaction of the minimum angle mesh quality control. By default the minimum angle suggested by ABAQUS (Simulia, 2011a) was 10 degrees and the maximum angle is set to 160 to satisfy mesh quality requirements. To reduce the chance of numerical errors all the elements in the research had a minimum internal angle of 20 degrees and the largest internal angle never exceeded 150 degrees. The maximum geometric deviation factor limit was 0.2. The Verify mesh tool in ABAQUS (Simulia, 2011a) was used to verify the mesh quality of each individual part of the assembly which was very useful in identifying poor elements and highlighting them for corrections.

All models developed in this thesis passed the software's mesh quality requirements before simulation. Figure 4.15 shows the finalized mesh design for one of the FE models developed. With the completion of the mesh design "instances" were created, which were representations of the parts used to define the interactions and connectivity between the components. The next step was to define the contact interactions which are explained in Section 4.3.7.

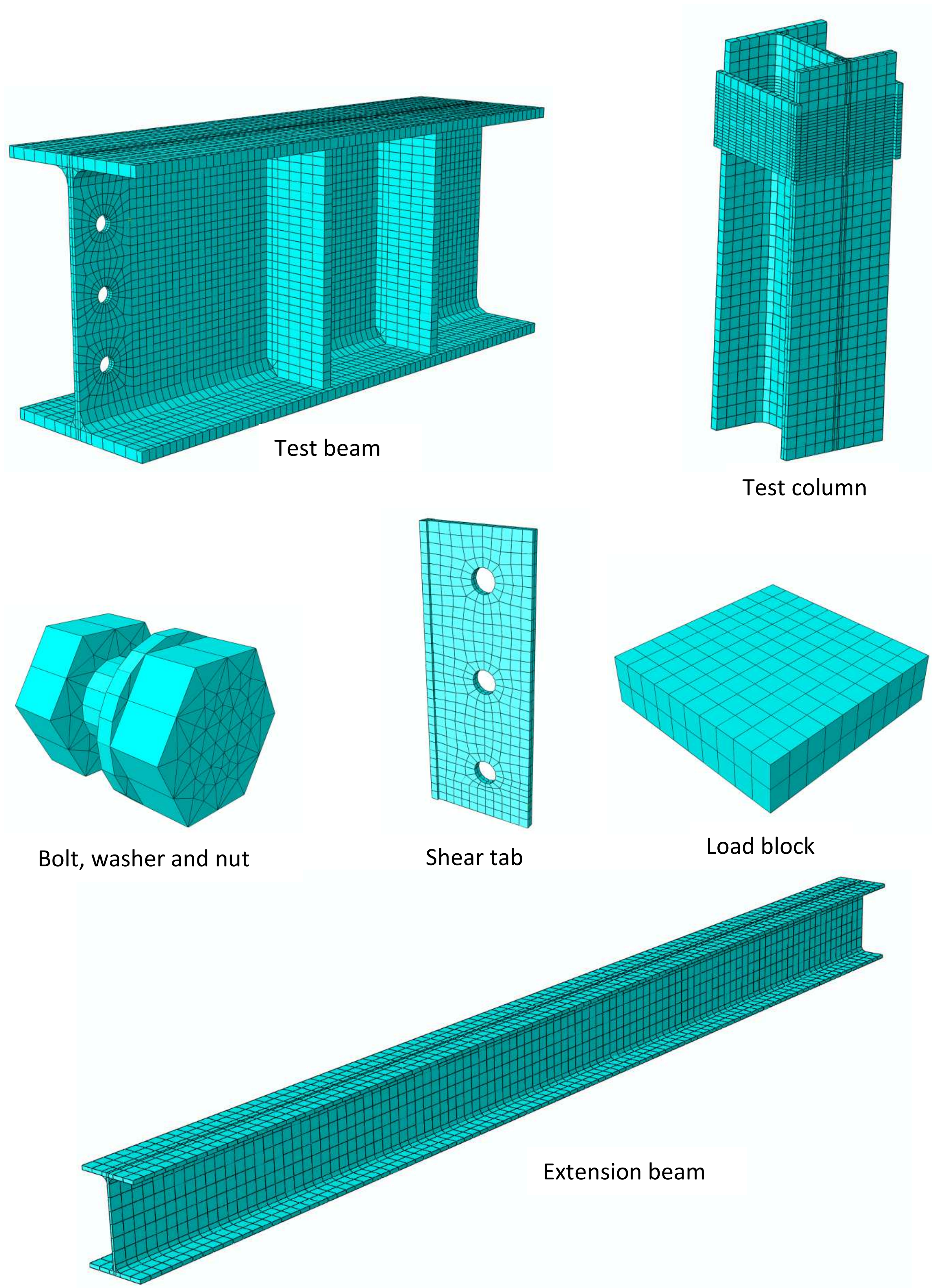

Figure 4.15- Mesh design of different parts of the assembly (Test M1 components shown)

4.3.7. Contact interactions

The FE model consisted of many contact interactions; all were defined as surface-to-surface contacts with the "Finite sliding" formulation and were based on a master-slave contact pair algorithm. The algorithm prevented penetration of nodes on the slave surface into the master surface; however there were no limitations for the nodes on the master surface; they could penetrate into the slave surface, therefore selecting the proper surface type was essential in the contact assignments. This was achieved by obeying two simple rules in the selection. First the surface with a finer mesh should be selected as the slave surface. Secondly if mesh densities on both surfaces were similar, the surface with the softer material should be assigned as the slave surface (Simulia, 2011b).

Two interaction properties were used in the modelling: Interaction with friction and frictionless interaction. "Hard contact" normal behaviour was defined in both interaction properties. This type of normal behaviour creates a contact constraint to surfaces when the clearance (distance between two surfaces) becomes zero and allows the transmission of contact pressures between the two surfaces. "Separation allowance" was used in the sub-options of normal behaviour to allow separation of surfaces and ABAQUS (Simulia, 2011b) executes this process by monitoring the transmitted contact pressure between the interacting surfaces; when the contact pressure drops to zero or becomes negative, the contact constraints created by the "Hard contact" feature are removed. "Penalty" was assigned as the tangential behaviour (also referred as sliding) for the interaction with friction property. The "Coulomb friction model" controlled the transmission of shear stresses between the interacting surfaces. No tangential motion exists between surfaces until a point when the shear stress reaches a critical value and ultimately slip occurs between the surfaces. The friction model is dependent on the normal contact pressure and the friction coefficient. Based on a research conducted by Rahman et al (2007), the friction coefficient of 0.3 was used in the models. The normal contact pressure was developed by "Hard contact". For the frictionless interaction property the friction coefficient is zero by default and slip occurs when contact is established (Simulia, 2011 b). The contacts assigned by the frictionless interaction property in the simulation were:

1) Contact between load block 1 (representing the main actuator) with the top surface of the test beam's flange. The slave surface was selected to be the top of the test beam's flange due to its higher mesh density compared to the mesh used in the load block.
2) Contact between load block 2 (representing the tip actuator) with the bottom surface of the test beam's flange. In this case the top face of the load block was selected to be the slave surface and the surface beneath the test beam was selected as the master surface since the far end of the test beam was meshed with a larger global seed size.

One important note to be highlighted is that the selection of the master and slave contact pair could vary based on the global seed size selected for the mesh design of each interacting component. It is important to realize that ABAQUS (Simulia, 2011b) automatically selects these surfaces based on the initial mesh density used when defining the contact iterations. If one would change the seeding of the mesh resulting in a different mesh density, these interaction surfaces will not be updated automatically; therefore, all the surfaces in the models were verified one last time to be properly assigned before the final run of the simulations.

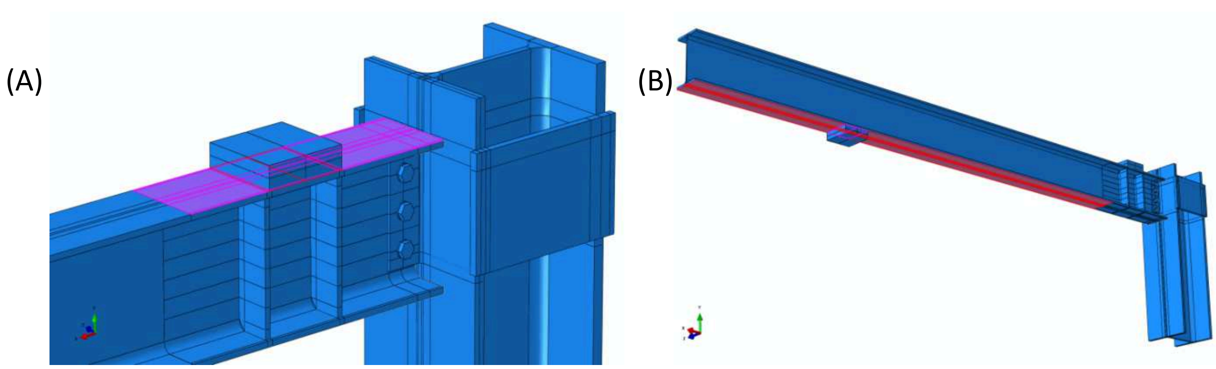

Figure 4.16-(A) Interaction region between the bottom face of load block 1 with the top surface of the test beam's flange, (B) Interaction region between the top face of load block 2 with the bottom surface of the test beam's flange

The remaining utilized contacts featuring the contact interaction with friction property are listed:
3) Contact between the washers and the outer face of the shear tab.
4) Contact between the nuts of the bolts and the web of the test beam.
5) Contact between the bolts' outer surfaces and the inner surface of the holes on the shear tab.
6) Contact between the bolts' outer surfaces and the inner surface of the holes on the test beam.

7) Contact between the inner face of the shear tab and the web of the test beam.
8) Contact between the end of the shear tab and the face of the connection column

Bearing simulation around the bolt holes was achieved by contacts 5 and 6. Figure 4.17-A shows a cross section of a bolt from the FE model built for Test M1. The contour shows the Von Mises stress distribution inside the bolt, which is caused mainly due to shear stress. The diameter used for the bolt was the same as the diameter of the hole on the shear tab. The reason for this selection was that in the FE model the 2mm gap between the surface of each bolt and the edge of the corresponding hole cannot exist due to a lack of continuity of the interaction surfaces. Since each bolt was assembled as an individual part in the FE assembly, this technique allowed for stability of the assembly at the initial stage of the analysis. Ashkul (2004) modelled this gap by utilizing special elements called "gap elements" but required an extremely fine mesh for the bolts, interacting members and gap elements. The preliminary FE results showed that without modelling the 2 mm gap the response of the connection would be slightly stiffer compared to the laboratory test results, but the overall predicted response of the connection was accurate; therefore, to increase the computational efficiency, it was decided not to include the gap in the FE models. Additional possible contacts that were experienced during laboratory testing were also embedded in the models such as:

9) Contact of the top of the shear tab with the curve between the test beam's flange and web (Figure 4.17-B)
10) Contact of the beam's flange and the column face (Only included in case of a penetration)

(A) 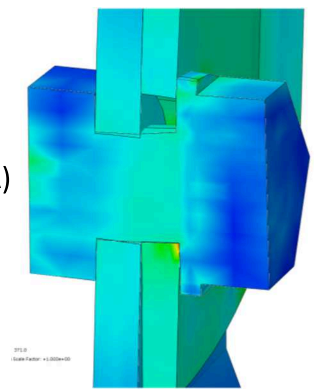

(B) 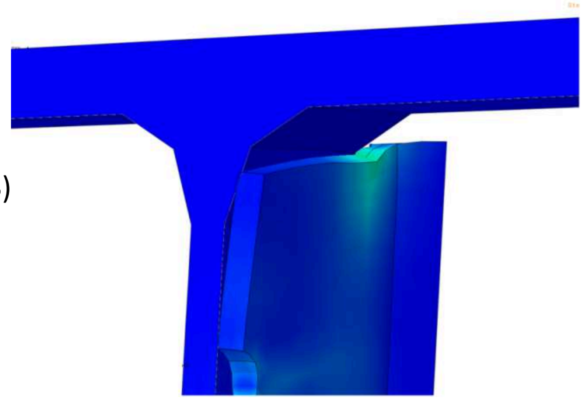

Figure 4.17-(A) Von-Mises stress distribution in a bolt, (B) Cross sectional view of the contact between the shear tab and the test beam

4.3.8. Actuator operation simulation

The loading generated from the main actuator and tip actuator was applied as a displacement boundary condition to the load blocks. In order to simulate the operation of the half cylinder–steel plate roller system used for applying the main load in the laboratory tests (Figure 4.18-A), a special simulation technique was used. All degrees of freedom at nodes A and B (Figure 4.18-B) were restrained in the initial analysis step to provide numerical stability of the load block in 3D space. In the next analysis step (loading step), the translation degree of freedom in the direction perpendicular to the ground was released to allow only vertical movement of the load block. An imposed unit displacement with an amplitude function corresponding to the measured displacements from lab testing was applied to line AB as shown in Figure 4.18-B. This technique allowed the load block to rotate freely as it displaced. For simulating the functionality of the roller with the two plates that eliminated friction between the load block and the test beams flange, a frictionless contact interaction was defined in the FE model at the interface location. The normal to surface interaction property used for contact was "hard contact" behaviour with a separation allowance feature. The same technique was used for the tip actuator with the difference that the load block was positioned underneath the test beam. A simple cantilever model was first used to certify the validity of this simulation technique and after approval it was embedded in the FE models. Other techniques were also investigated nevertheless the presented strategy yielded the most stable and acceptable results.

(A)

(B)

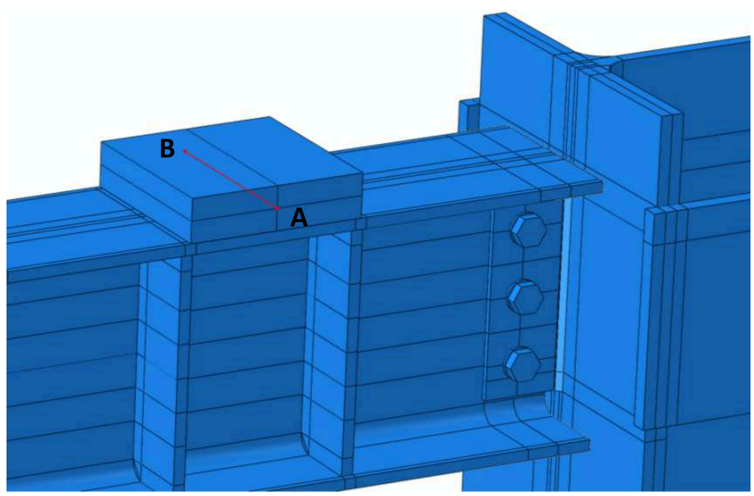

Figure 4.18-(A) Half cylinder–steel plate roller system used beneath the main actuator head used by Marosi (2011), (B) Location of the imposed displacement in the load block

4.3.9. Weld tearing simulation

To allow for weld tearing, the mesh assembly in Figure 4.19 was used. The problem with classical FE models was that all the components were usually modelled as one individual part, which would result in shared nodes between the shear tab, weld and supporting member. This would limit the ability to capture the shear tab separation from the column and would result in incorrect stresses in the weld leading to over-estimated shear resistance of the connection. To resolve this issue the steel plate, including an interface layer of 2 wedge elements on each side, was assembled as a separate part distinct from the column. The interface layer of wedge elements, which physically would be part of the weld, was tied with a tie constraint to the fillet weld. A contact interaction was also used between the vertical edge of the plate and the column flange which included a separation allowance. By using this technique and applying the damage properties to the shear tab and weld, tearing simulation was made possible. Once damaged, the weld was able to tear resulting in separation of the shear tab from the column and a more accurate compression stress distribution at the bottom of the shear tab due to contact with the column. The thickness of the wedge layer was minimized while still satisfying mesh quality requirements. By utilizing damage and weld tearing in the simulation, the final deformed shape of the FE models showed significant improvement in the failure progression of the connection compared to preliminary FE models which lacked these features.

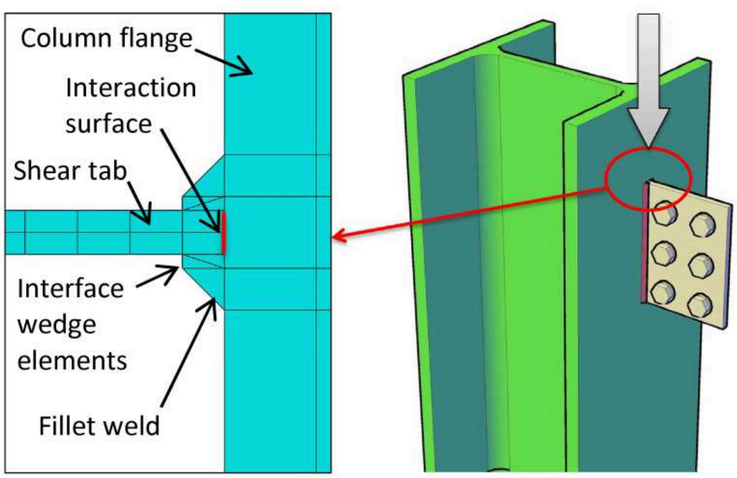

Figure 4.19-Mesh design representation at the interface of the shear tab with the connecting fillet weld

For connection simulations that experienced extreme weld tearing, the ultimate shear resistance of the connection was dependent on the mesh size; however limiting the maximum seed size of the shear tab to 10mm resulted in a close match of the ultimate shear resistance (within a margin of 5%) with the corresponding experimental results. A mesh sensitivity study was also performed; by using extremely small mesh sizes (less than 5mm seeding) the analysis was unable to proceed due to convergence issues because of satisfying a higher number of damage criteria.

4.4. Simulation results

The FE models were capable of simulating the behaviour and progressive damage observed in the six shear tab tests conducted by Marosi (2011). Most of the FE models where able to run completely but some terminated at just over 90% of the testing procedure due to numerical instabilities after damage evolution. The final deformed shape, shear tab vertical displacement and connection rotation versus the connections shear force were selected as the criteria for comparing the response from FE simulation with the lab test results. With the exclusion of the gap between the bolts and the holes on the shear tab and test beam in the FE models, it was expected that the simulation models would be stiffer compared to the laboratory tests especially when comparing rotations; therefore, the shear tab vertical displacement vs. the connection shear force was selected as the main criteria for comparison since an absolute measure was taken relative to the ground minimizing errors in measurements.

Another factor that affected the global stiffness in the finite element models compared to the laboratory experiments was their perfect initial condition nature. The geometry in the FE models was perfect, no accidental slips occurred between the components and no errors existed in exporting measurements. This was not the case for experimental work where even with high fabrication accuracies, some small gaps between components such as the bolts, the half cylinder–steel plate roller system, the base structure, etc., might have existed. These small gaps caused small deformations before complete load carrying capacity and slips might also occur at the beginning of the testing process. To account for this error the response curves of some FE models were shifted by a small initial deformation to achieve a better match with the laboratory test results. Each test simulation is presented individually and the response curves of each case were compared to the laboratory data of the matching shear tab test specimen. Observations from the simulation were also compared with the visual inspections by Marosi (2011). A summary of the simulation results is presented in Sections 4.4.1 to 4.4.6:

4.4.1. Test M1 simulation

Figure 4.20 compares the final deformed shape of the Test M1 shear tab specimen conducted by Marosi (2011) with its corresponding FE model (bolts removed). The shear tab was connected by a single vertical row of three 3/4 inch ASTM A325 bolts to a W310x 60 test beam. The colours in Figure 4.20-A represent the Von Mises stress distribution at the end of the simulation. As can be seen, the shear tab experienced flexural and shear plastic yielding between the bolt line and the fillet weld. The functionality of the applied weld tearing simulation technique can be clearly observed in the figure. Weld tearing was witnessed at the top of the shear tab in both the FE model and test. The load carrying capacity did not drop after the weld started to tear and the shear tab continued to carry shear force until the tearing reached the top bolt line. After excessive deformations, the top edge of the shear tab came into contact with the test beam's flange influencing the weld tearing progression.

(A) (B)

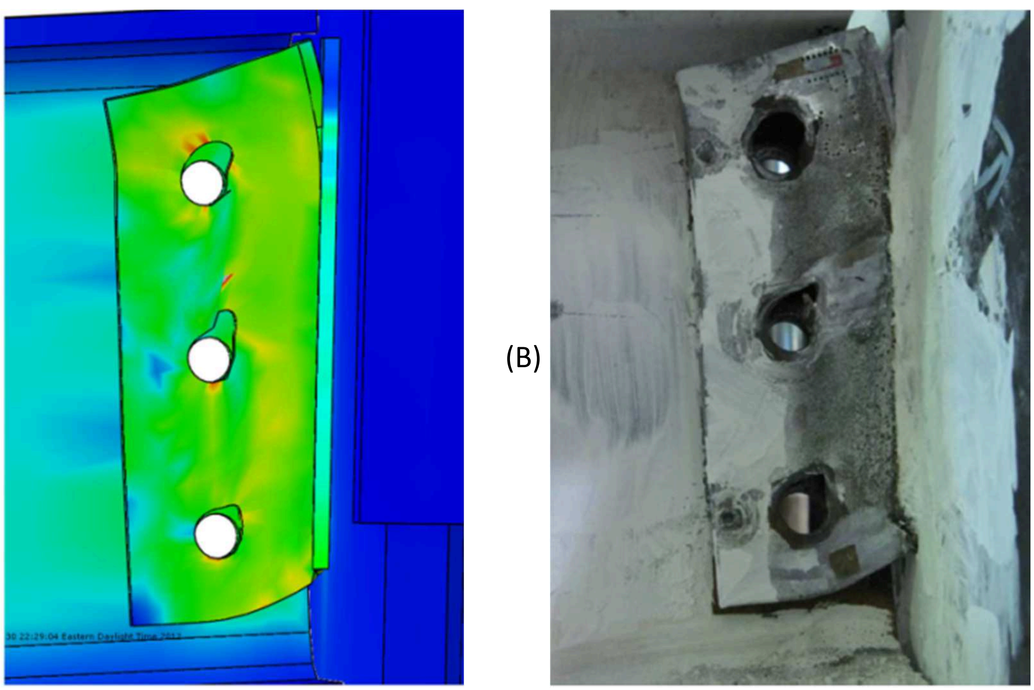

Figure 4.20- (A) FE simulation deformed shape of TestM1 vs. (B) Test result, Marosi (2011)

The corresponding shear force vs. vertical displacement and shear force vs. connection rotation response curves are shown in Figures 4.21 and 4.22, respectively. As it can be seen from the figures, the FE simulation results predicted the ultimate shear resistance of the shear tab specimen with acceptable accuracy (within a margin of 5%) with some differences in behaviour after the initiation of tearing in the weld. Based on Marosi's (2011) thesis, it should be noted that the force in the experiment did not drop due to the stroke limit having been reached for the end actuator.

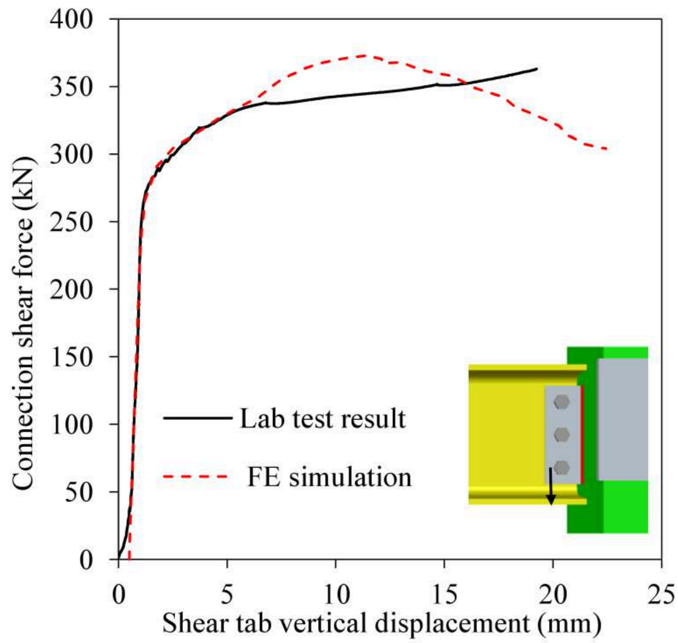

Figure 4.21-Shear force -shear tab vertical displacement response curves obtained from Test M1

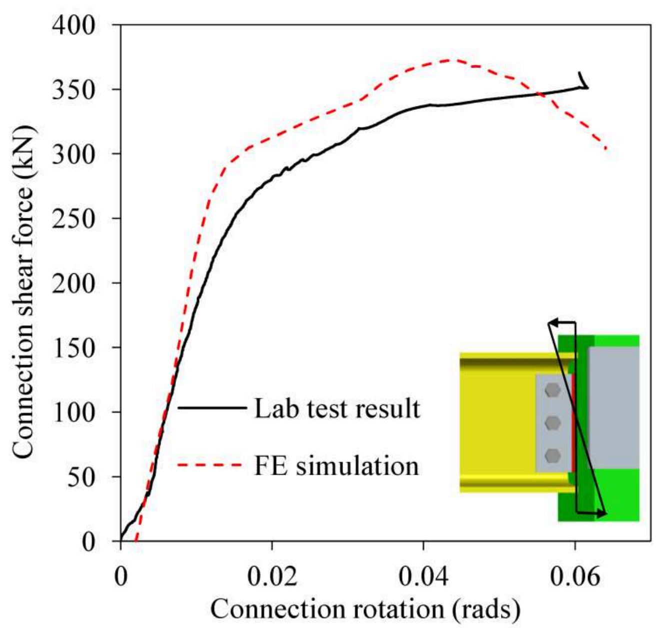

Figure 4.22-Shear force-connection rotation response curves obtained from Test M1

4.4.2. Test M7 simulation

The Test M7 specimen was a shear tab that was connected to a W610x140 beam by a single vertical row of six 7/8 inch ASTM A325 bolts. Due to the high height-to-width aspect ratio of the shear tab, net area failure was likely to occur. The FE element model of this test was performed by using two techniques for simulating net area failure. Both methods utilized damage simulation and differed in the inclusion of the element removal feature. Removing damaged elements in regions that were part of a contact interaction such as the bearing area around the holes could lead to high numerical instability. For this purpose the element removal feature could be disabled and instead the stiffness degradation can still be used in the models. Therefore the elements would be kept in the assembly but their stiffness would be degraded. A parameter called stiffness degradation was used to identify the loss of stiffness in the models and areas where crack prorogation could happen (Figure 4.23-A). By using the first technique and disabling element removal, some models were able to continue simulating the post ultimate behaviour more than models that included element removal.

The result of applying the second technique used in the FE model can be observed in Figure 4.23-B (Von-Mises stress distribution shown). In comparison with the deformed shape of the test specimen (Figure 4.23-C) it was successful to match the net area cracks in the shear tab. Net cracks can be observed between the top five holes on the shear tab and the FE model did not show any cracking between the two lower holes. Both techniques led to same shear resistance and did not differ much in regards to global response; however the model without element removal performed more stable with easier convergence. Bearing simulation was also deemed successful by comparing the deformed shape of the holes on the shear tab in the FE model with that observed in the laboratory. The weld did not tear during testing of this shear tab; the simulation results also did not indicate any tearing in the weld. Some out-of-plane bending of the shear tab at its top was observed due to the contact of the upper edge with the k-region between the flange and web of the beam. With the validation of the net area failure simulation method, the remaining FE models were embedded with this feature in order to predict possible cracking at extreme strain levels. Element removal was utilized for all other models since the differences were only related to the post-ultimate behaviour in the response curves of the tests.

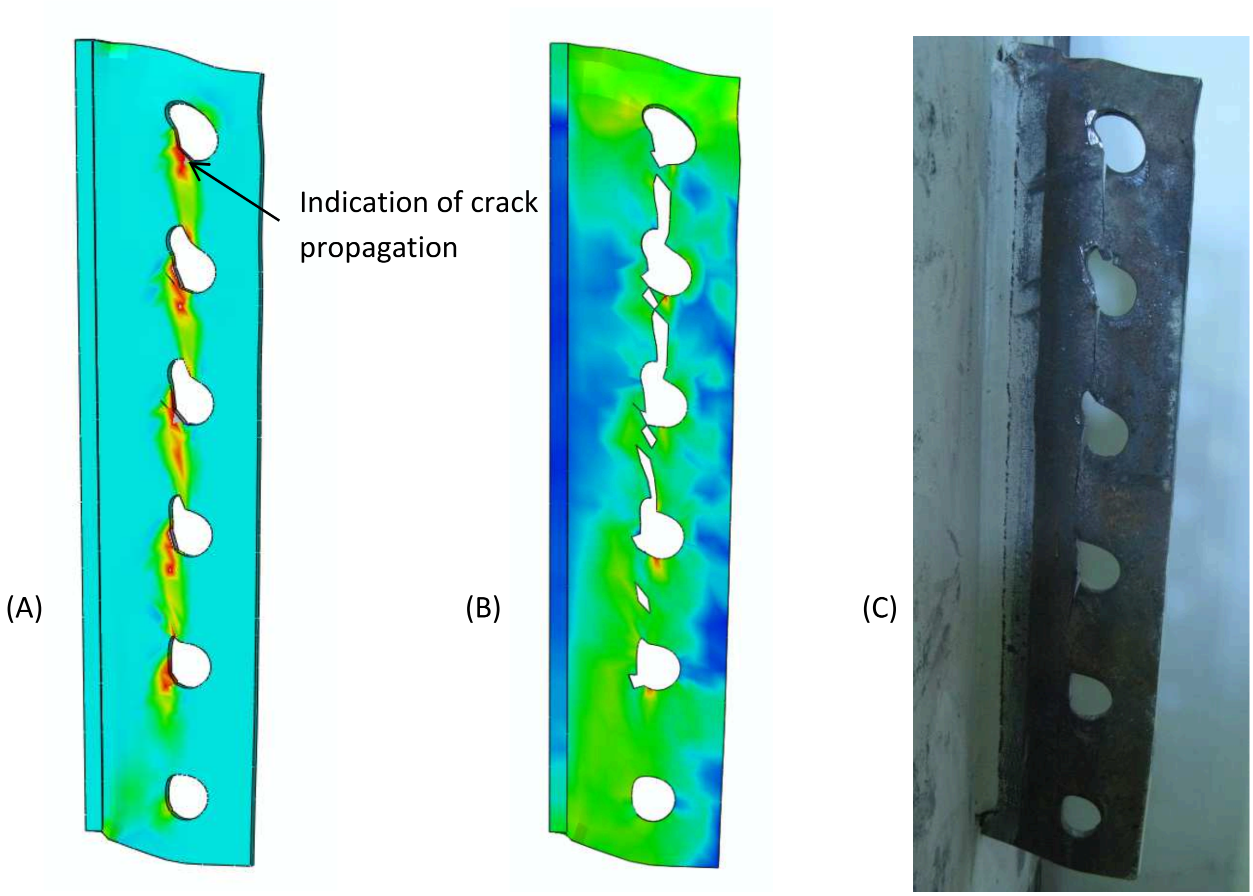

Figure 4.23- (A) FE simulation deformed shape of TestM1 with only stiffness degradation, (B) FE simulation deformed shape of TestM1 including element removal, (C) Deformed shape of Test M1 lab test result, Marosi (2011)

The corresponding shear force vs. vertical displacement and shear force vs. connection rotation response curves of Test M7 simulation are presented in Figures 4.24 and 4.25. The shear tab vertical displacement vs. the connection shear force matched the test results with the exception of some slight softening immediately after the elastic behaviour region. However, the predicted ultimate shear resistance was very close to Marosi's (2011) measured value. In terms of connection rotation some differences in the behaviour can be identified (Figure 4.25) and since the connection rotation was dependent on measurements by multiple instrumentations, the possibility of differences increases when comparing rotations. Overall the ultimate rotation of the connection was still predicted within a margin of 5%.

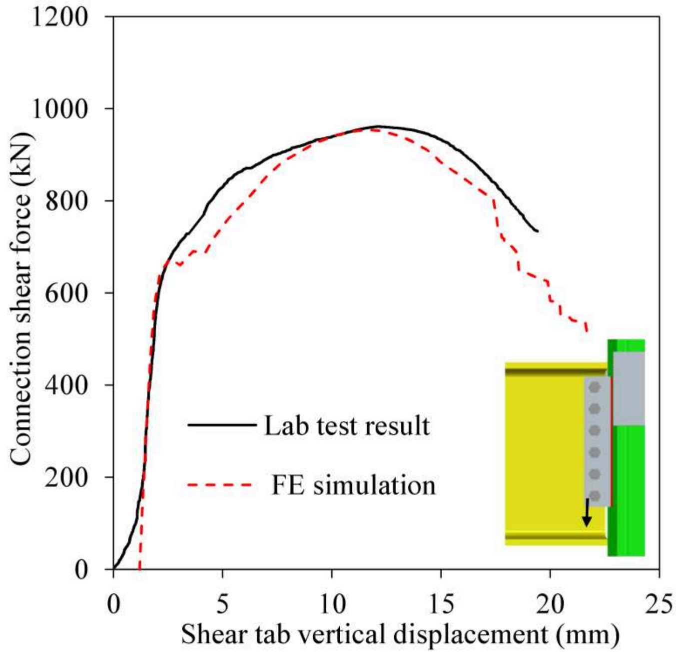

Figure 4.24-Shear force-shear tab vertical displacement response curves obtained from Test M7

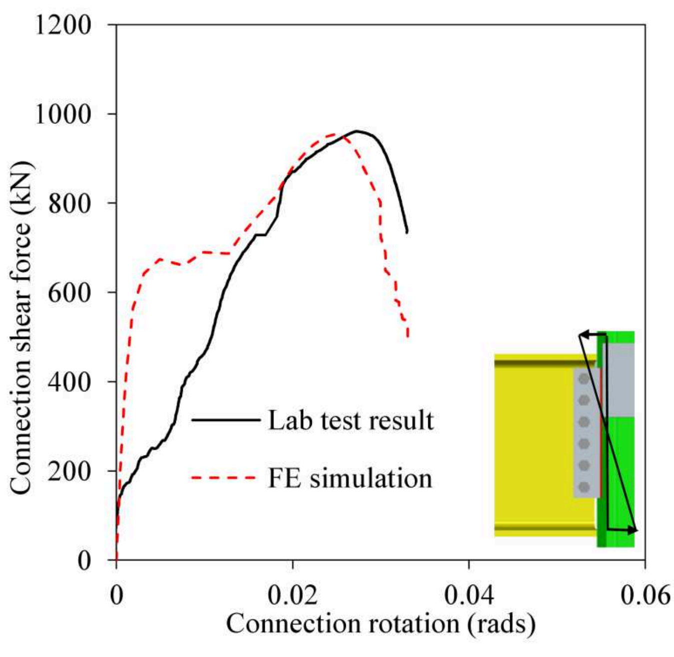

Figure 4.25-Shear force-connection rotation response curves obtained from Test M7

4.4.3. Test M13 simulation

Test M13 consisted of a single vertical row of ten bolts connecting a W920x223 test beam to a shear tab. One inch ASTM A325 bolts were used for the connection. The FE simulation showed that after some yielding between the bolt line and the connecting weld line, the weld on top of the shear tab started to tear. This fracture ultimately reached the bolt line third from the top. By continuing the loading and passing the ultimate shear resistance point, the stiffness started degrading and cracks developed between the five central bolt holes (Figure 4.26). This was the first connection FE model that simulated simultaneous weld tearing, shear yielding and net area failure.

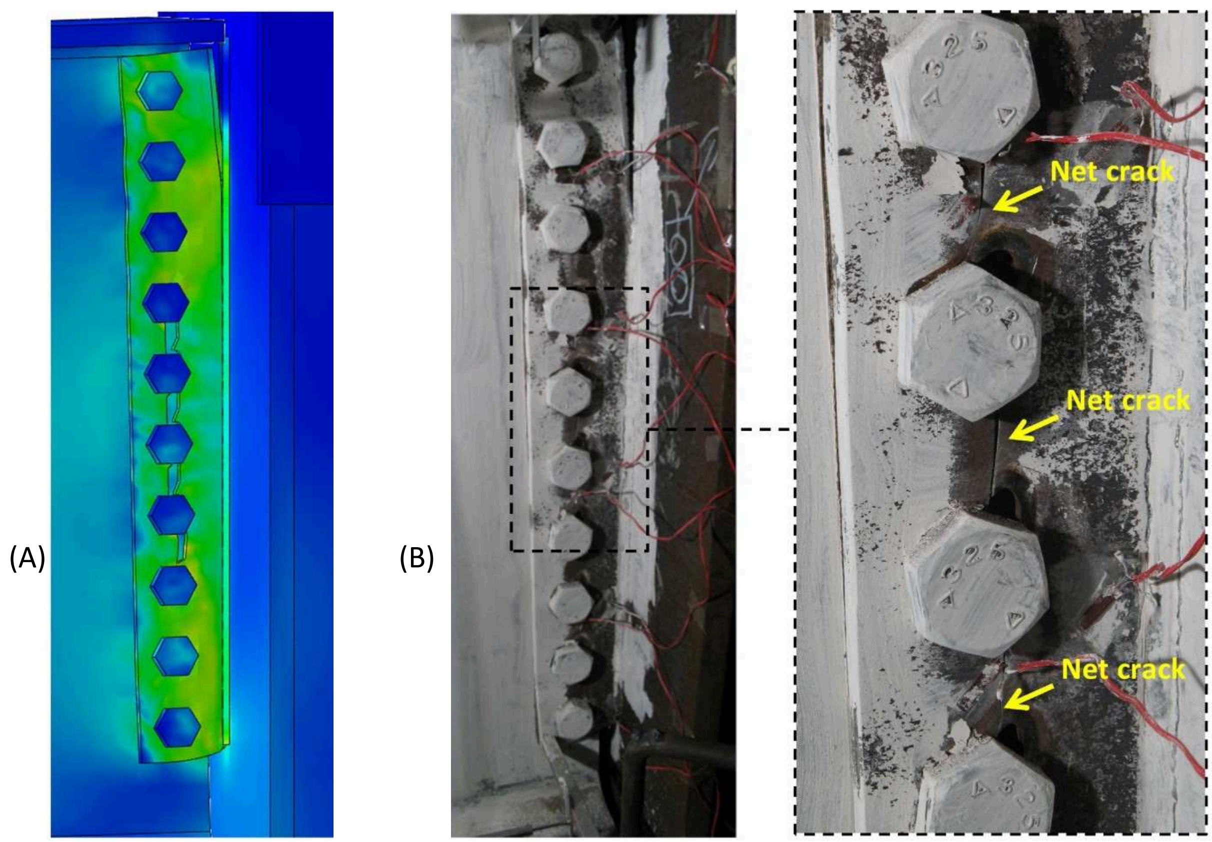

Figure 4.26-(A) FE simulation deformed shape of Test M13 vs. (B) lab test result, Marosi (2011)

In terms of structural response, the Test M13 FE model was able to simulate the testing procedure and the progressive damage mechanism of the connection. The model responded in a slightly more ductile fashion compared to the test response curve (Figure 4.27 and 4.28), however, the ultimate shear capacity of the connection was closely predicted. The sudden change and immediate drop of load in the experimental result (Figure 4.28) was due to stopping the end actuator when it reached its maximum stroke and further rotation could not been applied beyond that point.

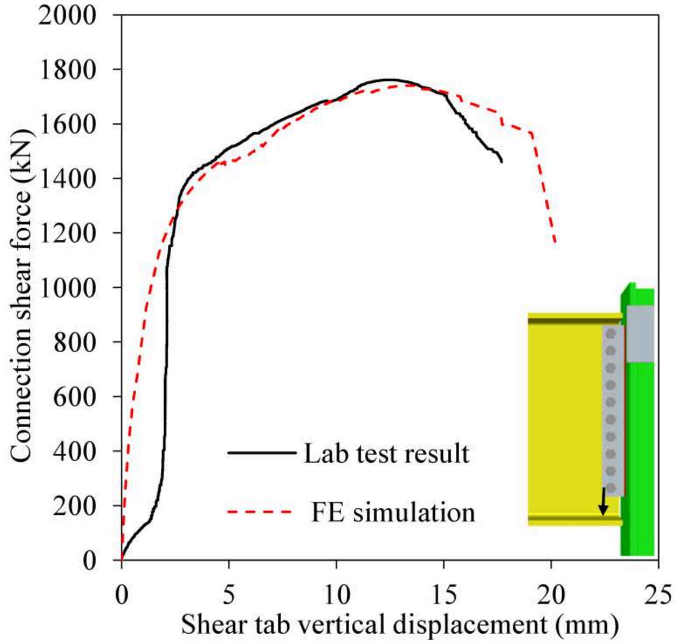

Figure 4.27-Shear force-shear tab vertical displacement response curves obtained from Test M13

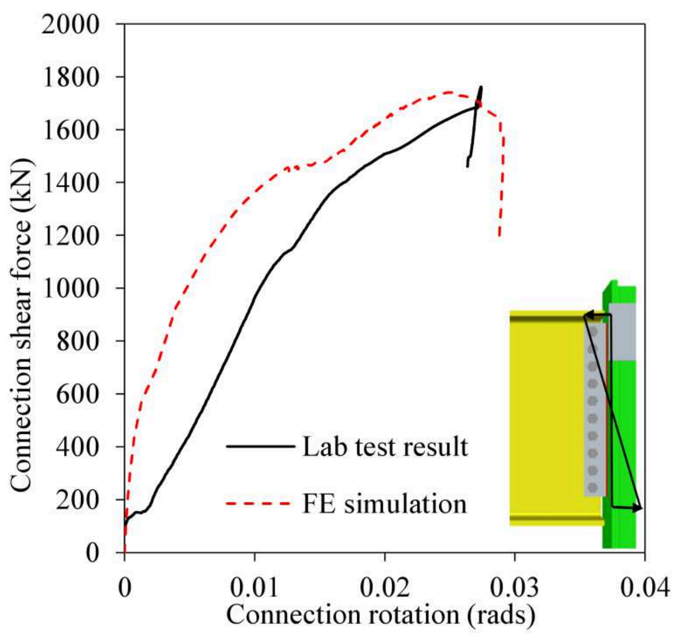

Figure 4.28-Shear force-connection rotation response curves obtained from Test M13

4.4.4. Test M2 simulation

The non-standard shear tab specimen of Test M2 was connected by two vertical rows of three 3/4 inch ASTM A325 bolts to a W310x 60 test beam. Due to the connection's higher eccentricity compared to the single vertical row of bolts shear tab simulated in Test M1, the flexural behaviour controlled the response. Some yielding was observed between the first bolt line and the weld line with minor bearing around the holes. The stiffness degraded with the rupture in the weld, whereas no extreme strains developed between the holes to propagate cracks. This behaviour was observed in both the FE model (Figure 4.29-A) and the captured images from laboratory testing (Figure 4.29-B). The colours on the deformed shape of the shear tab illustrated in Figure 4.29-A represents the Von-Mises stress distribution in the shear tab.

(A)

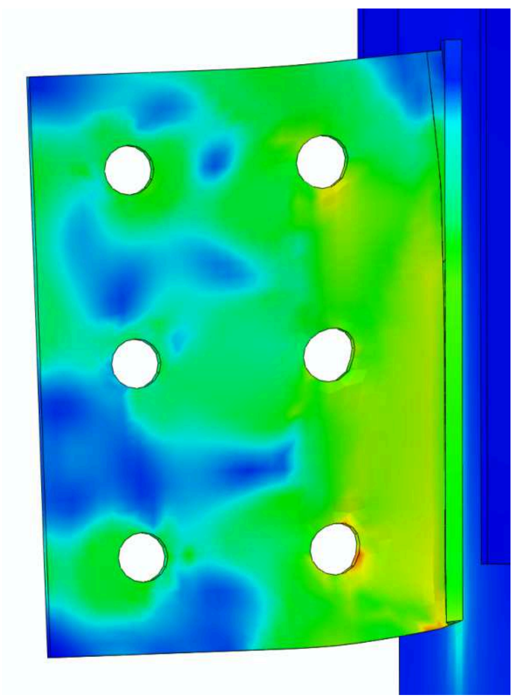

(B)

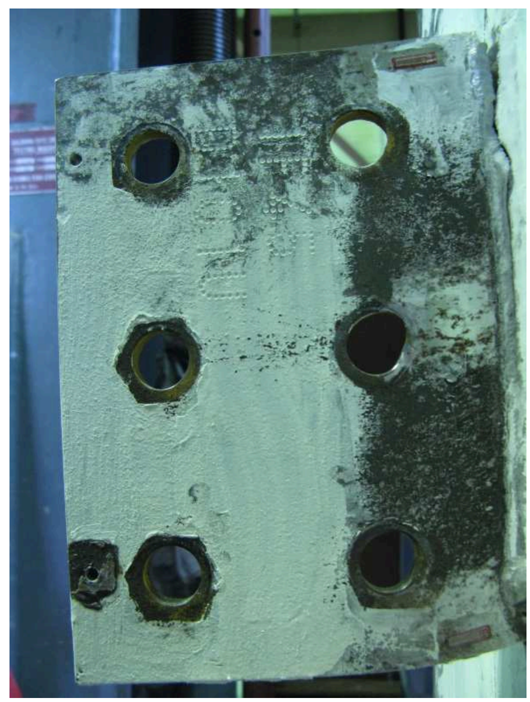

Figure 4.29- (A) FE simulation deformed shape of Test M2 vs. (B) lab test result, Marosi (2011)

The model's shear force vs. vertical displacement and shear force vs. connection rotation response curves showed a close match with the test results up to the ultimate shear resistance point; however beyond that point, the stiffness degradation in the FE model was more intensive compared to the lab test response curves (Figures 4.30 and 4.31). This is likely because the weld tearing simulation is dependent on the mesh size (10mm used), whereas in reality the weld does not tear suddenly every 10mm and tearing occurs more gradually.

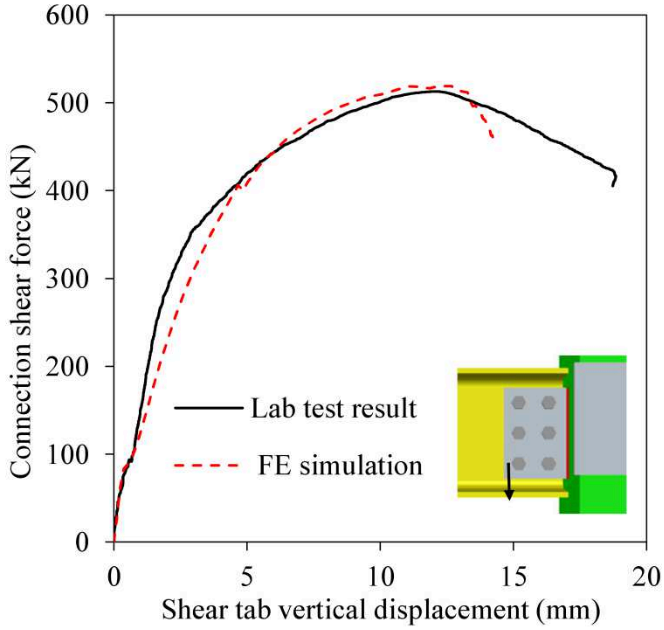

Figure 4.30-Shear force -shear tab vertical displacement response curves obtained from Test M2

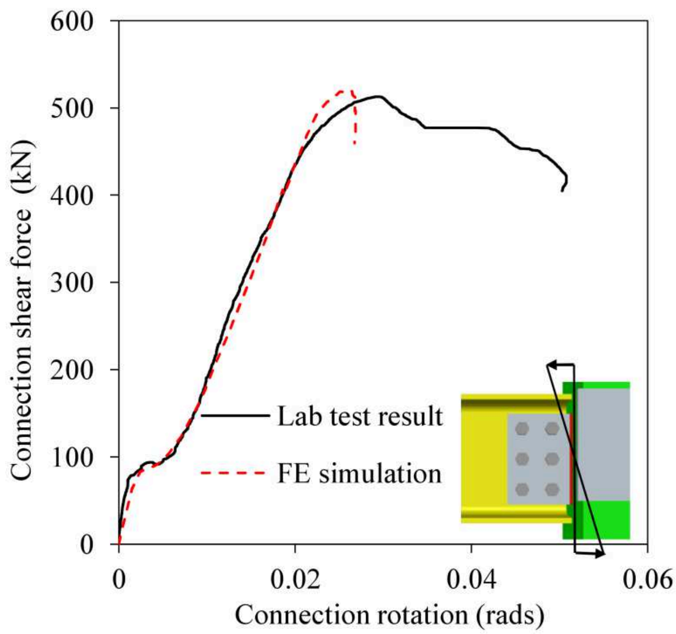

Figure 4.31-Shear force-connection rotation response curves obtained from Test M2

4.4.5. Test M8 simulation

Unlike Test M2, the shear tab specimen of Test M8 demonstrated a more ductile behaviour. The shear tab was connected by two vertical rows of six 7/8 inch ASTM A325 bolts to a W610x140 beam. Based on Figure 4.32, shear yielding was observed between the first bolt line and the weld line. Extensive bearing was identified mainly around the holes on the first bolt line of the shear tab (closer to the support) while the second bolt line did not show much bearing damage. Some weld tearing was observed at the top of the shear tab which ultimately extended to the top bolt line, and finally some cracks propagated between the central holes on the first bolt line.

(A)

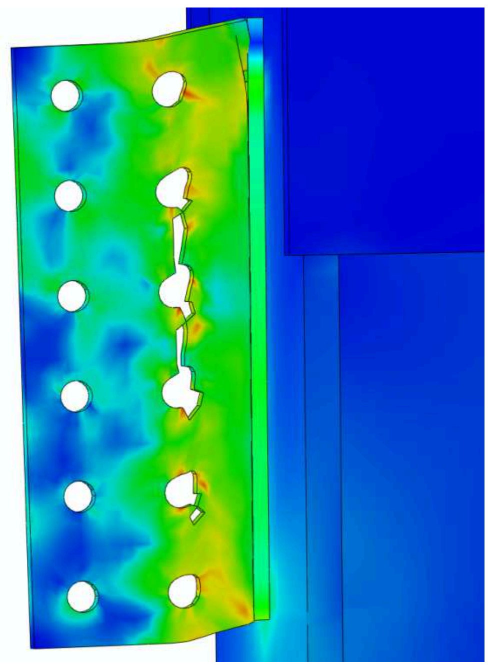

(B)

Figure 4.32- (A) FE simulation deformed shape of Test M8 vs. (B) lab test result, Marosi (2011)

The corresponding global shear force vs. vertical displacement and shear force vs. connection rotation response curves (Figures 4.33 and 4.34) demonstrate a slight over estimation of the ultimate shear resistance compared to the lab test result. The shear tab vertical displacement of the FE model shows a very good match with the lab test data; however the rotation response curves indicate that the FE model was stiffer than the laboratory test specimen.

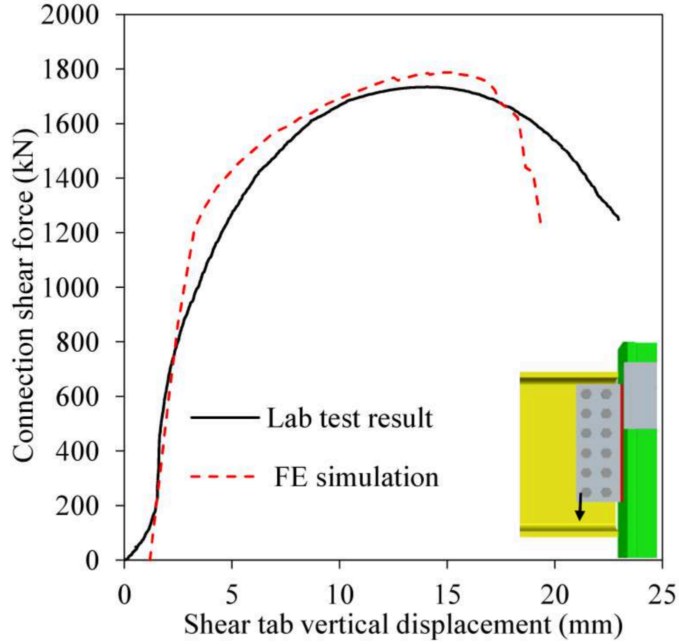

Figure 4.33-Shear force -shear tab vertical displacement response curves obtained from Test M8

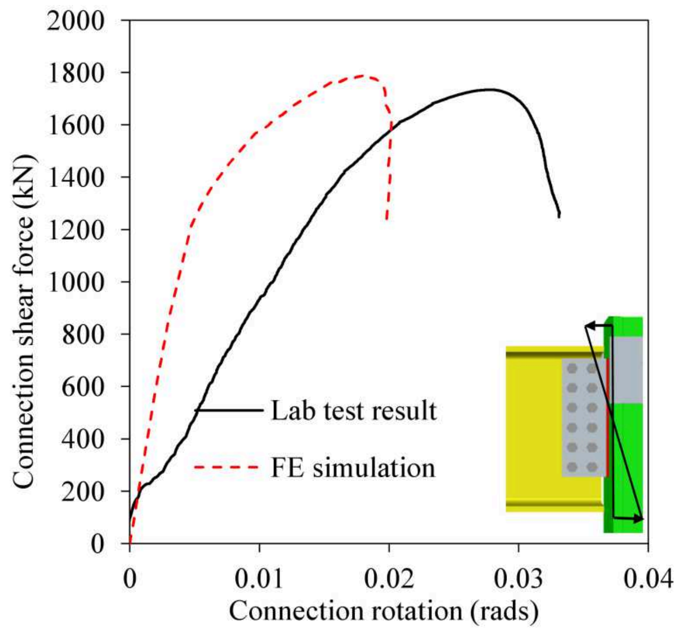

Figure 4.34-Shear force-connection rotation response curves obtained from Test M8

4.4.6. Test M15 simulation

Specimen M15 comprised the largest shear tab that Marosi (2011) had tested; it was connected by two vertical rows of ten 1 inch ASTM A325 bolts. The test beam used for the connection was a W920x223 wide flange member. Due to the large size of the components and the high capacity of the shear tab (around 3500 kN) the test setup was different compared to the other conducted tests. The tip actuator was replaced with two manually operated hydraulic cylinders (Figure 4.35-A). Another complication that occurred during the testing procedure was that the test beam did not have enough capacity to transfer the forces to the shear tab; as such the beam's web experienced large plastic strains with some minor out-of-plane buckling (Figure 4.35-B). Due to the failure of the beam it was not possible to reach the true capacity of the shear tab connection. However, the highest connection shear force recorded was 99% of the predicted value as determined using the modified AISC design method presented by Marosi (2011). With the exception of Test M15, the test results showed this prediction of shear tab resistance was approximately 20% less than that measured during testing.

(A) (B)

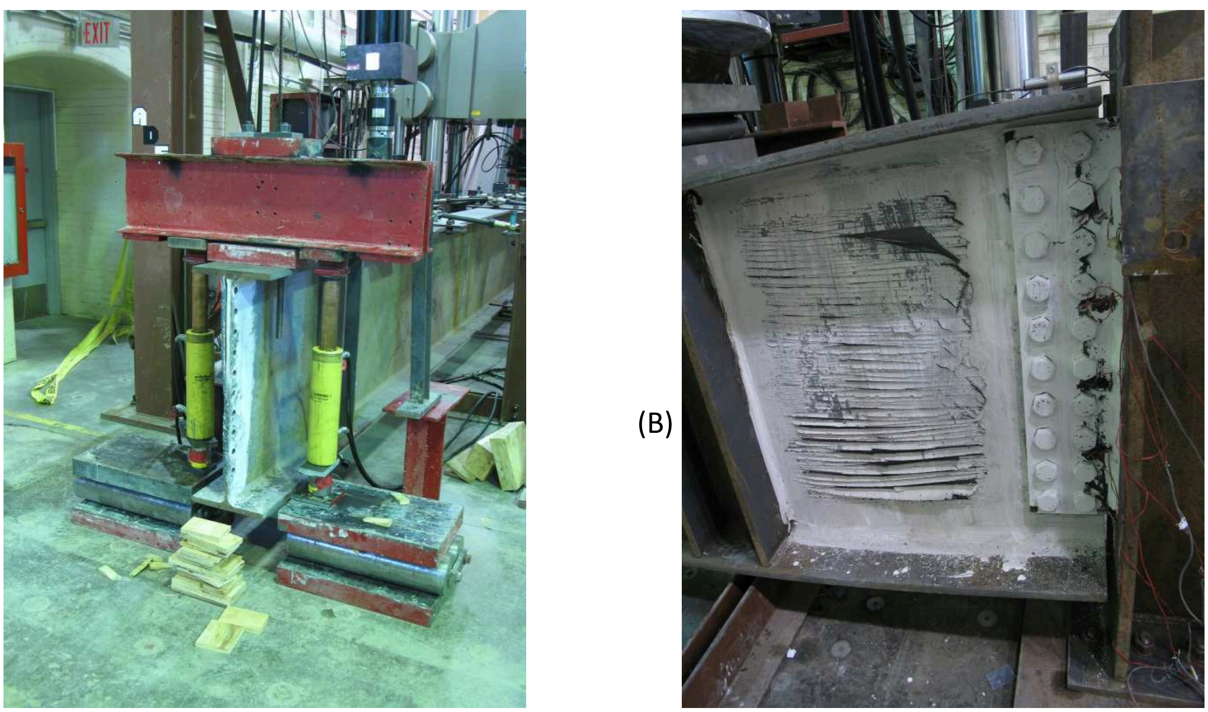

Figure 4.35- (A) Manual displacement application at the tip of Test M15's beam, (B) Large deformations in the web of the beam used in Test M15, Marosi (2011)

By utilizing finite element simulation it was possible to eliminate the limitations that existed in the laboratory testing, and as such the full capacity of this specific shear tab specimen could be determined. In order to achieve this, three different cases were investigated:

- **Model M15-A:** For this case, the same test performed by Marosi (2011) was replicated to determine the capability of the FE model in predicting the ultimate shear resistance of the shear tab. Figure 4.36 represents the final deformed shape of the simulation model including its response curve. As it can be seen from the figure the FE model was able to simulate the testing procedure with high accuracy. The initiation of the beam's web buckling can be observed in the deformed shape of the beam.

- **Model M15-B:** With the validation of the FE model, the loading on the FE model was continued beyond the final stage of the laboratory testing condition. With no limitations in terms of testing equipment, the displacements were increased and the connection shear force was recorded. After a very slight increase in applied force the beam's web continued to buckle out-of-plane thus limiting the capacity to that of the test beam (Figure 4.37) and not the shear tab connection. Therefore a third case was investigated.

- **Model M15-C:** In order to determine the ultimate shear resistance of the connection, the test beam was strengthened in the FE model to transfer the required shear force. For this purpose the original W920x223 test beam in the FE model was replaced with a larger beam size (W920x271). An additional stiffener was also included to reinforce the test beam's web and to prevent its buckling. By using this method, the ultimate resistance of the shear tab connection was increased from 3500 kN up to 4562 kN, proving that the shear resistance was underestimated by approximately 30% when calculated by Marosi's (2011) modified AISC method, which is a similar result compared with the other shear tab connections that were tested.

In all three of these cases the shear tab behaviour could be considered as very stiff without significant inelastic deformation, nor weld tearing. Furthermore, the connection resistance reached a level that caused some deformations in the stub column.

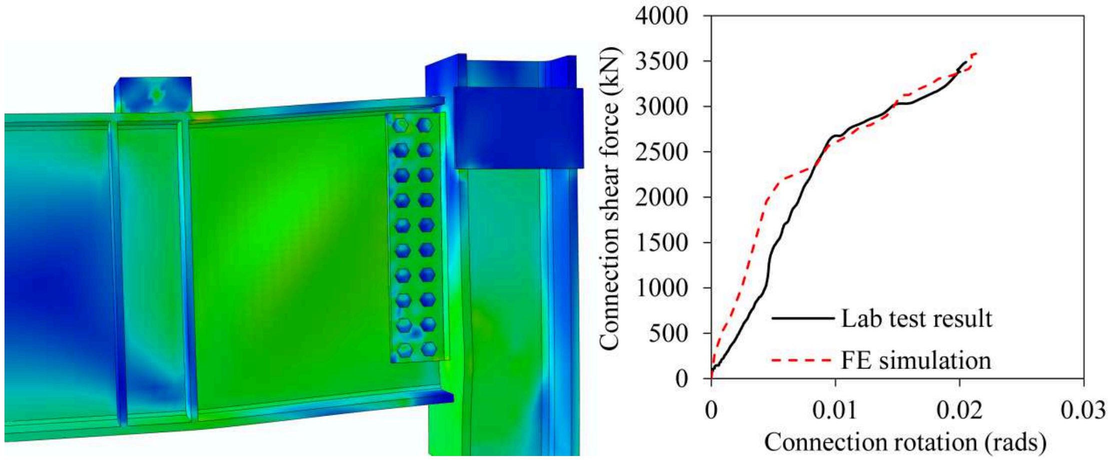

Figure 4.36-Model M15-A FE simulation vs. lab test result of Test M15

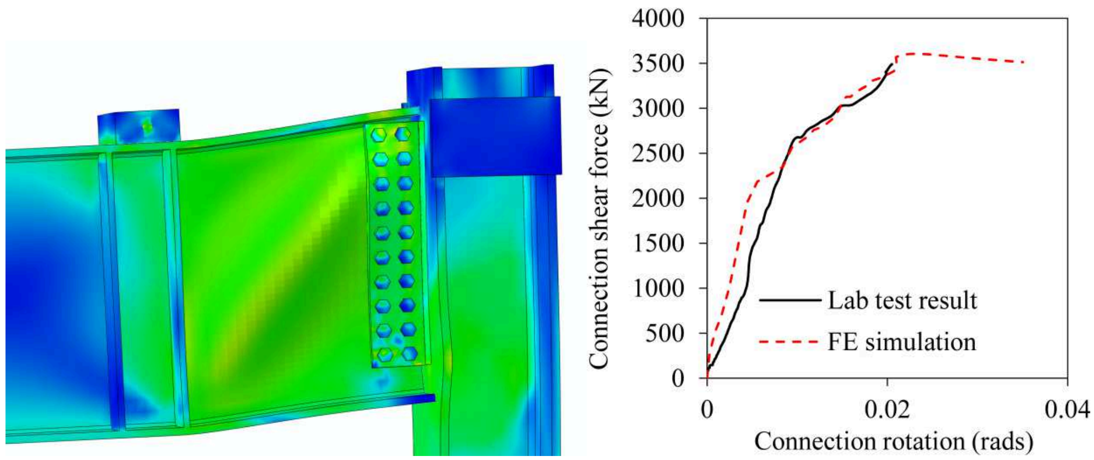

Figure 4.37- Model M15-B FE simulation vs. lab test result of Test M15

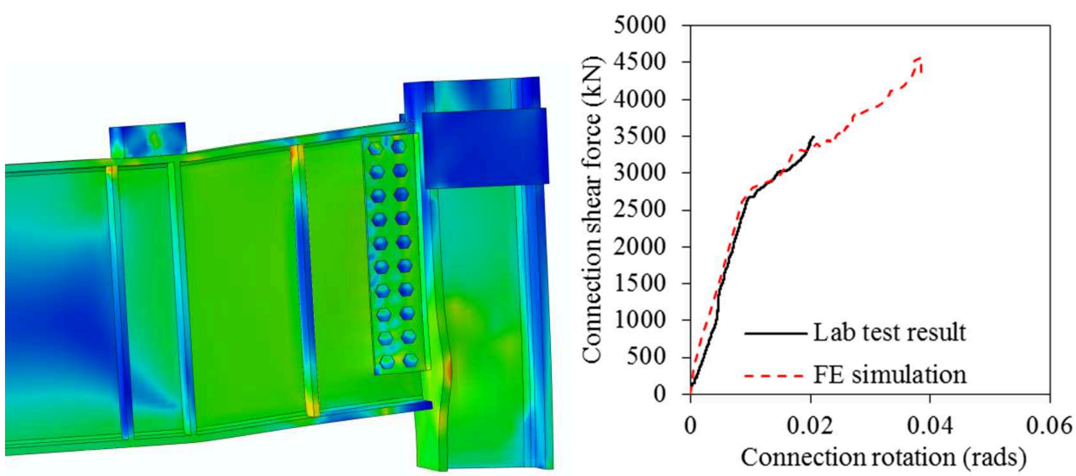

Figure 4.38- Model M15-C FE simulation vs. lab test result of Test M15

4.5. Summary

Finite element models representing six full-scale shear tab connections were created to replicate the laboratory testing procedure and connection configuration of the tests conducted by Marosi (2011). By implementing the FE simulation strategy equipped with the ductile damage for metals model and appropriate material properties it was possible to replicate weld tearing and net area fracture of the shear tab connections. The results showed the capability of the ABAQUS (Simulia, 2011a,b,c) models to closely match the behaviour of the shear tabs with that observed and measured during the testing. This has provided confidence in the models and their potential use for the evaluation of other loading scenarios such as combined axial and shear loading. Table 4.4 provides a summary of the finite element simulation results in comparison with the predicted and test results. As it can be seen from the table, the models provided predictions of the ultimate shear tab resistance with no more than 3% error compared with the measured test results.

Table 4.4- Experimental results compared to predicted values, Marosi (2011).

Test designation	*Predicted resistance based on nominal material properties (kN)*	*Predicted resistance based on actual material properties (kN)*	*Measured test result (kN), Marosi (2011)*	*FE simulation result (kN)*
M1	257	297	363	372
M2	405	424	513	519
M7	676	737	961	954
M8	1334	1476	1734	1787
M13	1323	1531	1762	1741
M15	2887	3515	3489	3596*

Note:

-The resistances were calculated based on the modified AISC method presented by Marosi (2011)

-Nominal refers to the minimum material strength specified for the components.

-Actual refers to material properties obtained from testing coupons extracted from test components

-A resistance factor of 1 was used for calculating the resistances

* FE simulation result of Model M15

Chapter 5

Laboratory testing of shear tab connections subjected to combined shear and axial forces

5. Chapter 5-Laboratory testing of shear tab connections subjected to combined shear and axial forces

5.1. Overview

In order to validate the results obtained from the preliminary FE simulation of the shear tab connections in Phase 2 and improve upon the numerical models in Phase 3 of the research program full-scale experimental work was performed (Phase 4). The response curves of these tests were used to validate the FE simulation of the connections when subjected to combined shear and axial forces. Once the FE simulation results were confirmed and improved by the verification tests, an extended study was performed with the enhanced FE models by using different values of axial loads on the connections (presented in Chapter 6). In this chapter the test methodology, specimens, setup design, stages of loading and outcome of the laboratory testing phase (Phase 4) are explained.

5.2. Methodology

Two shear tab configurations from Marosi's (2011) tests were selected to be tested in this phase. Applying axial load to a shear tab specimen that is undertaking shear force and some moment was extremely complex and expensive, hence a limited number of specimens were included in the scope of study. Each connection configuration comprised two nominally identical specimens, one of which was subjected to an axial tension force and the other an axial compression force, along with the applied shear and moment. To observe the effects of an axial force on the connections that Marosi tested, it was decided to replicate his connection specimens and test set-up in such a way that axial loads could be applied simultaneously; therefore a supplementary load application system was required to apply the axial loads to the connections. The axial load application system (ALAS) and its functionality are explained in Section 5.6. Figure 5.1 illustrates the overall test scheme. A main actuator applied the shear force close to the connection while a second actuator controlled the deflection close to the tip of the beam in order to apply the rotation and moment at the connection. The ALAS was then relied on to apply the axial force to the connection. The loading protocols from Marosi's tests were used to apply the vertical component of load on the connection. The loading protocol for the combined shear and axial forces is explained in Section 5.8.

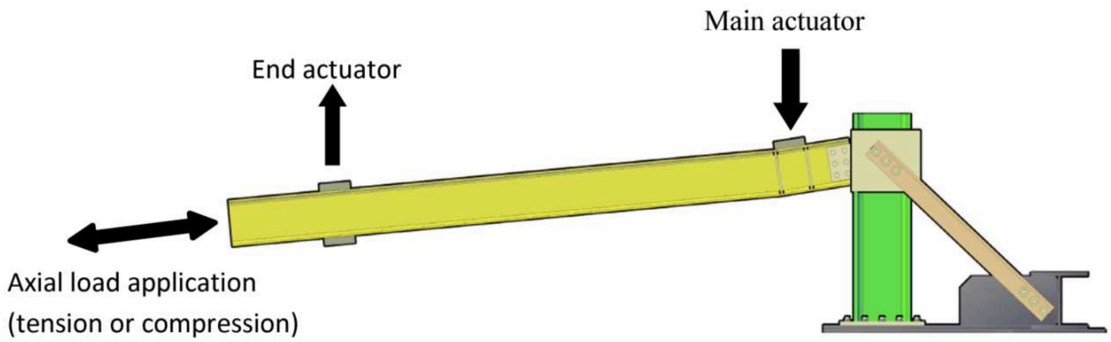

Figure 5.1- Illustration of the overall test setup concept

5.3. Test configurations

The global research program comprised different shear tab connection specimens varying in member size, plate size, number and size of bolts, number of bolts per row and support condition (Marosi, 2011; D'Aronco, 2014) .The shear tab connections shown in Figure 5.2 and described in Table 5.1 were selected to be tested under combined axial and shear forces because they are commonly used in construction. One of the methods to increase the axial capacity of shear tab connections is to use multiple vertical rows of bolts, which was also why these connections were selected for testing. The specimens were designed based on the modified AISC extended approach by Marosi (2011). These connections were not specifically designed for the combined shear and axial force. Instead, two shear tab connections designed for shear alone, and subsequently tested by Marosi, were subjected to combined shear and axial forces to observe and measure the change in behaviour and shear resistance.

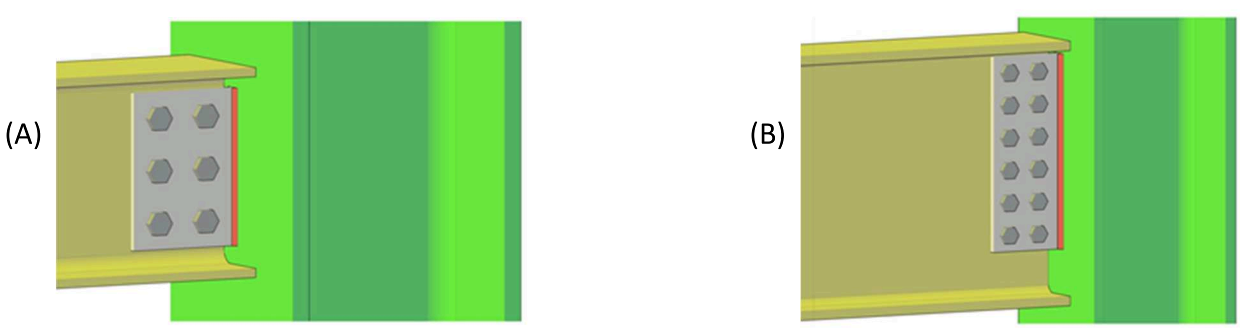

Figure 5.2- (A) Test #1 and #2 shear tab specimens, (B) Test #3 and #4 shear tab specimens

Table 5.1- Shear tab test configurations

Test no.	*#1*	*#2*	*#3*	*#4*
Shear tab dimensions (mm)	225x165x10	225x165x10	456x178x16	456x178x16
Shear tab weld size (mm)	6	6	10	10*
Test beam	W310 x 60	W310 x 60	W610 x 140	W610 x 140
Test column	W360 x 196	W360 x 196	W360 x 196	W360 x 196
Bolt size (mm (in))	19 (3/4)	19 (3/4)	22 (7/8)	22 (7/8)
Number of bolts per vertical row	3	3	6	6
Number of vertical rows	2	2	2	2
Axial load type	Compression	Tension	Compression	Tension
Axial load amplitude (KN)	215	215	512	512

* Weld for test #4 was designed to be 10mm but after the test it was measured to be 5mm

5.4. Coupon extraction and testing

The four combined loading shear tab tests were planned to be used to verify and enhance the finite element models which simulate the same connection and testing procedure. In order to accurately model the shear tab connections, replication of the material behaviour of the specimen components in the FE model was essential. The coupons were extracted from the beams' flanges, three from the web (Figure 5.3-A), and three for each shear tab specimen. These coupons were referred as Series B coupons, coupons that were extracted from the four conducted combined loading tests. The testing was performed based on the ASTM A370-12a Standard (2014) testing protocol. First they were cut into a standard ASTM A370 dog bone shape and measured precisely with a micrometer to determine the necessary dimensions and thickness of the specimens which was required during the data processing.

The coupons were then fixed at the bottom by a hydraulic clamp connected to a strong floor and clamped on top to a hydraulic grip attached to a 1000 kN actuator (Figure 5.3-B). The rate of cross-head displacement was first set at 0.0026 mm/s to capture the elastic region of the material. After yielding and reaching a flat plastic plateau, the rate was increased to twice this speed. Finally after passing beyond the initiation of strain hardening, the rate was changed to 0.026 mm/s for the remaining post plastic region until the point of fracture. Two strain gauges were installed at the centre of the specimen to capture the elastic behaviour, while both the elastic and the post yielding strains were measured by using a 200 mm gauge extensometer installed on the specimen. The installed extensometer reached its stroke limit after slightly passing the ultimate strain in most specimens and was readjusted to aid in capturing the post ultimate behaviour and degradation of the stiffness. However to prevent damage in the extensometer, it was removed from the coupon after about 10%-20% reduction of the stress depending on the possibility of fracture. Details of the coupon data processing and FE modeling are explained in Chapter 4 and a complete description of the material properties can be found in Appendix A.

(A)

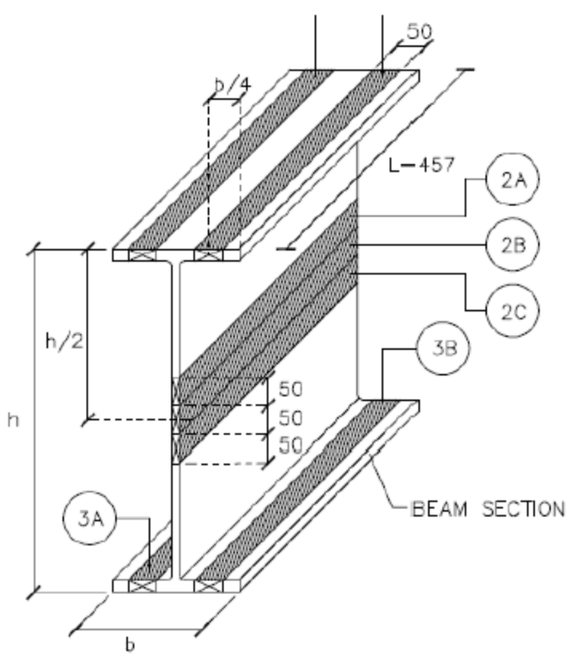

(B)

Figure 5.3- (A) Typical coupon extraction location and dimensions from the test beam (Image courtesy: DPHV) , (B) Clamped coupon specimen during testing

5.5. General shear tab test setup

The shear tabs were shop welded to a W360x196 ASTM A992 Grade 50 (F_y = 345 MPa) column which was connected to the strong floor of the laboratory. Fillet welding was performed on both sides of the shear tab by using a flux-cored arc welding (FCAW) process along with an additional shielding gas (CO_2) and an E71T (480 MPa) electrode. ASTM A572 Grade 50 (F_y = 345 MPa) hot rolled plate was used for the shear tab specimens. The base support structure (Fig. 5.4-A) allowed for the connection of the column baseplate to the strong floor (Fig. 5.4-B). A W360x196 steel beam welded to the top plate was attached to the strong floor using pre-tensioned 38mm diameter threaded rods to minimize horizontal slippage. To minimize column rotation, two 127x127x19 angles were used to brace the connection column to the gusset plates welded on the base support (Figure 5.4-B). This portion of the assembly was identical to that used by Marosi (2011)

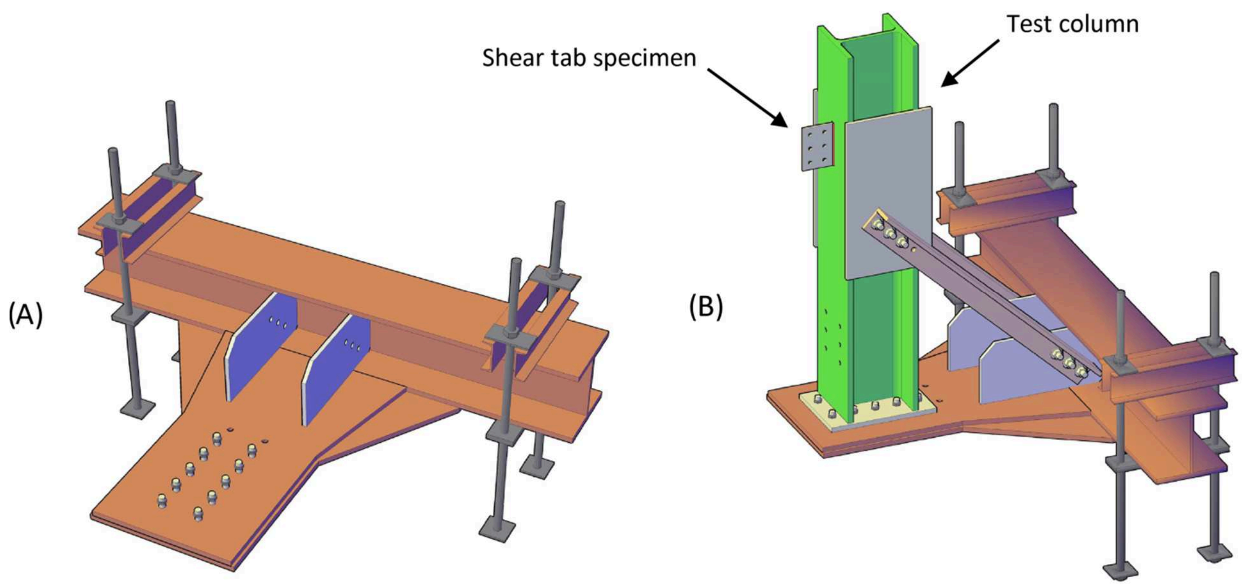

Figure 5.4- (A) Base support structure, (B) Connection column installation

Figure 5.5 illustrates the full test setup design of Specimen #4 which was subjected to combined tension and shear force. It includes the column support assembly, the lateral bracing assemblies and the ALAS. Transfer of forces from the actuators to the shear tab connection was through an ASTM A992 Grade 50 (Fy = 345 MPa) test beam which varied in size and length for different test configurations (Table 5.1). ASTM A325 snug tight bolts were used to connect the shear tab to the test beam; the shear plane did not intercept the bolt threads and the holes in the shear tabs and beams were drilled 1.6 mm (1/16") greater in diameter than the bolts.

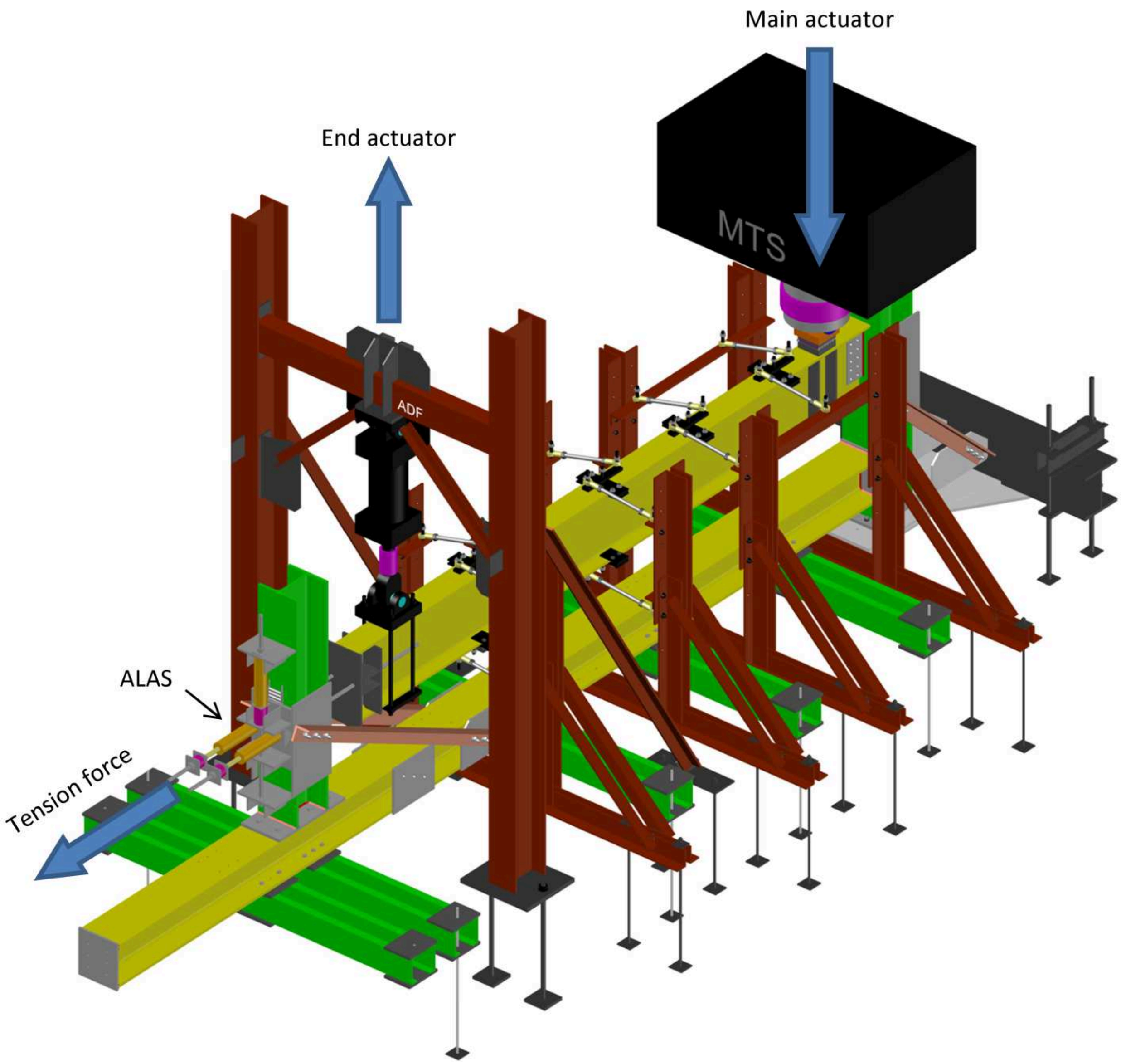

Figure 5.5- Full test setup for Specimen #4 combined shear and tension force shear tab test

The column member was positioned beneath a 12 MN hydraulic actuator, which generated the main shear force in the connection. Compatibility for free rotation and free friction was achieved by using a half steel cylinder, steel plate and roller system between the actuator head and the test beam's top flange (Figure 5.6-A). This system kept the applied force perpendicular to the top flange of the test beam during the testing procedure.

Close to the tip of the test beam (1337 mm for Tests #1 and #2, 512mm for Tests #3 and #4) , a 269 KN hydraulic actuator was suspended from a reaction frame that was fixed to the strong floor; this actuator was used to control the end displacement of the test beam which allowed for the control of rotation at the connection (Figure 5.6-B). This actuator was pinned on top which allowed the test beam to move in its axial direction as it displaced in the vertical direction.

(A) 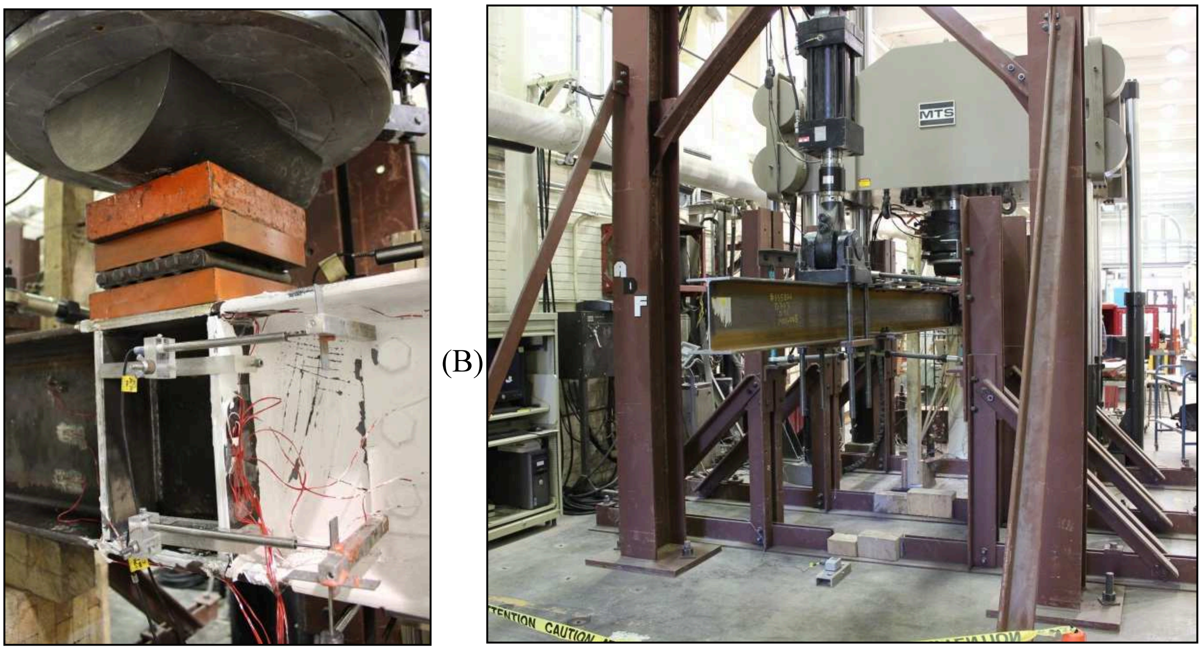 (B)

Figure 5.6- (A) Roller system under the head of the 12 MN actuator, (B) Test beam suspended by the secondary hydraulic actuator (ALAS out of view in background for axial compression loading)

In order to prevent lateral displacement of the test beam's compression flange lateral braces were utilized. Figure 5.7 shows the arrangement of the lateral bracing system with the supporting frame built of double steel angles that were anchored to the strong floor of the laboratory. These braces also simultaneously allowed the test beam to move vertically. This was achieved by using threaded rods with ball and socket joints from the support frames to the bolts on the pivot plates. Close to the connection, positive bending was expected; therefore the top flange of the test beam was laterally braced, whereas nearby the end actuator both flanges (top and bottom) were restrained from lateral movement.

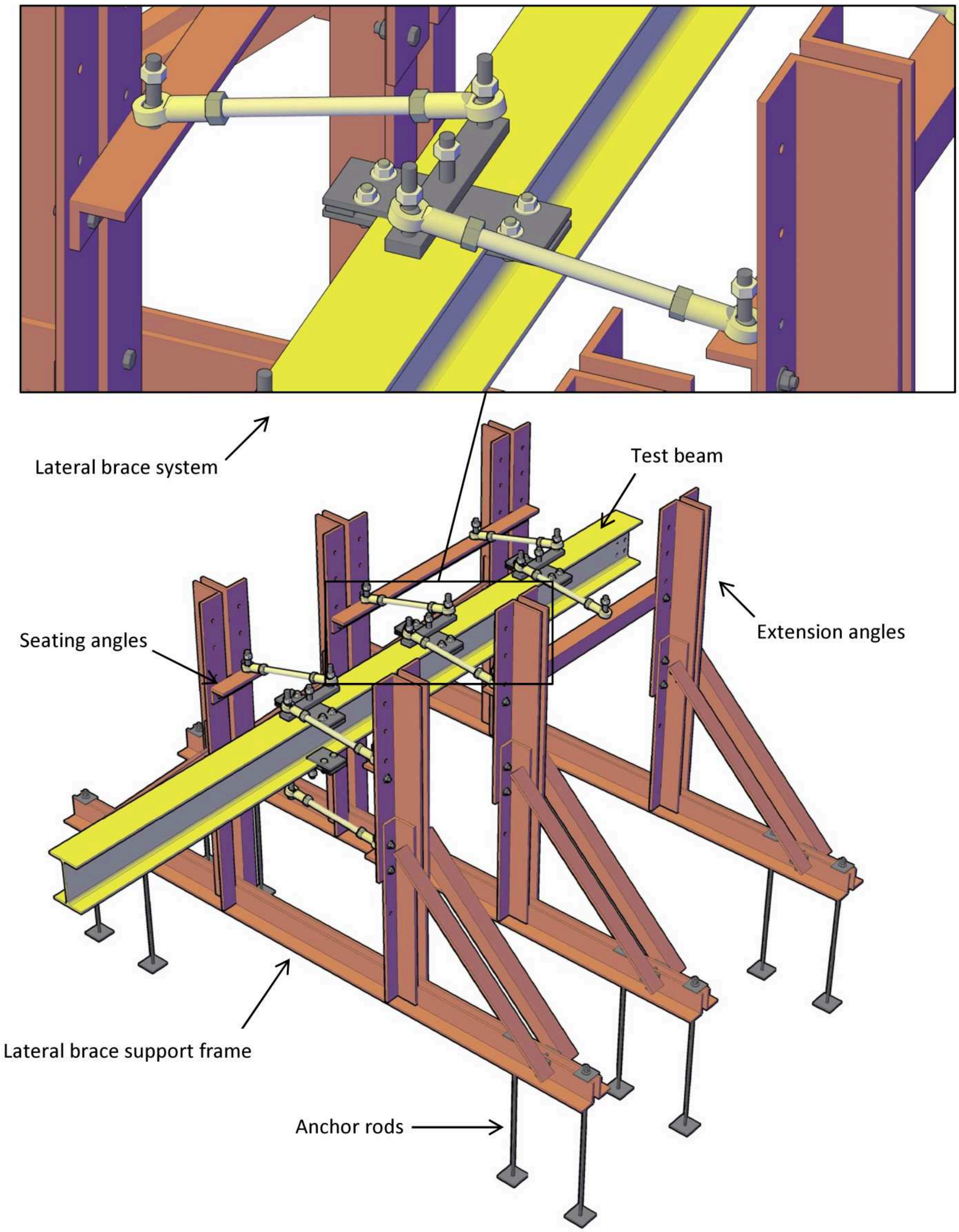

Figure 5.7-Lateral bracing system

5.6. Axial load application system (ALAS)

The axial load application system (ALAS) played an important role in allowing for either an axial tension or compression force to be applied to the shear tab connection. The ALAS was responsible for performing two main tasks. First it was required to apply a stable, controlled and constant axial force to the connection in either tension or compression. Second it was necessary to ensure that the axial force remained normal to the cross sectional area of the beam during the test . The axial force was then transferred through the beam to the shear tab connection. The ALAS was built of various components which functioned together to allow the system to perform these two tasks. Figure 5.8 shows an exploded view of the parts of the ALAS used to apply a tension axial force to the test beam and shear tab connection. Each component and its role are explained below.

In order to generate the required axial force for the tests two Enerpac RRH-3010 (300 KN) double acting hollow plunger cylinders were utilized. The force was transferred from these cylinders to a stiffened region on the test beam's web by using two threaded 31.8 mm (1 ¼") steel rods. These rods passed through a slotted column, aside a roller system, through the moving plate, half cylinder, load cells, axial load jacks and lastly were connected at the ends by an end plate and nut. For proper axial load transfer, these steel rods had to remain in line with the beam, which displaced vertically and rotated, during the testing procedure. To allow free rotation of the rods, a half cylinder steel plate was used to permit the rotation of the axial rods as the beam rotated. The moving plate acted as a moveable support for the half cylinder. The vertical movement of the moving plate was guided and stabilized by means of a vertical 31.8 mm (1 ¼") steel rod which passed through a third Enerpac cylinder, which controlled the vertical position of the moving plate. Two load cells, each with a capacity of 334 kN (75000 lbf) were used to monitor the axial force that was applied to the connection. The system was equipped with two manual hydraulic hand pumps. The first pump balanced the magnitude of the axial load that was applied. A second hand pump was utilized to control the third jack responsible for adjusting the vertical position of the moving plate. A steel roller system was placed between the moving plate and the supporting column eliminating friction and vertical force transfer and allowing only normal force interaction at the interface. Two strips of steel were installed on the moving plate to guide and stabilize its travel. In case of contact between the edges of the moving plate and side plates of the column greased Teflon strips were used to eliminate friction between the two components. The ALAS was used in both tension and compression tests but with different setup as explained in Section 5.7.

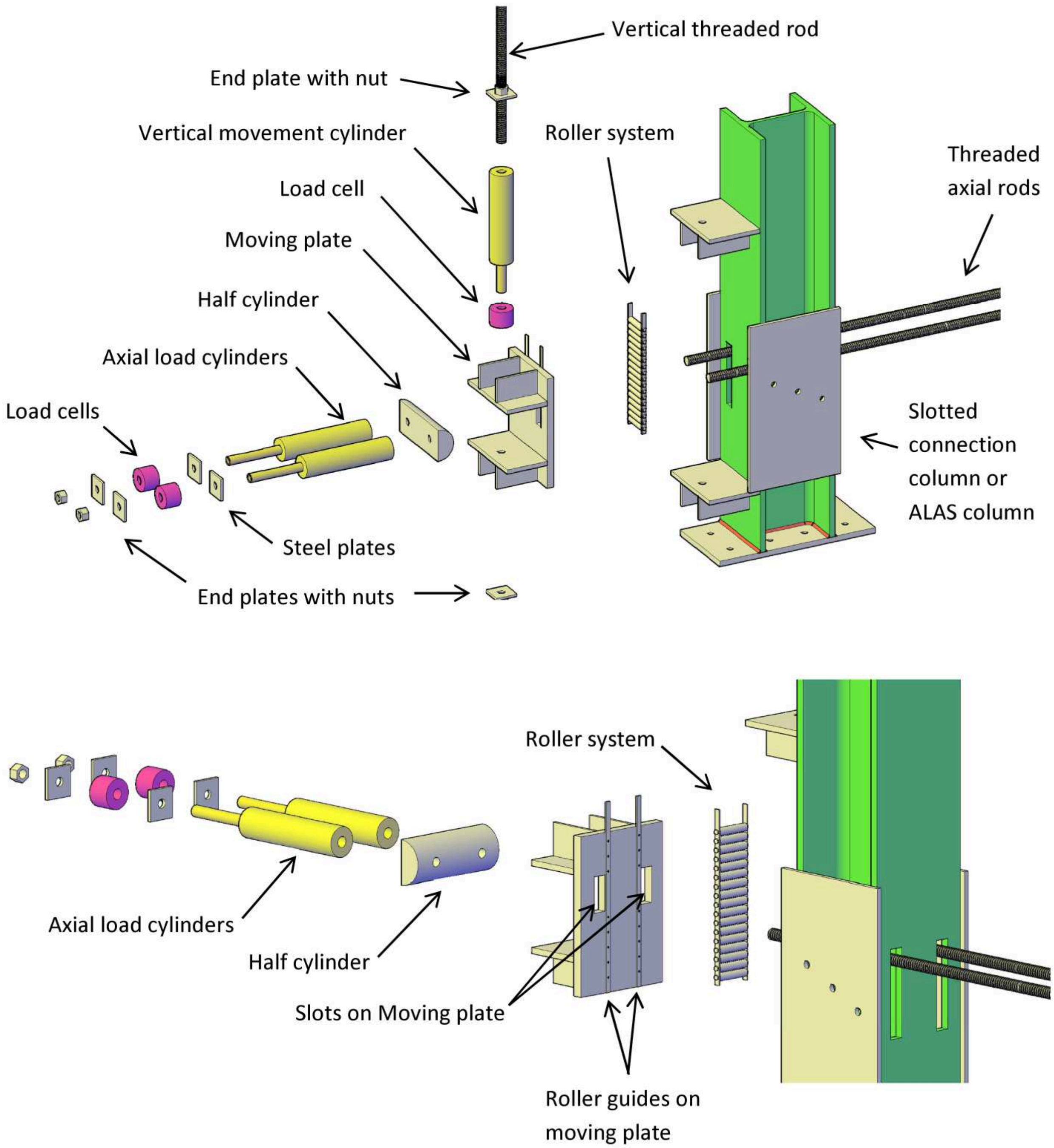

Figure 5.8-Exploded view of the axial load application system component

5.7. Compression and Tension application strategy

In this section the strategy for axial load application to the general test setup is explained. The ALAS generates tension in the axial rods, therefore the installation method for the system to function differs for the combined shear plus compression force compared to the shear plus tension forces. As can be seen in Figures 5.9 and 5.10 the ALAS is directly installed on the slotted connection column for the combined shear plus compression test configurations. Slots were placed in the column flanges to allow the axial rods to pass through and connect the stiffened region on the web of the test beams to the ALAS. As the axial rods extend, the test beam is pulled towards the face of the column therefore a compression force is developed in the connection. With the extension of the axial rods, the downward displacement of the beam and the positive rotation of the beam at the connection, the reaction of the ALAS caused the moving plate to move downward. Therefore the Enerpac jack that controlled the vertical travel of the moving plate was positioned below the moving plate. This simplifies the vertical movement control by extending the cylinder at the beginning of the test and then allowing the jack to retract as the force on the vertical load cell increases which is a sign that the moving plate is attempting to move down. In the compression test setup, the shear tab was expected to undergo high plastic shear yielding and the web of the test beam (between the loading point and the connection column) was also expected to experience some shear deformation. This caused noticeable vertical displacements of the beam close to the column and shows the importance of the vertical movement of the moving plate. If the ALAS lacked this feature, the rods would have bent and the direction of the axial force would not necessarily have been in line with the beam.

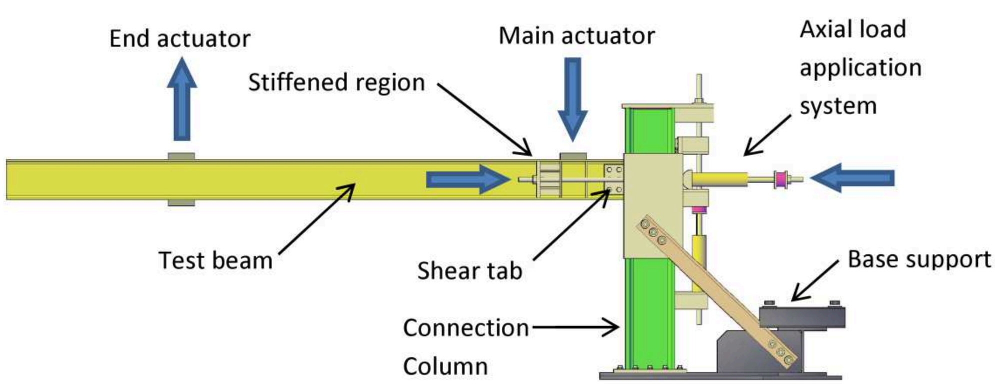

Figure 5.9-Typical setup used for combined shear & compression force shear tab testing (Test #1 shown)

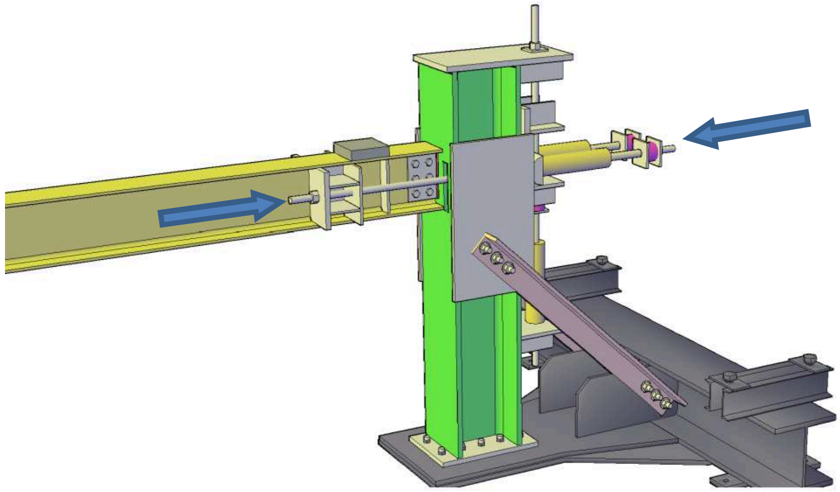

Figure 5.10-ALAS assembly for compression application (Test #1 shown)

The strategy used for the application of the combined shear and tension force was to pull the far end of the test beam, which resulted in a tension force in the connection. In order to apply this tension force a self-reacting frame was utilized such that the horizontal force was not transferred through the strong floor. The self-reacting frame was designed to be compatible for both combined shear plus tension force (Test#2 and Test#4) because they were of different beam lengths. The frame also acted as a support for the secondary slotted column at the far end of the test beam that supported the ALAS. Two angles were used to stiffen the intersection joint of the ALAS column and the self-reacting frame. The forces generated by the ALAS were transferred mainly by these angles to the self-reacting frame; therefore, the frame was subjected to a high axial compression force and bending due to the moment created at the intersection joint. As a result of the rotation at the intersection joint, the self-reacting frame was subjected to uplift forces. Floor beams built of two channels with double side plates at connections were used to perform two main tasks; first was to fill the gap between the self-reacting frame and the strong floor and allow the transfer of uplift forces to the strong floor. The floor beams were connected to the strong floor by using anchor rods to carry the uplift forces, while the bearing of the floor beam's steel plates resisted the compression. Since the self-reacting frame was subjected to combined compression and bending it behaved as a beam-column; hence, it was sensitive to buckling. The second responsibility of the floor beams was to provide bracing for the self-reacting frame so that the unbraced length was reduced which allowed for the selection of a smaller cross section. Because of the change in size and length of the test beam in Test #2 and #4, the number and position of the floor beams changed. For Test #4, five floor beams were required while for Test #2 (shown in Figure 5.11), three floor beams were used. Unlike the combined shear plus compression tests, the moving plate would have moved upward as the axial rods were placed in tension due to the inclination of the beam. It was therefore necessary to install the vertical Enerpac jack above the moving plate to force it to move vertically downwards as the tip of the test beam was lowered using the 269 kN end actuator. In a similar manner to the compression tests the movement of the vertical plate and axial force in the beam were controlled manually based on the displacement and load cell readings, respectively of the ALAS. Figure 5.12 demonstrates the installation of the ALAS on the ALAS column.

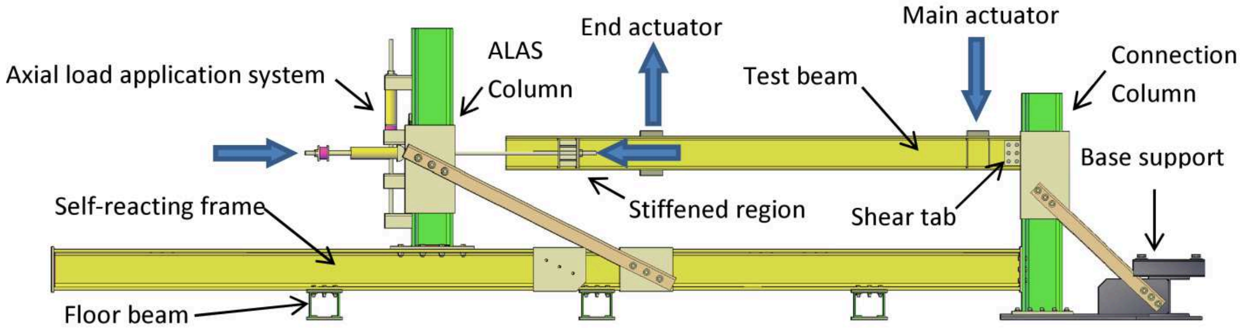

Figure 5.11-Typical setup used for combined shear & tension force shear tab testing (Test #2 shown)

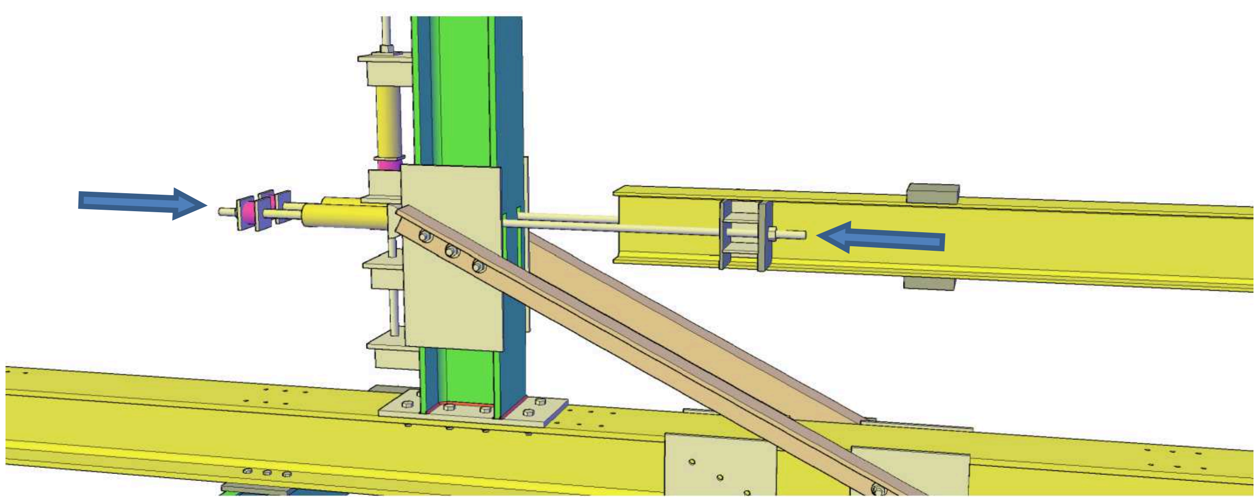

Figure 5.12-ALAS assembly for tension application (Test #2 shown)

In the combined tension plus shear force tests (Test #2 and Test #4), the hydraulic cylinder was positioned on top of the moving plate. Therefore the ALAS was suspended temporarily at the initial stage of the testing (Figure 5.13-A) prior to the application of the axial force. With the application of the axial load, the straps were released and the system remained stable. This was not the case for the combined compression plus shear force tests (Test #1 and Test #3) because the cylinder was extended at the initial stage, supporting the moving plate from below (Figure 5.13-B).

(A)

(B)

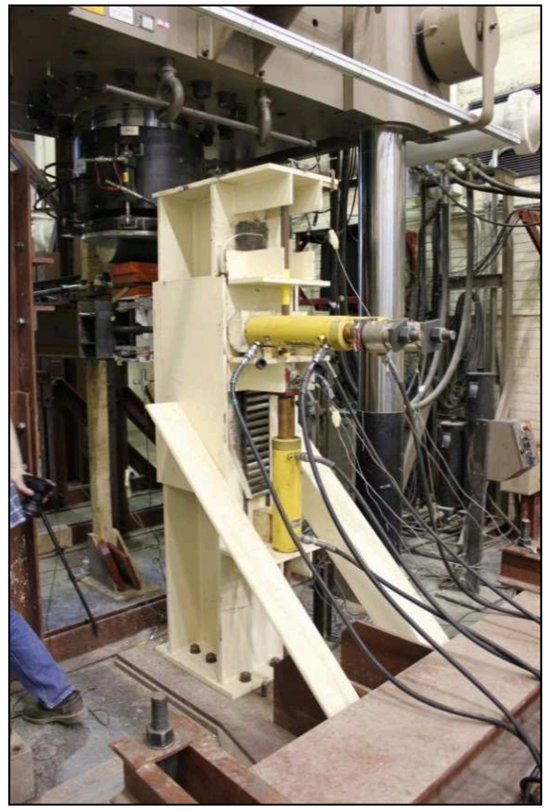

Figure 5.13- ALAS installation; (A) compression tests (Test #1 shown), (B) tension tests (Test #2 shown)

The shear tab plate for specimens #3 and #4 was installed with a slight vertical eccentricity to the mid-height of the test beam to comply with the standard distance used in steel detailing of 3” (76 mm) from the top-of-steel to the first bolt hole. That is, the shear tab edge was closer to the top flange of the test beam than the bottom flange. The axial force for these two tests was applied at the centre of the bolt group instead of the centroid of the beam’s cross-section, whereas for specimens #1 and #2 the line of action of the axial load coincided with the centroid of the beam’s cross-section and the bolt group since the shear tab was placed at the mid-height of the beam.

Figure 5.14 shows the final setup used for each test; further details such as dimensions, erection and shop drawings can be found in Appendix C.

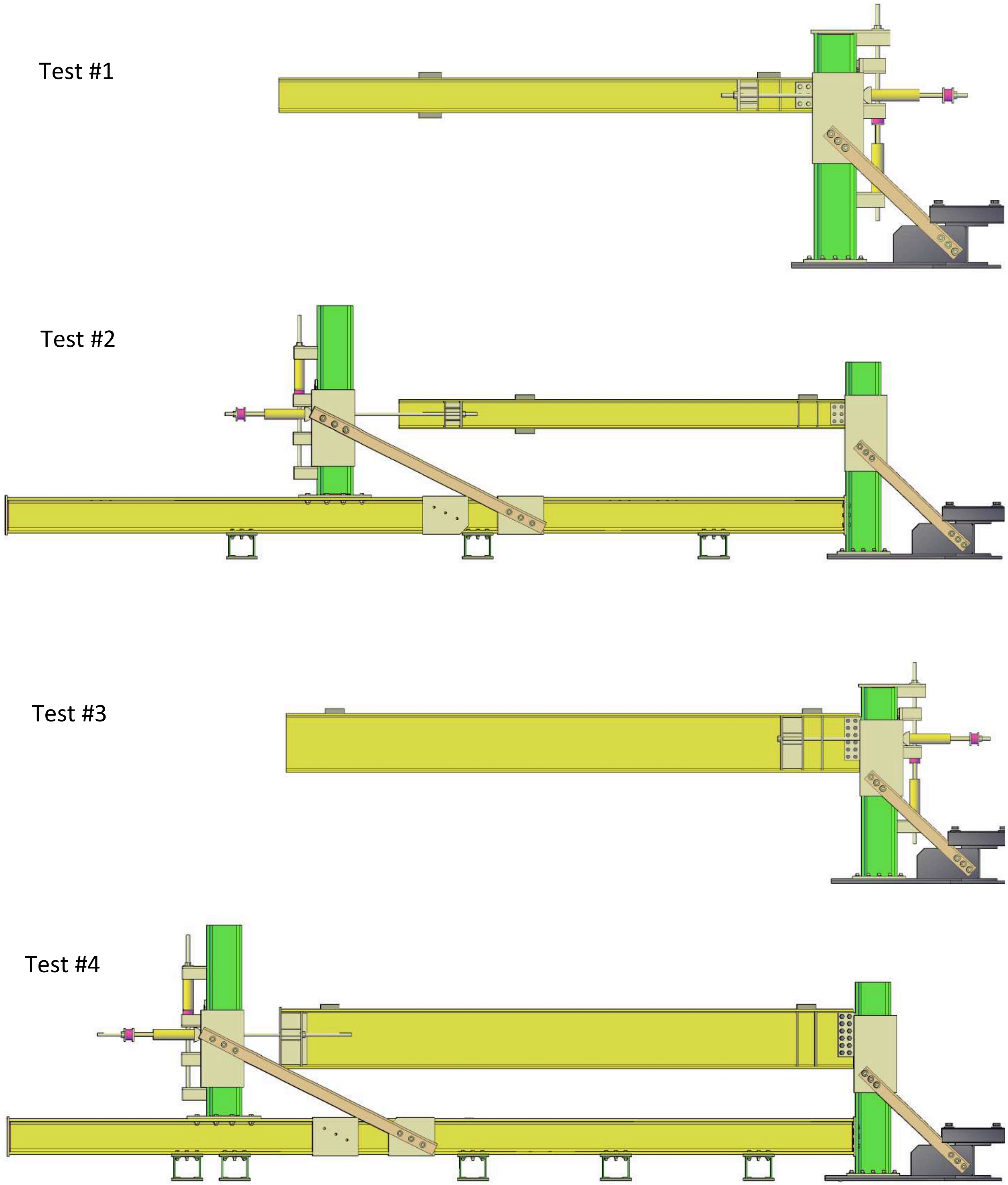

Figure 5.14-Final setup configuration designed for each test

5.8. Loading protocol

In order to have comparable results with the tests conducted by Marosi (2011), the same vertical load protocol was used. Marosi used a target rotation of 0.02 rads for the W310 beam connections and a target rotation of 0.015 rads for the W610 beam connections at the predicted ultimate shear resistance of the shear tab specimens. In addition to the shear loads an axial load was simultaneously applied in order to observe the change in behaviour and resistance of the specimens. The concept behind the load protocol for the axial load application was inspired by a typical beam during its lifespan which is normally subjected to gravity service loads until a stage where axial load may occur due to different possible sources such as wind, earthquake or other possible actions. Therefore a service level shear load was selected based on a statistical study and the global force vs. displacement response plots from Marosi's tests. Figure 5.15 illustrates the time of axial load application based on two tests from Marosi.

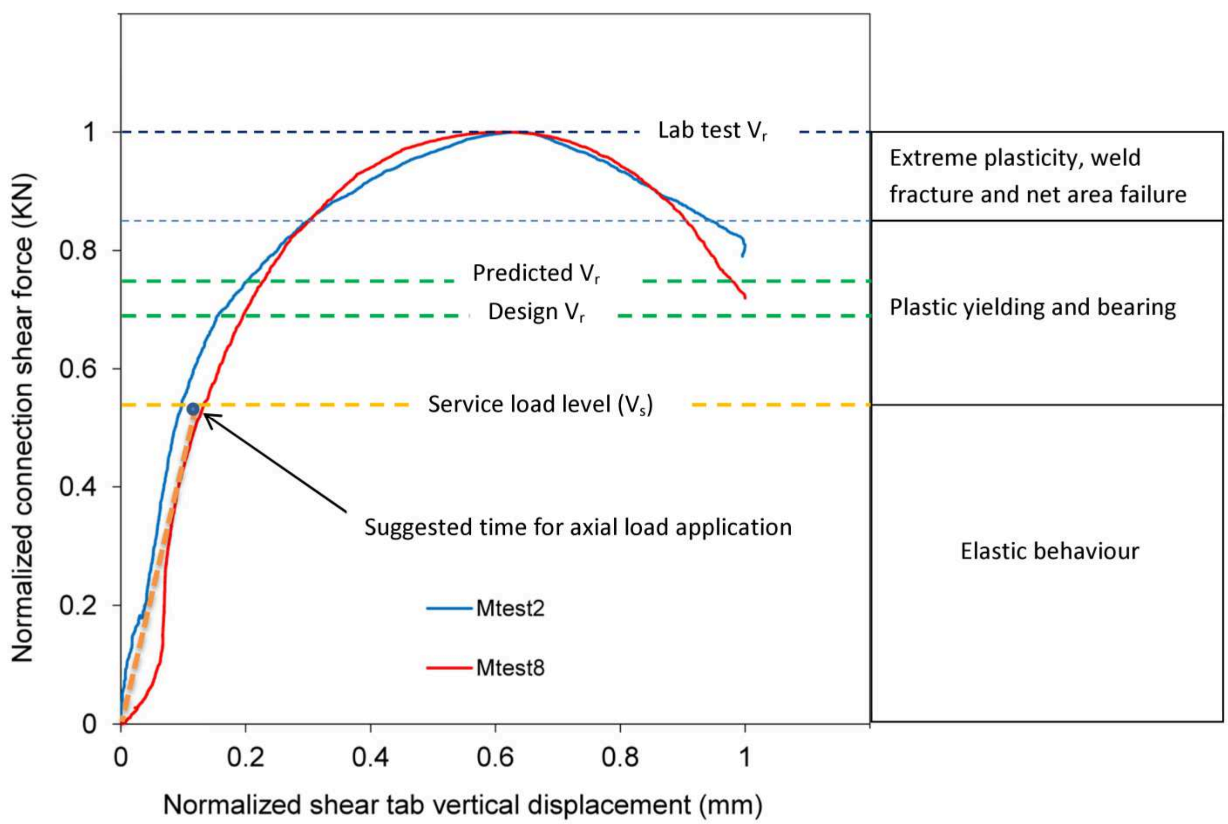

Figure 5.15-Representation of the axial load application time based on Marosi's tests (2011)

The vertical axis shows the shear force in the connection normalized to the ultimate shear resistance determined by full-scale lab testing. In a similar manner the horizontal axis represents the normalized deformation (vertical displacement) of the shear tab. The behaviour of the shear tab was classified into three regions based on the observations of Marosi (2011). With the initiation of vertical loading, the shear tab behaved elastically until it reached a normalized deformation of about 10% to 15% with a shear force level which was assumed to be the service load level. By continuing the vertical loading protocol, bearing around the holes, shear and flexural yielding was observed in the shear tab and the material softened leading to higher deformations. After significant deformation of the connection the weld between the shear tab and column started to tear and high stress between the bolt holes developed which led to fractures in the shear tab. The connections reached their ultimate resistance at approximately 65% of the total vertical displacement of the shear tab. By continuing the vertical loading, the shear tabs were still able to carry shear force but at a diminishing level because of the damage propagation in the shear tab.

Based on the information shown in Figure 5.15 and test results from Marosi, it was observed that the connection mainly behaves elastically before reaching a service load level of approximately 0.66 V_{ra} or 0.72 V_{rn}; where V_{ra} is the predicted ultimate shear resistance of the shear tab calculated using the modified AISC method recommended by Marosi (2011) and using $\phi = 1$ with measured material properties obtained from coupon testing. V_{rn} is also the predicted ultimate shear resistance of the shear tab but by using nominal material properties instead of measured. The point in the protocol when the axial load was applied was selected to be when the shear force in the connection reached the service load level; after which the axial force remained constant until final failure of the shear tab. For these series of tests, 0.66 V_{ra} (calculated based on the coupon tests that Marosi had conducted) was used for the load level at which the axial load was applied. Real-time monitoring was used during the testing procedure. Once the measured connection shear force reached the service load level, the actuators were stopped and temporarily held in their displaced position. The axial load was then applied gradually until the predetermined force level was reached. At this point in the testing protocol the axial load was held constant under force control and the vertical actuators were restarted at the same displacement rate as was being applied prior to their stoppage. The axial force used for Tests #1 and #2 was 215 kN, whereas 512 kN was applied for Tests #3 and #4. These axial force levels were selected based on different factors; first the force was required to be large enough to affect the connection's ultimate shear resistance. Based on an initial finite element investigation, if a small axial load was applied, the shear resistance would not have been significantly affected. Second the upper limit of the force was dependant on the axial capacity of the ALAS's cylinders and finally the axial load shouldn't be too large, failing the connection before continuing the vertical loading protocol. The possible axial force in a connection can vary significantly, therefore the test results only provide four data points of the intended interaction curves. The rest of the points of the interaction curves (for different axial force levels) were determined by using the FE simulation explained in Chapter 6.

5.9. Instrumentation

The instrumentation was selected and positioned in order to measure horizontal displacement, vertical displacement and rotation of the shear tab, beam and column, along with strains and forces in the connection. In order to have the ability to compare the response of this series of tests to those conducted by Marosi (shear tabs subjected to only vertical loading), the same instrumentation plans from Marosi with some modifications were used.

The actuators were equipped with internal load cells which measured the force that passed through each actuator. The connection shear force was calculated based on the readings from these load cells. Real time monitoring was used; therefore the connection shear force was monitored throughout the testing procedure. Three other load cells were used in the tests; the first one was used under the vertical cylinder which controlled the vertical force component of the moving plate in the ALAS (Figure 5.17-A). This information showed the tendency of the moving plate to move vertically. The other two load cells were used to monitor the axial force in the test beam and ultimately in the connection. (Figure 5.17- B). A separate display was provided for the axial load operator to control and keep the axial load level constant throughout the test. The actuators were also equipped with internal LVDTs, measuring the vertical displacement at their location throughout the testing procedure.

For redundancy purposes an additional vertical displacement measurement of the test beam was performed by placing a string potentiometer under the test beam at the end actuator position. This string potentiometer measured the vertical displacement of the test beam. A second string potentiometer was used to measure the horizontal movement of the test beam. The application of tension on the retracting frame used in Tests #2 and #4, was predicted to significantly deform the connection column, therefore a third string potentiometer was used to measure the horizontal movement of the connection column (Figure 5.17-C). Figure 5.16 illustrates a typical instrumentation plan showing the position of the main three string potentiometers used in Test #1 and test #2. Complete details of the instrumentation type and positions used for the performed tests can be found in in Appendix B.

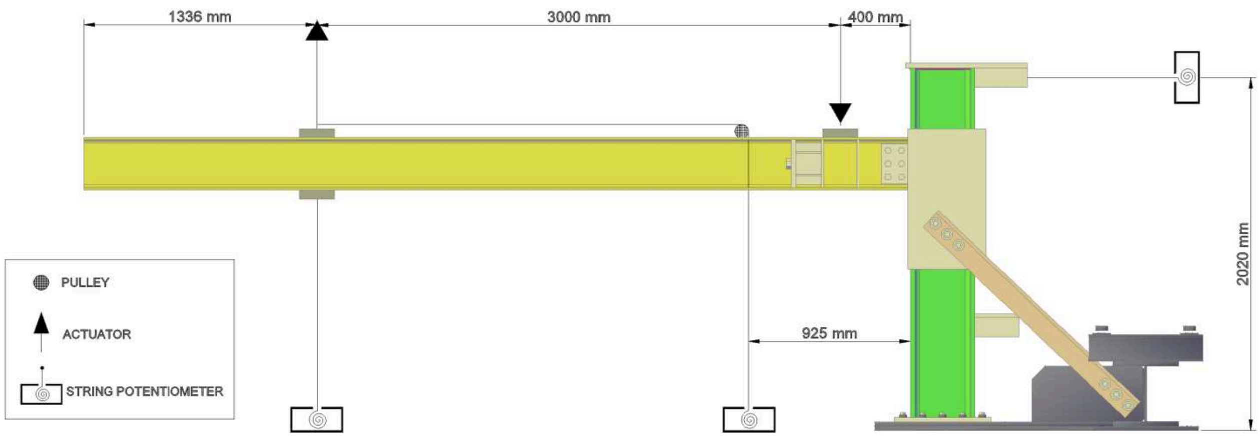

Figure 5.16- Position of the actuators and string potentiometers used in Test #1 and #2

A fourth string potentiometer (not shown in Figure 5.16) was used to measure the vertical displacement of the moving plate used in the axial load application system (Figure 5.17-A). For the combined compression and shear force tests it was directly installed on the connection column, but for the combined tension and shear force tests it was installed on the ALAS column. The reading from this potentiometer was used in controlling the position of the moving plate and minimizing bending in the axial rods.

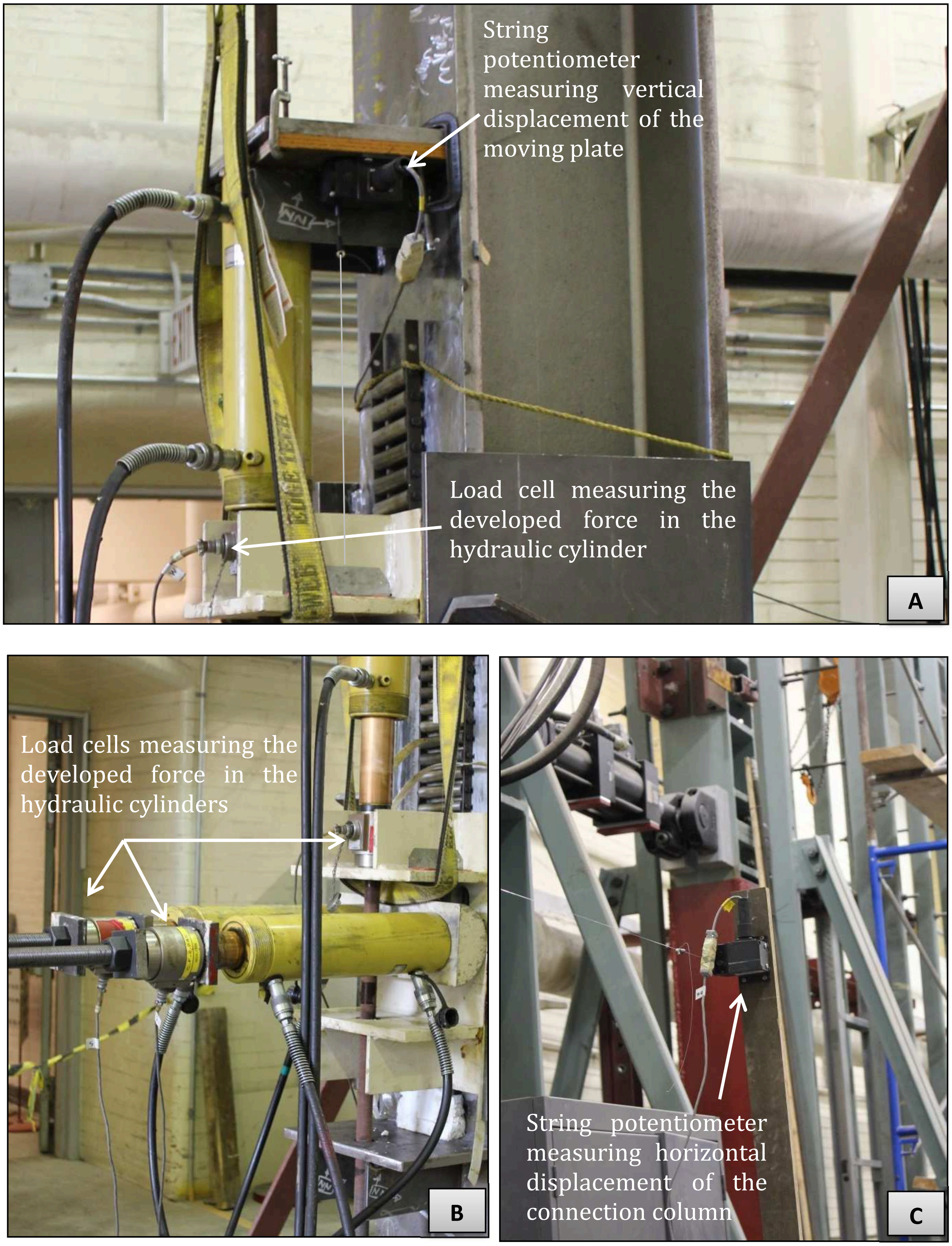

Figure 5.17-(A) Load cell and string potentiometer used for the moving plate, (B) Load cells used in the ALAS ,(C) String potentiometer installed on an external stand

In addition to string potentiometers, LVDTs (Linear variable differential transformer) were utilized to measure smaller displacements at locations close to the connection. Based on the required measurement range, two different types LVDTs were used. The first type had a stroke of +/-15 mm which were used to measure smaller displacements. The second type had a stroke of +/-25mm. Figure 5.18 to 5.20 shows different LVDTs positions prior to testing. Each LVDT application and purpose is explained below.

The shear tab's relative rotation to the test beam was measured by using two +/-25mm LVDTs installed on the stiffener of the test beam (Figure 5.18-B and 5.20-A). The connection's relative rotation to the column was measured by two horizontal +/-15 LVDTs installed on the top and bottom flange of the test beam close to the column face (Figure 5.18-B). The absolute (relative to the ground) vertical displacement of the test beam close to the connection was measured by using a +/-15 mm LVDT installed on an external stand underneath the bottom flange of the test beam (Figure 5.19-A). In the same manner the absolute shear tab vertical displacement was also measured by using a +/-15 LVDT on an external stand beside the test beam (Figure 5.18-B). To reduce the chance of slippage, the external stand was braced and weights were placed on its base. In order to measure the twist of the beam at the connection, two +/-25mm LVDTs were used to measure the lateral displacement of the top and bottom flange of the test beam. These LVDTs were installed on an external stand behind the test beam. (Figure 5.19-B).The final LVDT used was a +/-15 LVDT on an external stand beside the connection column which measured the absolute vertical displacement of the connection column (Figure 5.19-C). The application of axial force on the connection would possibly affect the readings from the LVDTs that were used to measure the rotation of the connection; therefore, for redundancy, digital inclinometers were installed on the top flange of the test beam and on the column face to measure the absolute rotation of the connection column and test beam (Figure 5.18-A). To measure strain, strain gauges were glued on different locations of the shear tab (Figure 5.20-A) as well as the web of the test beam (Figure 5.20-B). To visually demonstrate the progress of plastic yielding, a white lime compound was applied on the shear tab specimen and its surrounding region. The instruments were connected to Vishay Model 5100B scanners to record data at a rate of two readings per second (Figure 5.20-C). Vishay System 5000 StrainSmart software was used to control the data acquisition system.

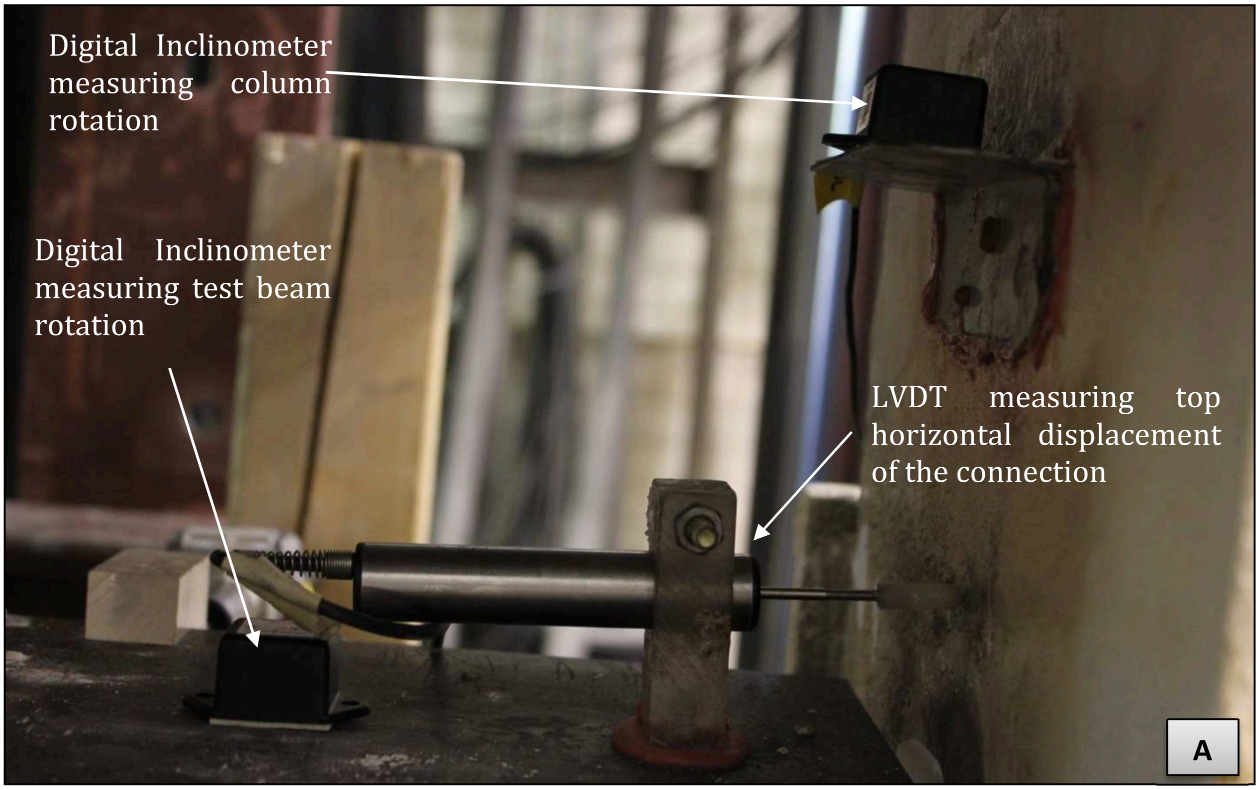

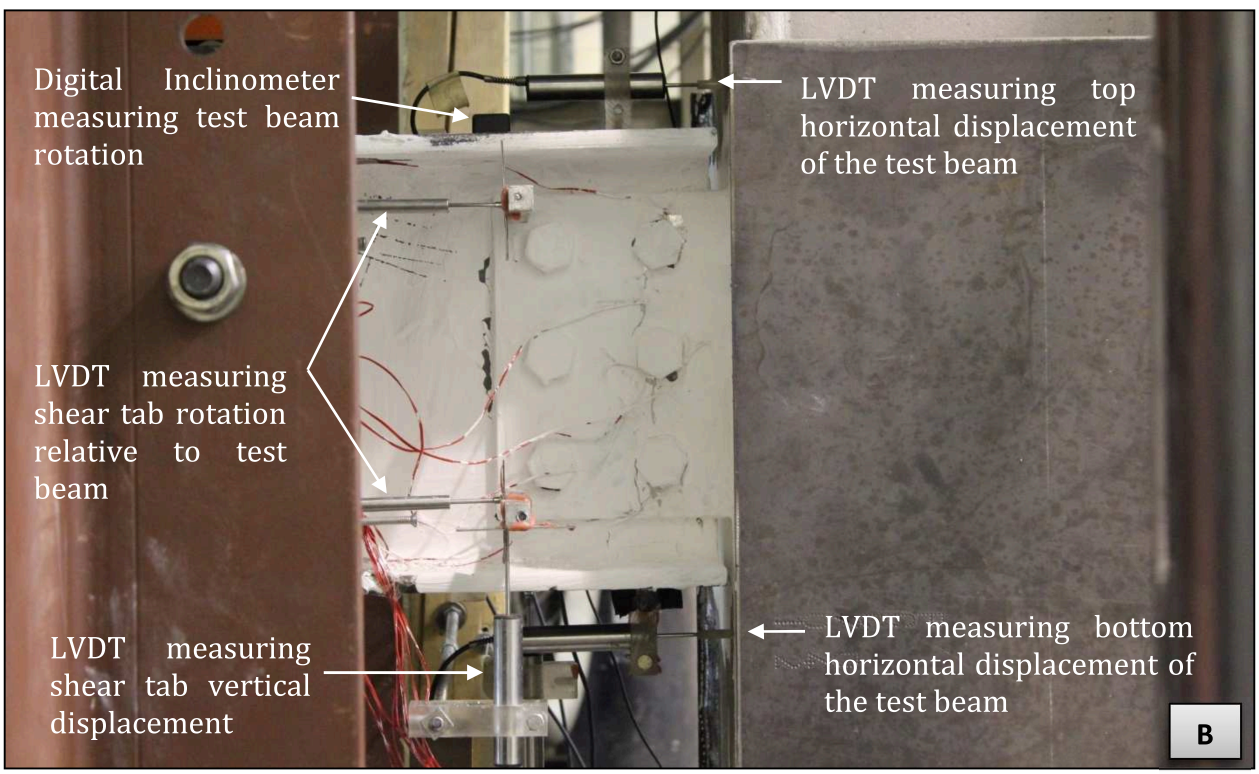

Figure 5.18-(A) Typical instrumentation installed over the test beam, (B) Typical LVDT arrangements and applications used for instrumentation

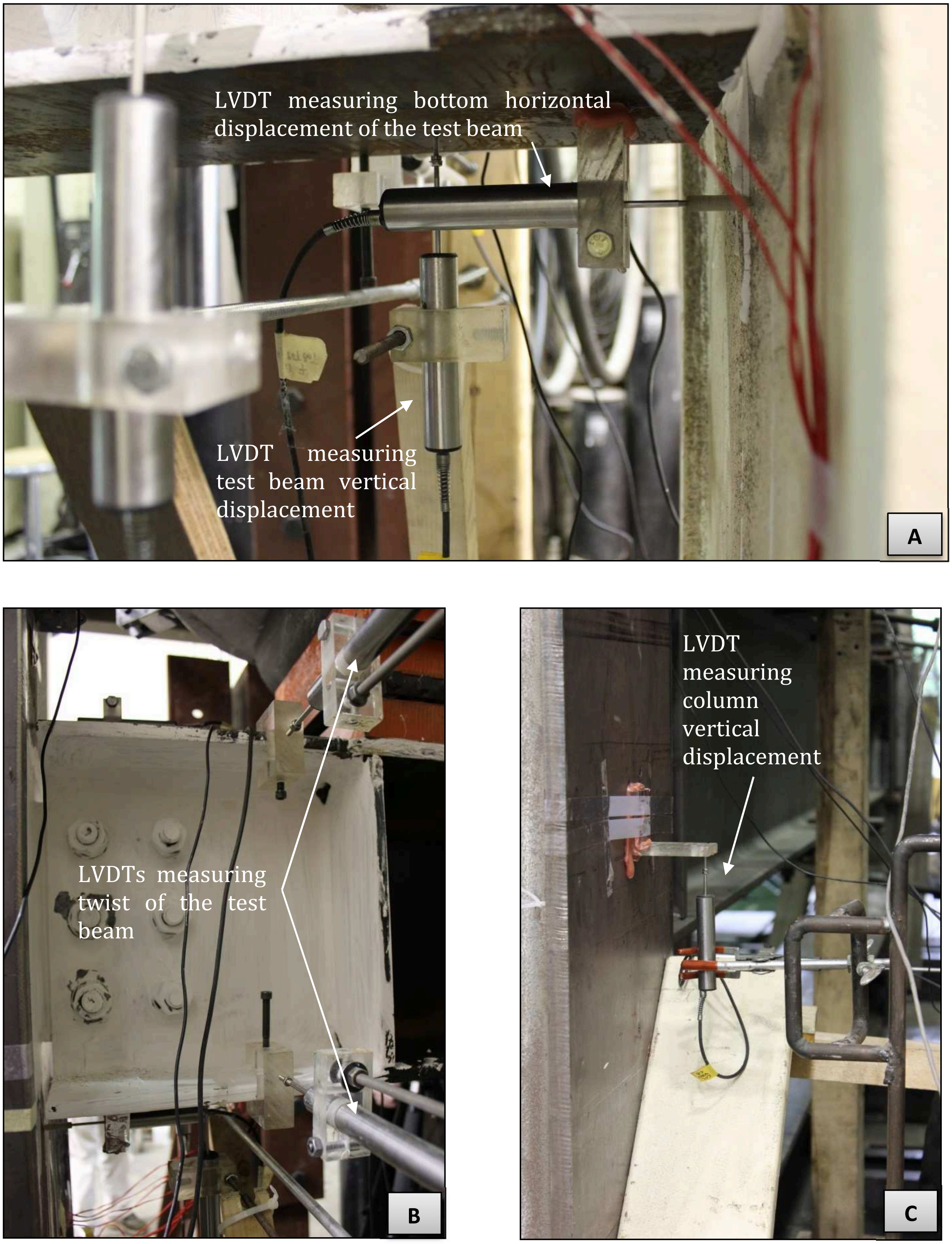

Figure 5.19-(A) Typical instrumentation installed beneath the test beam, (B) Typical LVDTs used for measuring beams twist, (C) LVDT used for measuring column vertical displacement

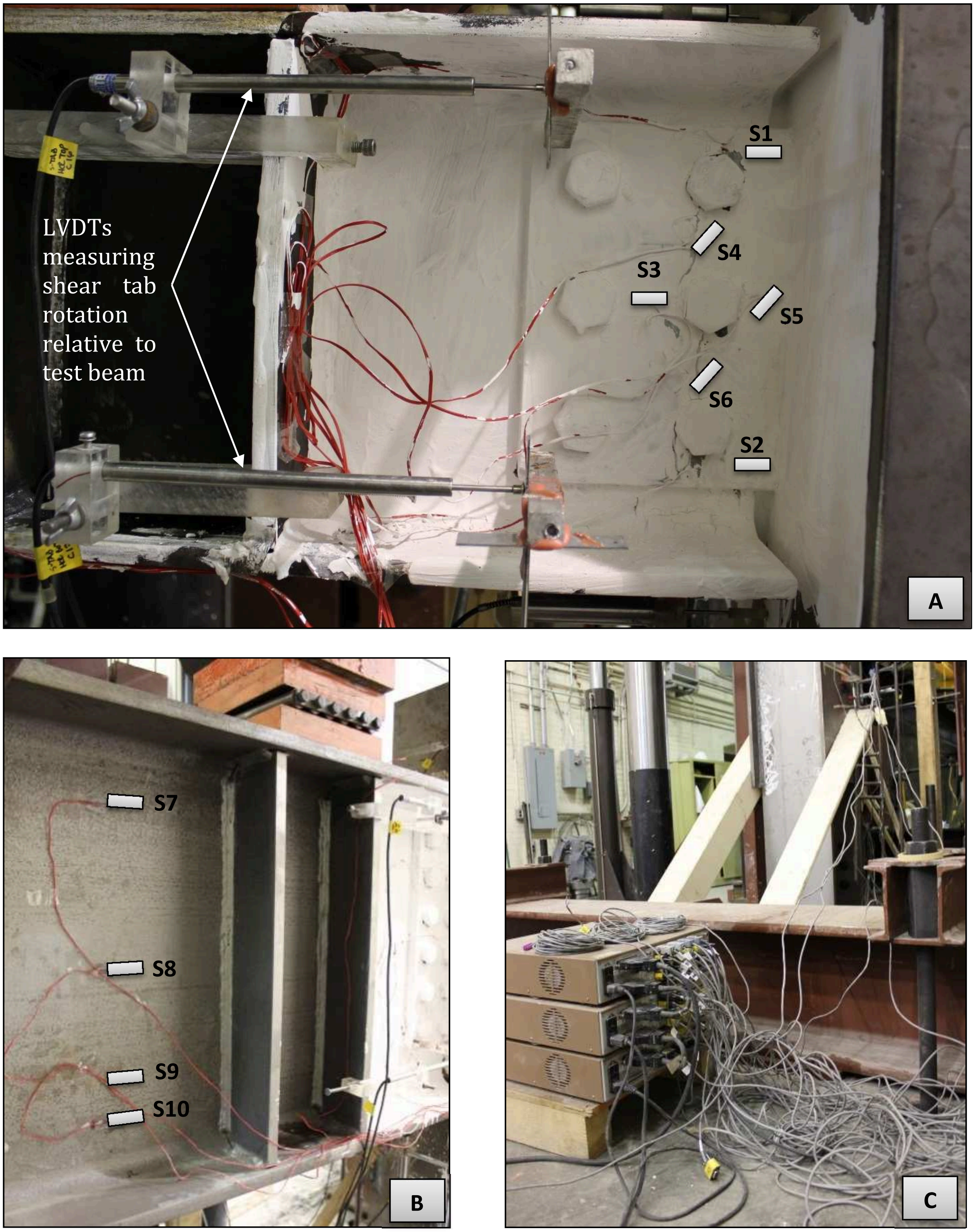

Figure 5.20- Typical strain gauge arrangement on (A) the shear tab (Test #2 shown), (B) the web of the test beam (Test #4 shown), and (C) Data acquisition boxes used for signal processing

5.10. Test results

The damage progression of the tested specimens, excluding Test #4, was very similar to that observed by Marosi (2011) for the shear tabs subjected to vertical loading alone. Flexural and shear yielding was observed in the shear tab, followed by a tear in the connecting weld after excessive yielding. Despite the fact that the weld started to tear, the connection was still able to carry loads by redistributing the stresses. Figure 5.21 shows the final deformed shape of the shear tabs at the end of testing. These can be compared with the same specimens as tested under shear loads alone by Marosi in Figure 5.22.

Observations of the compression and shear force tests (Test#1 and #3) showed that by continuing the loading protocol, regions on the first line of bolts on the shear tab strain hardened and cracks developed in the net area between the holes. Excessive bearing was also observed around the shear tab holes and some tearing in the connecting weld. On the other hand, Test #2 and #4 (combined tension and shear force) showed that the shear tab's final post-ultimate behaviour was governed mainly by the performance of the connecting weld to the support column.

Despite the fact that the same material and vertical loading protocol from Marosi was used for Test #1 and #2, the response of these tests resulted in significant higher ductility compared to Marosi's tests. Due to the lack of stroke at the end actuator, the testing had to be stopped after the connection shear force started to drop. Based on the coupon test results, the material used for the shear tabs had an 18% higher yield stress, 22% higher strain hardening strain, same ultimate stress and fracture strain compared to Series A coupons (extracted from the test components of Marosi). The second factor that could have affected this additional ductility was the performance of the connecting weld. The fabricated weld size, material behaviour, welding quality, temperature and welding stages could have differed to the welding conditions used by Marosi.

Test #3 revealed a similar final deformed shape and ductility in comparison with Marosi's test result with a 10% gain in shear resistance. Test #4 did not deform as expected and failed by complete weld rupture. The reason was later identified to be the shop weld of the shear tab to the column. It was 5mm instead of 10mm therefore the shear tab did not perform as designed and failed at less than 60% of its shear capacity (with a full size fillet weld) which is very close to the suggested service load level.

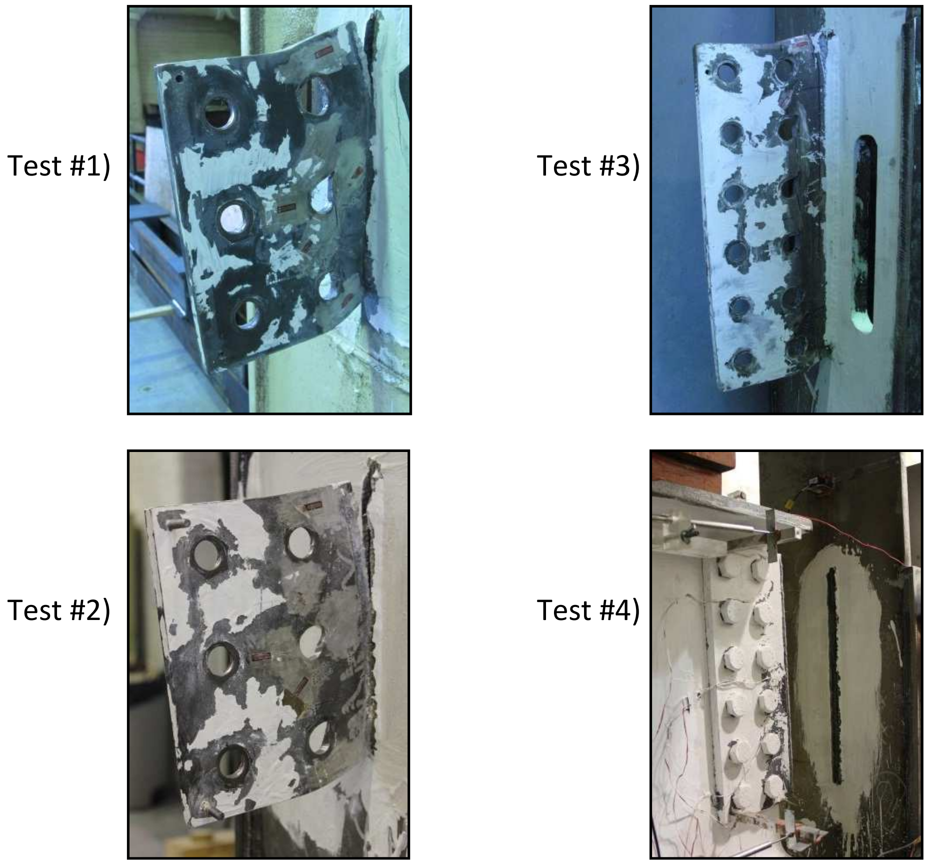

Figure 5.21-Final deformed shape of each of the four shear tab specimens subjected to combined shear and axial forces

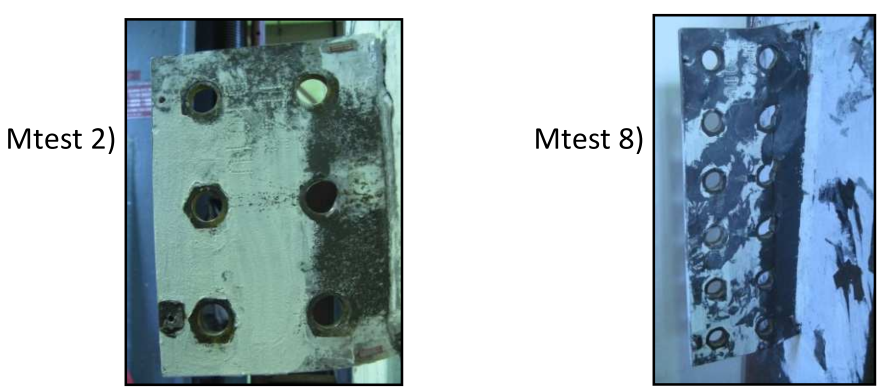

Figure 5.22- Final deformed shape of the corresponding shear tab specimens subjected to only shear load (Marosi, 2011)

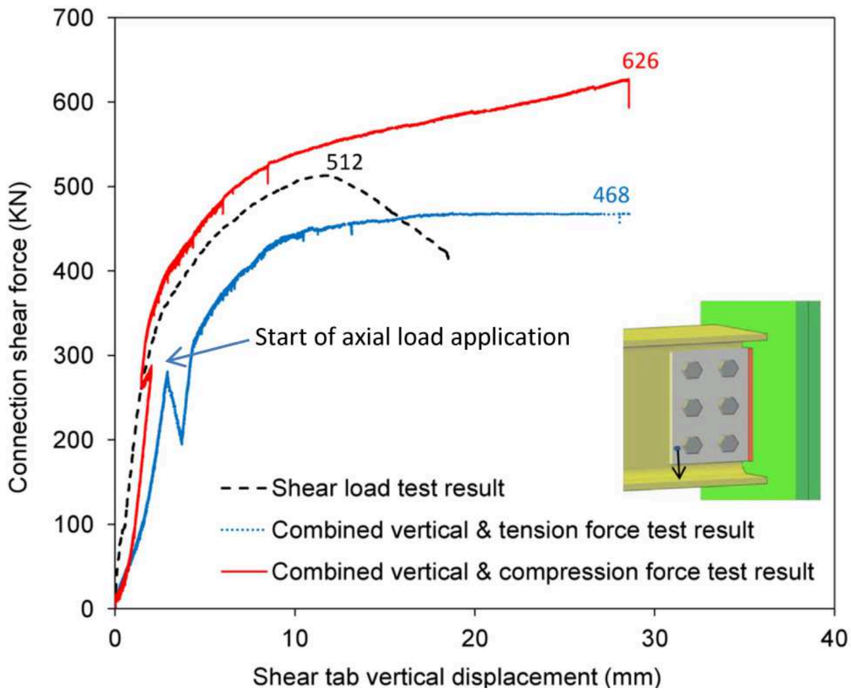

Figure 5.23-Shear tab connection shear force vs. vertical displacement test results for W310 beam connected by two vertical rows of three 19 mm (3/4") A325 bolts

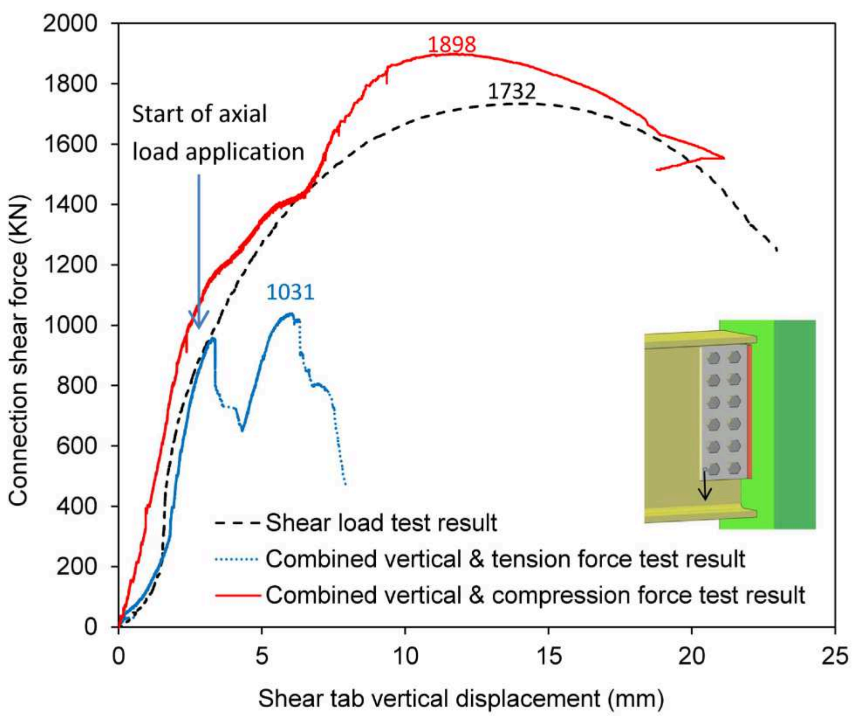

Figure 5.24- Shear tab connection shear force vs. vertical displacement test results for W610 beam connected by two vertical rows of three 22 mm (7/8") A325 bolts

A summary and comparison of the shear tab test results with those from Marosi (2011) are shown in Table 5.2. The shear tabs in Tests #1 and #2 vertically deformed almost 1.5 times more than the same shear tab subjected to only vertical loads (Figure 5.23). Unlike the first two tests, Tests #3 and #4 resulted in a lower vertical displacement (Figure 5.24). In terms of rotation the first three tests experienced a higher rotation level at the end of the test. Test #4 was also predicted to achieve higher deformations but due to the fabrication error, the specimen did not perform as expected. Overall as predicted, the compression force in the connection increased the shear capacity whereas the tension force decreased the shear resistance.

Table 5.2-Overall test results

Test no.	*#1*	*#2*	*#3*	*#4*
Axial load type	Compression	Tension	Compression	Tension
V_r for vertical load (KN) (Marosi.(2011))	512	512	1732	1732
V_r for combined forces (KN)	626	468	1898	1031*
Maximum connection rotation for vertical loading (rads) (Marosi.(2011))	0.042	0.042	0.033	0.033
Maximum connection rotation for combined forces (rads)	0.066	0.049	0.037	0.013*
Maximum shear tab vertical displacement for vertical loading (mm) (Marosi.(2011))	18.4	18.4	22.6	22.6
Maximum shear tab vertical displacement for combined forces (mm)	28.5	27.6	20.63	7.95*
Change in ultimate shear resistance (%)	22%	-8.60%	9.60%	-68% *

* Weld for test #4 was expected to be 10mm but after the test it was measured 5mm

5.11. Conclusions

A series of four full-scale tests were performed on double vertical row bolted shear tab connections subjected to a combined vertical (shear) force and axial force (tension and compression) along with the anticipated rotation of a typical beam-to-column joint. In comparison with the same shear tab specimens subjected to shear force alone conducted by Marosi (2011), the results showed a gain in shear resistance due to the presence of an axial compression force in the connection, while an axial tension decreased the shear resistance.

Test #1 and #2 specimens performed very ductile due to flexural and shear yielding of the steel plate, bearing, and ductile weld fracture resulting in a connection within high plastic deformation capabilities. By demonstrating the high ductility compared to Marosi's test that was subjected to only shear load, it was decided to compare the coupons from both tests. The coupons extracted from the specimens were investigated and a different material behaviour compared to Marosi's coupons was identified (explained in Section 5.10).

Specimen #3 demonstrated a similar behaviour and ductility in comparison with Marosi's test and did not perform more ductile compared to Marosi's test. The importance of the connecting weld in the performance of a shear tab was witnessed in specimen #4, which failed in a non-ductile fashion at a load level of approximately 60% of what was expected to be the shear capacity. The results of these tests were subsequently used to enhance and calibrate the finite element simulation models for further investigations (Chapter 6).

Chapter 6

Finite element modelling of shear tabs subjected to combined shear and axial forces

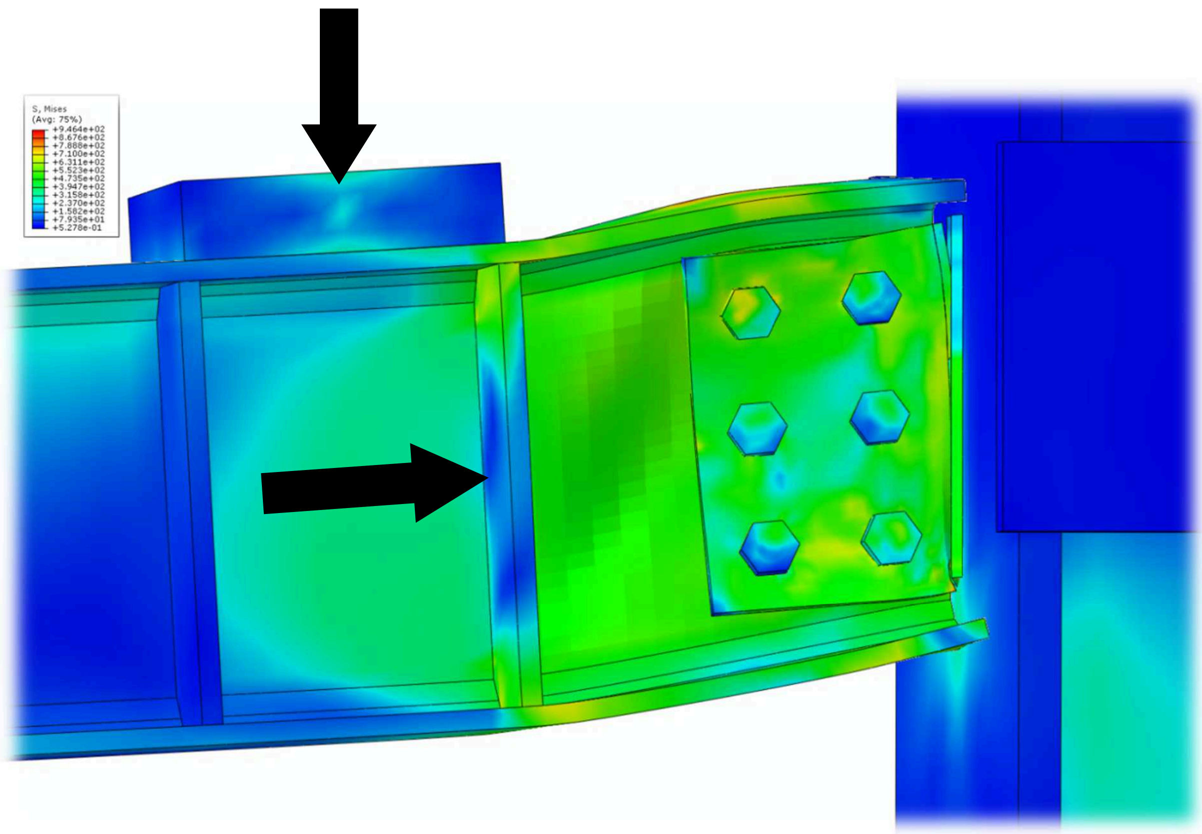

6. Chapter 6 - Finite element modelling of shear tabs subjected to combined shear and axial forces

This chapter presents the simulation strategy including the results obtained from the finite element simulation models built to investigate the performance of shear tabs subjected to combined shear and axial forces (Phase 3 of the research program). The performance of the single and double vertical row bolted shear tabs were investigated separately for compression and tension. Ultimately these results were used in the development of the suggested design approach.

6.1. Simulation strategy

A total of twelve finite element models were created for evaluating the performance of the six shear tab specimens (Figure 6.1) presented in Chapter 4 subjected to combined shear and axial force. Each specimen was investigated once for combined shear and compression force and once for combined shear and tension force.

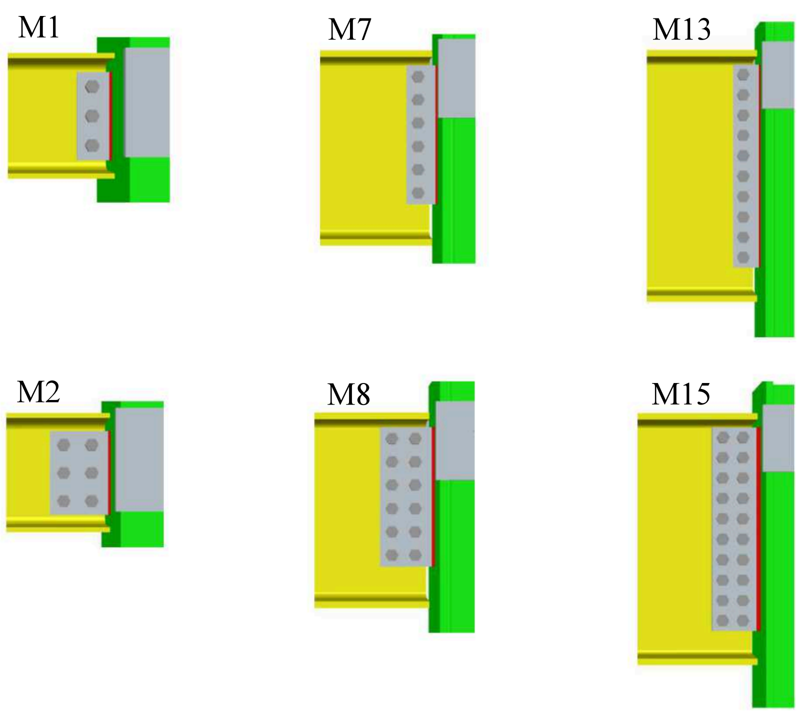

Figure 6.1- Shear tab specimens studied under combined shear and axial forces with test designations

The shear tab connections shown in Figure 6.1 were selected to be investigated under combined axial and shear forces because they represent commonly used connections in construction and because previous laboratory tests of the same connections under shear loading were carried out by Marosi (2011).These specimens were designed by Marosi solely for carrying gravity loads (pure shear) and axial force was not considered in their design The main objective of the performed simulations was to investigate the effect of a supplementary axial force on the connections behaviour and how it affects the ultimate shear resistance of the connection.

Different levels of axial force in forms of compression and tension were applied to the models. This was done by applying a uniform pressure equivalent to the desired axial compression or tension force at the end face of the test beam as shown in Figure 6.2. Tension application was easy to achieve but for compression application the test beam would have been sensitive to buckling, especially at high axial compression force levels. Assigning lateral restraints to the side face of the flanges of the test beam by using boundary conditions in ABAQUS eliminated the possibility of the test beam's buckling in compression, making compression application possible.

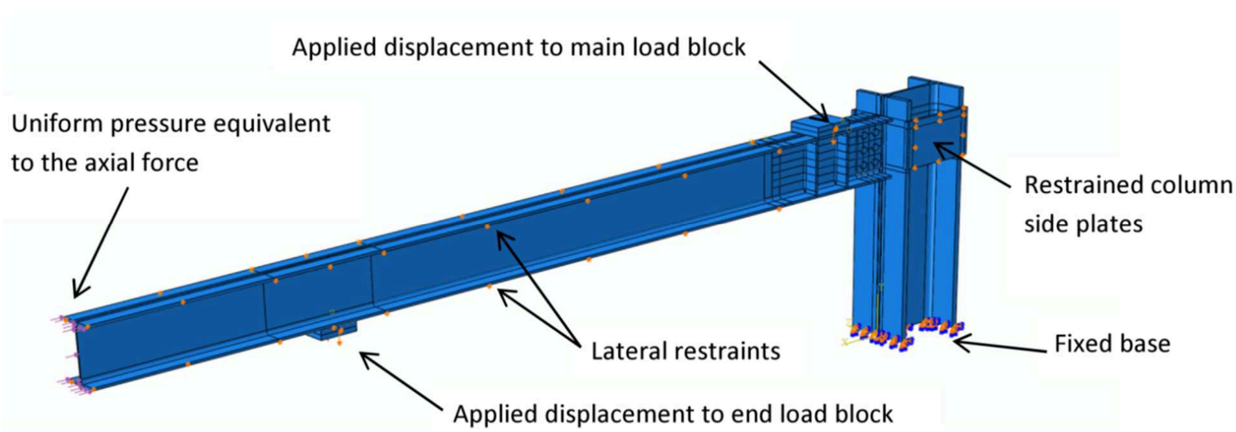

Figure 6.2- Representation of axial load application strategy for FE models

For a more realistic simulation, the selected primary load protocol for the axial load application was motivated by a typical beam during its lifespan which is generally subjected to gravity loads (service loads) until a stage where axial force may arise due to wind, earthquake or other possible sources. Based on the global force vs. displacement response plots from Marosi's

(2011) tests ,the suggested shear force level prior to axial load application was decided to be 0.72 V_{rn} where V_{rn} is the predicted shear resistance of the connection based on nominal material properties and ϕ =1.

The loading simulation was executed by first applying the same shear load protocol used to displace the main and end load block of the connections subjected to gravity loads alone, as described in Chapter 4. The time when the axial load was applied was determined based on the loading protocol methodology used for the verification laboratory tests, explained in Chapter 5. Once the shear force in the connection reached the suggested service shear force level, the axial load was applied and remained constant until the end of the simulation.

A secondary loading protocol was also investigated to determine the change in the ultimate shear resistance if the connection was loaded axially at the beginning of the simulation. The results of this investigation showed that the changes were negligible. For low axial force levels (about 25% of the measured ultimate shear resistance) a shear resistance decrease of less than 1% was observed and for high axial force levels (higher than 100% of the measured ultimate shear resistance) the reduction was approximately 2%. From the fact that the primary load protocol offered a more realistic representation, it was selected to be used for all the simulations.

This simulation process was repeated for various levels of axial loads. In order to achieve a better understanding of the magnitude of axial force and to avoid dependency on design code equations, the applied axial force magnitude was selected based on a percentage of the measured ultimate shear resistance of the connection, determined by means of FE simulation of the connections subjected to only gravity loads. The number of axial load levels to produce the interaction curves was dependant on the number of points required to match a linear, 2^{nd} or 3^{rd} order mathematical trend line with a coefficient of determination (R^2) of higher than 95% .Table 6.1 contains a summary of the twelve FE models built for the study including the connectivity configuration, beam size and loading protocol.

Table 6.1-FE model shear tab configurations and loading protocols

	Model designation.	Connectivity of shear tab (number of vertical rows of bolts & bolts per row)	Test beam	Number of axial load levels investigated	Predicted pure shear resistance based on nominal material properties and ϕ =1 (KN)	Suggested service shear force level for axial load application (KN)
					V_{rn}	0.72 V_{rn}
Combined shear and tension force	M1-T	1x3 bolts	W310 x 60	7	257	185
	M2-T	2x3 bolts	W310 x 60	8	405	292
	M7-T	1x6 bolts	W610 x 140	9	676	487
	M8-T	2x3 bolts	W610 x 140	9	1334	960
	M13-T	1x10 bolts	W920 x 223	8	1323	953
	M15-T	2x10 bolts	W920 x 223	8	2887	2079
Combined shear and compression force	M1-C	1x3 bolts	W310 x 60	9	257	185
	M2-C	2x3 bolts	W310 x 60	10	405	292
	M7-C	1x6 bolts	W610 x 140	12	676	487
	M8-C	2x3 bolts	W610 x 140	11	1334	960
	M13-C	1x10 bolts	W920 x 223	10	1323	953
	M15-C	2x10 bolts	W920 x 223	8	2887	2079

By using this technique the effect of each axial force level on the connection's behaviour was studied by monitoring the shear force vs. vertical displacement of the shear tab, plotting the ultimate shear resistance vs. axial force interaction curve, plotting the final deformed shape used to identify the failure progression of the connection, comparing the 4 verification test results (presented in Chapter 5) with the simulation results, identifying any other possible phenomena that could have affected the shear tab's behaviour, and ultimately applying final modifications such as material model, contact assignments ,simulation strategy ,etc. to the FE models (if necessary) for a more realistic simulation.

6.2. Initial investigation results

The major portion of assessing the performance of the connections under combined loading involved finite element (FE) simulation, therefore the first step was to optimize and calibrate the FE models for a combined shear and axial force scenario. For this purpose, the four FE models replicating the laboratory verification tests from Phase 3 were first built to investigate the capability of the models in simulating the behaviour and predicting the ultimate shear resistance of the connection.

The material properties used for models M2-T, M2-C, M8-T and M8-C were based on coupons extracted from the test components of the shear tab tests subjected to combined shear and axial forces, as described in Chapter 5 (Series B coupons), while the results of the coupons extracted from Marosi's (2011) shear tab tests (Series A) were used for the 8 remaining models because no combined shear and axial force experimental test was performed for the remaining shear tab specimens. In a same manner, the recorded actuator displacements from the four verification tests were specifically used for models M2-T, M2-C, M8-T and M8-C, while the remaining models used the data from Marosi's (2011) experimental work to simulate the shear force and connection rotation generated by gravity loads.

The four FE models (M2-T, M2-C, M8-T and M8-C) were built to simulate the laboratory testing procedure, predict the failure progression and the ultimate shear resistance of the connection. As such, they demonstrated how the connection was affected by the presence of axial tension and compression. Figure 6.3 contains a comparison of the final deformed shape with the Von-Mises stress distribution of the M8-C model vs. the experimental test result. As it can be seen from the Figure, the deformed shape is very similar and the simulation model was able to predict the cracks in the net area and the tearing in the weld. The ultimate shear resistance was also estimated within a margin of ± 5% as shown in Figure 6.4.

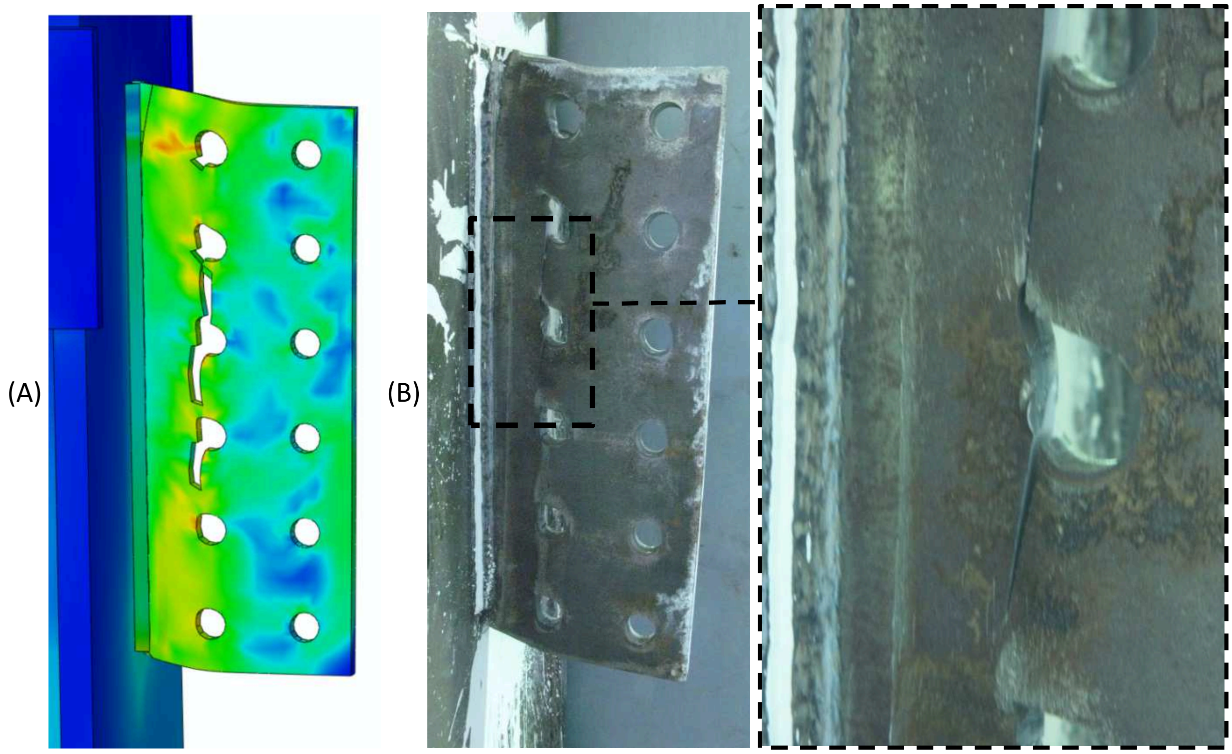

Figure 6.3-(A) Final simulation deformed shape of connection configuration M8-C subjected to combined shear and axial compression (B) Verification laboratory test deformed shape (Test #3)

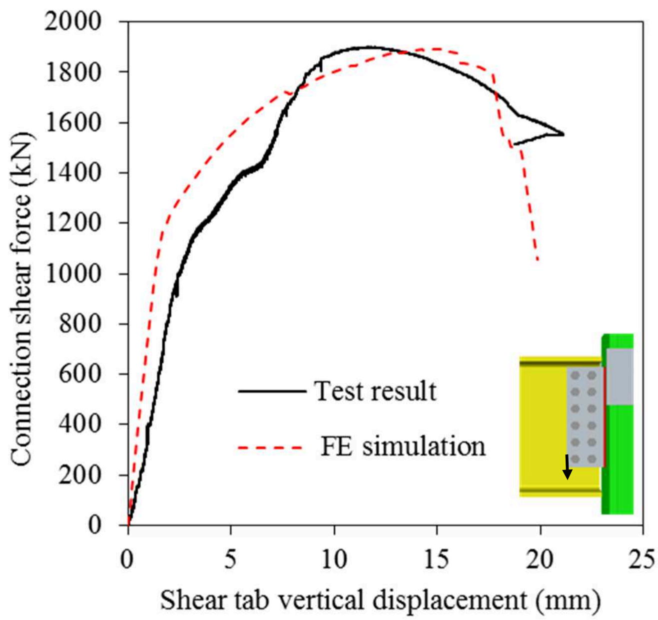

Figure 6.4-Connection configuration M8-C simulation response curve subjected to combined shear and axial compression vs. laboratory test (Test #3) result

Similarly Model M2-C was able to simulate the behaviour observed in verification Test #1 with a slight difference at the final stage of the failure progression. In the FE model, the bottom region of the steel plate that was subjected to extreme compression failed and the elements were deleted causing a sudden release triggering the cracks on the first line of bolts to propagate further compared to the experimental result (Figure 6.5). The corresponding response curve of Model M2-C and the experiment response curve are shown in Figure 6.6.

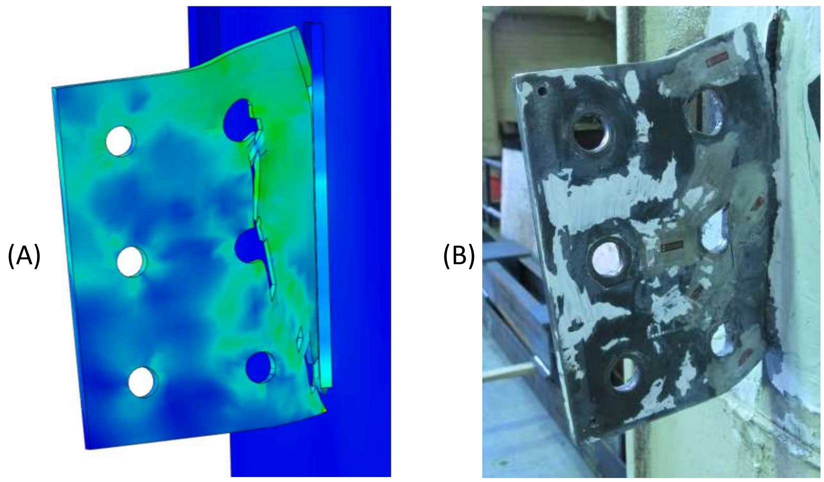

Figure 6.5-(A) Final simulation deformed shape of connection configuration M8-C subjected to combined shear and axial compression (B) Verification laboratory test deformed shape (Test #3)

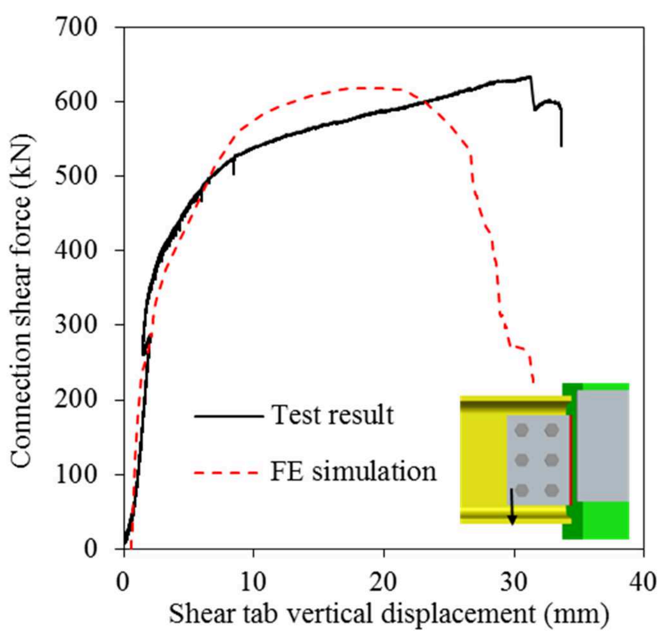

Figure 6.6-Connection configuration M8-C simulation response curve subjected to combined shear and axial compression vs. laboratory test (Test #3) result

The M2-T model simulated verification Test #2 with a more severe weld tearing degradation and less deformation in the shear tab itself (Figure 6.7). However this degradation affected the post ultimate behaviour and the ultimate shear resistance of the connection still matched the laboratory test result within a margin of ± 5% .The response curve of the FE model (Figure 6.8) is shifted with an initial displacement to achieve a better match with the test result (based on the methodology described in Chapter 4).The amount of shift was such that the time of the axial load application in both the test and FE simulation model occurred at the same vertical displacement and shear force level.

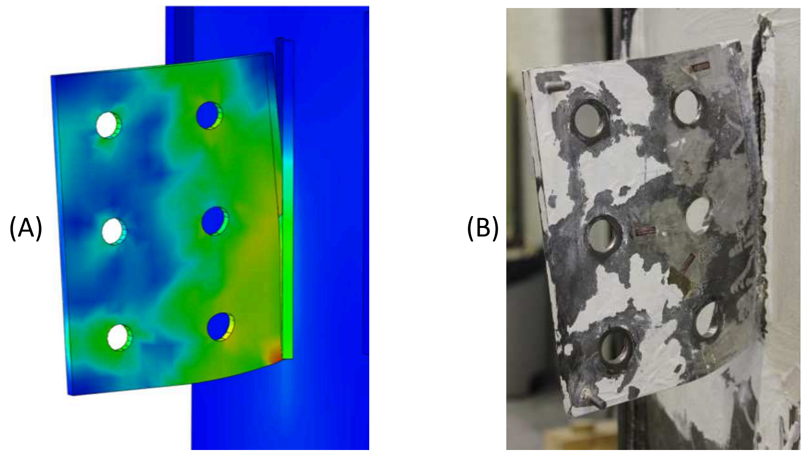

Figure 6.7-(A) Final simulation deformed shape of connection configuration M2-T subjected to combined shear and axial compression (B) Verification laboratory test deformed shape (Test #3)

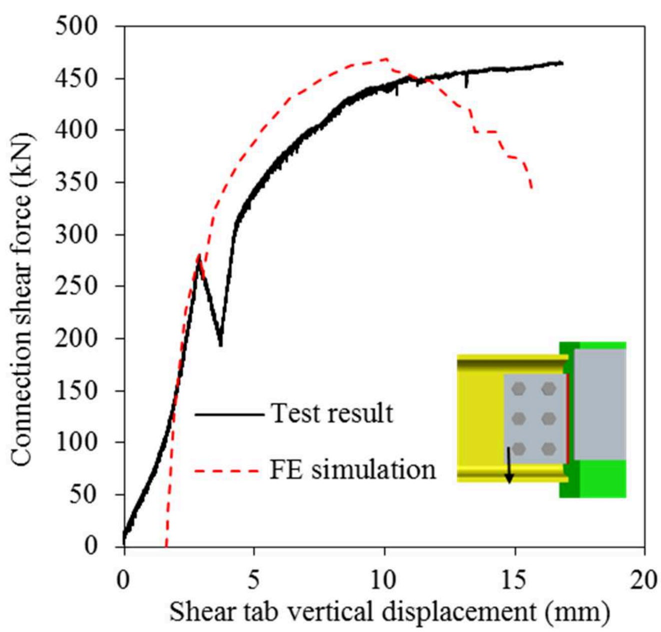

Figure 6.8-Connection configuration M8-C simulation response curve subjected to combined shear and axial compression vs. laboratory test (Test #3) result

The final deformed shape with the Von-Mises stress distribution of model M8-T subjected to combined shear and axial tension is shown in Figure 6.9-A.The connecting fillet weld size used in the model was 10mm, identical to the weld size that Marosi (2011) had designed and tested. Due to a fabrication error, the connecting fillet weld size of the specimen in verification Test #4 was measured as being 5mm, leading to a non-ductile fashion failure (Figure 6.9-B) at a load level of approximately 60% of what was expected to be the shear capacity (Figure 6.10). The purpose of building this model was to assess the performance of Marosi's specimen if it were subjected to combined shear and axial tension since it was not possible to compare the FE results to Test #3 described in Chapter 5.

(A)

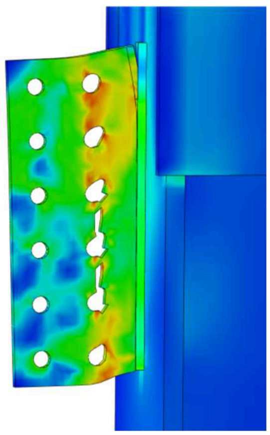

(B)

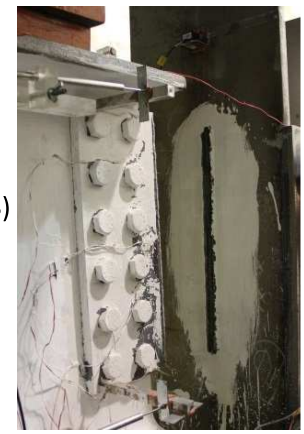

Figure 6.9-(A) Final simulation deformed shape of connection M8-T connected by a fillet weld size of 10mm (B) Verification laboratory Test #3 deformed shape (5mm weld size)

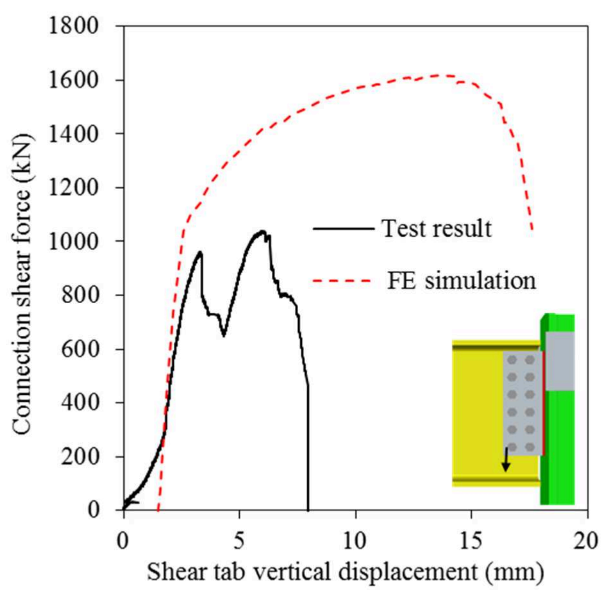

Figure 6.10-(A) Final simulation response curve of connection M8-T connected by a fillet weld size of 10mm (B) Verification laboratory Test #3 response curve (5mm weld size)

Table 6.2 presents a summary and comparison of the ultimate shear resistance obtained from the four FE models (M2-T, M2-C, M8-T and M8-C) simulating the four verification laboratory tests with the measured laboratory test results from Phase 3 of the research program.

Table 6.2- Comparison of the ultimate shear resistance obtained from FE models representing the four verification laboratory tests

FE model designation	M2-C	M2-T	M8-C	M8-T
Equivalent laboratory test no.	#1	#2	#3	#4
Shear tab dimension (mm)	225x165x10	225x165x10	456x178x16	456x178x16
Test beam	W310 x 60	W310 x 60	W610 x 140	W610 x 140
Axial load type	Compression	Tension	Compression	Tension
Axial load amplitude (kN)	215	215	512	512
FE simulation shear resistance (kN)	619	469	1889	1617
Measured laboratory shear resistance (kN)	626	468	1898	1031*

* Weld for test #4 was designed to be 10mm but after the test it was measured 5mm

According to Table 6.2, models M2-T, M2-C, and M8-C were capable of simulating the laboratory testing procedure and were able to predict the ultimate shear resistance of the connection within a margin of ± 5%. M8-T determined the shear resistance of the connection if the connecting weld was welded based on the design size (10mm). Based on the confidence gained by the results of the first four FE models, the next step was to apply different levels of axial force and investigate the impact on the connections behaviour.

Subsequently, the same four FE models were used to investigate the performance of the connections under higher and lower axial force levels in the form of tension and compression. However some problems were observed that affected the appropriateness of the outcome which needed to be resolved. The problems identified were:

1) The behaviour of the shear tabs subjected to combined shear and compression was complicated by the contact between the flanges of the test beam and the column face. For instance when the compression force exceeded 60% of the ultimate shear resistance of the shear tab specimen, as simulated in Test M2-C, the bottom flange of the test beam contacted the column face resulting in a sudden dramatic increase in the shear resistance of the connection (Figure 6.13). The corresponding deformed shapes with the Von Misses stress distribution of test M2-C for different levels of compression force can be observed in Figures 6.11 and 6.12.

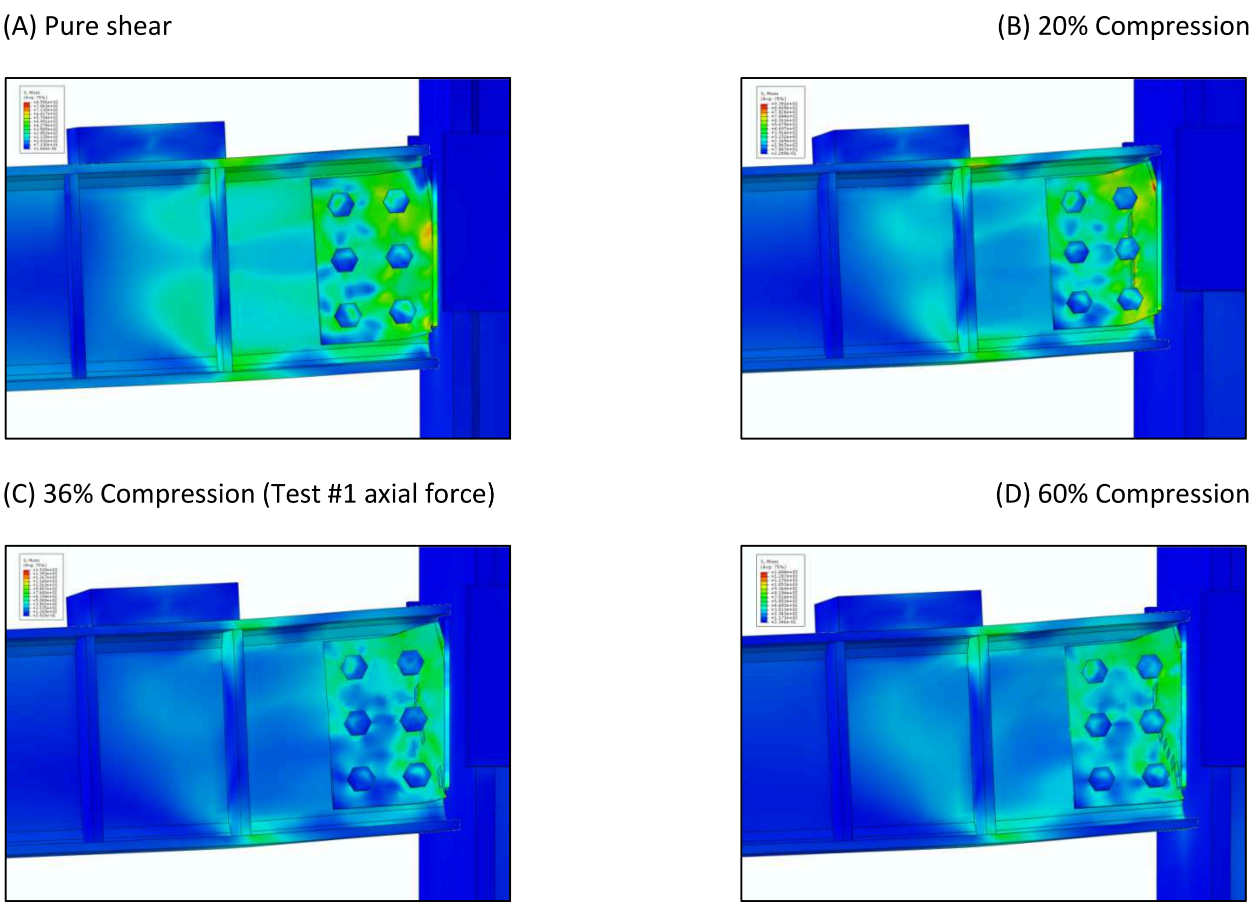

Figure 6.11– Final deformed shape of connection configuration M2-C subjected to combined shear and different levels of compression force (0%-60% of the ultimate shear resistance)

Axial compression forces of over 180% of the ultimate shear resistance caused the beam’s web to experience distortion and out of plate bending with the shear tab. The maximum compression force that the specimen resisted was 180% of the ultimate shear resistance. It failed immediately when the axial load was applied and was not able to take additional shear force. The plate was bent along a line near and parallel to the connecting weld as shown in Figure 6.12-J.

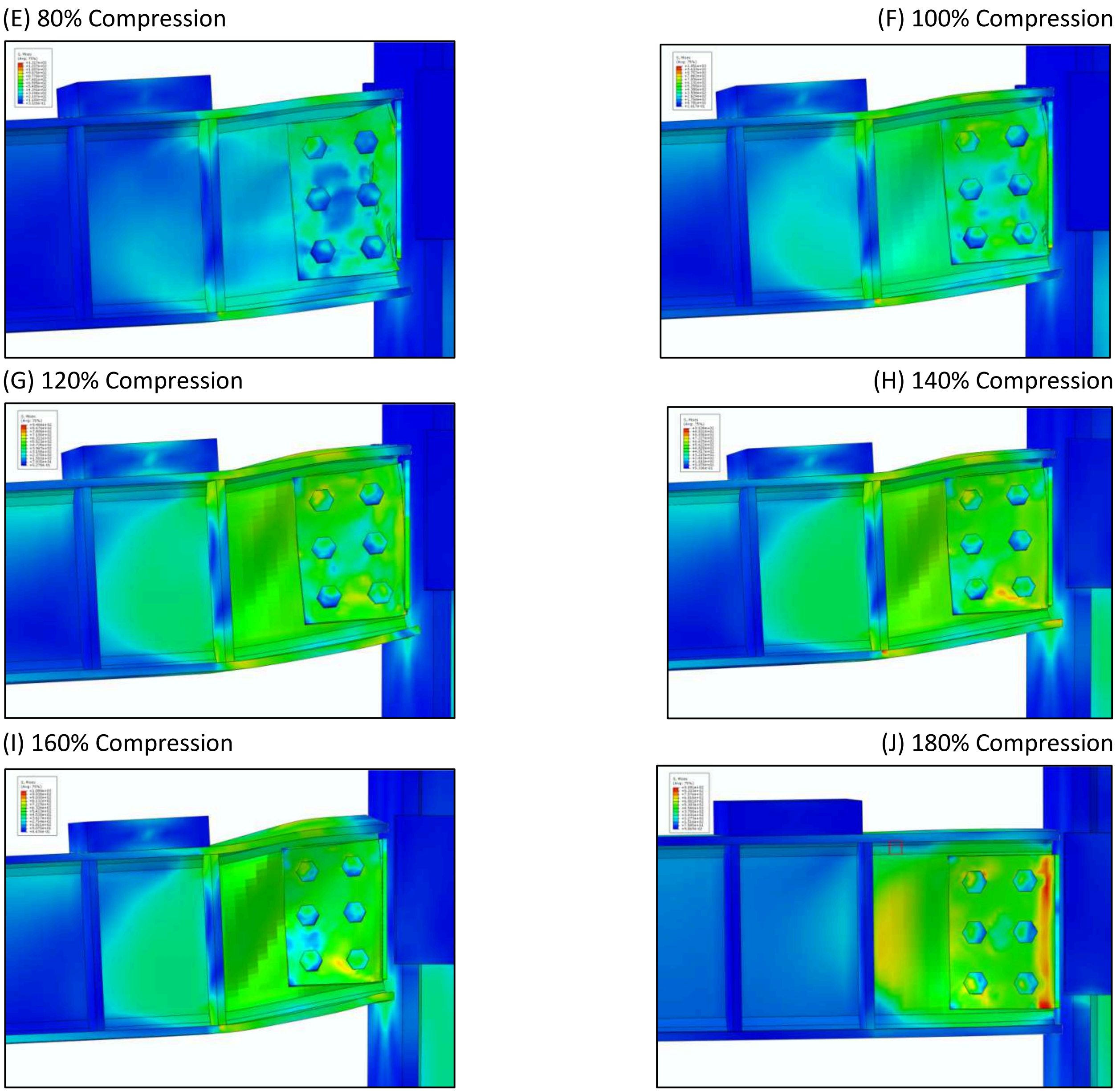

Figure 6.12– Final deformed shape of connection configuration M2-Csubjected to combined shear and different levels of compression force (120%-180% of the shear resistance)

The Von Mises stress development can be identified on the column face due to contact pressure between the bottom flange of test beam and the column flange for any compression force over 60% of the ultimate shear resistance, as shown in Figure 6.11 and Figure 6.12. Subsequently after contact, the beam participated in carrying shear force directly through to the column. The shear transfer from the beam to the column is partly the result of the contact between the beam flange and the column in addition to the shear tab. This phenomenon also caused the test beam's web and the steel plate to experience some out of plane bending.

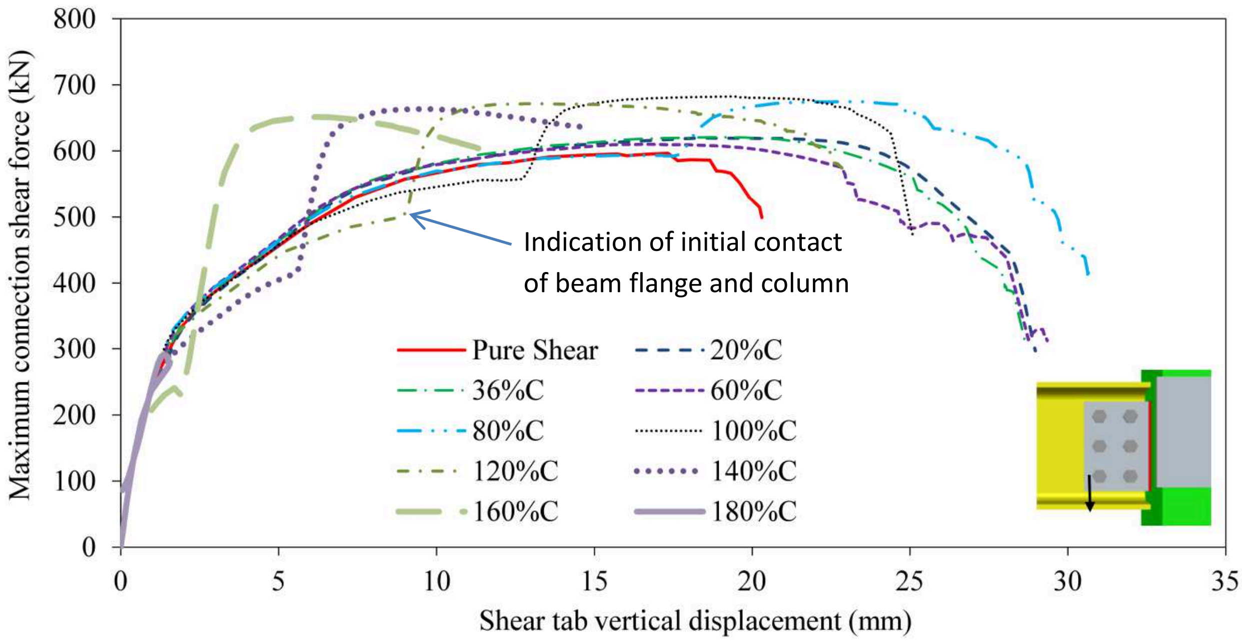

Figure 6.13–Connection configuration M2-C subjected to combined shear and different levels of compression force simulation response curves (including the contact interaction of the beam's flanges with the column face)

As illustrated in Figure 6.13, the ultimate shear resistance of the connection for all compression force levels over 60% of the ultimate shear resistance eventually reached a plateau of about 650 kN which is the highest shear force that is transferred though the test beam and connection. The proposed interaction curves were based on maximum shear resistance and axial force; therefore including the contact of the flange of the test beam affected the interaction curve and the performance of the connection alone could not be investigated. To resolve this issue the contact was removed from the FE models, which allowed penetration of the test beam's flange into the connection column. Although physically this is not possible, the intent was to limit the FE study to that of the shear tab's shear and axial resistance without incorporating the potential beneficial effect of increased shear resistance due to contact friction with the column face. The result of this adjustment can be realized in Figure 6.15 and the deformed shape of the shear tab subjected to 100% and 140% of the ultimate shear resistance compression force can be seen in Figure 6.14. Based on the Figure, the connections experienced higher bending and distortion compared to the models that included the contact of the beam's flange with the column. Further detail of the performance of this connection is explained in Section 6.3.

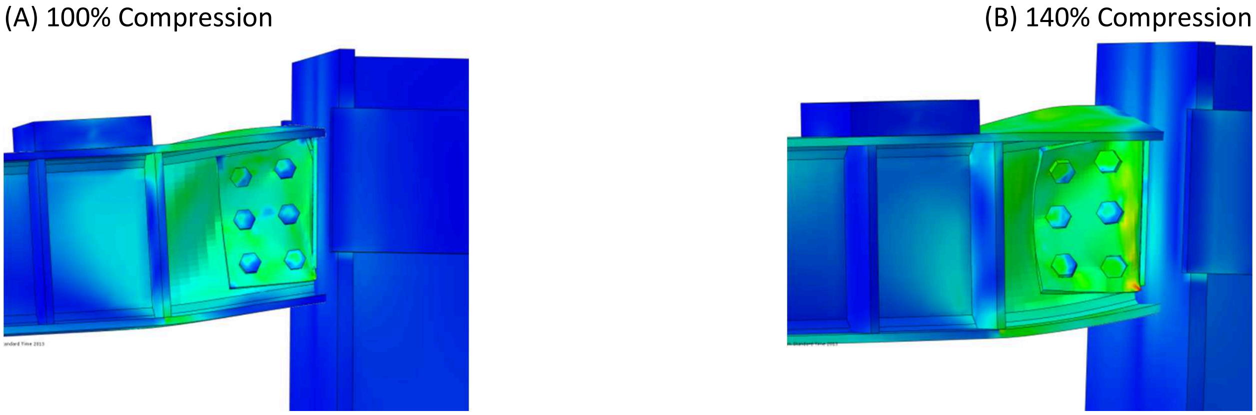

Figure 6.14– Final deformed shape of connection configuration M2 connection subjected to combined shear and two levels of compression force (100%&140% of the shear resistance) excluding the contact interaction of the beams' flanges with the column face)

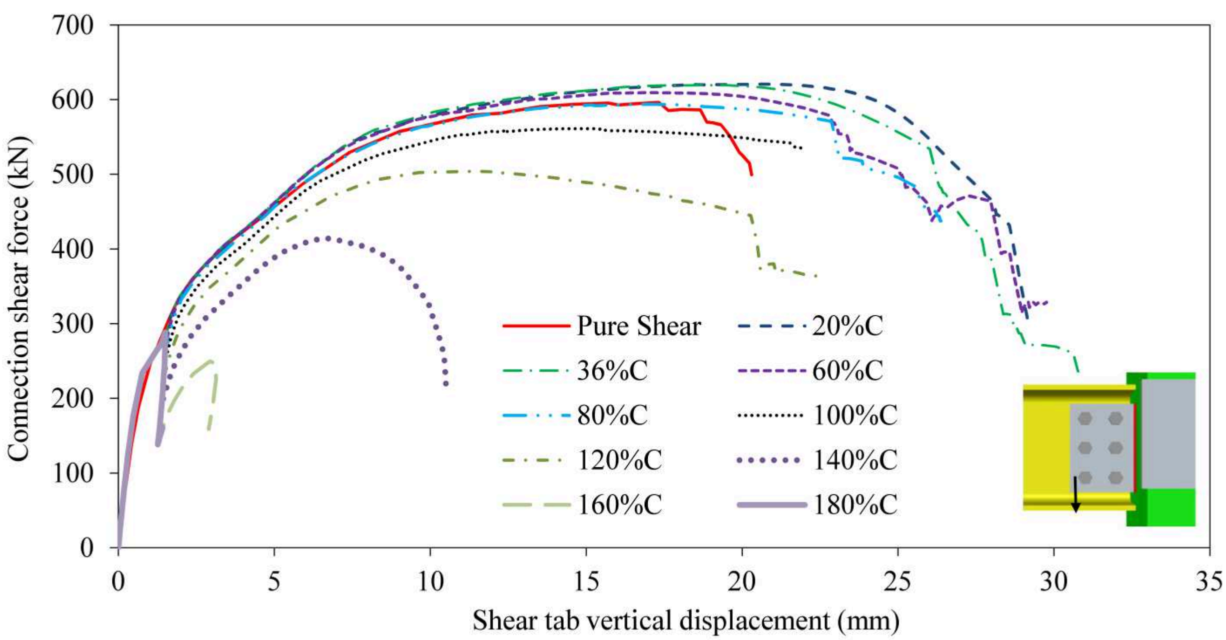

Figure 6.15– Connection configuration M2-C subjected to combined shear and different levels of compression force simulation response curves (excluding the contact interaction of the beams' flanges with the column face)

As illustrated in Figure 6.15 the sudden dramatic rise in the ultimate shear resistance of the connection was eliminated for all compression force levels and the change in shear resistance of the connection alone due to the presence of compression force was determined. This strategy was implanted in all the remaining FE models used for the investigation of combined shear and axial force (compression & tension).

2) The second issue that arose during the initial investigation was that the column experienced considerably large lateral displacement at high axial forces in the direction of the axial tension or compression force. In contrast, due to negligible lateral movements of the column when simulating the connections under shear loads alone, it was decided to exclude modelling the diagonal braces installed on the side plates of the column (See Section 4.3.1). However, the initial investigation of the connections' performance under a combined loading scenario showed that the lateral movement was no longer insignificant and that the column needed to be restrained. Hence, the side plates of the column in the direction of the axial force were restrained by applying a boundary condition over the external side plate surface in the FE models.

6.3. FE simulation results:

Once these two major modifications were applied to the FE models, they were used to investigate various levels of axial tension and compression force on the shear tab connections. The shear force vs. shear tab vertical displacement and the maximum shear force vs. axial force interaction curves were generated for all the connection configurations listed in Table 6.1. The final point shown on the interaction curves was the highest axial force level that the connection was able to sustain the minimum suggested service load level defined in Section 6.1. Axial forces beyond this point led to 55%-80% stiffness degradation for compression application and 41%-58% for tension force. Axial forces higher than this point were also investigated, which can be seen on the force-displacement plots; however, the interaction curves were stopped at the specified maximum axial force. The simulations were completed when an axial force that caused immediate failure of the connection was identified. The results obtained from the FE simulation of Marosi's (2011) experimental work (described in Chapter 4) were used as the ultimate pure shear resistance of the connection for zero axial force shown as the first point on the vertical axis of the interaction curve with the exception of models M2-T, M2-C, M8-T, and M8-C. For these models, the material data was based on the coupons extracted from the four verification laboratory tests. The same steel grade was used in both Marosi's testing and the verification tests presented in Chapter 5; however coupon test results showed different material properties. For this reason the pure shear resistance of connection configurations M2-T, M2-C, M8-T, and M8-C was different compared to the corresponding test conducted by Marosi. The final results of the connection FE simulations are presented in Section 6.3.1 and 6.3.2.

6.3.1. Combined shear and axial compression results:

The response plots, interaction curves, and simulation observations of six FE models M1-C, M2-C, M7-C, M8-C, M13-C, and M15-C subjected to combined shear and axial compression is presented:

Figure 6.16 illustrates the maximum connection shear force vs. shear tab vertical displacement response curve of the M1-C FE model. The corresponding generated shear force-axial force interaction curve is shown in Figure 6.17. A compression force up to 100 kN (25% of the ultimate shear resistance) did not show any difference in the failure progression compared to the pure shear FE model. The pure shear responses of the connections are explained in Chapter 4. At 186 kN (50%-C) compression force, the beam started to penetrate into the column face and weld tearing did not occur, instead the bottom part of the steel plate showed high distortion due to the compression force in the shear tab. Weld tearing was no longer observed for higher axial compression forces. By increasing the compression force up to 465 kN (125% -C), out of plane bending of the steel plate with the web of the test beam started to occur and the plastic strain between the bolt holes and the column face was higher compared to the plastic strains between the bolt holes. Ultimately after applying a compression force of over 600kN (160%-C) ,the connection showed significant out of plane bending and lost its shear capacity immediately after the application of compression force. The interaction curve in Figure 6.17 shows a 2.1% gain of shear resistance for an axial compression force up to 100kN and for higher compression force levels, the shear capacity of the shear tab starts to degrade. The shear resistance of the connection was reduced approximately 50% as a result of a 600kN compression force.

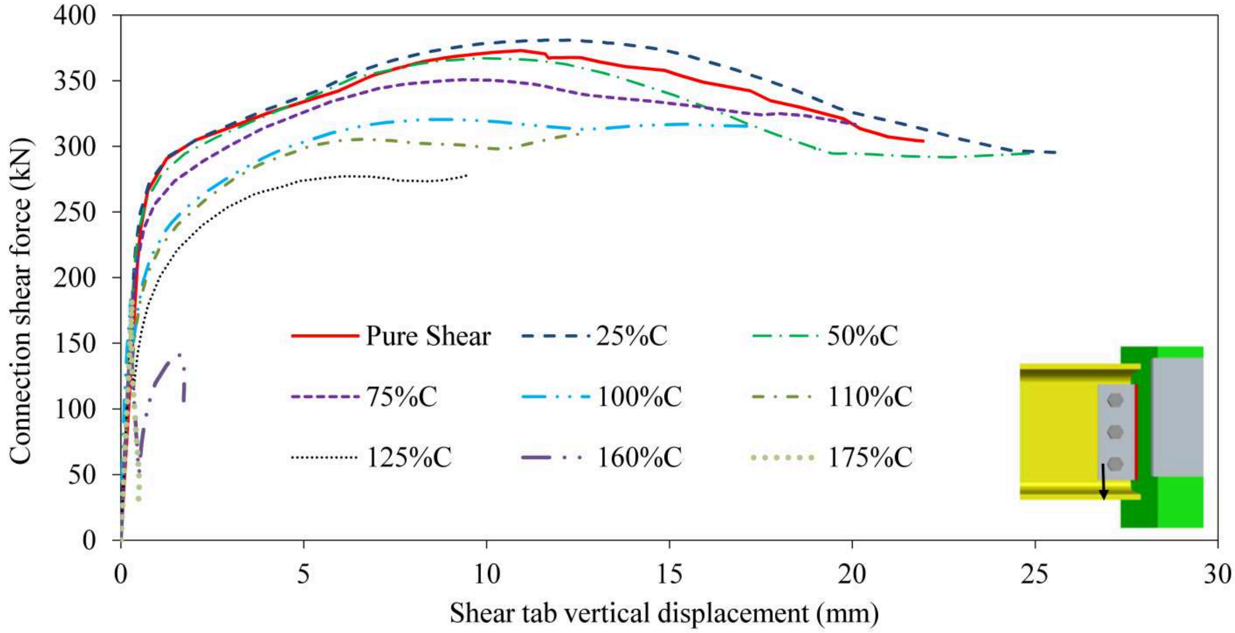

Figure 6.16–Connection configuration M1-C subjected to combined shear and different levels of axial compression force simulation response curves

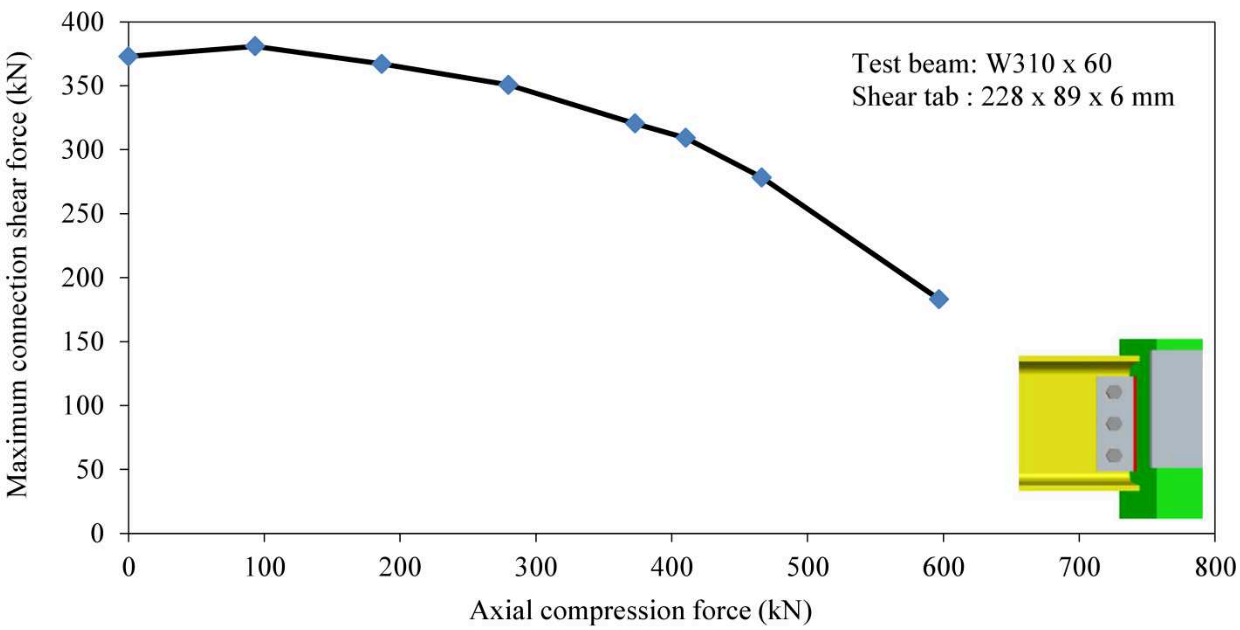

Figure 6.17– Connection configuration M1-C subjected to combined shear and axial compression force simulation interaction curve

FE model M7-C showed a higher capability in carrying axial compression force compared to connection configuration M1-C. For axial compression force levels up to 400 kN, the ultimate failure mode was similar to the pure shear model and reached its highest gain of shear resistance (8%) at 572 kN compression force (Figures 6.18 and 6.19). No contact of the test beam's flange with the column face, nor weld tearing was observed in the FE simulations and the main failure modes of the model for higher axial forces was crack propagation between the bolt line, failure at the bottom part of the steel plate connected to the column, and eventually out of plane bending of the steel plate with at an axial force higher than 1144 kN. Axial forces beyond this magnitude resulted in a significant degradation in shear resistance and ultimately the connection failed immediately after applying 1716kN (180%C) compression force.

The highest gain of shear resistance among all the connection configurations due to the impact of axial compression was observed in Model M13-C. Based on Figures 6.20 and 6.21, the maximum shear resistance of the connection increased about 17% at a compression force level of 1741 kN. With the increase of axial force beyond this magnitude, the shear resistance of the connection started to degrade and reached the same pure shear resistance at an axial compression force of 2089 kN. Lastly the connection failed with the application of a compression force higher than 2437 kN.

The failure progression of connection M13-C was similar to the pure shear FE model for axial compression force levels up to 696 kN. Weld tearing at the top of the plate and cracks between the central holes of the shear tab were observed. By increasing the axial force beyond 60% of the ultimate shear resistance (over 1044 kN), the weld tear length started to decrease and eventually at 1741 kN compression force, the length was minimized and the highest shear resistance (1741 kN) was predicted at this point. Out of plane bending of the shear tab became noticeable at axial compression force levels over 1392 kN. The deep web of the test beam also experienced twist and out of plane bending due to the continuity provided by the connected bolts. The possibility of impact between the beam flange and column was found to be at an axial compression force level of 2089 kN which was when the connection's stiffness severely degraded due to out of plane bending of the steel plate.

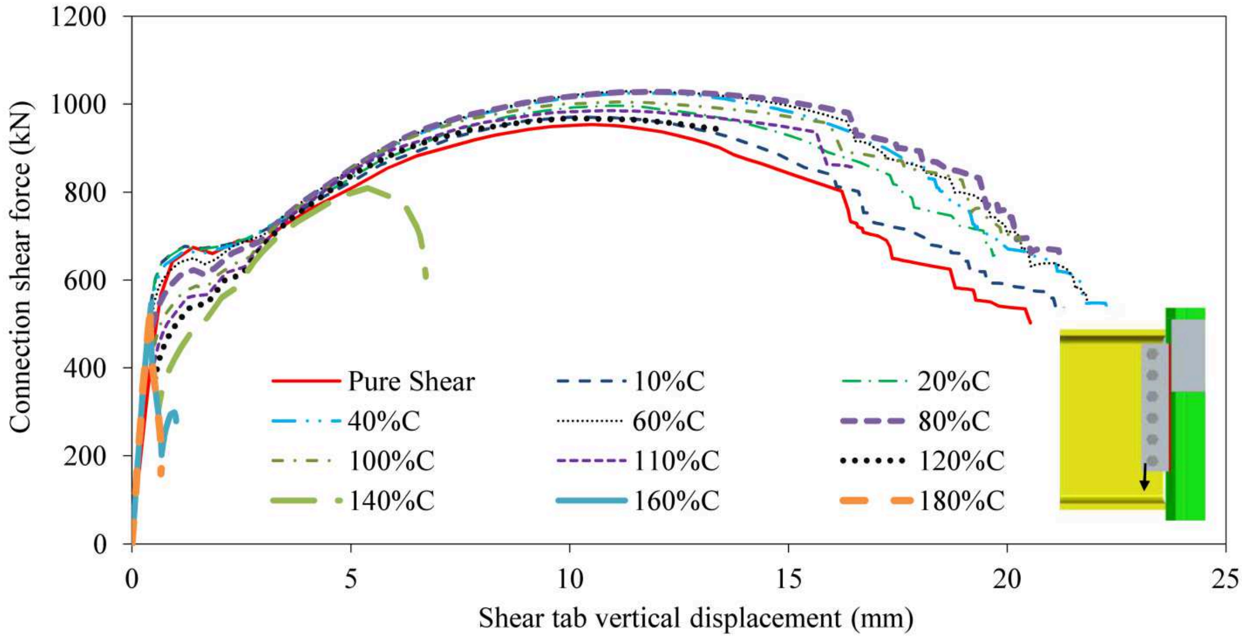

Figure 6.18– Connection configuration M7-C subjected to combined shear and different levels of axial compression force simulation response curves

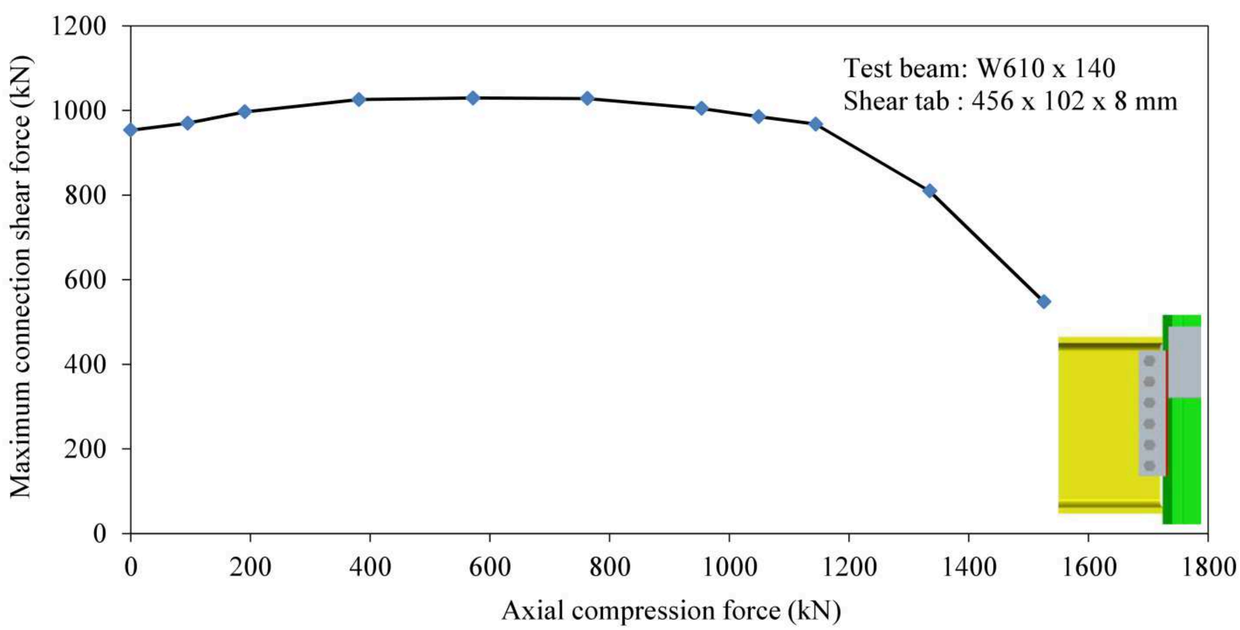

Figure 6.19– Connection configuration M7-C subjected to combined shear and axial compression force simulation interaction curve

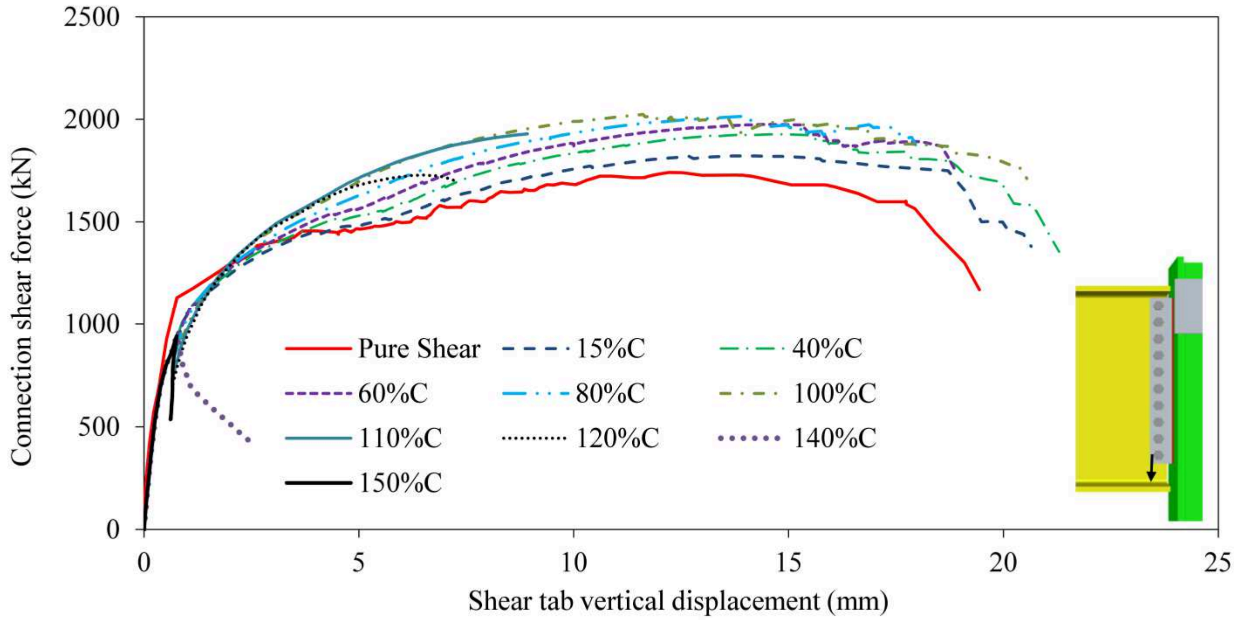

Figure 6.20– Connection configuration M13-C subjected to combined shear and different levels of axial compression force simulation response curves

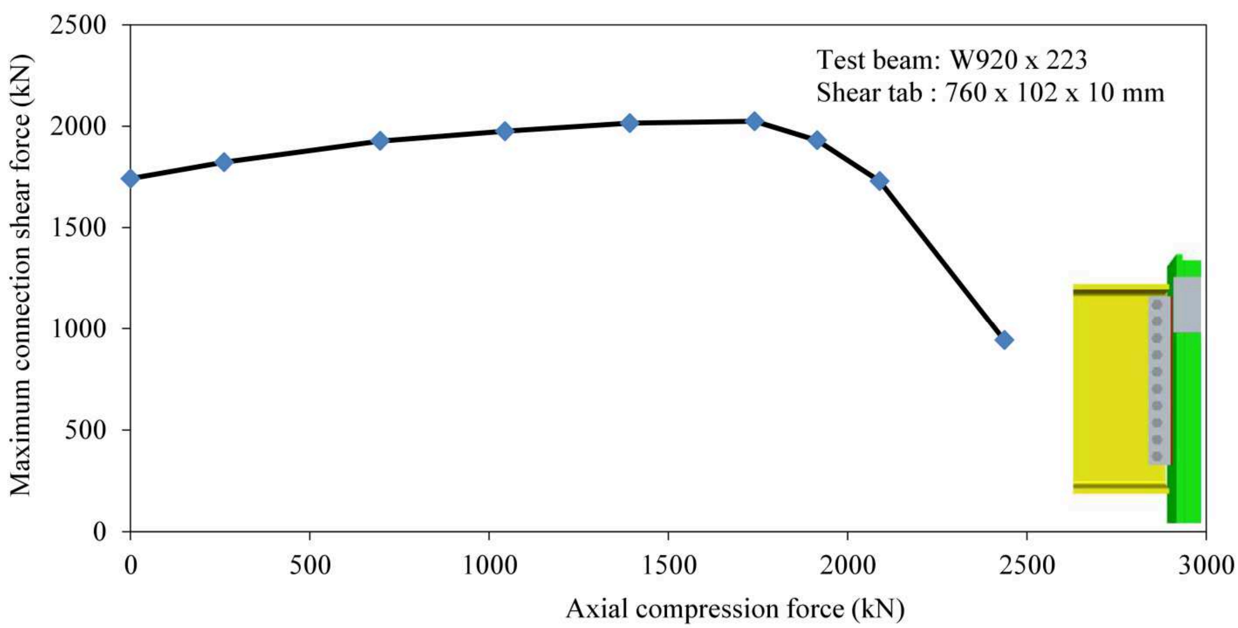

Figure 6.21– Connection configuration M13-C subjected to combined shear and axial compression force simulation interaction curve

Using the available test results from the experimental work of Phase 3 of the research program, connection configuration M2-C was the first connection that was simulated for combined shear and axial forces. Based on the initial investigations of this shear tab, modifications and improvements to the remaining FE models were implemented (explained in Section 6.2).

Figure 6.22 presents the response curve of model M2-C subjected to combined shear and various levels of compression force. The overall failure progression of the shear tab was not similar to the results obtained from the experimental work conducted by Marosi (2011) and the FE simulation result of this connection subjected to pure shear (presented in Chapter 4). Material property was the main reason for the alteration in behaviour. The coupons used for this model were based on coupons Series B which were extracted from the test components of tests subjected to combined shear and axial force. The reason for this selection was that the FE models were calibrated by using the verification test material data; therefore the ultimate pure shear resistance must have been determined based on the same material used to determine the points on the interaction curve. All FE models with different axial force level must have had the same condition. The material used for this shear tab had an 18% higher yield stress, 22% higher strain hardening strain, same ultimate stress and fracture strain compared to Series A coupons (extracted from the test components of Marosi). By using Series B coupons for the simulation, a more ductile failure mode was observed compared to the failure mode observed in Marosi's tests. The shear tab specimen tested by Marosi mainly failed due to tearing in the weld and no significant yielding was observed in the plate, whereas the FE simulation of the same shear tab resulted in shear and flexural yielding in the steel plate, tearing in the weld and finally development of cracks between the bolt holes on the first vertical row of bolts (closer to the column face). A similar behaviour was observed in connection configuration M2-C for axial compression force levels lower than 358 kN. Penetration of the beam's flange into the column was observed for axial compression force higher than 358kN, an indication of the possibility of contact. With the increase of compression force, out of plate bending of the plate with the beam's web was realised and ultimately the connection failed at an axial compression force of 955kN. Furthermore, the FE simulation result shows a close match (less than 5% difference) with the laboratory test result as shown in Figure 6.23.

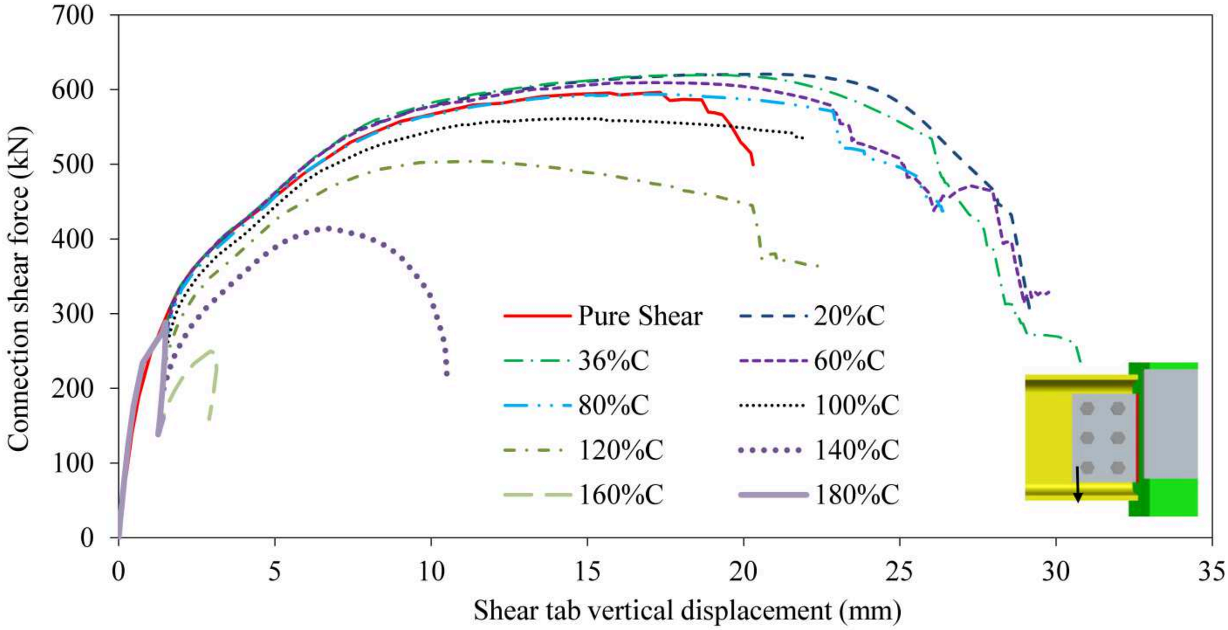

Figure 6.22– Connection configuration M2-C subjected to combined shear and different levels of axial compression force simulation response curves

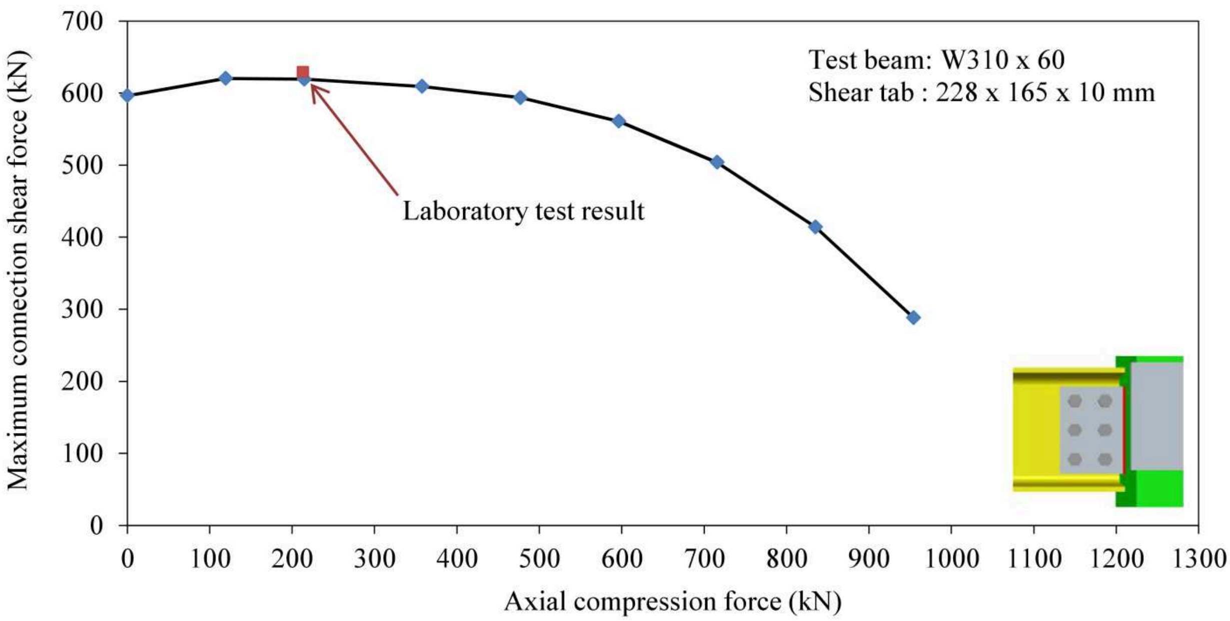

Figure 6.23– Connection configuration M2-C subjected to combined shear and axial compression force simulation interaction curve

The failure progression of connection configuration M8-C for axial compression force levels up to 716 kN (40%C) was very similar to the pure shear FE model's failure mode. Weld tearing at the top of the plate, development of cracks between the central bolts of the first vertical row of bolts (closer to column face) was identified. Axial compression forces over 716kN resulted in a shorter weld tear length and failure due to compression at the bottom of the steel plate; however the steel plate's shear capacity still did not drop until the axial compression reached 1432 kN which caused the initiation of out of plane bending of the steel plate and the ultimate shear resistance of the connection started to degrade. Applying a compression force over 2148 kN caused severe out of plane bending near and along a line parallel to the connecting weld as shown in Figure 6.24. However the connection was still able to sustain shear load. The contour in Figure 6.24 illustrates plastic strain. As can be seen from the Figure, the web of the beam was also affected and experienced yielding. Finally by applying an axial compression force of 2500 kN, the connection immediately failed.

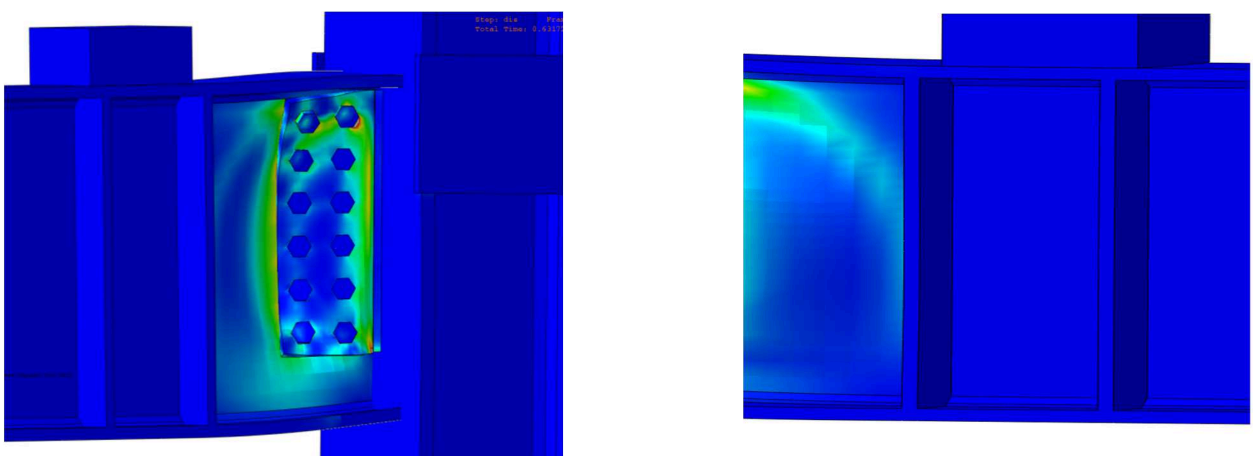

Figure 6.24- Final deformed shape and plastic strain distribution of connection configuration M8-C subjected to combined shear and 2148 kN compression (connection and beam web view)

Figure 6.24 illustrates the response curves of connection M8-C subjected to various levels of axial compression force; the corresponding interaction curve is presented in Figure 6.25. As can be seen from the Figures, the connection was capable of resisting compression forces up to 2500 kN in combination with shear. The highest capacity gained was 8.3 % at a compression force level of 1074 kN while the connection still behaved very ductile and stable.

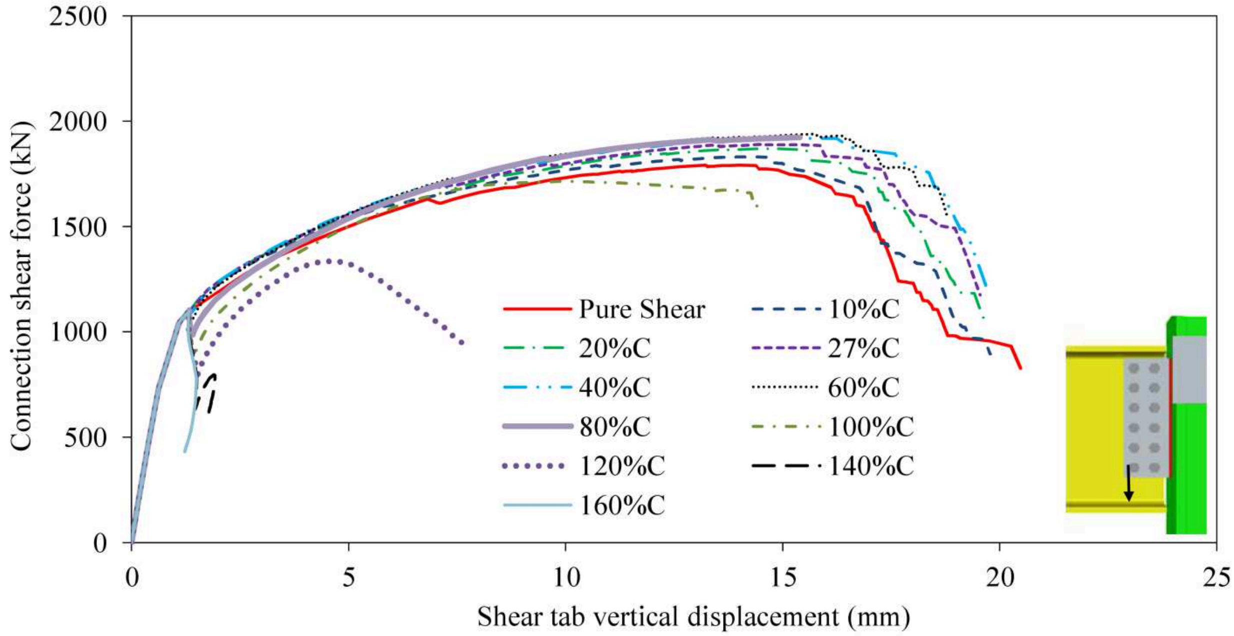

Figure 6.25– Connection configuration M8-C subjected to combined shear and different levels of axial compression force simulation response curves

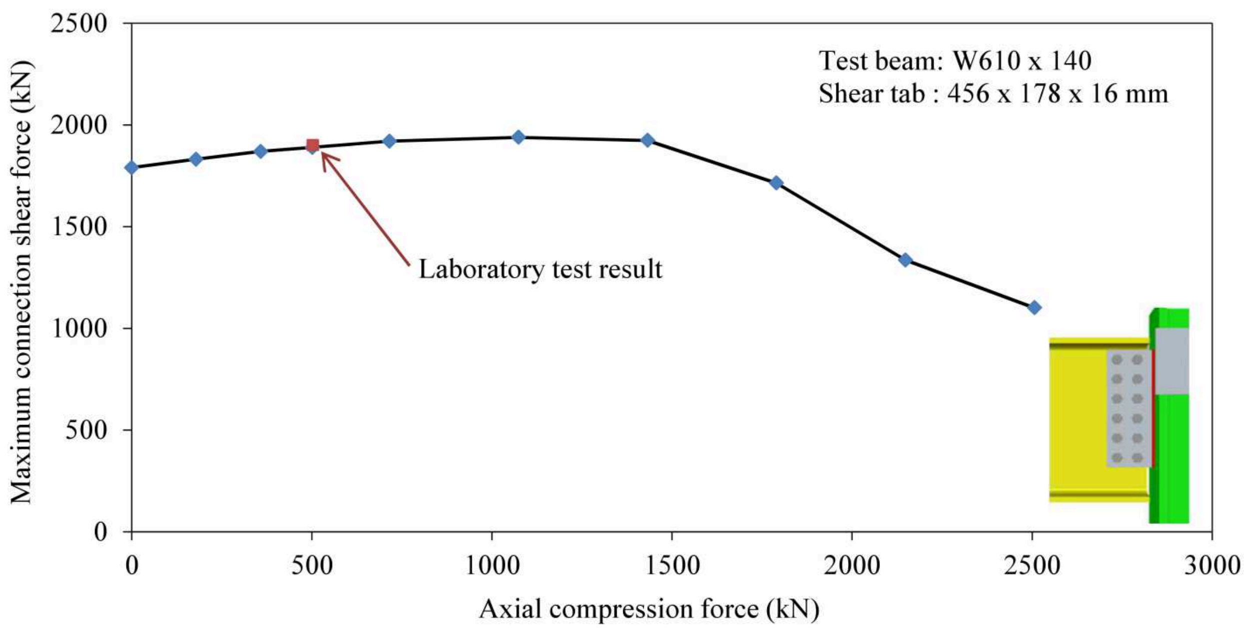

Figure 6.26– Connection configuration M8-C subjected to combined shear and axial compression force simulation interaction curve

Configuration M15-C was the stiffest and strongest connection that was investigated. The same modifications explained in Chapter 4 (Section 4.4.6) were implemented in the FE model. One major distinction that this specific model showed was that due to the high stiffness of the connection, the column was affected by the shear and compression force in the connection. The high depth of the beam's web also eased out of plane bending of the plate resulting in degradation of shear resistance at lower axial compression forces compared to the rest of the connections. Figure 6.27 shows the deformed shaped observed in the M15-C FE model for three axial compression force levels. The corresponding response curve and interaction curve can be demonstrated in Figures 4.28 and 4.29. Shear yielding in the web of the beam can be observed for all three cases as shown in Figure 4.27. Out of plane bending of the steel plate initiated at an axial compression force of 1827 kN. Axial compression forces over 2740kN significantly deformed the column support and resulted in failure of the web of the column. The extreme out of plate bending of the plate with the beams web caused the reduction of shear resistance; however the connection did not fail even at higher axial compression force levels; instead, failure was identified in the column. To maintain a consistent support condition for all configurations that were studied, it was decided to provide no further reinforcement to strengthen the column, and as such the interaction curve for this connection was generated based on the FE findings.

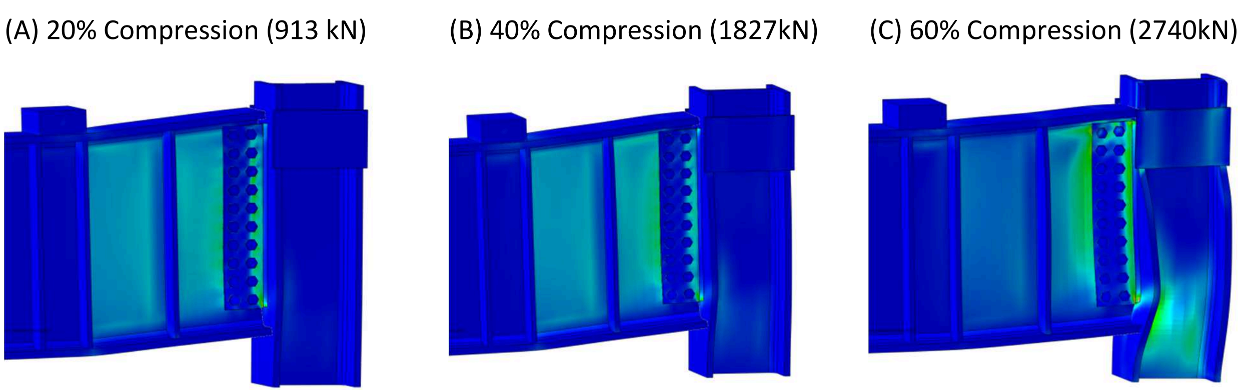

Figure 6.27- Final deformed shape and plastic strain distribution of connection configuration M15-C subjected to combined shear and different levels of compression force

The M15-C model was not able to complete the simulation for 10%C, 20%C, 40%C and 50%C; however the highest shear force recorded was approximately in the region were the response curves reached a plateau, therefore these shear forces were selected as the ultimate shear resistance in producing the interaction curve (Figure 6.29). The highest gain of shear resistance due to axial compression force was 10% at an axial compression force of 913kN.

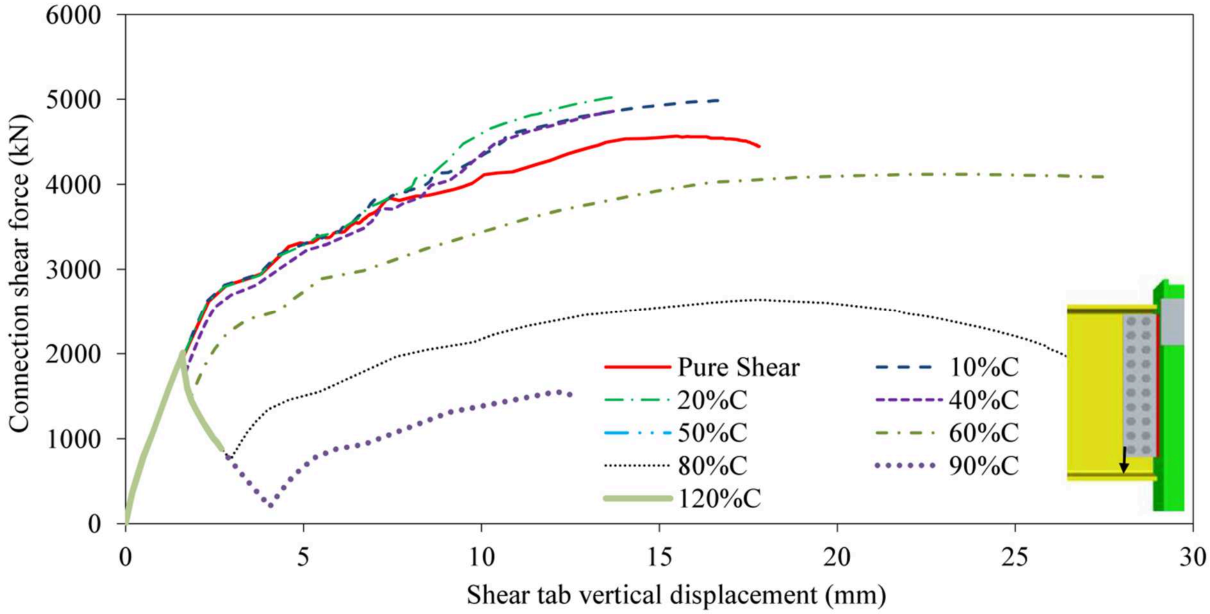

Figure 6.28 – Connection configuration M15-C subjected to combined shear and different levels of axial compression force simulation response curves

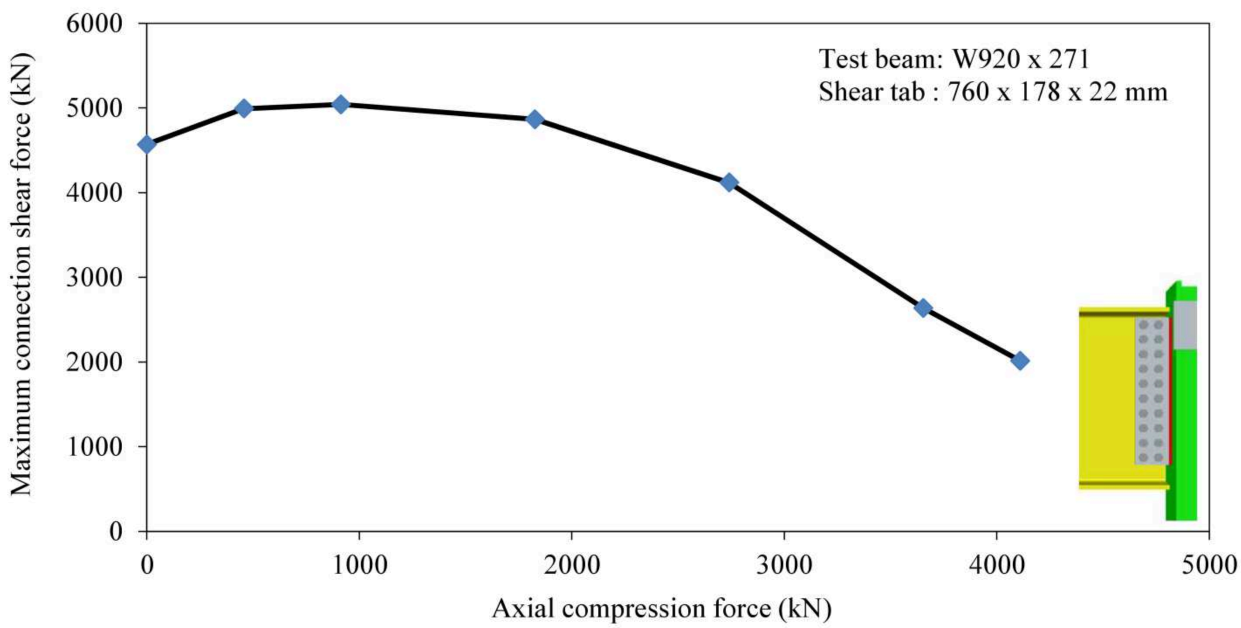

Figure 6.29– Connection configuration M15-C subjected to combined shear and axial compression simulation interaction curve

6.3.2. Combined shear and axial tension results

Subsequently, the performance of the same connections subjected to combined shear and tension force was investigated. For this purpose the direction of the axial force was reversed by changing the pressure direction at the end face of the beam. The response plots, interaction curves, and simulation observations of six FE models M1-T, M2-T, M7-T, M8-T, M13-T, and M15-T subjected to combined shear and axial tension is presented:

Connection configuration M1-T was the smallest connection that was investigated. Axial tension force lower than 50% of the ultimate shear resistance of the connection did not change the failure progression of the connection compared to the pure shear model (presented in Chapter 4); however the shear resistance was reduced due to the presence of axial tension force (Figures 6.31 and 6.32). Figure 6.30 demonstrates the final deformed shape including the plastic strain distribution of connection configuration M1-T for three axial tension force levels at the end of the FE simulations. As can be seen from Figure 6.30-A, 187 kN tension force resulted in yielding of the plate in shear, weld tearing on top of the plate, and excessive bearing around the bolt holes. Large plastic strain was developed between the two bottom holes which could have led to a brittle crack. By applying 280 kN axial tension force, the plastic strains started to spread towards the outer edge of the plate as shown in Figure 6.29-B. Finally by applying axial force tension over 373kN (100%T) the connection showed significant degradation of stiffness and bolt tear out was predicted as the failure mode.

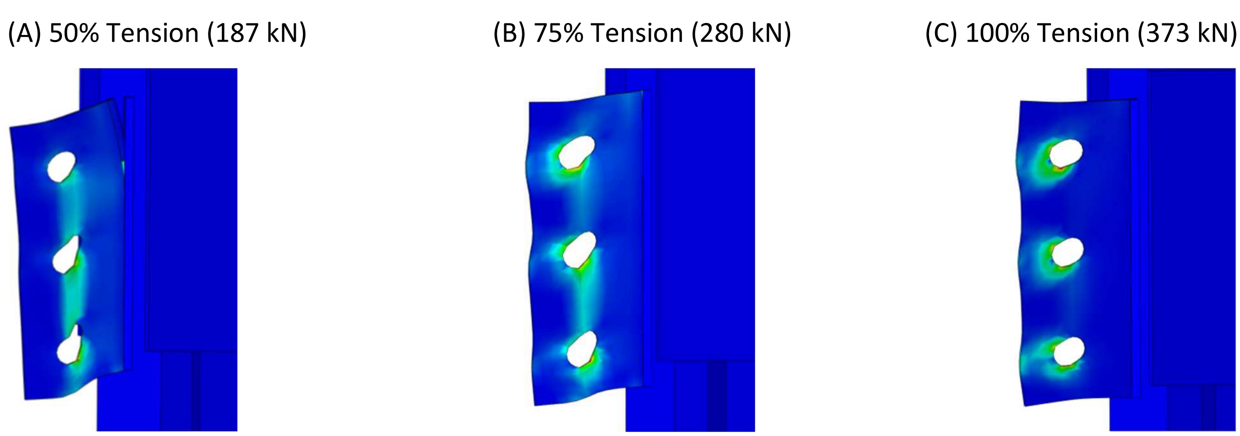

Figure 6.30- Final deformed shape and plastic strain distribution of connection configuration M15-C subjected to combined shear and different levels of compression force

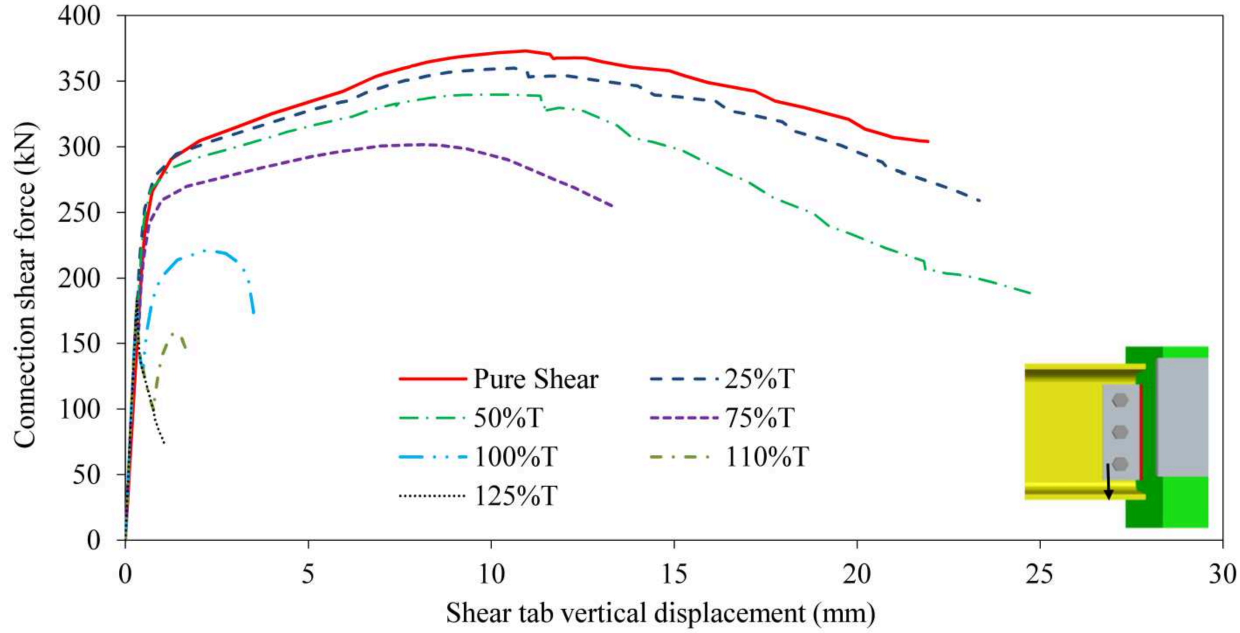

Figure 6.31– Connection configuration M1-T subjected to combined shear and different levels of axial tension force simulation response curves

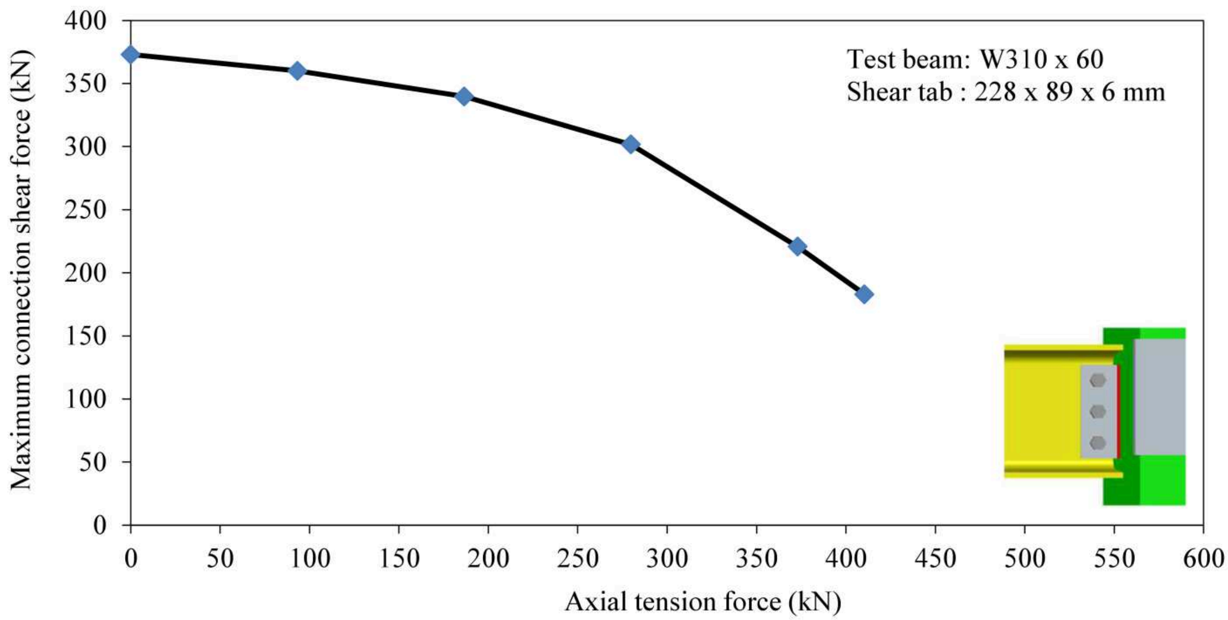

Figure 6.32– Connection configuration M1-T subjected to combined shear and axial tension simulation interaction curve

Connection configurations M7-T and M13-T both showed a quite linear degradation of shear resistance due to the presence of axial tension as shown in Figures 6.34 to 6.37. Both configurations failed in a same manner as a pure shear scenario for axial tension forces lower than 50% of their ultimate shear resistance.

Connection configuration M7-T did not show any tearing in the weld for any axial tension force level. Figure 6.33-A illustrates the deformed shape and plastic strain distribution of the connection subjected to combined shear and 573 kN (60%-T) axial tension force. As can be seen the highest plastic strains were located between the bolt holes which led to cracks in the net area. By applying higher axial tension forces, the plastic strain started to spread towards the outer edge of the plate, leading to a possible bolt tear out scenario at axial tension forces over 953kN (100%-T). Figure 6.33-B illustrates the deformed shape and plastic strain distribution of connection configuration M13-T subjected to combined shear and 1393 kN (80%-T) axial tension force. Unlike connection configuration M7-T, weld tearing was identified similar to the tearing in the pure shear simulation FE model and Marosi's (2011) test result. The failure mode determined for axial forces higher than 1740kN (100%-T) was bolt tear out.

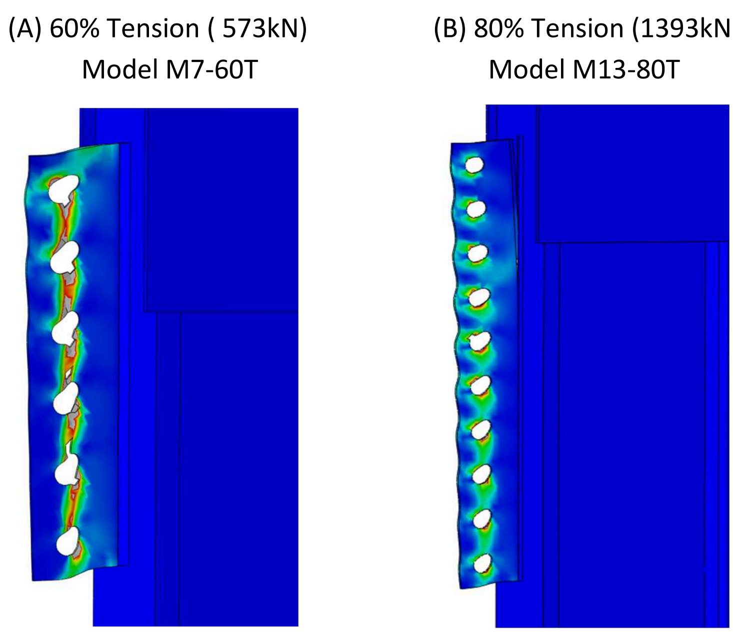

Figure 6.33- Final deformed shape and plastic strain distribution of connection configuration (A) M7-T subjected to combined shear and 573 kN axial compression force, (B) M13-T subjected to combined shear and 1393 kN axial compression force

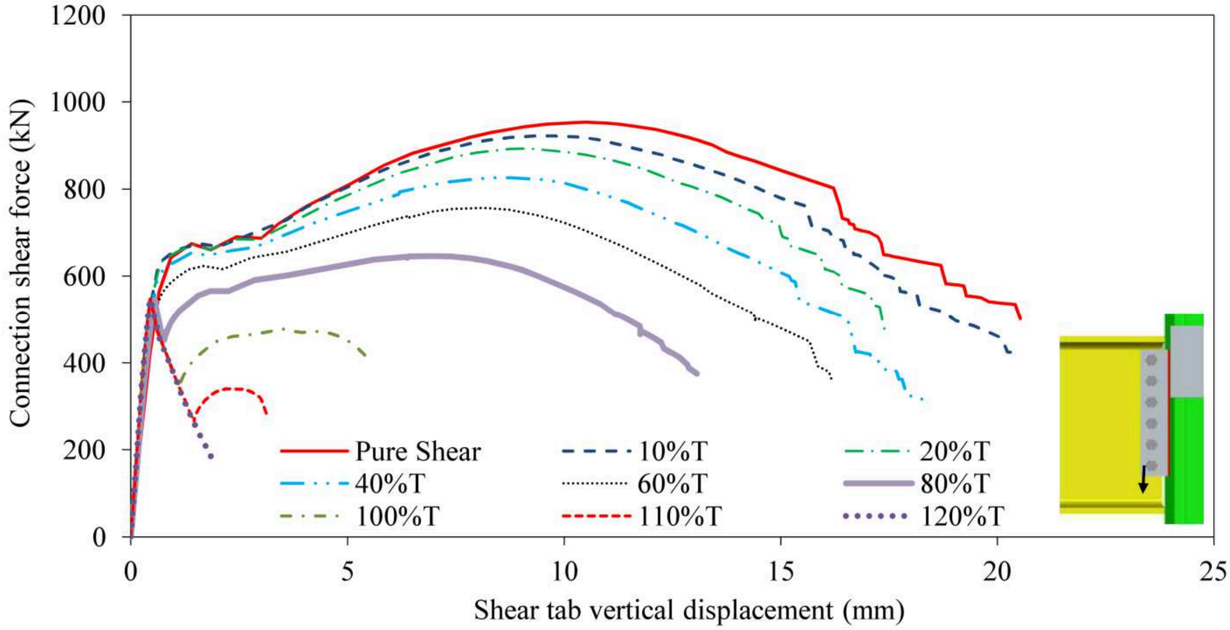

Figure 6.34– Connection configuration M7-T subjected to combined shear and different levels of tension force simulation response curves

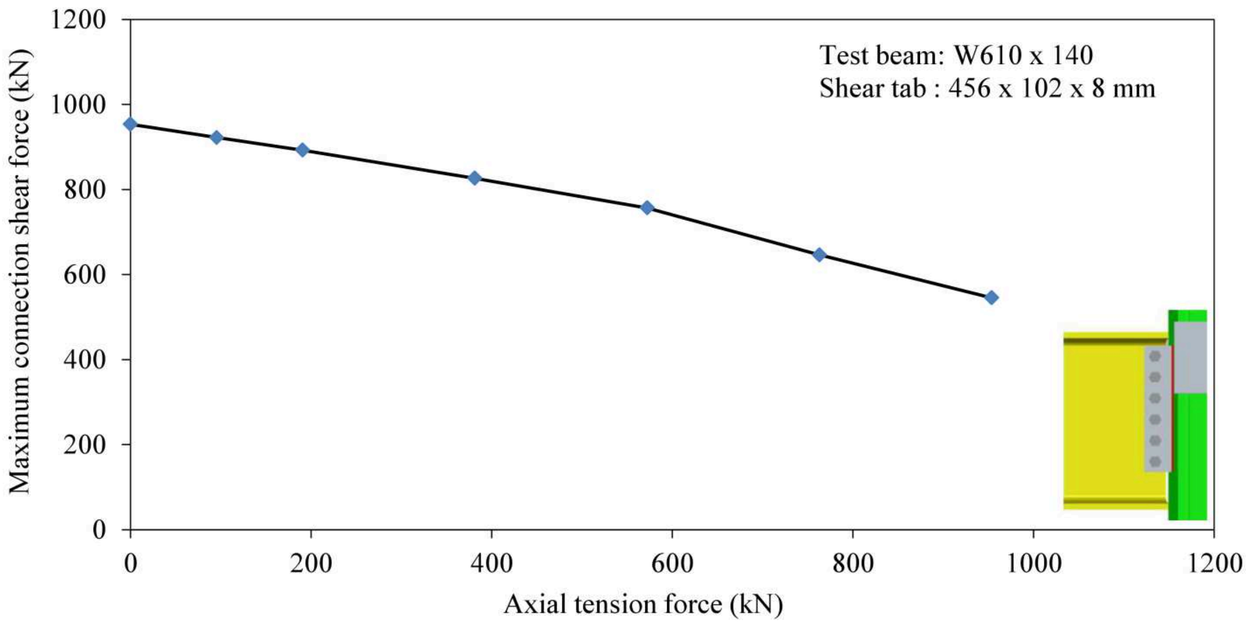

Figure 6.35– Connection configuration M7-T subjected to combined shear and tension simulation interaction curve

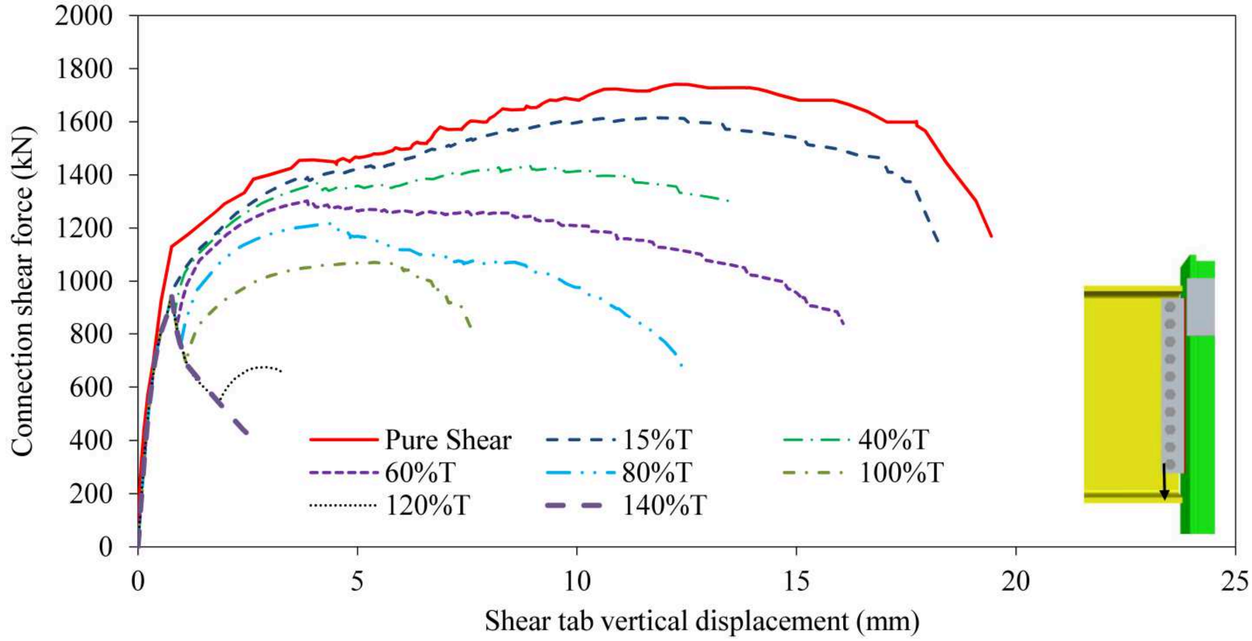

Figure 6.36 – Connection configuration M13-T subjected to combined shear and different levels of axial tension force simulation response curves

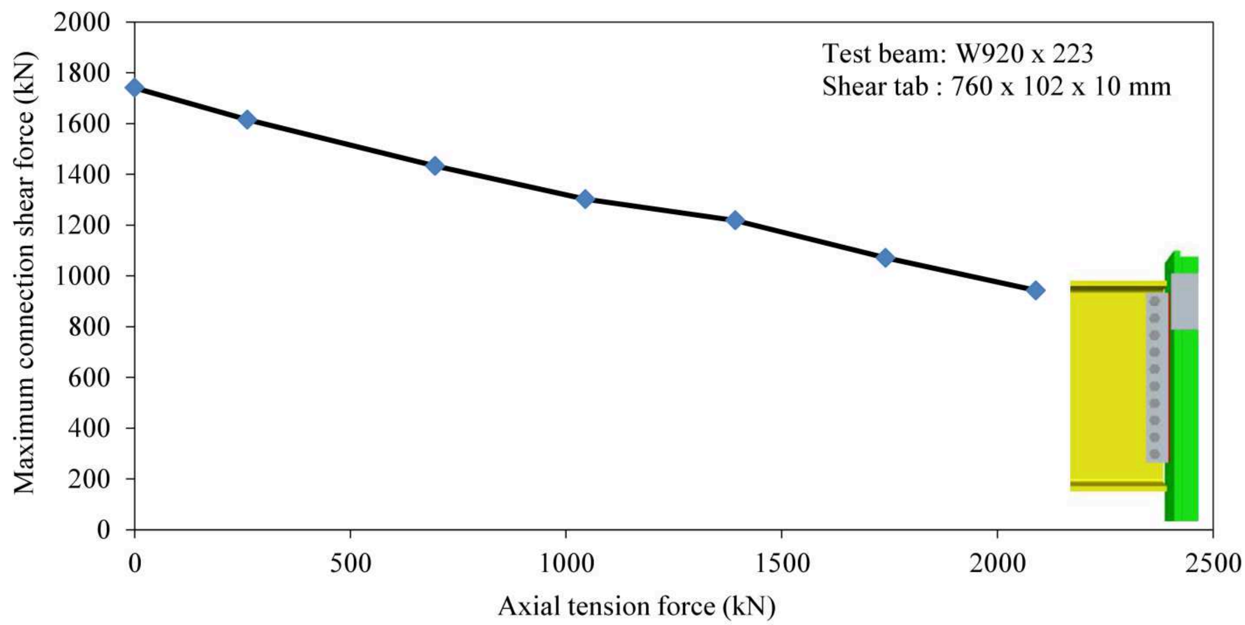

Figure 6.37– Connection configuration M13-T subjected to combined shear and axial tension simulation interaction curve

Figure 6.38 presents the response curve of model M2-T subjected to combined shear and various levels of axial tension force. The shear tab mainly failed due to tearing in the weld and no significant yielding was observed in plate. Greater axial tension force resulted in less shear yielding and lower ductility. Eventually a tension force over 596 kN (100%-T) resulted in a brittle weld failure with no yielding in the plate. Figure 6.39 illustrates the generated interaction curve of connection configuration M2-T.As can be seen from the figure, the connection experienced a linear degradation of shear resistance due to the presence of axial tension force.

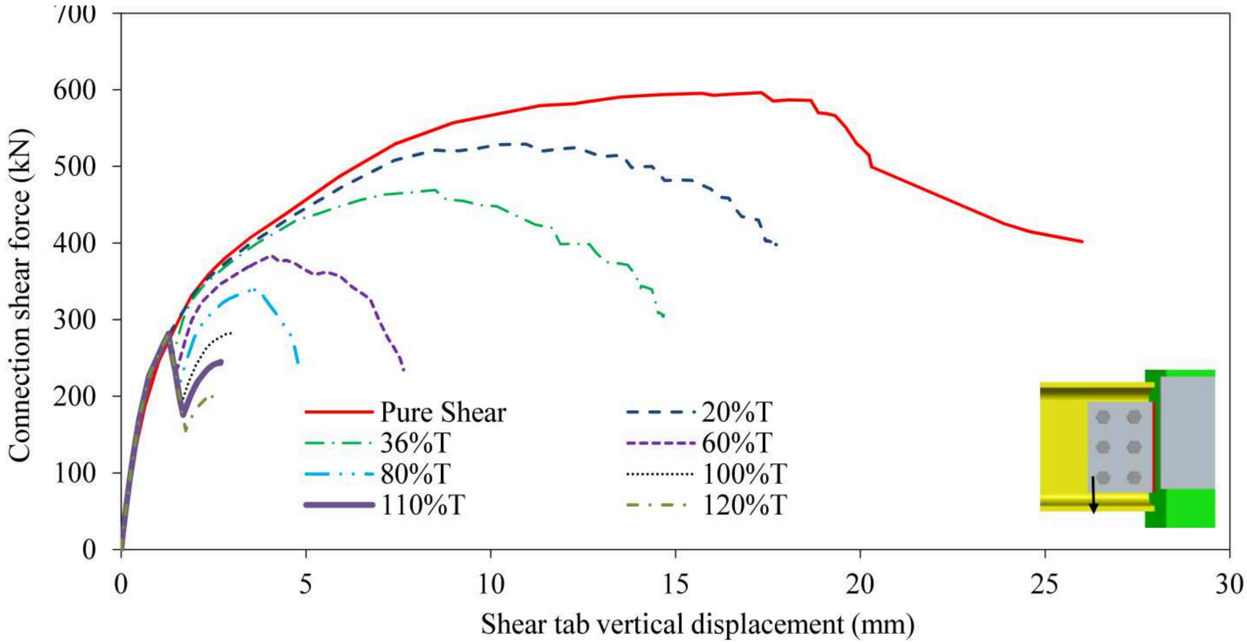

Figure 6.38– Connection configuration M2-T subjected to combined shear and different levels of tension force simulation response curves

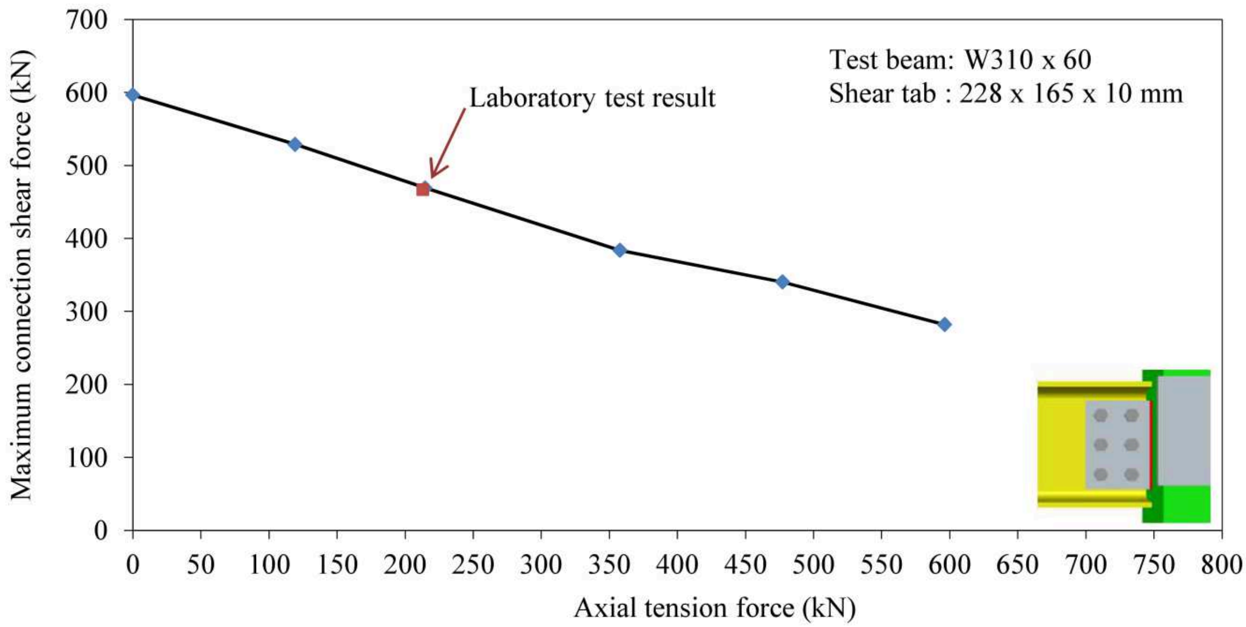

Figure 6.39– Connection configuration M2-T subjected to combined shear and tension simulation interaction curve

Model M8-T subjected to combined shear and 512 kN axial tension force was the simulation model replicating verification Test #4 (presented in Chapter 5) if the connecting fillet weld size used was 10mm identical to the weld size that Marosi (2011) had designed and tested. Due to a fabrication error the weld size was measured to be 5mm instead of 10mm. Figure 6.40-A shows the final deformed shape and plastic strain distribution of connection configuration M8-T for the same axial tension level used in the verification test (512kN) and Figure 6.40-B represents the effect of 1790kN (100%T) axial tension on the connections performance. Axial tension forces lower than 1074 kN resulted in shear yielding of the plate between the first bolt line and the column, followed by some tearing in the connecting weld, and eventually the development of cracks between bolt holes. Axial tension force higher than 1432 kN decreased plastic strain distribution in the plate and led to the possibility of a brittle weld tear failure.

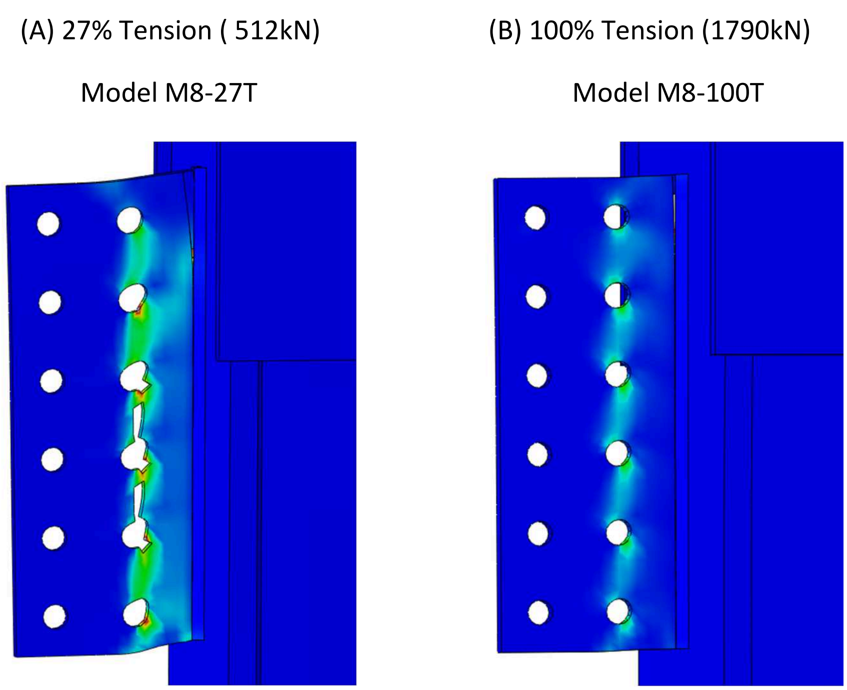

Figure 6.40- Final deformed shape and plastic strain distribution of connection configuration (A) M7-T subjected to combined shear and 573 kN axial compression force, (B) M13-T subjected to combined shear and 1393 kN axial compression force

Figure 6.41 illustrates the corresponding response curve of connection configuration M8-T subjected to shear and various levels of axial tension force. The shear-axial tension interaction curve of connection configuration M8-T (Figure 6.42) shows a linear degradation of shear resistance due to the impact of axial tension force.

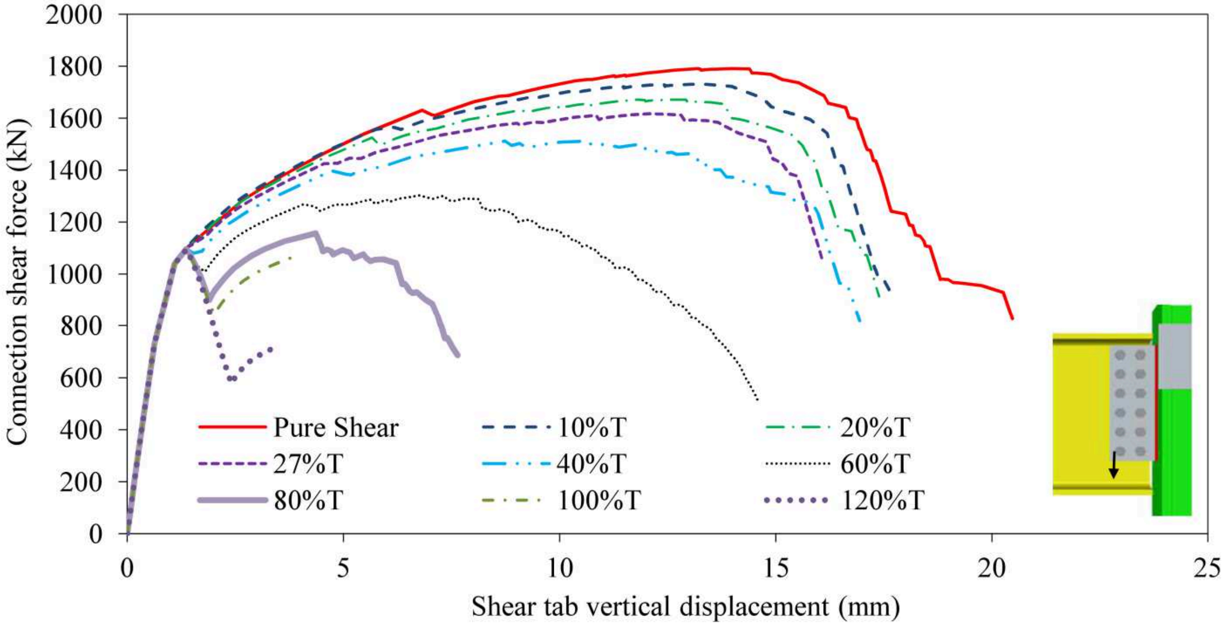

Figure 6.41– Connection configuration M8-T subjected to combined shear and different levels of tension force simulation response curves

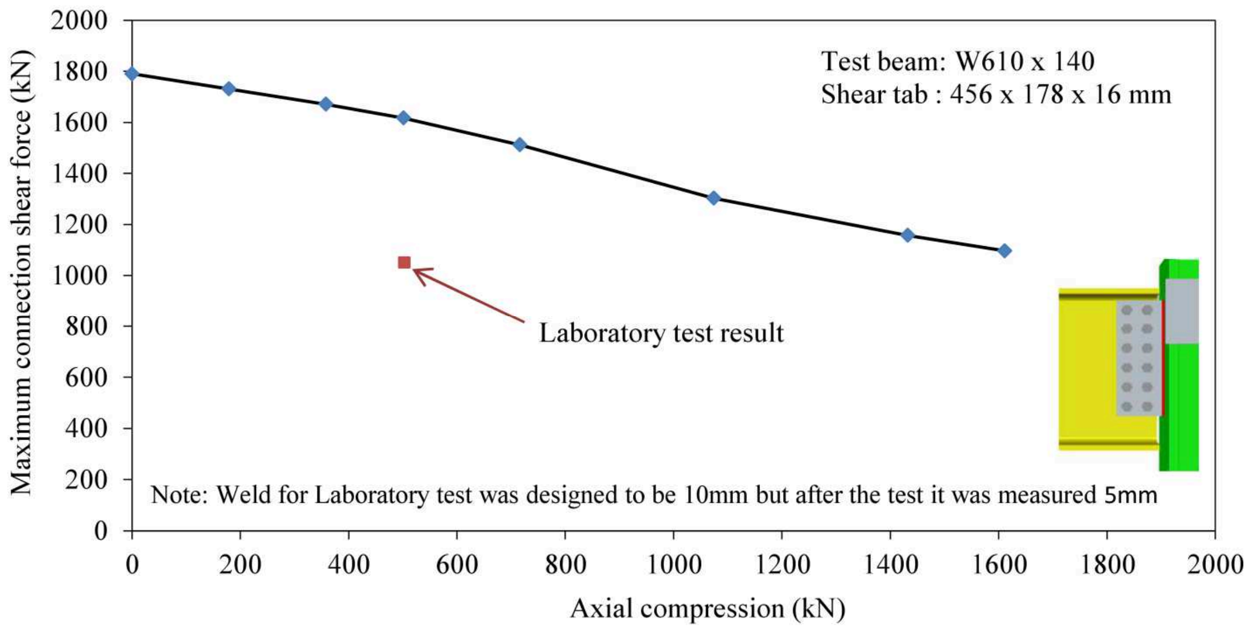

Figure 6.42– Connection configuration M8-T subjected to combined shear and tension simulation interaction curve

Similarly to the FE model simulating connection configuration M15-C, the behaviour of connection configuration M15-T was affected due to its high stiffness. For axial tension forces below 913 kN (20%T), the behaviour was similar to the pure shear FE model presented in Chapter 4. After exceeding axial tension force over 1826 kN (40%T) the rate of shear resistance degradation changed but eventually continued to degrade with the initial rate (Figure 6.45). The reason for this change in behaviour compared to the remaining models was the high stiffness of the connection and its influence on the beams web. Figure 6.43 shows the final deformed shape of connection configuration M15-T subjected to shear and 2740 kN tension force.As can be seen from the figure,the beam's web between the main actuator load block and the connection column has yielded in shear.The shear tab experienced some yielding along the first line of bolts (closer to the column); however, no significant plastic deformations was observed in the shear tab itself.On the other hand, the beam's web experienced high plastic strains between the holes on the second vertical row and the plastic strain spreaded towards the end face of the test beam at the the top and botom leading to a possible block shear failure at higher axial force levels.

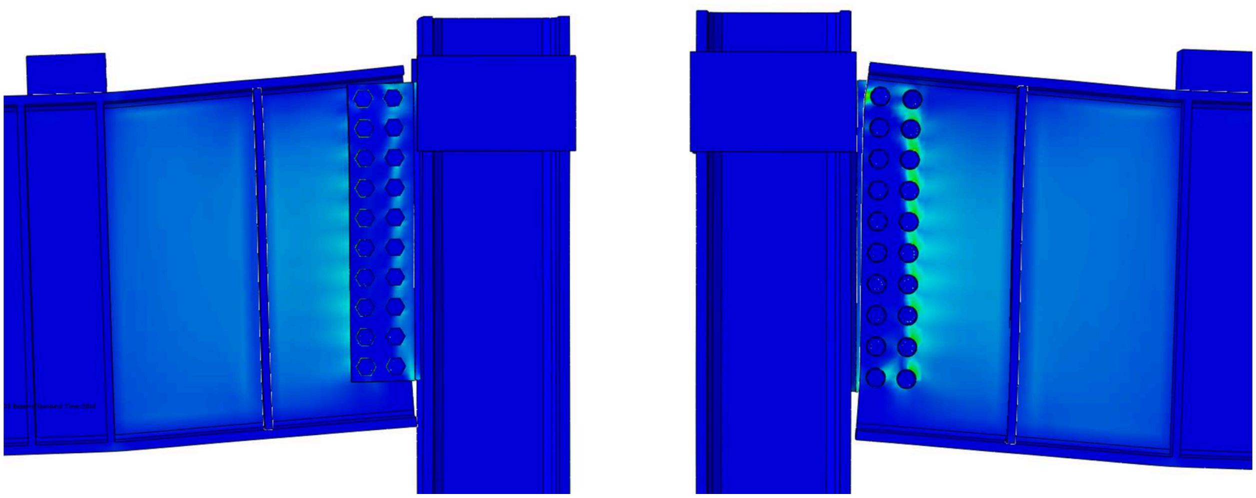

Figure 6.43- Final deformed shape and plastic strain distribution of connection configuration M15-T subjected to combined shear and 2740 kN compression (connection and beam web view)

Figure 6.44 illustrates the response curve of connection configuration M15-T subjected to shear and various levels of axial tension force .The corresponding shear force-axial tension force interaction curve of connection configuration M15-T is shown in Figure 6.45.

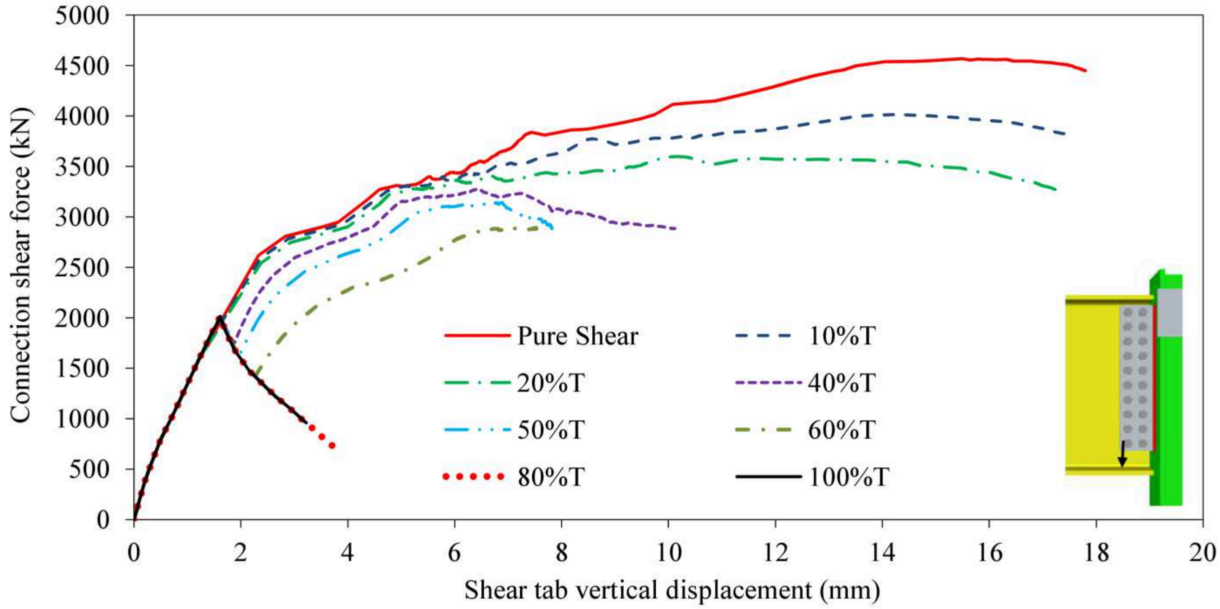

Figure 6.44– Connection configuration M15-T subjected to combined shear and different levels of tension force simulation response curves

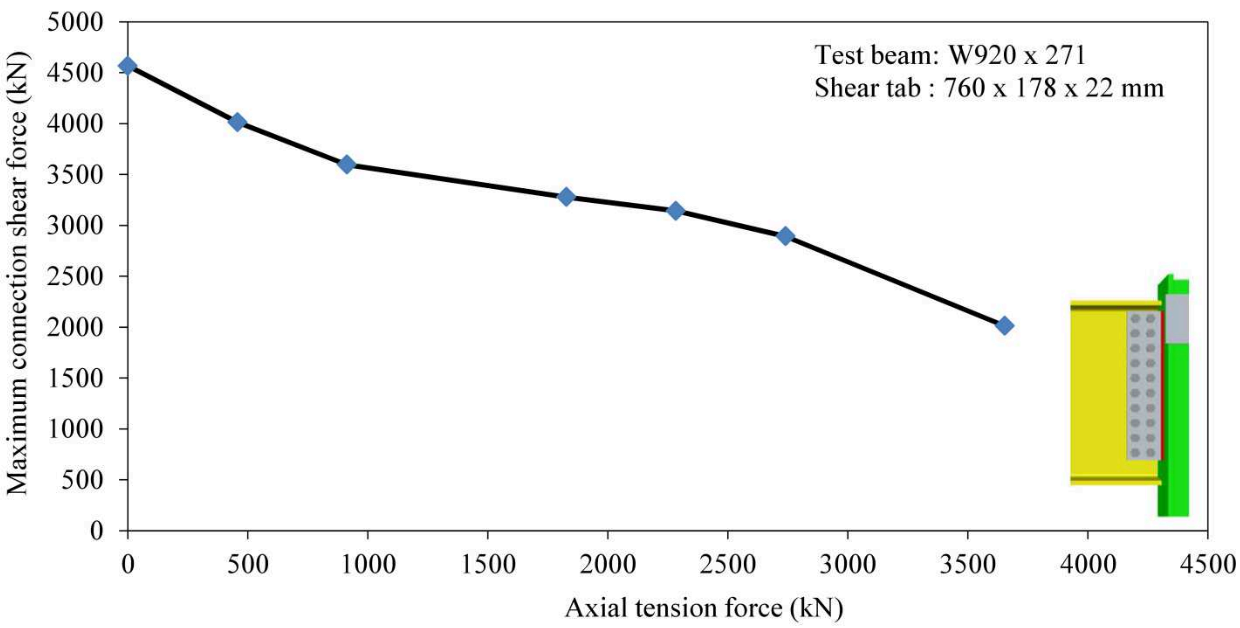

Figure 6.45– Connection configuration M15-T subjected to combined shear and tension simulation interaction curve

6.4. Summary

The FE models of connection configurations M2-T, M2-C, and M8-C were capable of simulating the verification laboratory testing procedure and were able to predict the ultimate shear resistance of the connection within a margin of ± 5%. M8-T determined the shear resistance of the connection if the connecting weld was welded based on the design size (10mm). Based on the confidence gained by the simulations of connection configurations M2-T, M2-C, M8-C and M8-T, the remaining FE models were used to determine the interaction of shear and axial force.

Six connection configurations were investigated under the influence of combined shear and axial compression force. Overall the combined shear and axial compression FE model interaction curves showed a 2nd or 3rd order trend curve which demonstrated an initial gain in shear resistance for lower axial forces and continued by degradation of the shear resistance when the axial compression exceeded a specific level and ultimately the shear resistance dropped below the suggested service load level. Connection configurations with two vertical rows of bolts were identified to be more sensitive to axial compression, since their shear capacity degraded at lower axial compression force levels compared to the shear tabs connected by a single vertical row of bolts.

The same six connection configurations were then subjected to combined shear and axial tension. The resulted interaction curves for combined shear and axial tension force showed a linear degradation trend of shear resistance with the exception of models M1-T and M15T where the stiffness degraded non-linearly. Overall, the shear tabs that were connected by a single vertical row of bolts showed at least 12% higher axial tension capacity in comparison with the shear tabs connected by two vertical rows of bolts.

Further details on how the interaction curves were used in the development of the design approach is explained in Chapter 7.

Chapter 7

Design approach

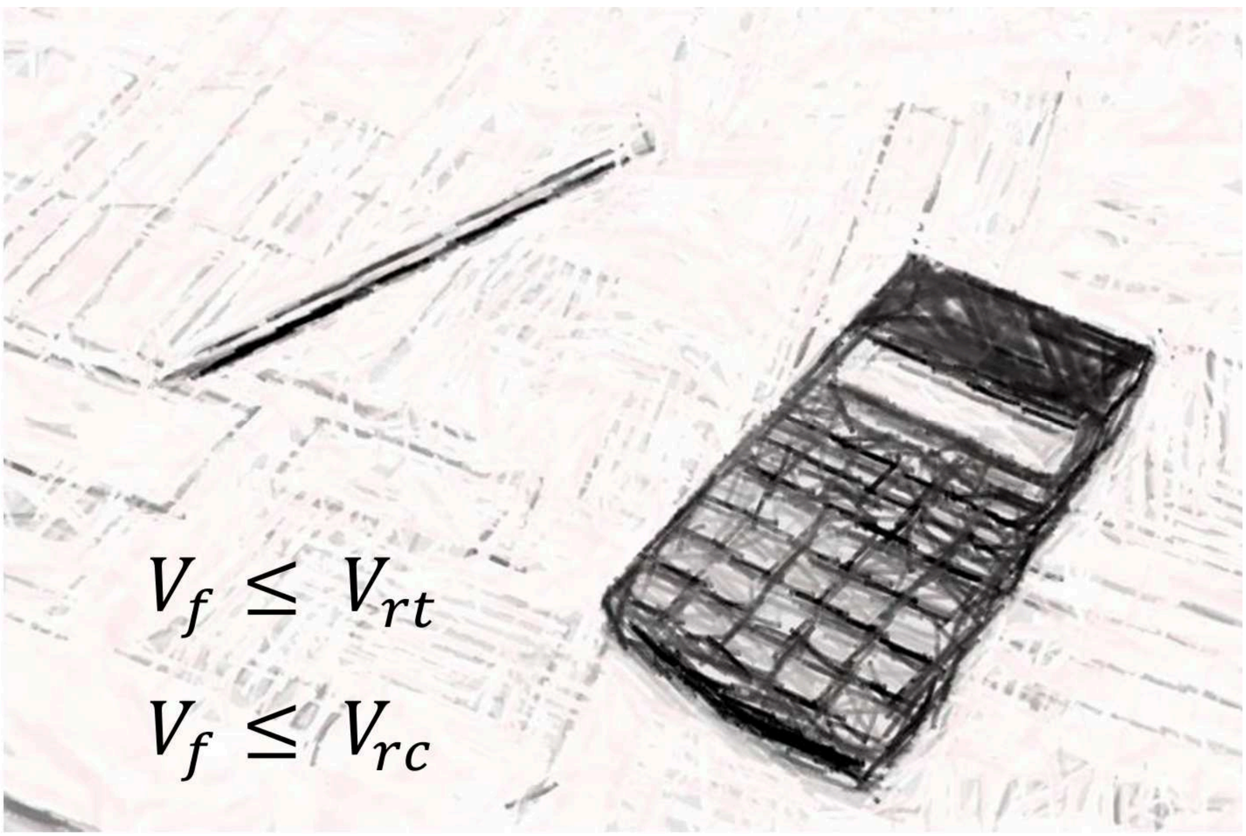

7. Chapter 7 – Design approach

This chapter summarizes the FE simulation results obtained from Chapter 6 and presents the suggested approach for the design of shear tab connections subjected to combined shear and axial forces.

7.1. Development of design approach

The design approach was developed by completing the following steps:

1. Establishing a relation for the variation of shear resistance with the magnitude of axial tension or axial compression force by producing a shear force-axial force interaction curve for each connection configuration, which was accomplished in Chapter 6.
2. Determining the maximum allowable tension or compression force that could be applied to the connection configurations while sustaining a suggested minimum gravity service load level (V_s) as explained in Section 6.1.
3. Normalizing the interaction curves with the maximum pure shear resistance on the vertical axis and the maximum allowable axial force on the horizontal axis.
4. Determining a linear, 2nd or 3rd order polynomial trend line or curve with a coefficient of determination (R2) of higher than 95% for each configuration.
5. Establishing a relation between the connection size and the corresponding interaction trend line or curve.
6. Introducing the axial modification factor used for design, which modifies the ultimate shear resistance of the connection to account for the factored applied axial load.

The performance of the shear tab configurations under combined shear plus tension force was different compared with a combined shear plus compression force scenario; therefore, the results and the design approach are presented separately. In addition, the performance of the shear tabs connected by a single or double vertical row of bolts was investigated individually. Figure 7.1 and 7.2 illustrates the normalized shear force vs. axial tension force interaction curves including trend functions of shear tab configurations connected by one and two vertical rows of bolts. V_{max} is the maximum shear resistance of the connection for pure shear; V is the ultimate shear resistance of the connection subjected to axial forces. T and C are the axial tension and compression forces that are applied to the connection. T_{max} and C_{max} are the highest axial tension and compression forces that can be applied to the connection. Any axial force higher than T_{max} and C_{max} will result in failure of the connection or a shear resistance lower than V_s, the minimum gravity service load level.

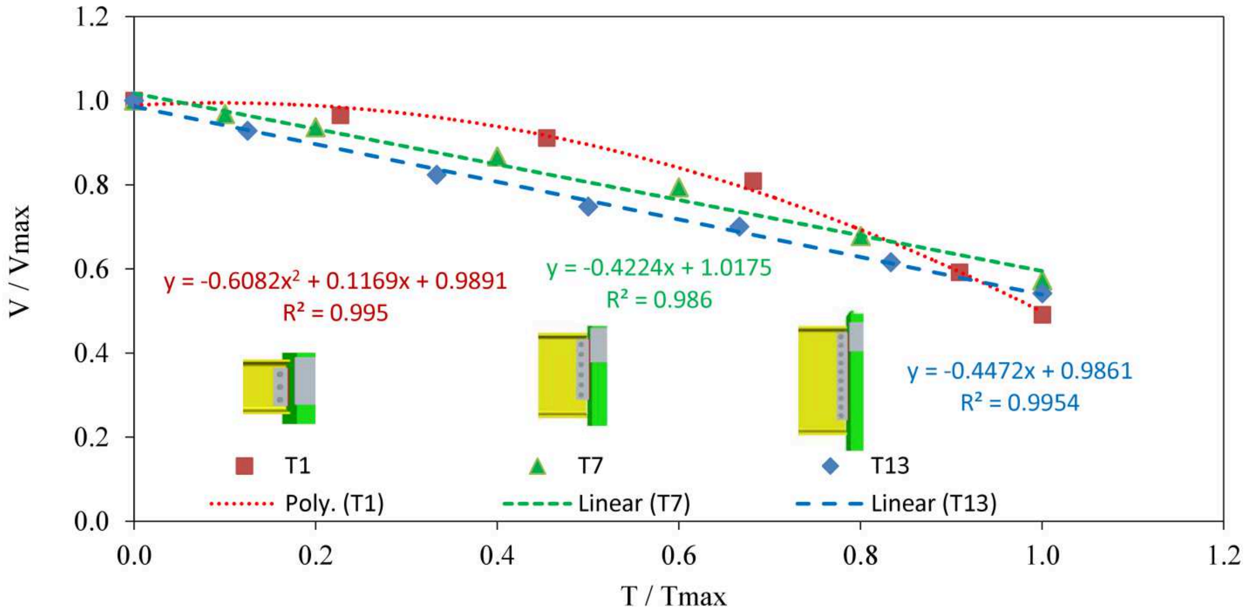

Figure 7.1-Normalized shear-axial tension force interaction curves for shear tab configurations connected by a single vertical row of bolts

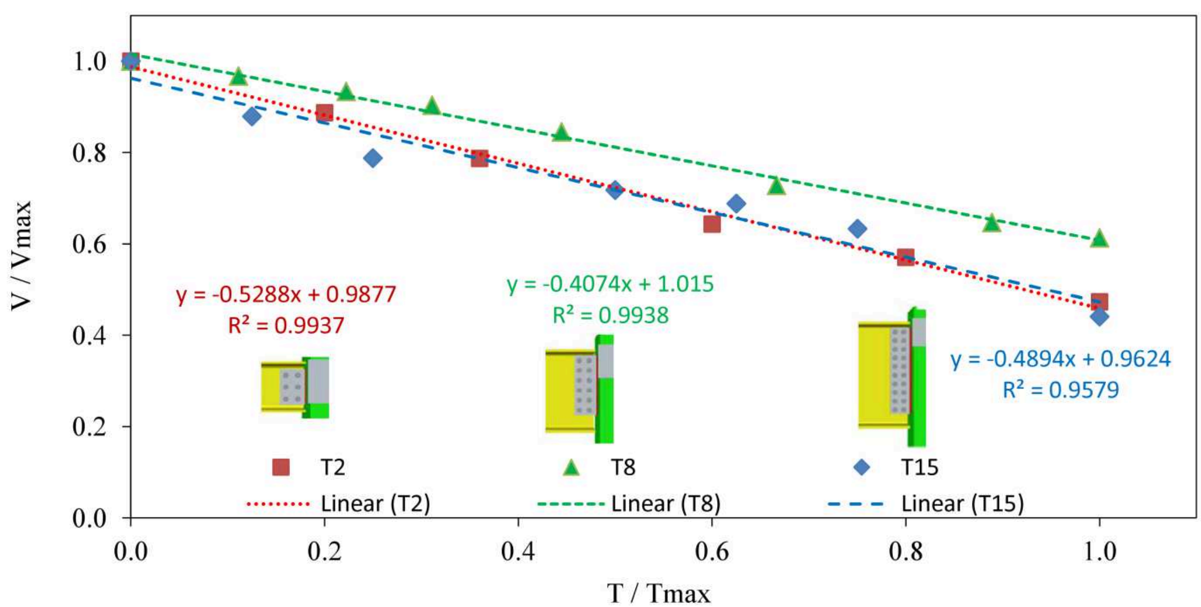

Figure 7.2- Normalized shear-axial tension interaction curves for shear tab configurations connected by two vertical rows of bolts

As can be seen from Figures 7.1 and 7.2, with the exception of Model T1, the remaining connection models showed a linear degradation trend of shear resistance as the axial tension force was increased. Based on this observation it was decided to introduce a linear reduction of shear resistance for combined shear and axial tension force. By combining each three series of data points of Figure 7.1 and 7.2, an average degradation linear trend line (Figure 7.3 and 7.4) was introduced which is used for the design model presented in Section 7.2. The slope of this trend line for the single vertical row configurations was found to be -0.4562 and -0.4731 for the double vertical row configurations.

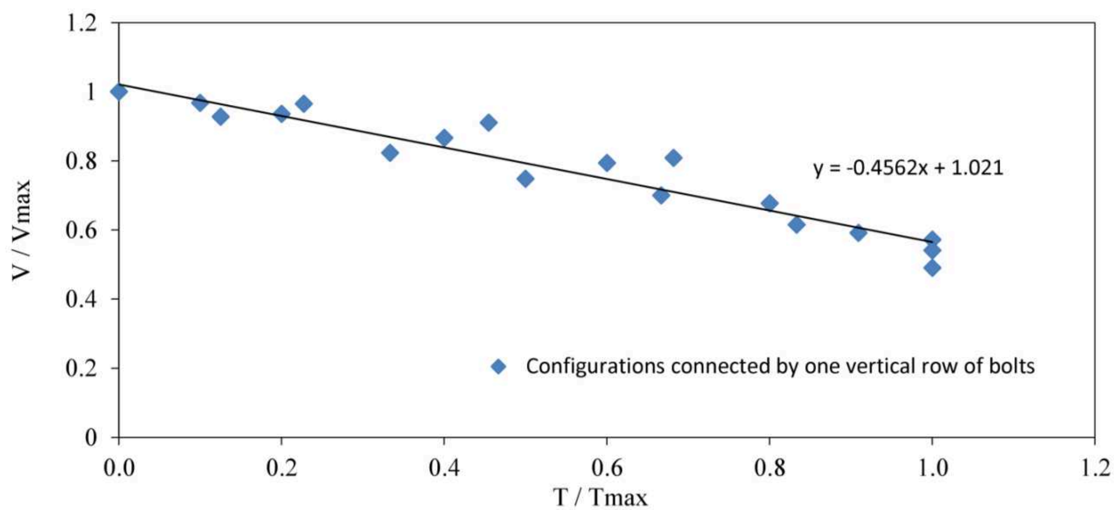

Figure 7.3- Shear-axial tension interaction line for shear tab configurations connected by one vertical row of bolts

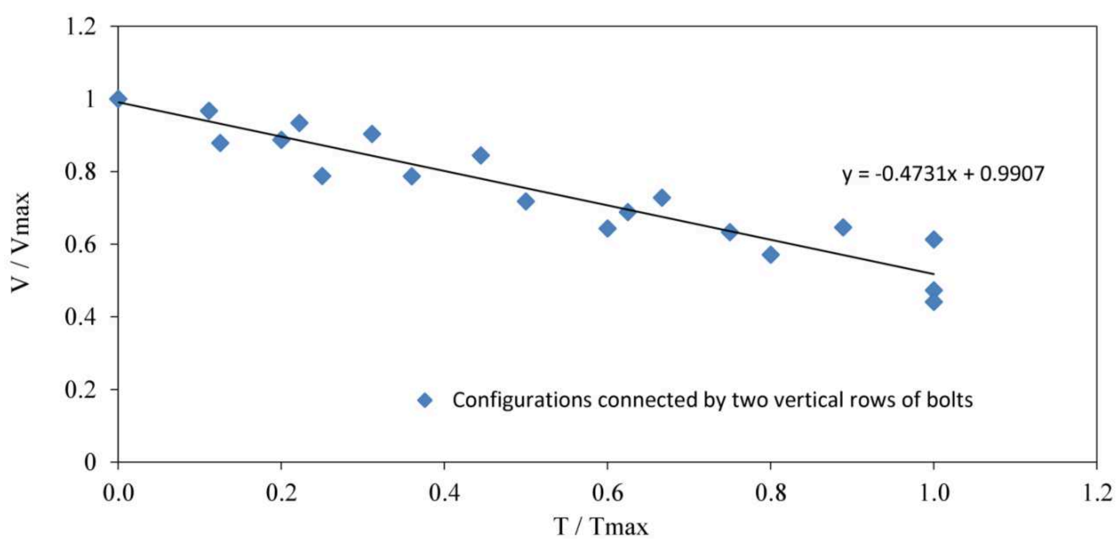

Figure 7.4- Shear-axial tension interaction line for shear tab configurations connected by two vertical rows of bolts

In a similar manner the process was repeated for the combined shear and axial compression force interaction curves; however an average linear trend line was found not to be suitable for representing the overall behaviour. Instead a 3rd order polynomial trend curve was determined for each configuration as shown in Figures 7.5 and 7.6.

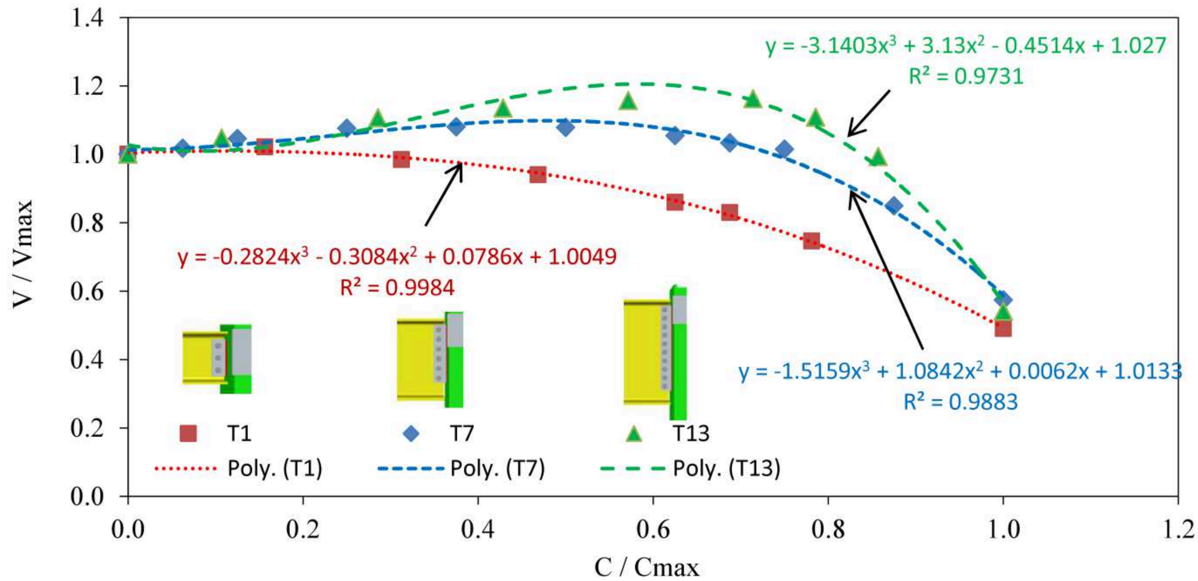

Figure 7.5-Normalized shear-axial compression force interaction curves for shear tab configurations connected by a single vertical row of bolts

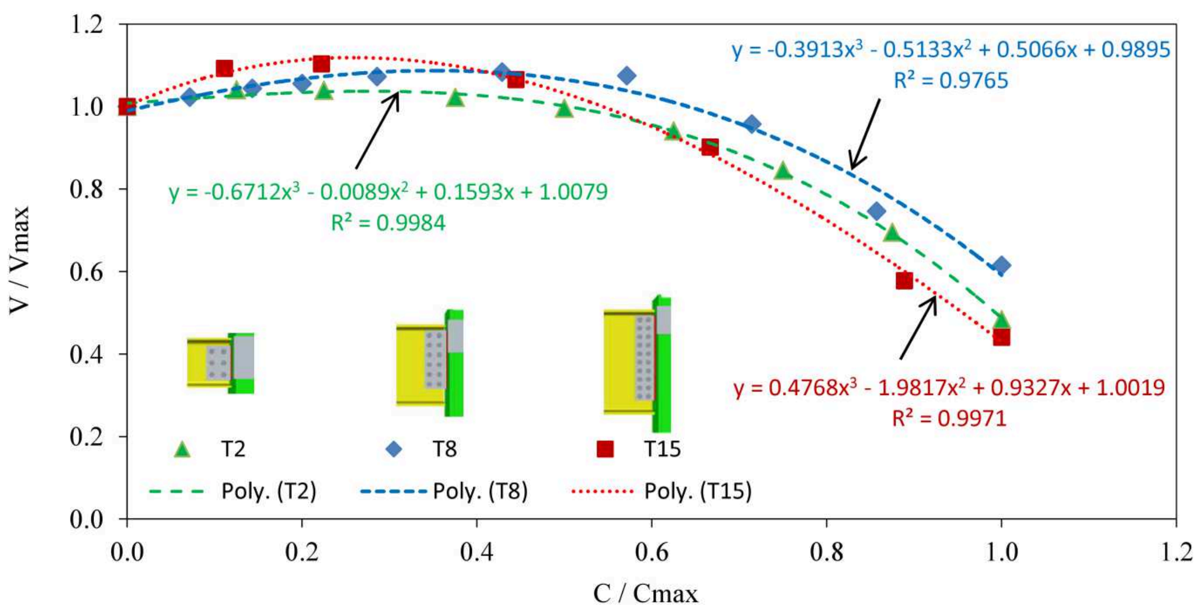

Figure 7.6-Normalized shear-axial compression force interaction curves for shear tab configurations connected by a single vertical row of bolts

Unlike the combined shear and axial tension force interaction, the single and double vertical row configurations showed an initial increase of shear resistance due to the presence of axial compression force in the connection. Eventually the connection lost its stiffness leading to degradation of the shear resistance; therefore a change of curvature was required for the representative interaction trend curve that varies based on the connection size and number of vertical row of bolts used.

In order to determine the relation between the polynomial coefficients with the connection size, the values of the coefficients versus the number of bolts per vertical row of bolts was plotted and the change of each coefficient value (A, B, and C) was determined as a function of the number of bolts. Figure 7.7–A illustrates the coefficients of the 3rd order polynomial trend curve established for the single vertical row connected shear tab configurations and Figure 7.7-B shows the coefficient trend functions for shear tabs connected by two vertical rows of bolts. Ultimately the results of Figures 7.7 were used for the suggested design approach for designing shear tabs subjected to combined shear and compression force. These coefficients were used to determine the shear force resistance modification factor for compression (C_c) described in Section 7.4.

(A)

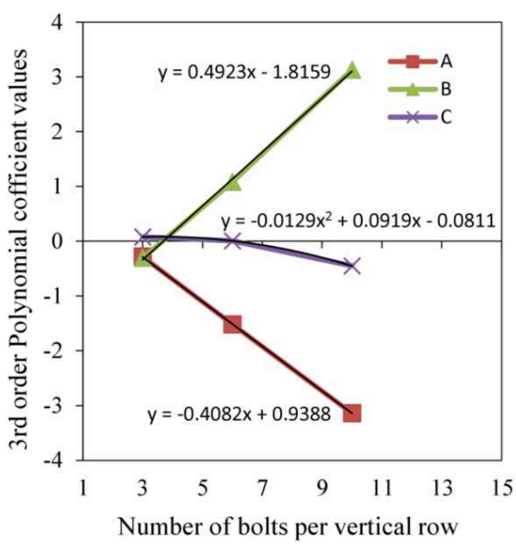

(B)

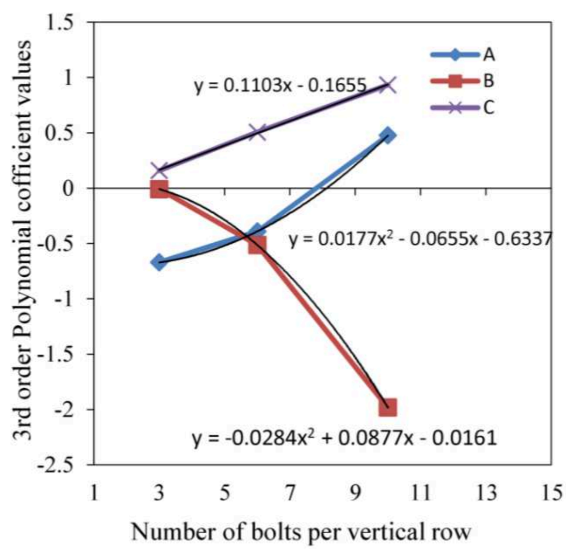

Figure 7.7-Variation of polynomial trend curve coefficients with respect to the number of bolts for shear tabs connected by (A) Single vertical row of bolts, (B) Two vertical rows of bolts

7.2. Design approach methodology

This section introduces the methodology used in the development of the design approach. A list of symbols used for the design approach is presented:

V_{max}: Measured shear resistance of connection determined by means of experiment or equivalent FE simulation (independent of design code used)

V_{rp} : Predicted shear resistance of connection based on design limit state equations for shear tab connections and by using a resistance ϕ factor of 1

V_{rd} : Design shear resistance of connection based on design limit states for shear tab connections with required resistance ϕ factors for each limit state

V_{rt} : Modified design shear resistance of connection including the effect of axial tension force

V_{rc} : Modified design shear resistance of connection including the effect of axial compression force

T_f : Factored applied axial tension force

C_f : Factored applied axial compression force

T_r : Pure tensile resistance of connection calculated based on the minimum tensile resistance of the shear tab and beam.

T_{max} : Maximum allowable axial tension force

C_{max} : Maximum allowable axial compression force

C_t : Shear resistance modification factor for combined shear and axial tension force

C_c : Shear resistance modification factor for combined shear and axial compression force

n : Number of bolts per vertical row (3-10)

S : Design code over-strength margin

Figure 7.8 demonstrates the design model used for designing shear tab connections subjected to combined shear and axial tension. The true interaction curve is the average linear trend line determined in Section 7.1 which is used to provide the degraded shear resistance based on the axial tension force that is being applied. This interaction curve is generated based on laboratory testing and FE simulation by using actual material properties (determined from coupon testing); therefore it is independent of a design code.

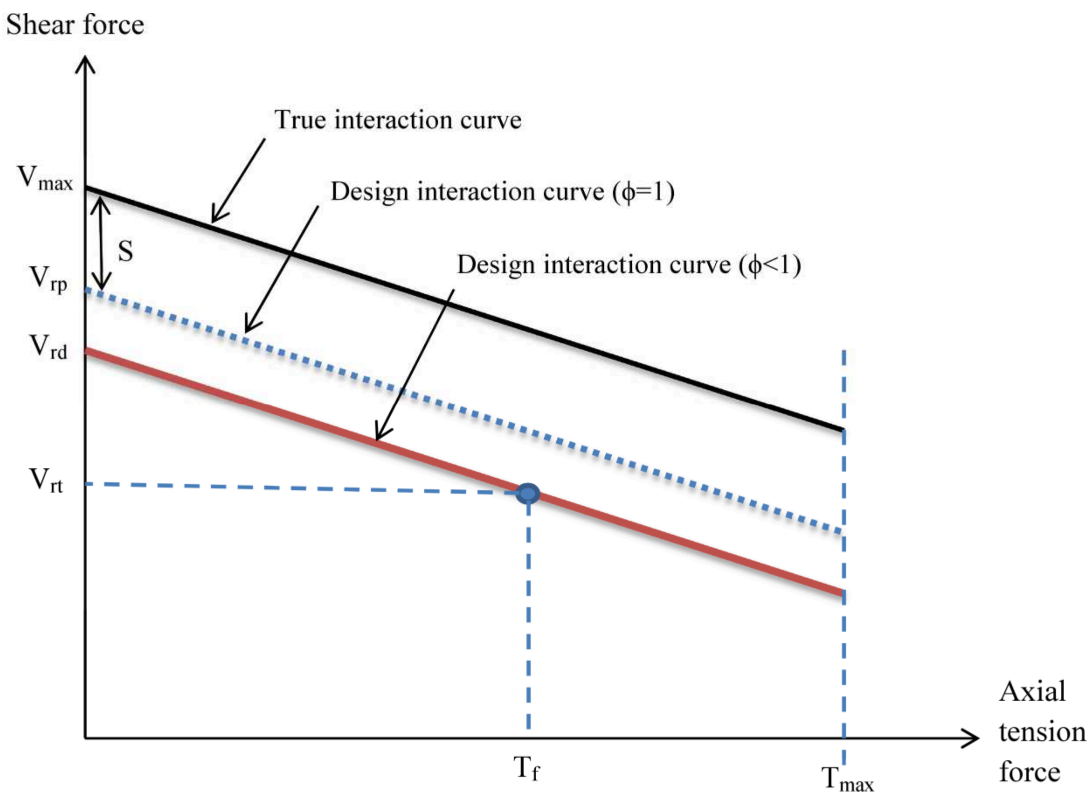

Figure 7.8-Representation of the design model for combined shear and axial tension force

The difference of V_{max} and V_{rp} is referred as "S". Based on Marosi's (2011) experimental work, S varies from 27% to 71% dependent on connection configuration, material properties and design code used for predicting the ultimate shear resistance. V_{rp} is the predicted shear resistance of the connection based on design limit state equations and is determined by using minimum nominal material properties and a resistance ϕ factor of 1.The design interaction curve (ϕ=1) is defined as an offset line from the true interaction curve with a vertical offset spacing of "S". This curve defines the change of shear resistance of the connection if the maximum pure shear resistance of the connection was equal to V_{rp}. V_{rd} is the design pure shear resistance which is dependent on design code. An additional safety margin is also provided by the ϕ factor of the controlling limit state (difference of V_{rp} and V_{rd}), therefore a minimum factor of safety of 30% is considered for the anticipated design approach. The final design interaction curve (ϕ<1) is shaped by an offset line from the true interaction curve with a spacing of "S" plus the difference between V_{rp} and V_{rd}. By using this technique the reduced shear resistance (V_{rt}) for an axial force (T_f) lower than T_{max} can be determined. T_{max} is defined as a percentage of V_{max} based on the interaction curves produced in Chapter 6.

The same methodology was used for the combined shear and compression; however a 3rd order polynomial function was used instead of a straight line as the design interaction curve (Figure 7.9)

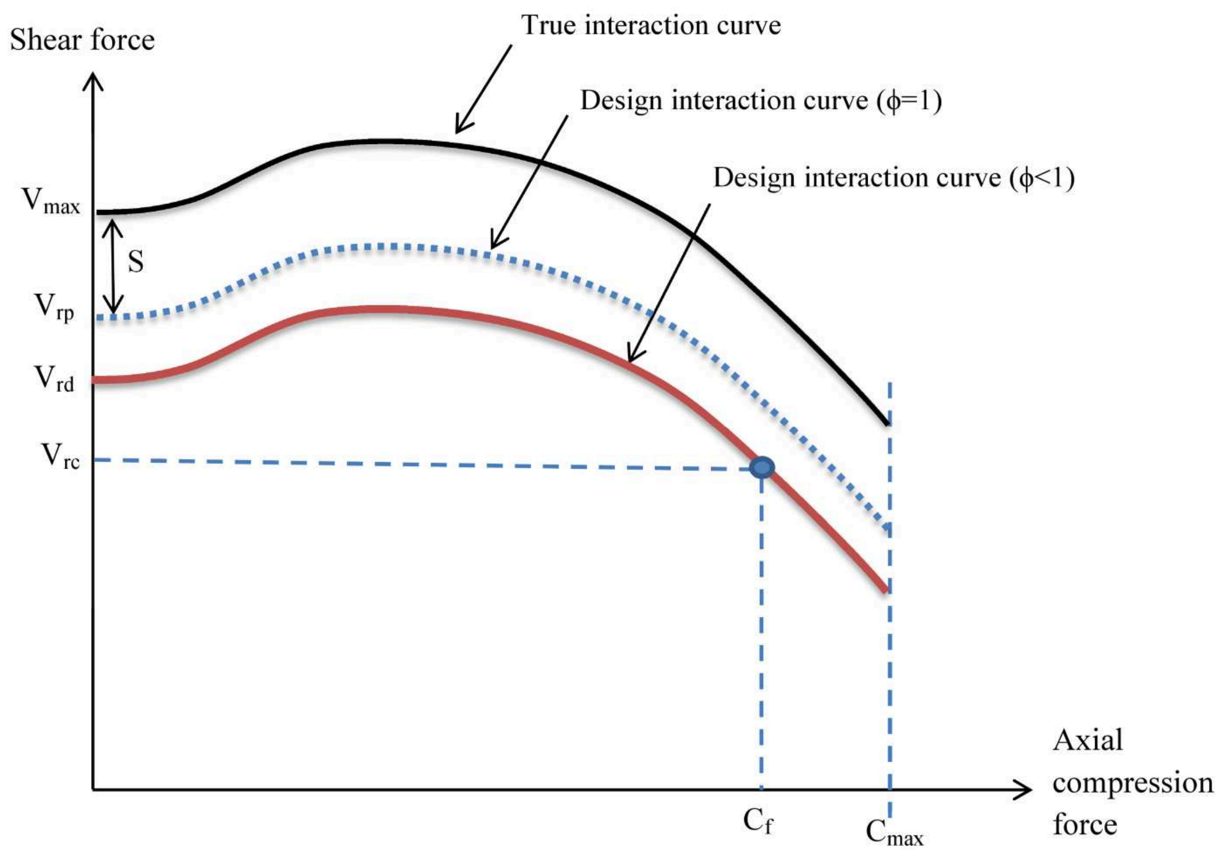

Figure 7.9-Representation of the design model for combined shear and axial compression force

7.3. Combined shear and axial tension force design procedure

The suggested approach for designing a shear tab subjected to a combined shear force of V_f and an axial tension force of T_f is to:

1) Calculate the pure shear resistance of the connection V_{rd} based on the design code of interest. The design approach presented in the AISC 14th edition manual of steel construction (AISC, 2011) or the modified approach suggested by Marosi (2011) is recommended.

2) Calculate the design pure tensile resistance of the connection T_r , which is the minimum of the tensile capacity of the shear tab, beam web, connecting weld and the shear capacity of the bolt group.

3) Use Equations 7.1 and 7.2 to determine the maximum allowable tensile force.

For one vertical row of bolts: $T_{max} = V_{rd} \leq T_r$ Equation 7.1

For two vertical rows of bolts: $T_{max} = (1.08 - 0.028\,n)\,V_{rd} \leq T_r$ Equation 7.2

n : Number of bolts per vertical row (3-10)

4) Calculate the shear force reduction factor C_t by using Equations 7.3 and 7.4.

For one vertical row of bolts: $C_t = 1 - 0.456\left(\frac{T_f}{T_{max}}\right)$ Equation 7.3

For two vertical rows of bolts: $C_t = 1 - 0.473\left(\frac{T_f}{T_{max}}\right)$ Equation 7.4

5) Calculate the reduced shear resistance of the connection (V_{rt}) and compare it with the factored shear force (Equation 7.5)

$V_{rt} = C_t\,V_{rd}\,, \quad V_f \leq V_{rt}$ Equation 7.5

7.4. Combined shear and axial compression force design procedure

The suggested approach for designing a shear tab subjected to a combined shear force of V_f and an axial compression force of C_f is to:

1) Calculate the pure shear resistance of the connection V_{rd} based on the design code of interest. The design approach presented in the AISC 14th edition manual of steel construction (AISC, 2011) or the modified approach suggested by Marosi (2011) is recommended.

2) Calculate the design pure compression resistance of the connection C_r , which is determined based on the minimum of the squash capacity of the shear tab loaded in the direction perpendicular to the connecting weld and the shear capacity of the bolt group.

3) Use Equations 7.6 and 7.7 to determine the maximum allowable compression force where n is the number of bolts per vertical row (3-10):

For one vertical row of bolts: $C_{max} = (1.86 - 0.1n)\, V_{rd} \le C_r$ Equation 7.6

For two vertical rows of bolts: $C_{max} = 1.6\, V_{rd} \le C_r \qquad n \le 6$ Equation 7.7

$C_{max} = 1.4\, V_{rd} \le C_r \qquad n > 6$

4) Calculate the shear force modification factor C_c by using Equations 7.8.

$C_c = 1 + A\left(\frac{C_f}{C_{max}}\right)^3 + B\left(\frac{C_f}{C_{max}}\right)^2 + C\left(\frac{C_f}{C_{max}}\right)$ Equation 7.8

For one vertical row of bolts:

$A = 0.939 - 0.408n\,, \quad B = 0.492n - 1.816\,, \qquad C = -0.013n^2 + 0.092n - 0.081$

For two vertical rows of bolts:

$A = 0.018n^2 - 0.066n - 0.634, B = -0.028n^2 + 0.088n - 0.016\,, C = 0.11n - 0.166$

5) Calculate the modified shear resistance of the connection (V_{rc}) and compare it with the factored shear force (Equation 7.9)

$V_{rc} = C_c\, V_{rd}\;, \quad V_f \le V_{rc}$ Equation 7.9

Chapter 8

Conclusions and recommendations

8. Chapter 8 – Conclusions and recommendations

This chapter summarizes the performed research and highlights the conclusions and recommendations for future studies.

8.1. Conclusions

The final conclusions of the research are:

- The performed research presented in this thesis led to a design approach which can be used to include the influence of axial compression or tension force on the ultimate shear resistance of a shear tab connection. The design approach is applicable for shear tab connections connected by 3 to 10 bolts per vertical row and can be used for a single or double vertical row bolted configuration. Based on the tension or compression axial force value, the modified shear resistance is calculated and is compared with the factored applied shear force.

- The finite element models representing six full-scale shear tab tests were able to replicate the laboratory testing procedure and connection configuration. The simulation strategy with appropriate material properties and equipped with a damage model was able to simulate weld tearing and net area fracture of the connections. The results showed the capability of ABAQUS (Simulia, 2011a,b,c) to closely match the shear tabs behaviour observed in previous test programs, which has provided confidence in the models and their potential use for the evaluation of other loading scenarios such as combined shear and axial force.

- A series of four full-scale tests were performed on double row bolted shear tab connections subjected to combined vertical (shear) force and axial tension or compression force along with the anticipated rotation of a typical beam-to-column joint. In comparison with the same shear tab specimens subjected to only shear force conducted by Marosi et al. (2011a,b), the results showed a gain in shear resistance due to the presence of an axial compression force in the connection, while an axial tension decreased the shear resistance.

- The importance of the connecting plate-to-column fillet weld in the performance of a shear tab connection was witnessed in Test #4 (presented in Chapter 5), which failed suddenly at a load level of about 60% of its predicted shear resistance due to an undersized weld.
- The established interactions of axial and shear force from this research can be used to evaluate the performance of the currently designed shear tab connections that are designed for pure shear.

8.2. Recommendations for further research

The gravity load testing protocol defined by Astaneh et al. (1989) which controls the rotation of the connection was used to apply the vertical load. Based on Marosi's (2011) experimental work, the highest rotation measured for the most flexible specimen was 0.06 rads. The suggested design approach does not cover shear tab connections subjected to higher rotations and covers shear tabs with a typical rotation level (less than 0.06 rads). Higher rotations can occur due to a column collapse in a building were the catenary actions cause the development of significant axial force and rotations in the connection with a reduction of shear force; therefore further studies is required to investigate the compatibility of the design approach for including this feature. All possible failure modes of the studied connections was not observed such as bolt shear failure; therefore this method should also be evaluated such that it is proven that it works irrespective of the failure mode in the prediction of the shear resistance of the shear tab. Recommendations regarding laboratory work:

- Due to limited resources, only four laboratory tests were conducted on the connection specimens subjected to combined shear and axial forces. To increase the reliability of the design approach further experimental work is recommended.

- The test beam sizes used were selected by Marosi (2011) based on typical beams commonly found in construction. They were selected such that their strength was adequate to fail the connection under the loading scenario used in the laboratory; however, the W920 test beam for the stiffest configuration showed some influence on the connection's behaviour and as such required additional stiffeners. As a result, the effect of the test beam on the connection's performance and special requirements for deep beams need to be investigated.

- The suggested design method is limited to cases where the beam is laterally braced such that no extensive lateral movement of the connection occurs that would magnify weak axis bending in the shear tab; therefore the effect of lateral bracing should be investigated.

- The usage of one and two vertical rows of bolts was studied and the use of more than two vertical rows of bolts requires further research.

- The axial load application system designed for this research program showed its capability for future applications; however the capacity of the system is dependent on the hydraulic cylinders used for applying tension in the axial rods. If a connection is to be subjected to axial force higher than 500 kN, adjustments need to be made to the system and the axial rods need to be checked for the desired axial force.

Sophisticated FE modeling techniques such as contact and damage simulation were utilized in this study; however some simplifications were made and require further development. Further improvements for enhancing the FE simulation models are:

- Determining an approach to obtain the weld material properties for use in the finite element modeling. The shear tab steel plate material behaviour was used for the connecting weld in this research. Connections involving severe weld tearing will be influenced by the damage parameters used for stiffness degradation therefore further studies are required for developing the simulation technique used for simulating weld tearing.

- The size of the bolts used in the FE models was based on the diameter of the holes on the shear tab in order to fill the gap between the bolts outer surface with the inner surface of the holes leading to a stiffer connection compared with the real laboratory test specimen. This caused lower deformations in the FE models compared to the experimental displacements and rotation. Another improvement can be developing a technique to exclude this additional stiffness due to direct contact of the bolts with the holes.

References

ABAQUS (2000a), *ABAQUS/Standard User's Manual Volume I-III* , by Hibbitt, Karlsson & Sorenson Inc., Pawtucket, RI

ABAQUS (2000b), *Getting Started with ABAQUS/Standard*, by Hibbitt, Karlsson &Sorenson Inc., Pawtucket, RI

ANSYS (1996), *ANSYS Verification Manual Release 5.3* , ANSYS Inc., , Pittsburg, PA

ANSYS (2000), *ANSYS User manual version 5.7*, ANSYS Corporation, Pittsburg, PA

AISC (1989), *AISC Manual of Steel Construction: Allowable Stress Design, 9th Edition*, by the American Institute of Steel Construction, Chicago, IL

AISC (1992), AISC *Manual of Steel Construction: Vol II-connections* by the American Institute of Steel Construction, Chicago, IL

AISC (2003), *AISC Manual of Steel Construction: Load and Resistance Factor Design 3rd Edition*, by the American Institute of Steel Construction, Chicago, IL

AISC (2005), *AISC Manual of Steel Construction, 13th Edition*, by the American Institute of Steel Construction, Chicago, IL

AISC (2010), *Specification for Structural Steel Buildings,* by the American Institute of Steel Construction, Chicago, IL

AISC (2011), *AISC Manual of Steel Construction, 14th Edition*, by the American Institute of Steel Construction, Chicago, IL

Arasaratnam P., Sivakumaran K. S., and Tait M. J. (2011), "True Stress-True Strain Models for Structural Steel Elements", *ISRN Civil Engineering,Volume 2011*, Article ID 656401

Ashakul, A. (2004), "Finite Element Analysis of Single Plate Shear Connections", PhD Dissertation, Virginia Polytechnic Institute and State University

Astaneh, A. (1989), "Demand and Supply of Ductility in Steel Shear Connections", *Journal of Constructional Steel Research*, 14, pp. 1-19.

Astaneh, A., Call, S. M., and McMullin, K. M (1989), “Design of Single Plate Shear Connections,” *AISC Engineering Journal*, AISC, First Quarter, Vol. 26, 21-32

Astaneh, A., McMullin, K.M., and Call, S.M. (1993), “Behaviour and Design of Steel Single Plate Shear Connections”, *ASCE Journal of Structural Engineering*, ASCE, Volume 119, No. 8, pp. 2421-2440.

Astaneh, A., Liu, J., and McMullin, K.M., (2002), “Behaviour and Design of Single Plate Shear Connections”, *Journal of Constructional Steel Research*, Volume 58, pp. 1121-1141.

Astaneh (2005), “*Steel Tips: Design of Shear Tab Connection for Gravity and Seismic Loads*” by Abolhassan Astaneh-Asl, Ph.D., P.E., Professor, University of California, Berkeley

ASTM (2014), *Annual Book of ASTM Standards”, Volume 01.01*, American Society for Testing and Materials. Philadelphia, PA.

Autodesk Inc. (2010), *AutoCAD 2011 User Guide*, San Rafael, CA

CAN/CSA-G40.20/G40.21-98 (1998), *General Requirements for Rolled or Welded Structural Quality Steel/Structural Quality Steel*, Standard Council of Canada, Ottawa,ON

CISC (2010), *Handbook of Steel Construction – 10th Edition*, Markham, ON Canada

Creech, D.D. (2005), “Behaviour of Single Plate Shear Connections with Rigid and Flexible Supports”, MSc. Thesis, North Carolina State University

Crocker, Joseph. P and Chambers, Janice J. (2004), “Single Plate Shear Connection Response to Rotation Demands Imposed by Frames Undergoing Cyclic Lateral Displacements,” Journal of Structural Engineering, ASCE, June 2004, Vol. 130, No. 6, 934-941.

CSA. (2000), *Limit states design of steel structures, Standard CAN/CSA-S16.1-94*, Canadian Standards Association, Toronto, Ont.

Dassault Systèmes, D. (2009). *ABAQUS analysis user's manual*, Simulia Corp., Providence, RI.

Daneshvar H. and Driver R. G., “Behaviour of Shear Tab Connections under Column Removal Scenario”, *ASCE Structures 2011 Congress proceedings*, pp. 2905 -2916

Ghorbanpoor, A. & Sherman, D.R. (2002), “Design Procedures for Extended Shear Tabs”, AISC Final report, University of Wisconsin-Milwaukee

Goodrich, W. (2005), “Behaviour of Extended Shear Tabs In Stiffened Beam-To-Column Web Connections”, MSc. Thesis, Vanderbilt University.

Guravich, S. J., & Dawe, J. L. (2006). “Simple Beam Connections in Combined Shear and Tension”, *Canadian Journal of Civil Engineering* ,Vol. 33, 357-372.

Larson, P.C. (1996) “The design and behaviour of bolted beam-to-column frame connections under cyclical loading,” MSc. thesis, University of Texas at Austin, TX

Lipson (1968), “Single-Angle and Single-Plate Beam Framing Connections”. *Proceedings of Canadian Structural Engineering Conference*. pp. 141-162. Toronto, ON.

Liu, J. and Astaneh-Asl, A., (2000), “Cyclic testing of simple connections including effects of slab,” *Journal of Structural Engineering*, Vol. 126(1), pp. 32-39

Marosi, M., (2011), “Behaviour of Single and Double Row Bolted Shear Tab Connections and Weld Retrofits”. Dept. of Civil Eng. & Applied Mechanics, McGill University, Montreal, QC, Canada: Research Report.

Marosi, M., D’Aronco, M., Tremblay, R., Rogers, C.A. 2011, “Multi-Row Bolted Beam to Column Shear Tab Connections”, *6th European Conference on Steel and Composite Structures*, Budapest, Hungary. 555-560.

Metzger, K. A. (2006), “Experimental Verification of a New Single Plate Shear Connection Design Model”. MSc. Thesis, Virginia Polytechnic Institute and State University

Oosterhof, S. A. and Driver, R. G.(2011), “Performance of Steel Shear Connections under combined Moment, Shear, and Tension”, University of Alberta, AB

Rahman, A., Mahamid, M., Amro, A., & Ghorbanpoor, A. (2007), “The Analyses of Extended Shear Tab Connections Part I: The Unstiffened Connections”, *AISC Engineering Journal* - Second Quarter, 117-132.

Richard, R.M., Gillett, P.E., Kriegh, J.D., and Lewis, B.A. (1980), “The Analysis and Design of Single Plate Framing Connections”, *American Institute of Steel Construction Engineering Journal*, Volume 17, 2nd Quarter, pp. 38-52.

Sarkar, D. (1992) “Design of Single Plate Framing Connections”, MSc. Thesis, University of Oklahoma

Schroeder J.M, (2012), "Moment-Rotation Curves for Shear Tab Connections using Finite Element Modeling and Experimental Data”, MSc. thesis, School of Advanced Structures, College of Engineering and Applied Science, University of Cincinnati, Cincinnati , OH

Simulia (2011a), *ABAQUS/CAE 6.11 User’s Manual*, by Dassault Systèmes Simulia Corp., Providence, RI, USA

Simulia (2011b), *ABAQUS/CAE 6.11 Analysis User’s Manual*, by Dassault Systèmes Simulia Corp., Providence, RI, USA

Simulia (2011c), *ABAQUS/CAE 6.11 Theory Manual*, by Dassault Systèmes Simulia Corp., Providence, RI, USA

St-Onge E. (2012) , “Étude Expérimentale et Conception de Fusibles Ductiles Travaillant en Traction pour L’amélioration de L’efficacité des Contreventements Parasismiques en Acier”, MSc. thesis, École Polytechnique de Montréal, Montreal,CA

Thompson, S. L. (2009), "Axial, shear and moment interaction of single plate shear tab connections”, MSc. thesis, Milwaukee School of Engineering, Milwaukee, WI

Weigand and Berman (2014), “Integrity of Steel Single Plate Shear Connections Subjected to Simulated Column Removal”, *ASCE Journal of structural engineering*, Volume 140, Issue 5.

Yim, Hyun Chang and Krauthammer, Theodor (2012), “Mechanical Properties of Single-Plate Shear Connections under Monotonic, Cyclic, and Blast Loads,” *Engineering Structures*, Vol. 37, April 2012, 24-35.

Appendix A

Material information

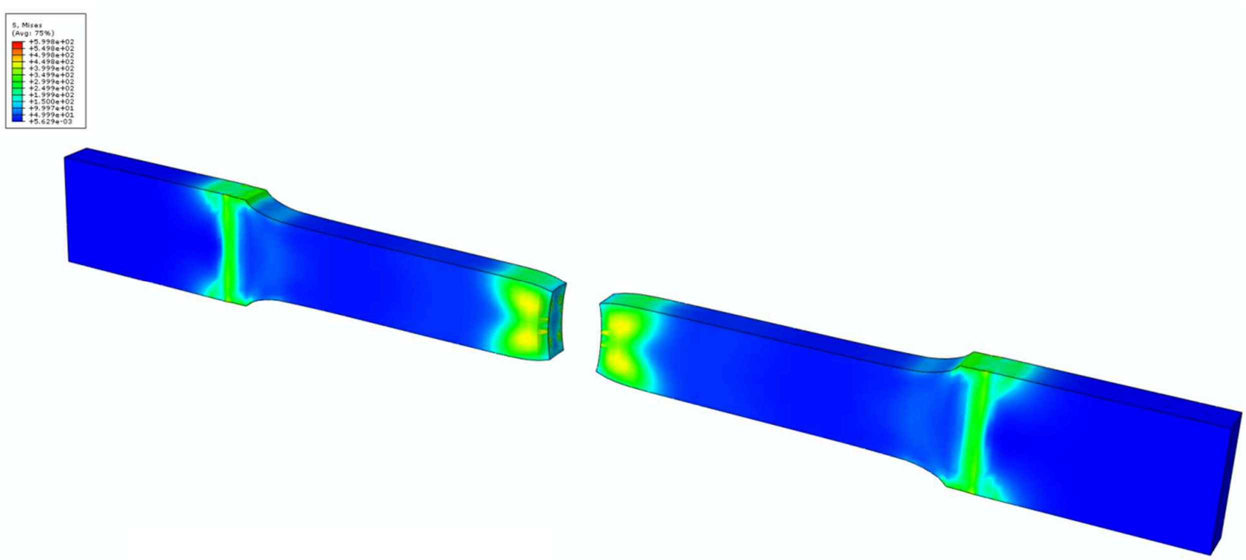

Appendix A – Material information from Series A coupons

Series A coupons were extracted from the components of the 6 full-scale shear tab tests subjected to gravity loads conducted by Marosi (2011). The data processed from the coupon tests was used to develop the material input curves.

Table A1-Steel plate material information with ABAQUS input (Series A)

Steel plate									
Coupon	6A	Coupon	7A	Coupon	8A	Coupon	9A	Coupon	10A
Test used	M1	Test used	M7	Test used	M2,M13	Test used	M8	Test used	M15
Fy (Mpa)	422	Fy (MPa)	390	Fy (MPa)	385	Fy (MPa)	388	Fy (MPa)	403
Fu (MPa)	486	Fu (MPa)	515	Fu (MPa)	526	Fu (MPa)	543	Fu (MPa)	565
E (MPa)	207593	E (MPa)	206171	E (MPa)	206171	E (MPa)	205840	E (MPa)	204727
True stress (MPa)	True strain	True stress (MPa)	True strain	True stress (MPa)	True strain	True stress (MPa)	True strain	True stress (MPa)	True strain
422.0	0.0000	390.0	0.0000	385.0	0.0000	388.0	0.0000	403.0	0.0000
424.2	0.0031	391.2	0.0013	386.2	0.0013	389.3	0.0015	404.3	0.0012
425.5	0.0062	391.8	0.0026	386.7	0.0026	389.9	0.0030	404.8	0.0024
426.8	0.0092	392.3	0.0039	387.2	0.0038	390.5	0.0045	405.3	0.0036
428.0	0.0123	392.8	0.0052	387.7	0.0051	391.1	0.0060	405.7	0.0048
429.3	0.0153	393.3	0.0065	388.2	0.0064	391.6	0.0075	406.2	0.0060
430.6	0.0184	393.8	0.0078	388.7	0.0077	392.2	0.0090	406.7	0.0072
431.9	0.0214	394.3	0.0091	389.2	0.0090	392.8	0.0105	407.2	0.0084
433.2	0.0244	394.8	0.0104	389.6	0.0102	393.4	0.0120	407.7	0.0096
434.4	0.0274	395.3	0.0117	390.1	0.0115	394.0	0.0135	408.2	0.0108
435.7	0.0304	395.8	0.0130	390.6	0.0128	394.5	0.0150	408.6	0.0120
439.6	0.0323	402.8	0.0153	399.6	0.0151	403.2	0.0170	418.8	0.0143
443.5	0.0342	409.5	0.0176	408.1	0.0174	411.5	0.0190	428.5	0.0165
447.1	0.0361	416.0	0.0199	416.3	0.0197	419.5	0.0209	437.7	0.0187
450.7	0.0380	422.2	0.0222	424.1	0.0220	427.2	0.0229	446.6	0.0209
454.1	0.0399	428.3	0.0245	431.6	0.0243	434.6	0.0249	455.0	0.0231
457.5	0.0418	434.1	0.0268	438.8	0.0266	441.7	0.0269	463.0	0.0253
460.7	0.0437	439.7	0.0291	445.6	0.0289	448.5	0.0288	470.7	0.0275
463.8	0.0456	445.2	0.0313	452.1	0.0311	455.0	0.0308	478.1	0.0297
466.8	0.0475	450.4	0.0336	458.4	0.0334	461.3	0.0328	485.1	0.0319
469.7	0.0493	455.5	0.0359	464.4	0.0357	467.4	0.0347	491.8	0.0341
472.5	0.0512	460.4	0.0381	470.1	0.0380	473.2	0.0367	498.2	0.0362
475.3	0.0531	465.1	0.0404	475.6	0.0402	478.8	0.0386	504.4	0.0384
477.9	0.0549	469.7	0.0427	480.9	0.0425	484.2	0.0406	510.3	0.0406
480.5	0.0568	474.2	0.0449	486.0	0.0447	489.3	0.0425	515.9	0.0427
483.0	0.0586	478.5	0.0471	490.8	0.0470	494.3	0.0445	521.3	0.0449
485.4	0.0605	482.6	0.0494	495.5	0.0492	499.1	0.0464	526.5	0.0471
487.7	0.0623	486.6	0.0516	499.9	0.0514	503.7	0.0483	531.5	0.0492

Table A1-Steel plate material information with ABAQUS input (Series A)-cont.

490.0	0.0642	490.5	0.0538	504.2	0.0537	508.2	0.0503	536.2	0.0513
492.2	0.0660	494.3	0.0560	508.4	0.0559	512.5	0.0522	540.8	0.0535
494.4	0.0679	498.0	0.0583	512.3	0.0581	516.6	0.0541	545.2	0.0556
496.5	0.0697	501.5	0.0605	516.1	0.0603	520.6	0.0560	549.4	0.0578
498.5	0.0715	505.0	0.0627	519.8	0.0625	524.5	0.0579	553.5	0.0599
500.5	0.0734	508.3	0.0649	523.4	0.0647	528.2	0.0599	557.4	0.0620
502.4	0.0752	511.5	0.0671	526.8	0.0669	531.8	0.0618	561.1	0.0641
504.3	0.0770	514.7	0.0693	530.0	0.0691	535.3	0.0637	564.7	0.0662
506.1	0.0788	517.7	0.0715	533.2	0.0713	538.6	0.0656	568.2	0.0683
507.9	0.0806	520.7	0.0736	536.3	0.0735	541.8	0.0675	571.5	0.0704
509.7	0.0825	523.6	0.0758	539.2	0.0757	545.0	0.0694	574.8	0.0725
511.4	0.0843	526.4	0.0780	542.1	0.0779	548.0	0.0712	577.9	0.0746
513.0	0.0861	529.1	0.0801	544.8	0.0800	550.9	0.0731	580.9	0.0767
514.6	0.0879	531.8	0.0823	547.5	0.0822	553.8	0.0750	583.8	0.0788
516.2	0.0897	534.3	0.0845	550.1	0.0843	556.5	0.0769	586.6	0.0809
517.8	0.0915	536.9	0.0866	552.6	0.0865	559.2	0.0788	589.3	0.0830
519.3	0.0933	539.3	0.0888	555.0	0.0887	561.8	0.0806	591.9	0.0850
520.8	0.0950	541.7	0.0909	557.3	0.0908	564.3	0.0825	594.5	0.0871
522.2	0.0968	544.0	0.0931	559.6	0.0929	566.7	0.0844	597.0	0.0892
523.6	0.0986	546.3	0.0952	561.8	0.0951	569.1	0.0862	599.3	0.0912
525.0	0.1004	548.5	0.0973	564.0	0.0972	571.4	0.0881	601.7	0.0933
526.4	0.1022	550.6	0.0994	566.1	0.0993	573.6	0.0899	603.9	0.0953
527.8	0.1039	552.8	0.1016	568.1	0.1015	575.7	0.0918	606.1	0.0974
529.1	0.1057	554.8	0.1037	570.1	0.1036	577.9	0.0936	608.2	0.0994
530.4	0.1075	556.8	0.1058	572.0	0.1057	579.9	0.0955	610.3	0.1015
531.6	0.1092	558.8	0.1079	573.9	0.1078	581.9	0.0973	612.3	0.1035
532.9	0.1110	560.7	0.1100	575.8	0.1099	583.8	0.0992	614.3	0.1055
534.1	0.1128	562.6	0.1121	577.6	0.1120	585.7	0.1010	616.2	0.1076
535.3	0.1145	564.5	0.1142	579.3	0.1141	587.6	0.1028	618.1	0.1096
536.5	0.1163	566.3	0.1163	581.0	0.1162	589.4	0.1046	619.9	0.1116
537.7	0.1180	568.0	0.1184	582.7	0.1183	591.2	0.1065	621.7	0.1136
538.8	0.1198	569.8	0.1205	584.4	0.1204	592.9	0.1083	623.5	0.1156
540.0	0.1215	571.5	0.1225	586.0	0.1225	594.6	0.1101	625.2	0.1176
541.1	0.1233	573.1	0.1246	587.6	0.1245	596.2	0.1119	626.9	0.1196
542.2	0.1250	574.8	0.1267	589.1	0.1266	597.8	0.1137	628.5	0.1216
543.3	0.1267	576.4	0.1287	590.6	0.1287	599.4	0.1155	630.1	0.1236
544.4	0.1285	578.0	0.1308	592.1	0.1307	601.0	0.1173	631.7	0.1256
545.4	0.1302	579.5	0.1329	593.6	0.1328	602.5	0.1191	633.2	0.1276
546.5	0.1319	581.1	0.1349	595.0	0.1349	604.0	0.1209	634.8	0.1296
547.5	0.1336	582.6	0.1370	596.5	0.1369	605.4	0.1227	636.3	0.1316
548.6	0.1353	584.1	0.1390	597.9	0.1390	606.8	0.1245	637.7	0.1335
549.6	0.1371	585.5	0.1410	599.2	0.1410	608.2	0.1263	639.2	0.1355
550.6	0.1388	587.0	0.1431	600.6	0.1430	609.6	0.1281	640.6	0.1375
551.6	0.1405	588.4	0.1451	601.9	0.1451	611.0	0.1299	642.0	0.1394
552.6	0.1422	589.8	0.1471	603.3	0.1471	612.3	0.1316	643.4	0.1414

Table A1-Steel plate material information with ABAQUS input (Series A)-cont.

553.5	0.1439	591.1	0.1492	604.6	0.1491	613.6	0.1334	644.8	0.1434
554.5	0.1456	592.5	0.1512	605.8	0.1511	614.9	0.1352	646.1	0.1453
555.5	0.1473	593.8	0.1532	607.1	0.1532	616.2	0.1370	647.5	0.1473
556.4	0.1490	595.2	0.1552	608.4	0.1552	617.5	0.1387	648.8	0.1492
557.4	0.1507	596.5	0.1572	609.6	0.1572	618.7	0.1405	650.1	0.1511
558.3	0.1524	597.8	0.1592	610.9	0.1592	619.9	0.1423	651.4	0.1531
559.2	0.1541	599.0	0.1612	612.1	0.1612	621.1	0.1440	652.6	0.1550
560.1	0.1557	600.3	0.1632	613.3	0.1632	622.3	0.1458	653.9	0.1569
561.0	0.1574	601.5	0.1652	614.5	0.1652	623.5	0.1475	655.1	0.1589
561.9	0.1591	602.8	0.1672	615.6	0.1672	624.7	0.1493	656.4	0.1608
562.8	0.1608	604.0	0.1692	616.8	0.1692	625.8	0.1510	657.6	0.1627
563.7	0.1624	605.2	0.1711	618.0	0.1711	626.9	0.1527	658.8	0.1646
564.6	0.1641	606.4	0.1731	619.1	0.1731	628.1	0.1545	660.0	0.1665
565.5	0.1658	607.6	0.1751	620.3	0.1751	629.2	0.1562	661.2	0.1684
566.4	0.1674	608.8	0.1770	621.4	0.1771	630.3	0.1579	662.4	0.1703
567.3	0.1691	609.9	0.1790	622.5	0.1790	631.4	0.1597	663.6	0.1722
568.1	0.1708	611.1	0.1810	623.7	0.1810	632.4	0.1614	664.7	0.1741
569.0	0.1724	612.2	0.1829	624.8	0.1829	633.5	0.1631	665.9	0.1760
569.8	0.1741	613.4	0.1849	625.9	0.1849	634.6	0.1648	667.0	0.1779
570.7	0.1757	614.5	0.1868	627.0	0.1868	635.6	0.1666	668.2	0.1798
571.5	0.1774	615.6	0.1888	628.1	0.1888	636.7	0.1683	669.3	0.1817
572.4	0.1790	616.7	0.1907	629.1	0.1907	637.7	0.1700	670.4	0.1836
573.2	0.1807	617.8	0.1926	630.2	0.1927	638.7	0.1717	671.6	0.1854
574.1	0.1823	618.9	0.1946	631.3	0.1946	639.7	0.1734	672.7	0.1873
574.9	0.1839	620.0	0.1965	632.4	0.1965	640.8	0.1751	673.8	0.1892
575.7	0.1856	621.1	0.1984	633.4	0.1985	641.8	0.1768	674.9	0.1910
576.5	0.1872	622.2	0.2004	634.5	0.2004	642.8	0.1785	676.0	0.1929
577.4	0.1888	623.2	0.2023	635.5	0.2023	643.7	0.1802	677.1	0.1948
578.2	0.1905	624.3	0.2042	636.6	0.2042	644.7	0.1819	678.2	0.1966
579.0	0.1921	625.3	0.2061	637.6	0.2061	645.7	0.1836	679.2	0.1985
579.8	0.1937	626.4	0.2080	638.7	0.2081	646.7	0.1852	680.3	0.2003
580.6	0.1953	627.4	0.2099	639.7	0.2100	647.7	0.1869	681.4	0.2022
581.4	0.1969	628.5	0.2118	640.7	0.2119	648.6	0.1886	682.5	0.2040
582.2	0.1986	629.5	0.2137	641.8	0.2138	649.6	0.1903	683.5	0.2058
583.0	0.2002	630.5	0.2156	642.8	0.2157	650.5	0.1920	684.6	0.2077
583.8	0.2018	631.6	0.2175	643.8	0.2175	651.5	0.1936	685.6	0.2095
584.6	0.2034	632.6	0.2194	644.8	0.2194	652.4	0.1953	686.7	0.2113
585.4	0.2050	633.6	0.2213	645.8	0.2213	653.4	0.1970	687.8	0.2131

Table A2-Test beam flange and web material information with ABAQUS input (Series A)

Flange						Web					
Beam	W310x60	Beam	W610x140	Beam	W920 x 223	Beam	W310x60	Beam	W610x140	Beam	W920 x 223
Coupon	1-(1a)	Coupon	2-(1a)	Coupon	5-(1a)	Coupon	1-(2a)	Coupon	4-2c	Coupon	5-(2a)
Fy (MPa)	372.2	Fy (MPa)	413.8	Fy (MPa)	387.2	Fy (MPa)	400.3	Fy (MPa)	454.0	Fy (MPa)	425.9
Fu (MPa)	492	Fu (MPa)	576	Fu (MPa)	518	Fu (MPa)	500	Fu (MPa)	543	Fu (MPa)	537
E (MPa)	207532	E (MPa)	206043	E (MPa)	202854	E (MPa)	208819	E (MPa)	207143	E (MPa)	201662
True stress (MPa)	True strain	True stress (MPa)	True strain	True stress (MPa)	True strain	True stress (MPa)	True strain	True stress (MPa)	True strain	True stress (MPa)	True strain
372.2	0.0000	413.8	0.0000	387.2	0.0000	400.3	0.0000	454.0	0.0000	425.9	0.0000
379.2	0.0188	420.9	0.0168	394.6	0.0188	411.9	0.0286	474.8	0.0237	446.6	0.0207
379.6	0.0198	426.0	0.0178	395.0	0.0198	418.3	0.0310	477.6	0.0247	449.7	0.0217
390.7	0.0207	431.0	0.0188	411.3	0.0207	424.5	0.0335	480.3	0.0257	452.9	0.0227
394.7	0.0217	435.9	0.0198	414.7	0.0217	430.5	0.0359	480.5	0.0257	455.9	0.0237
398.6	0.0227	440.7	0.0207	418.1	0.0227	436.3	0.0383	487.2	0.0282	458.9	0.0246
402.4	0.0237	445.3	0.0217	421.4	0.0237	441.9	0.0407	493.5	0.0306	461.8	0.0256
406.1	0.0246	449.9	0.0227	424.7	0.0246	447.4	0.0431	499.5	0.0330	462.0	0.0257
409.8	0.0256	454.4	0.0237	427.8	0.0256	452.6	0.0454	505.3	0.0354	469.1	0.0281
410.0	0.0257	458.8	0.0246	428.1	0.0257	457.7	0.0478	510.7	0.0378	475.9	0.0305
418.6	0.0281	463.0	0.0256	435.8	0.0281	462.6	0.0502	515.9	0.0402	482.3	0.0329
426.7	0.0305	463.3	0.0257	443.1	0.0305	467.4	0.0526	520.8	0.0426	488.4	0.0354
434.3	0.0330	473.6	0.0281	450.1	0.0330	472.0	0.0549	525.6	0.0450	494.3	0.0378
441.4	0.0354	483.3	0.0305	456.8	0.0354	476.4	0.0573	530.1	0.0474	499.9	0.0402
448.1	0.0378	492.5	0.0330	463.2	0.0378	480.7	0.0597	534.4	0.0498	505.3	0.0426
454.4	0.0402	501.2	0.0354	469.3	0.0402	484.9	0.0620	538.5	0.0521	510.4	0.0449
460.3	0.0426	509.4	0.0378	475.2	0.0426	489.0	0.0643	542.4	0.0545	515.3	0.0473
465.9	0.0450	517.2	0.0402	480.7	0.0450	492.9	0.0667	546.2	0.0569	520.0	0.0497
471.1	0.0473	524.6	0.0426	486.1	0.0473	496.7	0.0690	549.8	0.0592	524.4	0.0521
476.0	0.0497	531.6	0.0449	491.2	0.0497	500.4	0.0713	553.2	0.0616	528.7	0.0544
480.7	0.0521	538.3	0.0473	496.1	0.0521	504.0	0.0737	556.5	0.0639	532.8	0.0568
485.1	0.0545	544.6	0.0497	500.8	0.0545	507.5	0.0760	559.7	0.0662	536.8	0.0592
489.3	0.0568	550.6	0.0521	505.3	0.0568	510.9	0.0783	562.8	0.0686	540.6	0.0615
493.2	0.0592	556.3	0.0544	509.6	0.0592	514.2	0.0806	565.7	0.0709	544.2	0.0638
496.9	0.0615	561.7	0.0568	513.7	0.0615	517.4	0.0829	568.6	0.0732	547.7	0.0662
500.5	0.0639	566.8	0.0592	517.7	0.0639	520.5	0.0852	571.3	0.0755	551.1	0.0685
503.8	0.0662	571.7	0.0615	521.5	0.0662	523.5	0.0875	574.0	0.0778	554.3	0.0708
507.0	0.0685	576.4	0.0639	525.2	0.0685	526.4	0.0898	576.5	0.0802	557.5	0.0732
510.1	0.0709	580.9	0.0662	528.7	0.0709	529.3	0.0920	579.0	0.0825	560.5	0.0755
513.0	0.0732	585.1	0.0685	532.1	0.0732	532.0	0.0943	581.4	0.0847	563.4	0.0778
515.7	0.0755	589.2	0.0709	535.4	0.0755	534.7	0.0966	583.7	0.0870	566.2	0.0801
518.4	0.0778	593.1	0.0732	538.5	0.0778	537.4	0.0988	586.0	0.0893	568.9	0.0824
520.9	0.0801	596.8	0.0755	541.5	0.0801	539.9	0.1011	588.2	0.0916	571.5	0.0847

Table A2-Test beam flange and web material information with ABAQUS input (Series A)-cont.

523.3	0.0824	600.4	0.0778	544.5	0.0824	542.4	0.1033	590.3	0.0939	574.1	0.0870
525.7	0.0847	603.8	0.0801	547.3	0.0847	544.9	0.1056	592.4	0.0961	576.5	0.0893
527.9	0.0870	607.1	0.0824	550.0	0.0870	547.2	0.1078	594.4	0.0984	578.9	0.0915
530.1	0.0893	610.2	0.0847	552.7	0.0893	549.6	0.1101	596.4	0.1007	581.2	0.0938
532.2	0.0916	613.2	0.0870	555.2	0.0916	551.8	0.1123	598.3	0.1029	583.5	0.0961
534.2	0.0938	616.1	0.0893	557.7	0.0938	554.0	0.1145	600.2	0.1052	585.7	0.0984
536.1	0.0961	618.9	0.0916	560.1	0.0961	556.2	0.1168	602.1	0.1074	587.8	0.1006
538.0	0.0984	621.7	0.0938	562.5	0.0984	558.3	0.1190	603.9	0.1096	589.9	0.1029
539.8	0.1006	624.3	0.0961	564.7	0.1006	560.4	0.1212	605.7	0.1119	591.9	0.1051
541.6	0.1029	626.8	0.0984	566.9	0.1029	562.4	0.1234	607.4	0.1141	593.9	0.1074
543.3	0.1051	629.2	0.1006	569.1	0.1051	564.4	0.1256	609.1	0.1163	595.9	0.1096
545.0	0.1074	631.6	0.1029	571.2	0.1074	566.4	0.1278	610.8	0.1185	597.7	0.1118
546.7	0.1096	633.9	0.1051	573.2	0.1096	568.3	0.1300	612.5	0.1208	599.6	0.1141
548.3	0.1119	636.2	0.1074	575.2	0.1118	570.1	0.1322	614.1	0.1230	601.4	0.1163
549.9	0.1141	638.3	0.1096	577.1	0.1141	572.0	0.1344	615.7	0.1252	603.2	0.1185
551.4	0.1163	640.4	0.1118	579.0	0.1163	573.8	0.1365	617.3	0.1274	605.0	0.1207
552.9	0.1185	642.5	0.1141	580.8	0.1185	575.5	0.1387	618.9	0.1296	606.7	0.1229
554.4	0.1207	644.5	0.1163	582.7	0.1207	577.3	0.1409	620.4	0.1318	608.4	0.1251
555.9	0.1230	646.5	0.1185	584.4	0.1229	579.0	0.1431	622.0	0.1339	610.0	0.1273
557.3	0.1252	648.4	0.1207	586.2	0.1251	580.7	0.1452	623.5	0.1361	611.7	0.1295
558.7	0.1274	650.3	0.1229	587.9	0.1273	582.3	0.1474	625.0	0.1383	613.3	0.1317
560.1	0.1296	652.1	0.1251	589.5	0.1295	583.9	0.1495	626.5	0.1405	614.9	0.1339
561.5	0.1317	653.9	0.1273	591.2	0.1317	587.1	0.1538	628.0	0.1426	616.4	0.1361
562.8	0.1339	655.7	0.1295	592.8	0.1339					618.0	0.1382
564.2	0.1361	657.5	0.1317	594.4	0.1361					619.5	0.1404
565.5	0.1383	659.2	0.1339	596.0	0.1383						
566.9	0.1405	660.9	0.1361	597.5	0.1404						

Appendix A – Coupon material information from Series B

Series B were coupons extracted from the test components of shear tab tests subjected to combined shear and axial forces (described in Chapter 5).

Table A3-Steel plate and test beam flange material information with ABAQUS input (Series B)

Shear tab steel plate			
Coupon	B4	Coupon	A4
Test used	#1,#2	Test used	#3,#4
Fy (MPa)	450	Fy (MPa)	360
Fu (MPa)	525	Fu (MPa)	510
E (MPa)	205526	E (MPa)	241391
True stress (MPa)	True strain	True stress (MPa)	True strain
450.0	0.0000	360.0	0.0000
451.7	0.0016	361.0	0.0012
452.4	0.0032	361.4	0.0023
453.2	0.0049	361.8	0.0035
453.9	0.0065	362.2	0.0047
454.6	0.0081	362.6	0.0058
455.4	0.0097	363.1	0.0070
456.1	0.0113	363.5	0.0081
456.8	0.0129	363.9	0.0093
457.5	0.0145	364.3	0.0105
458.2	0.0161	364.7	0.0116
463.0	0.0179	372.3	0.0134
467.6	0.0197	379.7	0.0151
472.0	0.0215	386.7	0.0168
476.2	0.0232	393.6	0.0186
480.3	0.0250	400.1	0.0203
484.3	0.0268	406.5	0.0220
488.2	0.0285	412.6	0.0238
491.9	0.0303	418.5	0.0255
495.5	0.0321	424.2	0.0272
498.9	0.0338	429.7	0.0289
502.3	0.0356	435.0	0.0306
505.5	0.0373	440.2	0.0323
508.7	0.0390	445.1	0.0341
511.7	0.0408	449.9	0.0358
514.7	0.0425	454.5	0.0375
517.5	0.0443	459.0	0.0392

Flange							
Coupon	A1-702	Coupon	A1-706	Coupon	A3-711	Coupon	A1-713
Test used	#1	Test used	#2	Test used	#3	Test used	#4
Fy (MPa)	370.0	Fy (MPa)	371.0	Fy (MPa)	382.0	Fy (MPa)	378.0
Fu (MPa)	482	Fu (MPa)	490	Fu (MPa)	492	Fu (MPa)	478
E (MPa)	206222	E (MPa)	209406	E (MPa)	201635	E (MPa)	201665
True stress (MPa)	True strain	True stress (MPa)	True strain	True stress (MPa)	True strain	True stress (MPa)	True strain
370.0	0.0000	371.0	0.0000	382.0	0.0000	378.0	0.0000
371.2	0.0016	372.2	0.0015	383.3	0.0016	379.4	0.0018
371.8	0.0031	372.8	0.0030	384.0	0.0032	380.1	0.0036
372.4	0.0047	373.3	0.0045	384.6	0.0049	380.8	0.0054
373.0	0.0063	373.9	0.0061	385.2	0.0065	381.4	0.0072
373.6	0.0078	374.5	0.0076	385.8	0.0081	382.1	0.0090
374.1	0.0094	375.0	0.0091	386.4	0.0097	382.8	0.0108
374.7	0.0109	375.6	0.0106	387.1	0.0113	383.5	0.0126
375.3	0.0125	376.1	0.0121	387.7	0.0129	384.1	0.0144
375.8	0.0140	376.7	0.0136	388.3	0.0145	384.8	0.0162
376.4	0.0156	377.3	0.0151	388.9	0.0161	385.5	0.0179
382.0	0.0171	384.3	0.0169	394.9	0.0180	391.2	0.0197
387.3	0.0185	391.0	0.0188	400.7	0.0198	396.7	0.0215
392.5	0.0200	397.5	0.0206	406.4	0.0216	402.0	0.0232
397.5	0.0215	403.7	0.0225	411.8	0.0235	407.1	0.0250
402.4	0.0230	409.6	0.0243	417.0	0.0253	412.0	0.0267
407.0	0.0245	415.3	0.0261	422.0	0.0271	416.7	0.0285
411.6	0.0260	420.8	0.0279	426.8	0.0289	421.2	0.0302
415.9	0.0275	426.1	0.0298	431.5	0.0307	425.6	0.0319
420.2	0.0290	431.1	0.0316	436.0	0.0325	429.8	0.0337
424.2	0.0304	436.0	0.0334	440.4	0.0343	433.8	0.0354
428.2	0.0319	440.7	0.0352	444.6	0.0361	437.7	0.0372
432.0	0.0334	445.2	0.0370	448.7	0.0379	441.5	0.0389
435.7	0.0349	449.5	0.0388	452.6	0.0397	445.1	0.0406
439.3	0.0363	453.7	0.0406	456.4	0.0415	448.6	0.0423
442.8	0.0378	457.7	0.0424	460.0	0.0433	452.0	0.0441
446.1	0.0393	461.6	0.0442	463.6	0.0451	455.2	0.0458

Table A3-Steel plate and test beam flange material information with ABAQUS input (Series B) -cont.

520.3	0.0460	463.3	0.0409	449.4	0.0407	465.3	0.0460	467.0	0.0469	458.4	0.0475
523.0	0.0477	467.5	0.0425	452.5	0.0422	468.9	0.0478	470.3	0.0486	461.4	0.0492
525.6	0.0494	471.5	0.0442	455.6	0.0436	472.3	0.0496	473.5	0.0504	464.3	0.0509
528.1	0.0512	475.4	0.0459	458.5	0.0451	475.6	0.0514	476.6	0.0522	467.2	0.0526
530.6	0.0529	479.2	0.0476	461.4	0.0465	478.8	0.0532	479.6	0.0539	469.9	0.0543
533.0	0.0546	482.8	0.0493	464.1	0.0480	481.9	0.0549	482.5	0.0557	472.6	0.0560
535.3	0.0563	486.3	0.0510	466.8	0.0494	484.9	0.0567	485.4	0.0575	475.1	0.0577
537.6	0.0580	489.7	0.0526	469.4	0.0509	487.8	0.0585	488.1	0.0592	477.6	0.0594
539.8	0.0597	493.0	0.0543	472.0	0.0523	490.6	0.0603	490.7	0.0610	480.0	0.0611
541.9	0.0614	496.2	0.0560	474.4	0.0538	493.3	0.0620	493.3	0.0627	482.3	0.0628
544.0	0.0631	499.3	0.0577	476.8	0.0552	495.9	0.0638	495.8	0.0645	484.6	0.0645
546.0	0.0648	502.3	0.0593	479.1	0.0567	498.4	0.0656	498.2	0.0662	486.8	0.0662
548.0	0.0665	505.2	0.0610	481.3	0.0581	500.8	0.0673	500.5	0.0680	488.9	0.0678
549.9	0.0682	508.1	0.0626	483.5	0.0595	503.2	0.0691	502.8	0.0697	490.9	0.0695
551.7	0.0699	510.8	0.0643	485.6	0.0610	505.5	0.0708	505.0	0.0715	492.9	0.0712
553.6	0.0716	513.4	0.0660	487.7	0.0624	507.7	0.0726	507.2	0.0732	494.9	0.0729
555.4	0.0733	516.0	0.0676	489.7	0.0638	509.8	0.0743	509.3	0.0749	496.8	0.0745
557.1	0.0750	518.5	0.0693	491.6	0.0653	511.9	0.0760	511.3	0.0767	498.6	0.0762
558.8	0.0766	520.9	0.0709	493.5	0.0667	513.9	0.0778	513.3	0.0784	500.4	0.0779
560.5	0.0783	523.3	0.0725	495.4	0.0681	515.9	0.0795	515.2	0.0801	502.1	0.0795
562.1	0.0800	525.6	0.0742	497.2	0.0695	517.8	0.0812	517.1	0.0818	503.8	0.0812
563.7	0.0817	527.8	0.0758	498.9	0.0709	519.6	0.0830	518.9	0.0835	505.4	0.0828
565.2	0.0833	530.0	0.0775	500.6	0.0724	521.4	0.0847	520.7	0.0852	507.0	0.0845
566.7	0.0850	532.1	0.0791	502.3	0.0738	523.2	0.0864	522.4	0.0870	508.6	0.0861
568.2	0.0867	534.1	0.0807	503.9	0.0752	524.9	0.0881	524.1	0.0887	510.1	0.0878
569.7	0.0883	536.1	0.0824	505.4	0.0766	526.5	0.0899	525.8	0.0904	511.6	0.0894
571.1	0.0900	538.1	0.0840	507.0	0.0780	528.2	0.0916	527.4	0.0921	513.0	0.0911
572.5	0.0916	539.9	0.0856	508.5	0.0794	529.7	0.0933	529.0	0.0938	514.5	0.0927
573.9	0.0933	541.8	0.0872	509.9	0.0808	531.3	0.0950	530.5	0.0955	515.8	0.0943
575.3	0.0949	543.6	0.0888	511.4	0.0822	532.8	0.0967	532.0	0.0972	517.2	0.0960
576.6	0.0966	545.3	0.0904	512.8	0.0836	534.2	0.0984	533.5	0.0989	518.5	0.0976
577.9	0.0982	547.0	0.0921	514.1	0.0850	535.7	0.1001	534.9	0.1005	519.8	0.0992
579.2	0.0999	548.7	0.0937	515.5	0.0864	537.1	0.1018	536.3	0.1022	521.1	0.1009
580.4	0.1015	550.3	0.0953	516.8	0.0878	538.4	0.1035	537.7	0.1039	522.3	0.1025
581.7	0.1031	551.9	0.0969	518.0	0.0892	539.8	0.1052	539.1	0.1056	523.5	0.1041
582.9	0.1048	553.5	0.0985	519.3	0.0906	541.1	0.1069	540.4	0.1073	524.7	0.1057
584.1	0.1064	555.0	0.1001	520.5	0.0920	542.4	0.1086	541.7	0.1089	525.9	0.1073
585.3	0.1080	556.5	0.1017	521.7	0.0934	543.6	0.1102	543.0	0.1106	527.1	0.1090
586.5	0.1096	557.9	0.1033	522.9	0.0948	544.9	0.1119	544.3	0.1123	528.2	0.1106
587.6	0.1113	559.4	0.1049	524.0	0.0961	546.1	0.1136	545.5	0.1139	529.3	0.1122
588.7	0.1129	560.7	0.1064	525.1	0.0975	547.3	0.1153	546.7	0.1156	530.4	0.1138
589.9	0.1145	562.1	0.1080	526.2	0.0989	548.5	0.1169	547.9	0.1173	531.5	0.1154
591.0	0.1161	563.5	0.1096	527.3	0.1003	549.6	0.1186	549.1	0.1189	532.5	0.1170
592.1	0.1177	564.8	0.1112	528.4	0.1017	550.8	0.1203	550.2	0.1206	533.6	0.1186
593.1	0.1193	566.1	0.1128	529.4	0.1030	551.9	0.1219	551.4	0.1222	534.6	0.1202

Table A3-Steel plate and test beam flange material information with ABAQUS input (Series B) -cont.

594.2	0.1209	567.3	0.1143
595.3	0.1225	568.6	0.1159
596.3	0.1241	569.8	0.1175
597.3	0.1257	571.0	0.1191
598.4	0.1273	572.2	0.1206
599.4	0.1289	573.3	0.1222
600.4	0.1305	574.5	0.1238
601.4	0.1321	575.6	0.1253
602.4	0.1337	576.7	0.1269
603.3	0.1353	577.8	0.1284
604.3	0.1369	578.9	0.1300
605.3	0.1384	579.9	0.1315
606.2	0.1400	581.0	0.1331
607.1	0.1416	582.0	0.1346
608.1	0.1432	583.0	0.1362
609.0	0.1447	584.0	0.1377
609.9	0.1463	585.0	0.1392
610.8	0.1479	586.0	0.1408
611.8	0.1494	587.0	0.1423
612.7	0.1510	587.9	0.1438
613.6	0.1525	588.9	0.1454
614.5	0.1541	589.8	0.1469
615.3	0.1556	590.7	0.1484
616.2	0.1572	591.7	0.1499
617.1	0.1587	592.6	0.1514
618.0	0.1603	593.5	0.1530
618.9	0.1618	594.4	0.1545
619.7	0.1634	595.3	0.1560
620.6	0.1649	596.1	0.1575
621.4	0.1664	597.0	0.1590
622.3	0.1680	597.9	0.1605
623.1	0.1695	598.7	0.1620
624.0	0.1710	599.6	0.1635
624.8	0.1725	600.4	0.1650
625.7	0.1741	601.3	0.1665
626.5	0.1756	602.1	0.1680
627.3	0.1771	602.9	0.1695
628.2	0.1786	603.8	0.1710
629.0	0.1801	604.6	0.1725

530.5	0.1044	553.0	0.1236	552.5	0.1239	535.6	0.1218
531.5	0.1058	554.1	0.1252	553.6	0.1255	536.6	0.1233
532.5	0.1072	555.1	0.1269	554.7	0.1272	537.6	0.1249
533.5	0.1085	556.2	0.1286	555.8	0.1288	538.6	0.1265
534.4	0.1099	557.2	0.1302	556.8	0.1304	539.5	0.1281
535.4	0.1112	558.2	0.1319	557.9	0.1321	540.5	0.1297
536.3	0.1126	559.3	0.1335	558.9	0.1337	541.4	0.1313
537.2	0.1140	560.3	0.1351	559.9	0.1353	542.3	0.1328
538.1	0.1153	561.2	0.1368	560.9	0.1370	543.2	0.1344
539.0	0.1167	562.2	0.1384	561.9	0.1386	544.1	0.1360
539.9	0.1180	563.2	0.1400	562.9	0.1402	545.0	0.1375
540.8	0.1194	564.1	0.1417	563.9	0.1418	545.9	0.1391
541.6	0.1207	565.1	0.1433	564.8	0.1434	546.8	0.1407
542.5	0.1221	566.0	0.1449	565.8	0.1451	547.7	0.1422
543.3	0.1234	566.9	0.1465	566.7	0.1467	548.5	0.1438
544.1	0.1248	567.9	0.1482	567.7	0.1483	549.4	0.1453
545.0	0.1261	568.8	0.1498	568.6	0.1499	550.2	0.1469
545.8	0.1275	569.7	0.1514	569.5	0.1515	551.1	0.1484
546.6	0.1288	570.6	0.1530	570.4	0.1531	551.9	0.1500
547.4	0.1301	571.5	0.1546	571.3	0.1547	552.7	0.1515
548.1	0.1315	572.3	0.1562	572.2	0.1563	553.6	0.1531
548.9	0.1328	573.2	0.1578	573.1	0.1579	554.4	0.1546
549.7	0.1341	574.1	0.1594	574.0	0.1595	555.2	0.1562
550.4	0.1355	574.9	0.1610	574.8	0.1611	556.0	0.1577
551.2	0.1368	575.8	0.1626	575.7	0.1626	556.8	0.1592
551.9	0.1381	576.7	0.1642	576.6	0.1642	557.6	0.1608
552.7	0.1394	577.5	0.1658	577.4	0.1658	558.4	0.1623
553.4	0.1408	578.3	0.1674	578.3	0.1674	559.1	0.1638
554.1	0.1421	579.2	0.1690	579.1	0.1690	559.9	0.1653
554.9	0.1434	580.0	0.1706	580.0	0.1705	560.7	0.1669
555.6	0.1447	580.8	0.1721	580.8	0.1721	561.5	0.1684
556.3	0.1460	581.7	0.1737	581.6	0.1737	562.2	0.1699
557.0	0.1474	582.5	0.1753	582.4	0.1752	563.0	0.1714
557.7	0.1487	583.3	0.1769	583.3	0.1768	563.8	0.1729
558.4	0.1500	584.1	0.1784	584.1	0.1784	564.5	0.1744
559.1	0.1513	584.9	0.1800	584.9	0.1799	565.3	0.1759
559.8	0.1526	585.7	0.1816	585.7	0.1815	566.0	0.1774
560.5	0.1539	586.5	0.1831	586.5	0.1830	566.8	0.1789
561.1	0.1552	587.3	0.1847	587.3	0.1846	567.5	0.1804

Table A4-Test beam web material information with ABAQUS input (Series B)

Web							
Coupon	C2-702	Coupon	C2-706	Coupon	A2-711	Coupon	B2-713
Test used	#1	Test used	#2	Test used	#3	Test used	#4
Fy (MPa)	387.4	Fy (MPa)	385.0	Fy (MPa)	407.0	Fy (MPa)	428.0
Fu (MPa)	490	Fu (MPa)	484	Fu (MPa)	506	Fu (MPa)	509
E (MPa)	209558	E (MPa)	220000	E (MPa)	200566	E (MPa)	203400
True stress (MPa)	True strain	True stress (MPa)	True strain	True stress (MPa)	True strain	True stress (MPa)	True strain
387.4	0.0000	385.0	0.0000	407.0	0.0000	428.0	0.0000
389.0	0.0023	386.3	0.0017	408.6	0.0020	429.9	0.0024
389.9	0.0046	387.0	0.0034	409.4	0.0040	430.9	0.0048
390.8	0.0069	387.7	0.0052	410.3	0.0060	432.0	0.0071
391.6	0.0092	388.3	0.0069	411.1	0.0079	433.0	0.0095
392.5	0.0115	389.0	0.0086	411.9	0.0099	434.0	0.0119
393.4	0.0138	389.6	0.0103	412.7	0.0119	435.0	0.0142
394.3	0.0160	390.3	0.0120	413.5	0.0139	436.0	0.0166
395.2	0.0183	390.9	0.0137	414.3	0.0158	437.0	0.0189
396.1	0.0206	391.6	0.0154	415.1	0.0178	438.0	0.0212
396.9	0.0228	392.2	0.0171	415.9	0.0197	439.0	0.0236
402.3	0.0246	398.0	0.0189	421.4	0.0215	442.8	0.0251
407.5	0.0263	403.6	0.0208	426.7	0.0233	446.5	0.0266
412.5	0.0280	408.9	0.0227	431.9	0.0251	450.2	0.0281
417.4	0.0297	414.1	0.0245	436.9	0.0269	453.7	0.0295
422.2	0.0313	419.1	0.0264	441.7	0.0286	457.2	0.0310
426.7	0.0330	423.9	0.0283	446.3	0.0304	460.5	0.0325
431.2	0.0347	428.5	0.0301	450.8	0.0322	463.8	0.0340
435.5	0.0364	433.0	0.0320	455.1	0.0340	467.0	0.0355
439.7	0.0381	437.3	0.0338	459.3	0.0357	470.1	0.0370
443.8	0.0398	441.4	0.0356	463.3	0.0375	473.2	0.0385
447.7	0.0415	445.4	0.0375	467.2	0.0392	476.2	0.0399
451.5	0.0431	449.3	0.0393	471.0	0.0410	479.1	0.0414
455.2	0.0448	453.0	0.0411	474.7	0.0427	481.9	0.0429
458.8	0.0465	456.7	0.0430	478.2	0.0445	484.7	0.0444
462.3	0.0481	460.1	0.0448	481.6	0.0462	487.4	0.0458
465.7	0.0498	463.5	0.0466	484.9	0.0480	490.0	0.0473
469.0	0.0515	466.8	0.0484	488.1	0.0497	492.6	0.0488
472.2	0.0531	469.9	0.0503	491.2	0.0515	495.1	0.0502
475.3	0.0548	473.0	0.0521	494.2	0.0532	497.5	0.0517
478.3	0.0564	476.0	0.0539	497.2	0.0549	499.9	0.0531
481.3	0.0581	478.8	0.0557	500.0	0.0566	502.3	0.0546
484.1	0.0597	481.6	0.0575	502.7	0.0584	504.6	0.0561

Table A4-Test beam web material information with ABAQUS input (Series B)-cont.

486.9	0.0614	484.3	0.0593	505.4	0.0601	506.8	0.0575
489.6	0.0630	486.9	0.0611	508.0	0.0618	509.0	0.0590
492.3	0.0646	489.4	0.0629	510.5	0.0635	511.2	0.0604
494.8	0.0663	491.8	0.0647	512.9	0.0652	513.3	0.0618
497.3	0.0679	494.2	0.0664	515.3	0.0669	515.3	0.0633
499.7	0.0695	496.5	0.0682	517.6	0.0687	517.3	0.0647
502.1	0.0712	498.8	0.0700	519.8	0.0704	519.3	0.0662
504.4	0.0728	500.9	0.0718	522.0	0.0721	521.2	0.0676
506.6	0.0744	503.1	0.0736	524.1	0.0738	523.1	0.0690
508.8	0.0760	505.1	0.0753	526.1	0.0755	524.9	0.0705
510.9	0.0777	507.1	0.0771	528.1	0.0771	526.7	0.0719
513.0	0.0793	509.1	0.0789	530.1	0.0788	528.5	0.0733
515.0	0.0809	511.0	0.0806	532.0	0.0805	530.2	0.0748
517.0	0.0825	512.8	0.0824	533.8	0.0822	531.9	0.0762
519.0	0.0841	514.6	0.0841	535.6	0.0839	533.6	0.0776
520.8	0.0857	516.4	0.0859	537.4	0.0856	535.2	0.0790
522.7	0.0873	518.1	0.0876	539.1	0.0872	536.8	0.0805
524.5	0.0889	519.7	0.0894	540.8	0.0889	538.4	0.0819
526.2	0.0905	521.4	0.0911	542.4	0.0906	539.9	0.0833
527.9	0.0921	523.0	0.0929	544.0	0.0922	541.4	0.0847
529.6	0.0937	524.5	0.0946	545.6	0.0939	542.9	0.0861
531.3	0.0953	526.0	0.0963	547.1	0.0956	544.4	0.0875
532.9	0.0969	527.5	0.0981	548.6	0.0972	545.8	0.0889
534.4	0.0984	529.0	0.0998	550.1	0.0989	547.2	0.0903
536.0	0.1000	530.4	0.1015	551.5	0.1005	548.6	0.0917
537.5	0.1016	531.8	0.1032	552.9	0.1022	549.9	0.0931
539.0	0.1032	533.2	0.1049	554.3	0.1038	551.3	0.0945
540.4	0.1048	534.5	0.1067	555.7	0.1055	552.6	0.0959
541.8	0.1063	535.8	0.1084	557.0	0.1071	553.9	0.0973
543.2	0.1079	537.1	0.1101	558.3	0.1088	555.1	0.0987
544.6	0.1095	538.4	0.1118	559.6	0.1104	556.4	0.1001
545.9	0.1110	539.6	0.1135	560.9	0.1120	557.6	0.1015
547.2	0.1126	540.8	0.1152	562.1	0.1137	558.8	0.1029
548.5	0.1142	542.0	0.1169	563.3	0.1153	560.0	0.1043
549.8	0.1157	543.2	0.1186	564.5	0.1169	561.2	0.1057
551.0	0.1173	544.4	0.1203	565.7	0.1185	562.3	0.1070
552.3	0.1188	545.5	0.1220	566.8	0.1202	563.5	0.1084
553.5	0.1204	546.7	0.1236	568.0	0.1218	564.6	0.1098
554.7	0.1219	547.8	0.1253	569.1	0.1234	565.7	0.1112
555.8	0.1235	548.9	0.1270	570.2	0.1250	566.8	0.1125
557.0	0.1250	550.0	0.1287	571.3	0.1266	567.8	0.1139
558.1	0.1265	551.0	0.1304	572.4	0.1282	568.9	0.1153
559.2	0.1281	552.1	0.1320	573.5	0.1298	569.9	0.1167
560.3	0.1296	553.1	0.1337	574.5	0.1314	571.0	0.1180
561.4	0.1312	554.1	0.1354	575.6	0.1330	572.0	0.1194
562.5	0.1327	555.2	0.1370	576.6	0.1346	573.0	0.1208

Table A4-Test beam web material information with ABAQUS input (Series B)-cont.

563.5	0.1342	556.2	0.1387	577.6	0.1362	574.0	0.1221
564.6	0.1357	557.2	0.1404	578.6	0.1378	575.0	0.1235
565.6	0.1373	558.1	0.1420	579.6	0.1394	575.9	0.1248
566.6	0.1388	559.1	0.1437	580.6	0.1410	576.9	0.1262
567.6	0.1403	560.1	0.1453	581.6	0.1426	577.8	0.1275
568.6	0.1418	561.0	0.1470	582.5	0.1442	578.8	0.1289
569.6	0.1433	562.0	0.1486	583.5	0.1457	579.7	0.1302
570.5	0.1448	562.9	0.1503	584.4	0.1473	580.6	0.1316
571.5	0.1464	563.8	0.1519	585.3	0.1489	581.5	0.1329
572.4	0.1479	564.7	0.1535	586.3	0.1505	582.4	0.1343
573.3	0.1494	565.6	0.1552	587.2	0.1520	583.3	0.1356
574.3	0.1509	566.5	0.1568	588.1	0.1536	584.2	0.1370
575.2	0.1524	567.4	0.1584	589.0	0.1552	585.0	0.1383
576.1	0.1539	568.3	0.1600	589.9	0.1567	585.9	0.1396
577.0	0.1554	569.2	0.1617	590.8	0.1583	586.8	0.1410
577.9	0.1569	570.1	0.1633	591.7	0.1599	587.6	0.1423
578.8	0.1584	570.9	0.1649	592.6	0.1614	588.4	0.1436
579.6	0.1598	571.8	0.1665	593.4	0.1630	589.3	0.1450
580.5	0.1613	572.7	0.1681	594.3	0.1645	590.1	0.1463
581.3	0.1628	573.5	0.1697	595.1	0.1661	590.9	0.1476
582.2	0.1643	574.4	0.1714	596.0	0.1676	591.7	0.1490
583.0	0.1658	575.2	0.1730	596.9	0.1691	592.5	0.1503
583.9	0.1673	576.0	0.1746	597.7	0.1707	593.3	0.1516
584.7	0.1687	576.9	0.1762	598.5	0.1722	594.1	0.1529
585.5	0.1702	577.7	0.1778	599.4	0.1738	594.9	0.1542
586.4	0.1717	578.5	0.1794	600.2	0.1753	595.7	0.1555
587.2	0.1732	579.4	0.1809	601.0	0.1768	596.4	0.1569
588.0	0.1746	580.2	0.1825	601.9	0.1784	597.2	0.1582
588.8	0.1761	581.0	0.1841	602.7	0.1799	598.0	0.1595
589.6	0.1776	581.8	0.1857	603.5	0.1814	598.7	0.1608
590.4	0.1790	582.6	0.1873	604.3	0.1829	599.5	0.1621
591.2	0.1805	583.4	0.1889	605.1	0.1845	600.2	0.1634

Appendix B

Instrumentation details

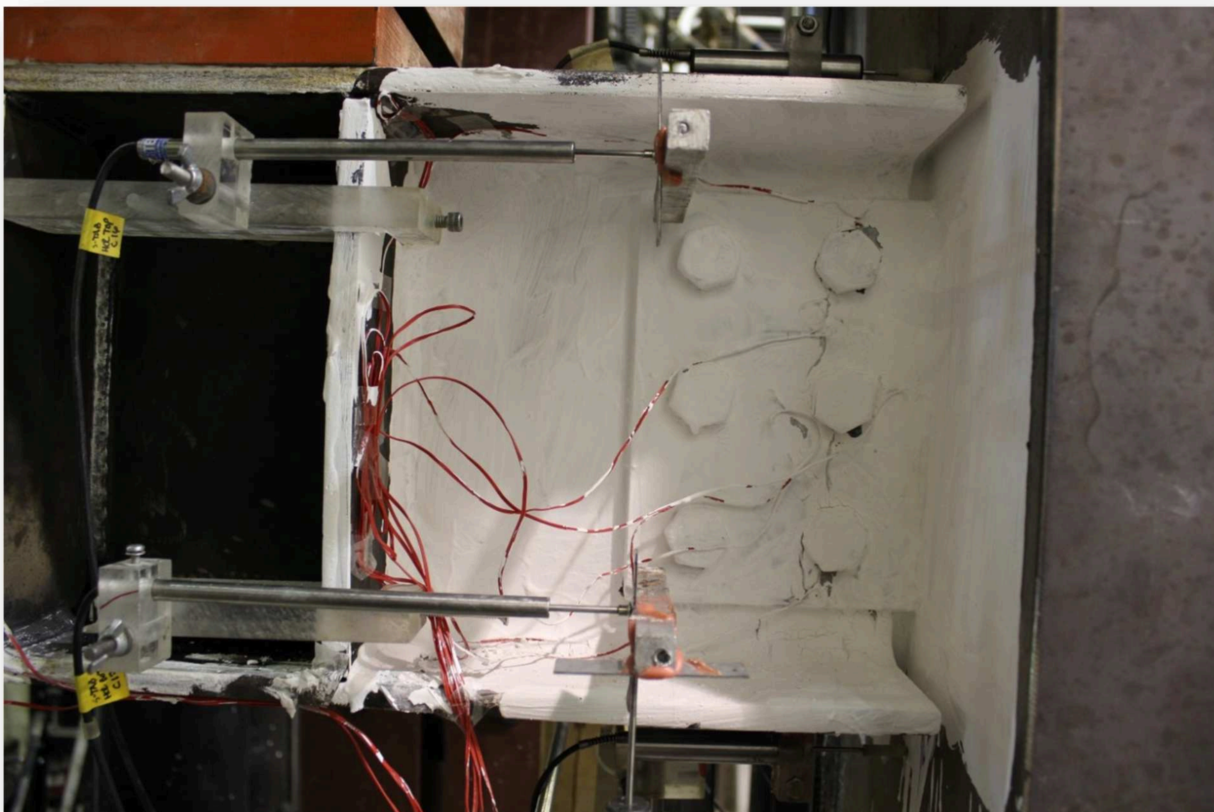

Appendix B – Shear tab test instrumentation details

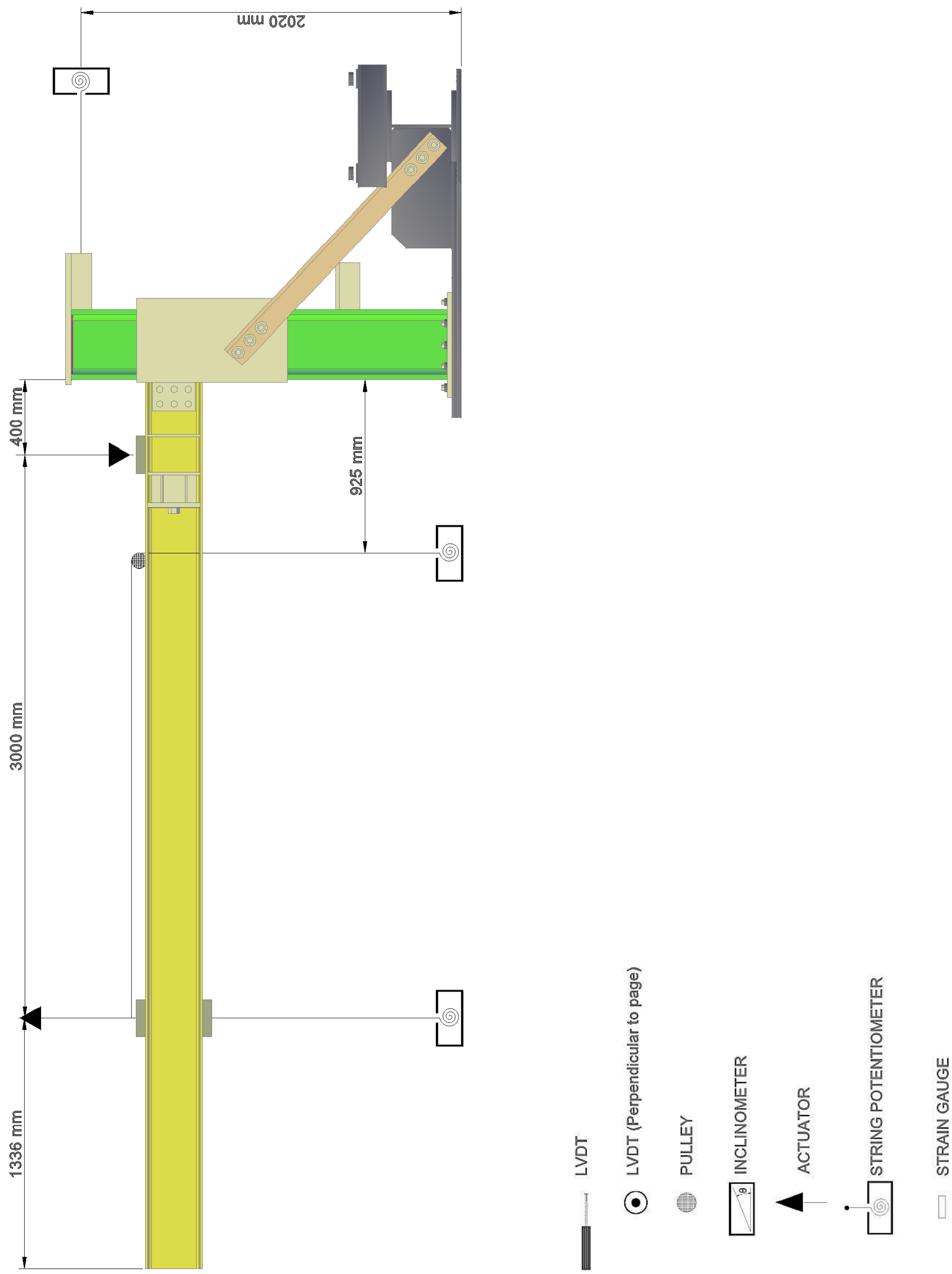

Figure B1- String potentiometer and actuator locations used in Test #1 and #2

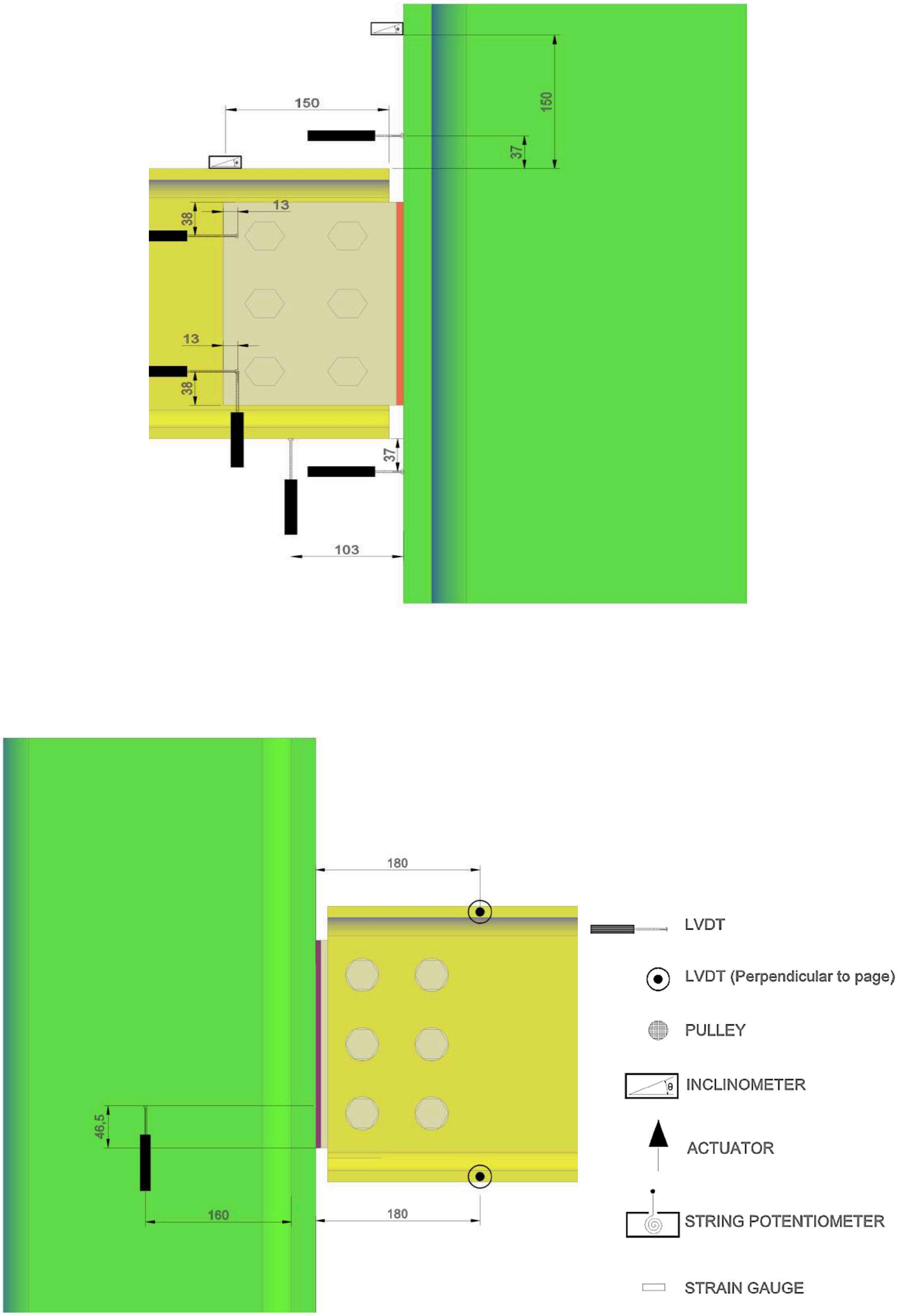

Figure B2- LVDT and Inclinometer locations used in Test #1 and #2

Figure B3- Strain gauge locations used in Test #1 and #2

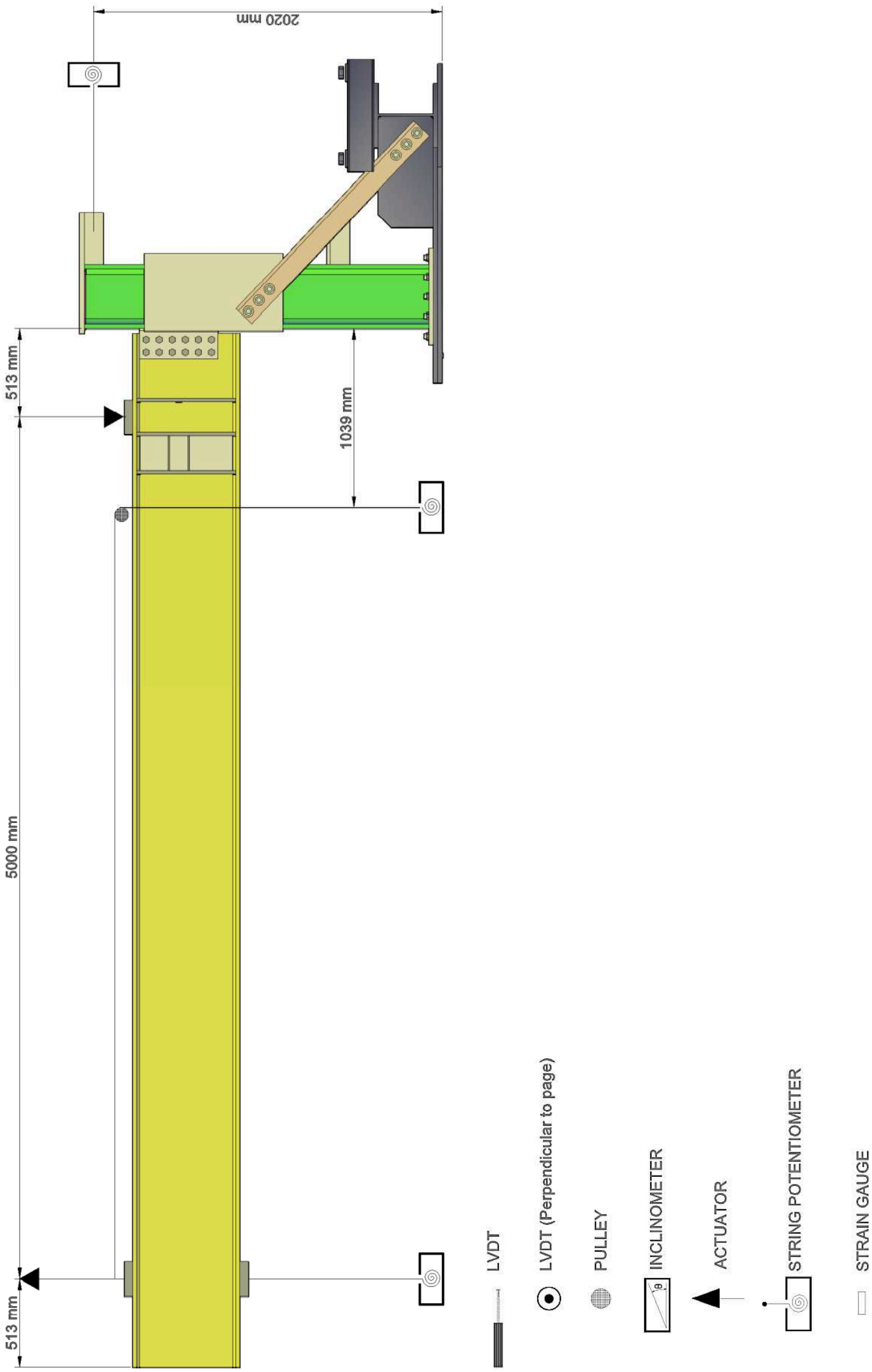

Figure B4- String potentiometer and actuator locations used in Test #3 and #4

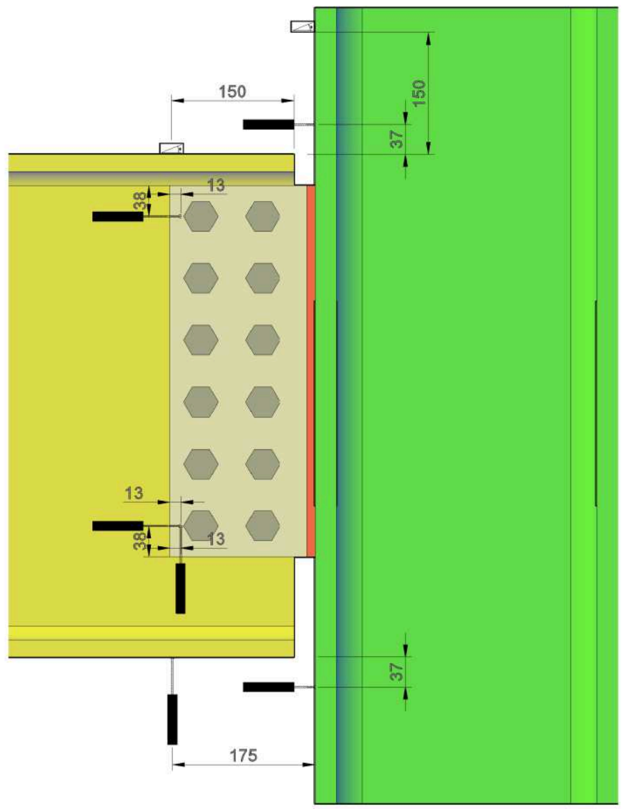

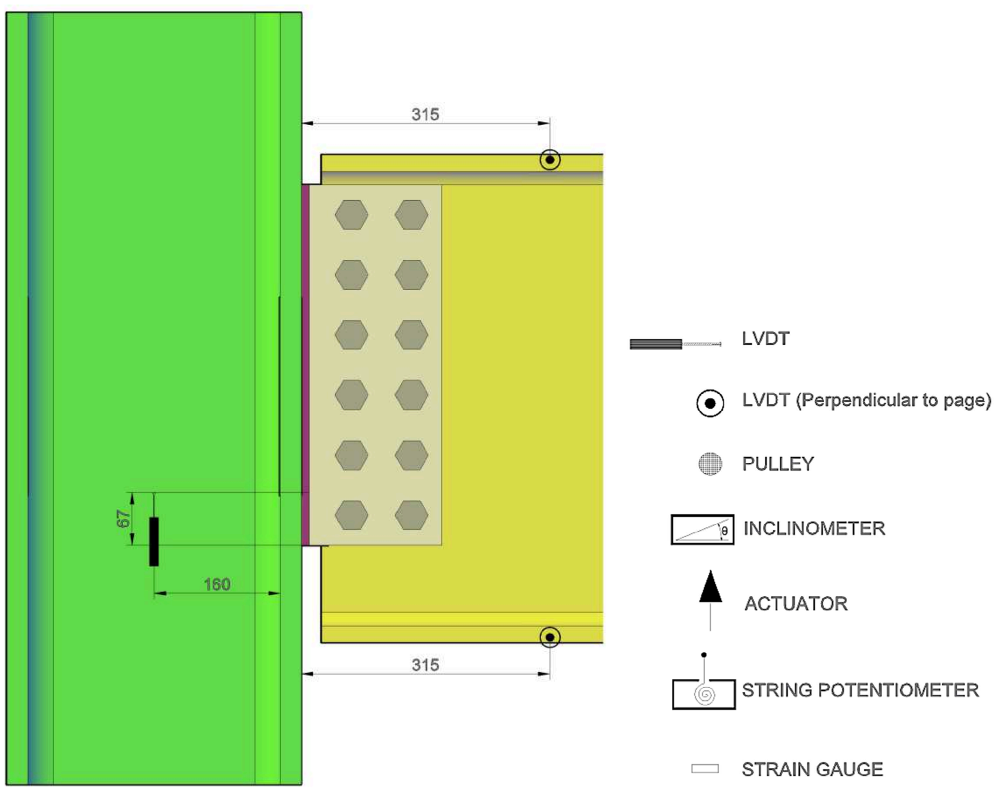

Figure B5- LVDT and Inclinometer locations used in Test #3 and #4

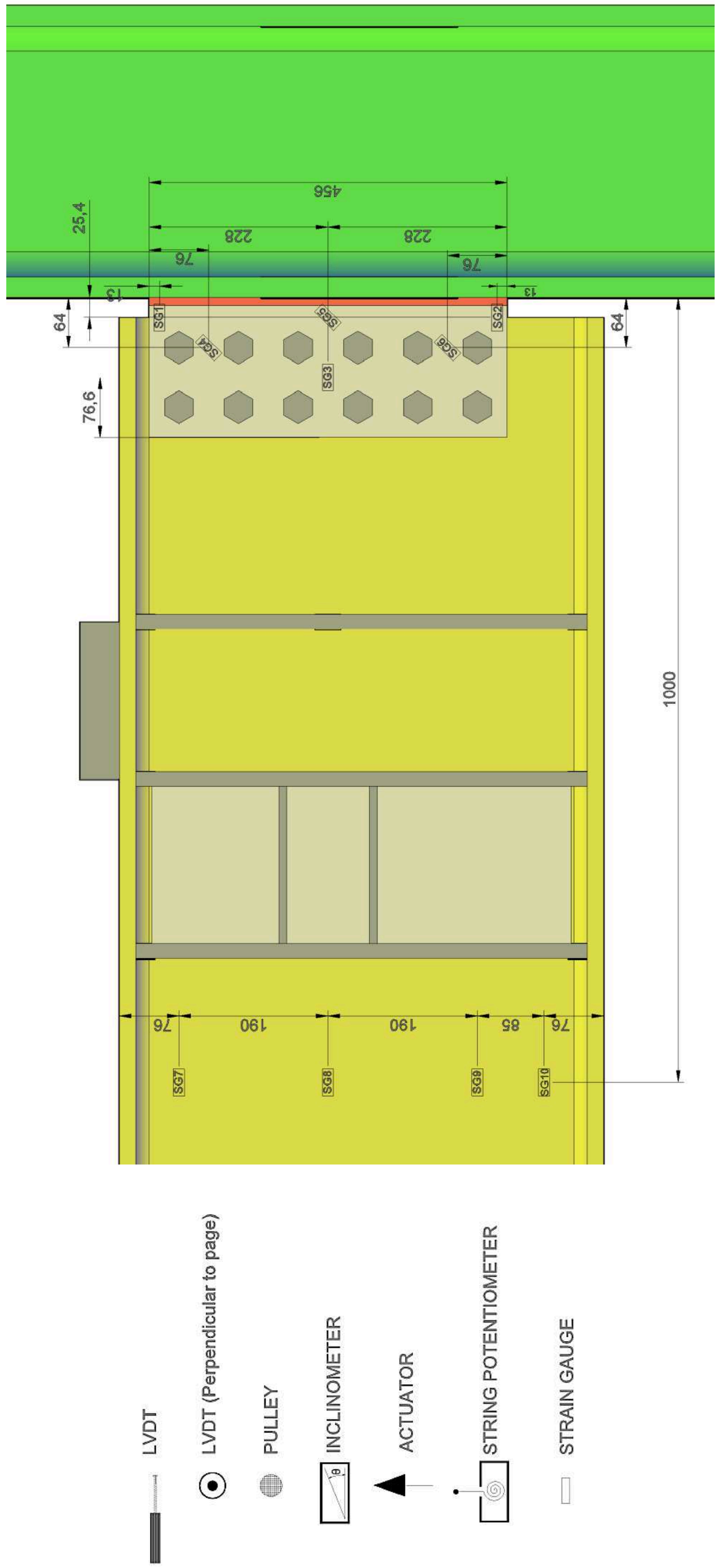

Figure B6 -Strain gauge locations used in Test #3 and #4

Appendix C

Erection and shop drawings

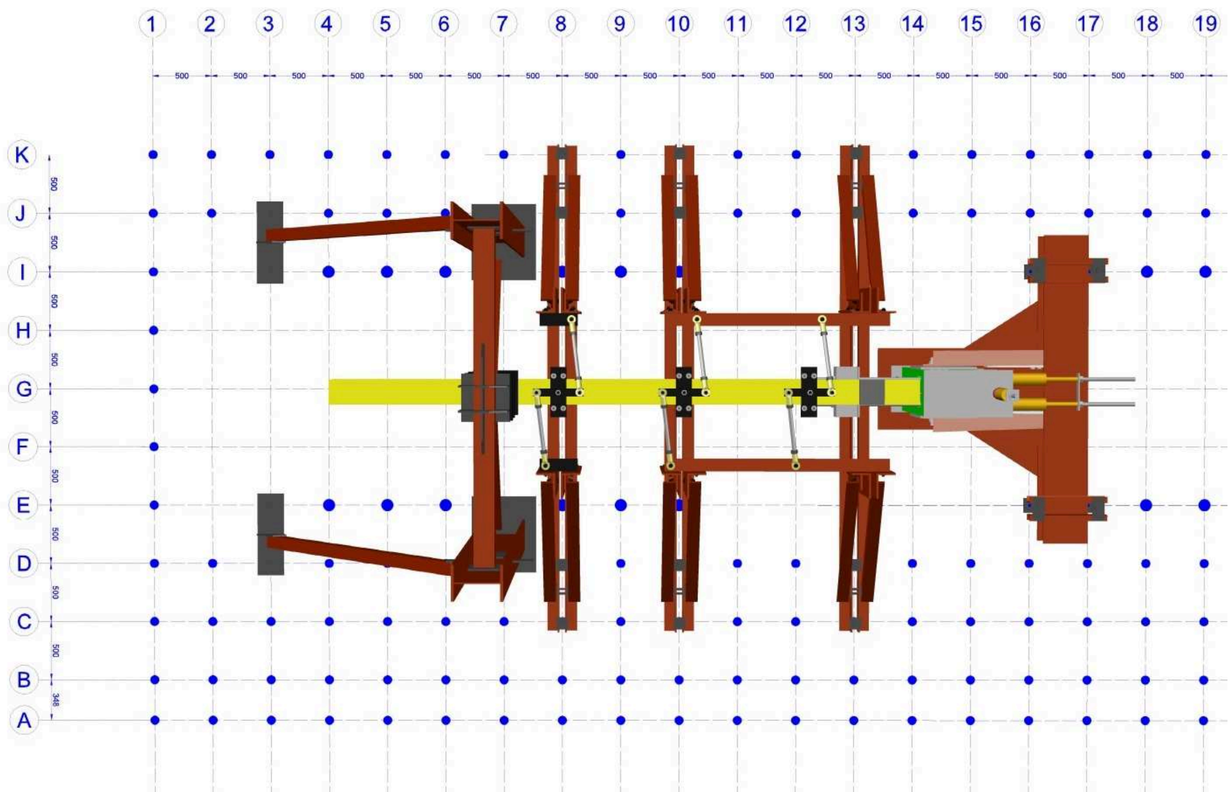

Appendix C – Erection and shop drawings

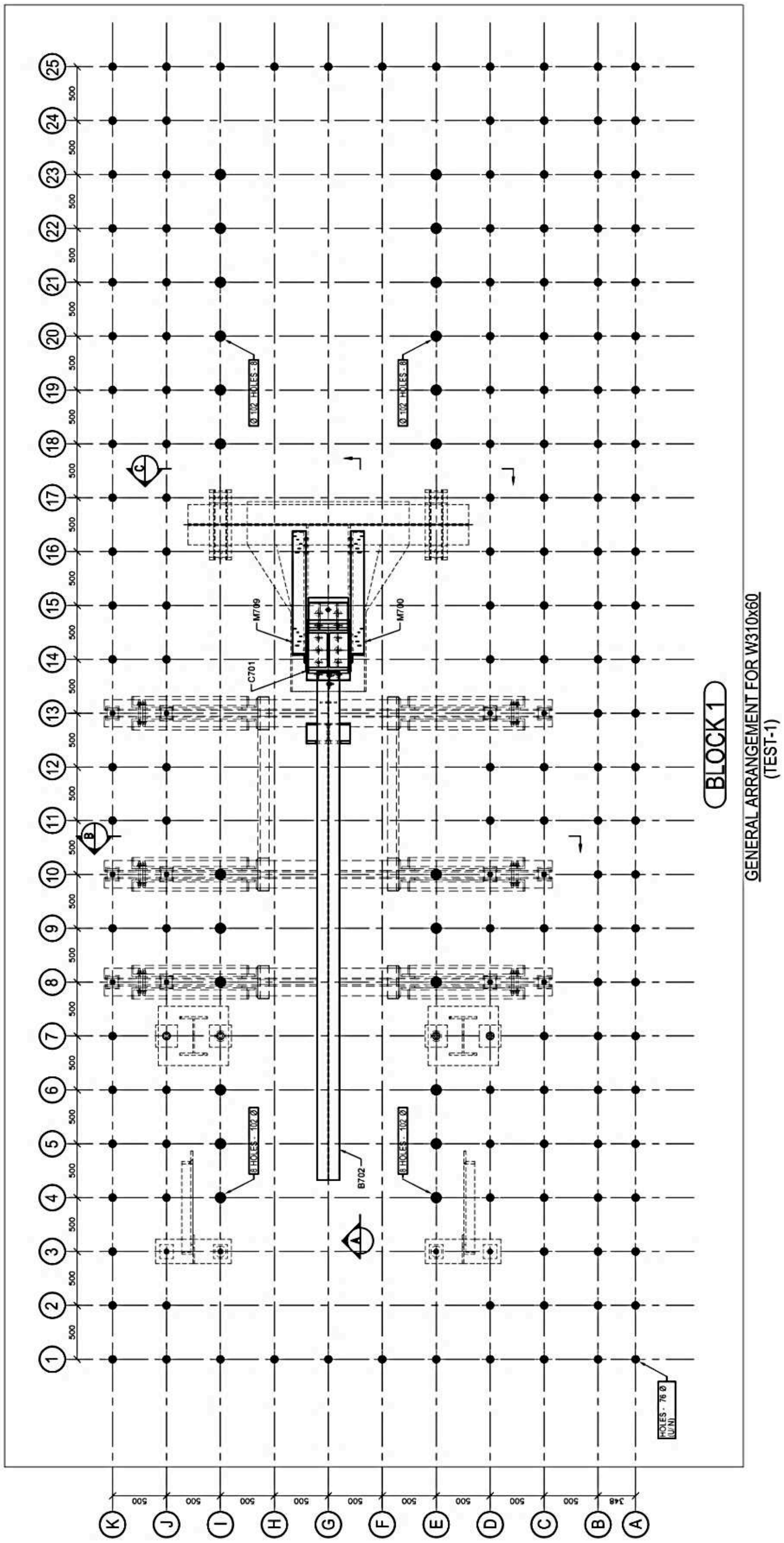

Figure C1−General arrangement used in Test #1

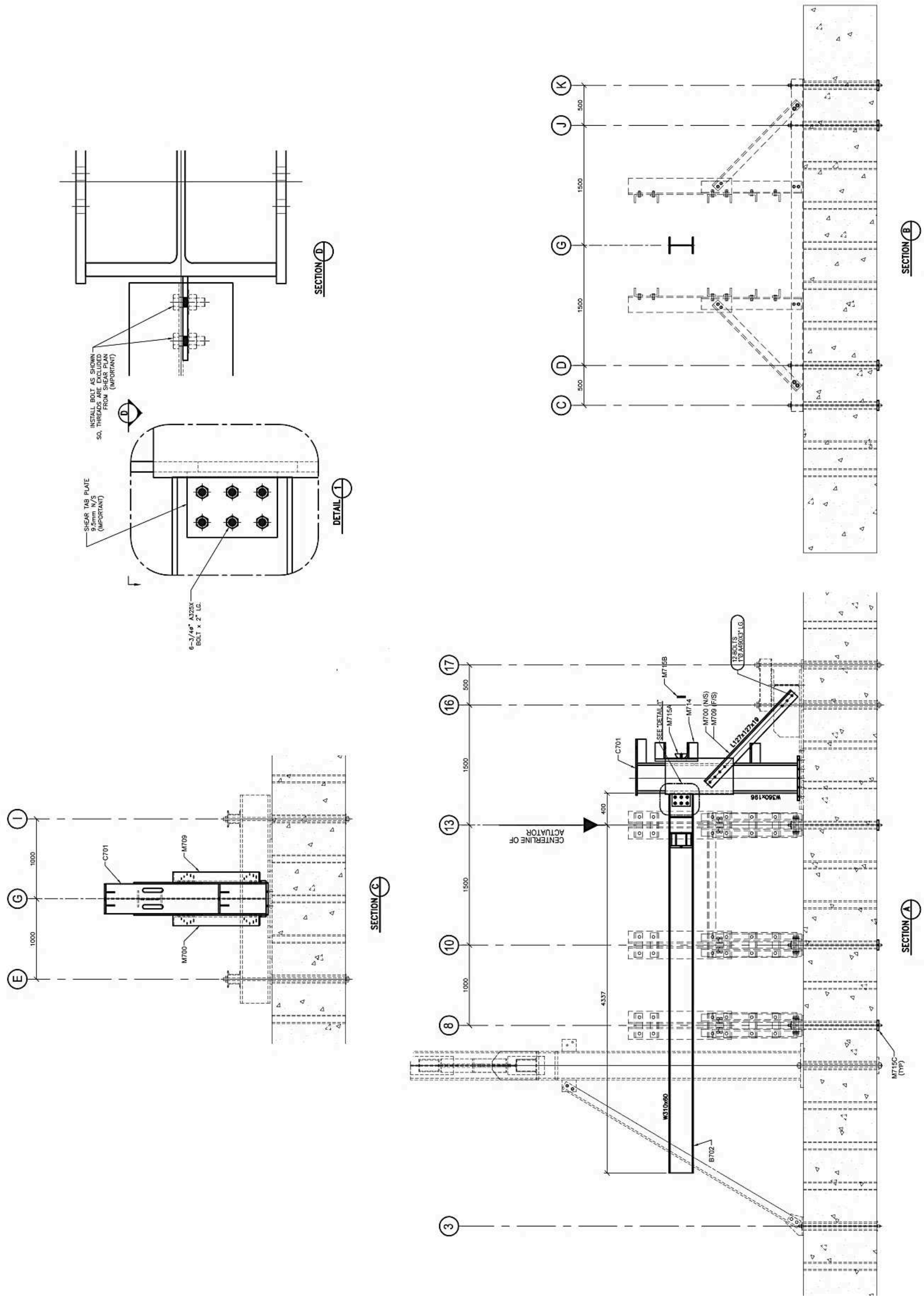

Figure C2–Erection details of Test #1

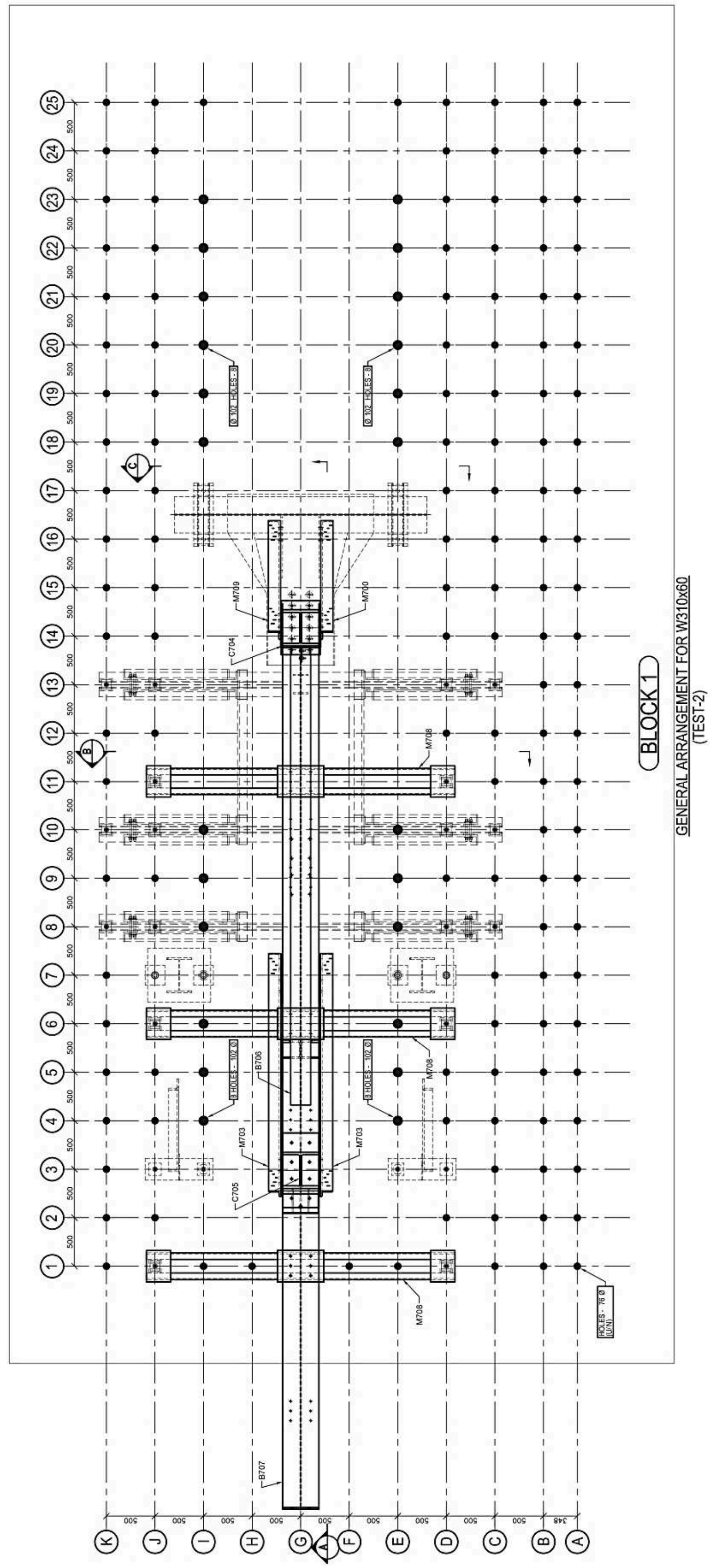

Figure C3−General arrangement used in Test #2

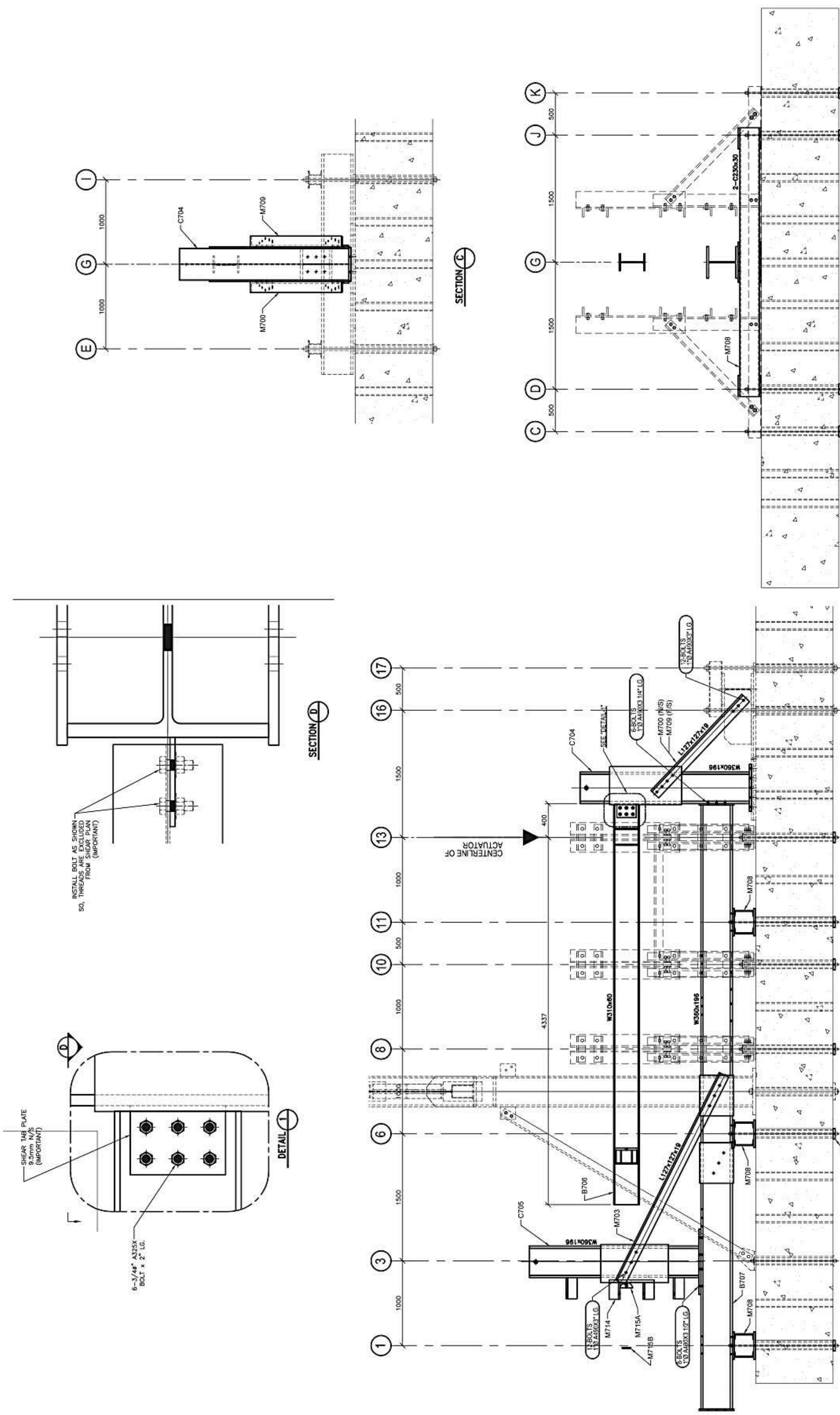

Figure C4−Erection details of Test #2

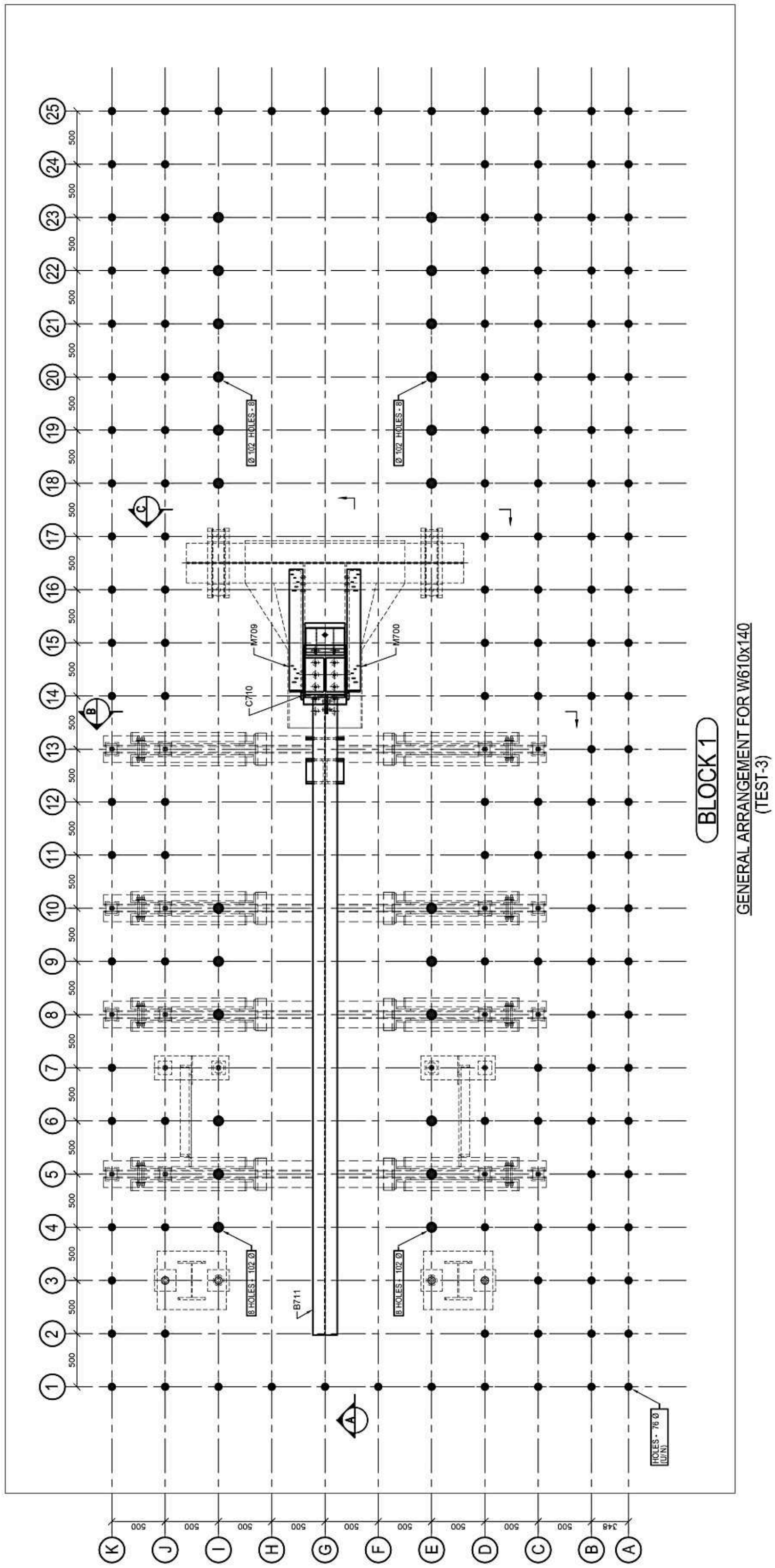

Figure C5−General arrangement used in Test #3

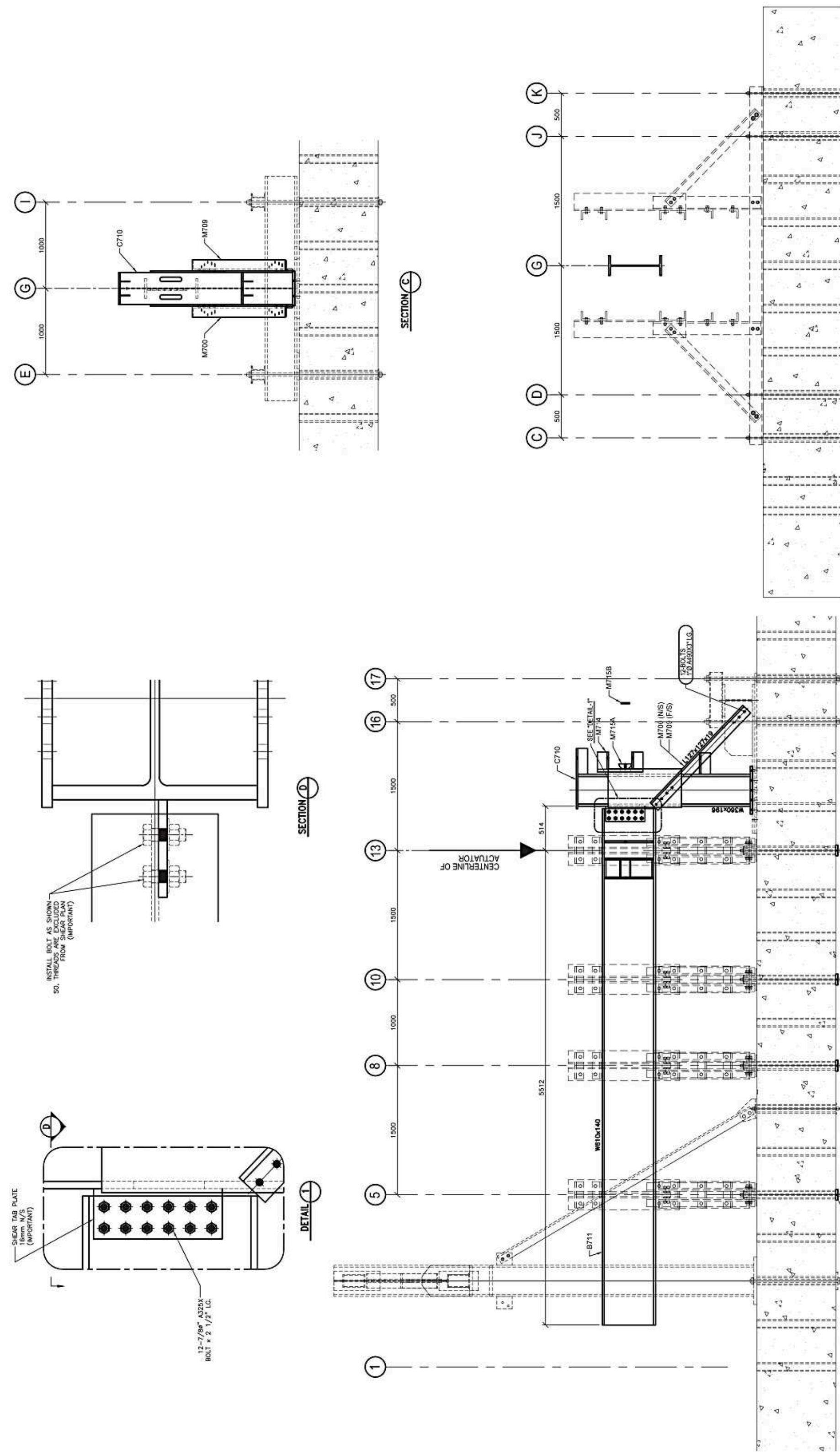

Figure C6–Erection details of Test #3

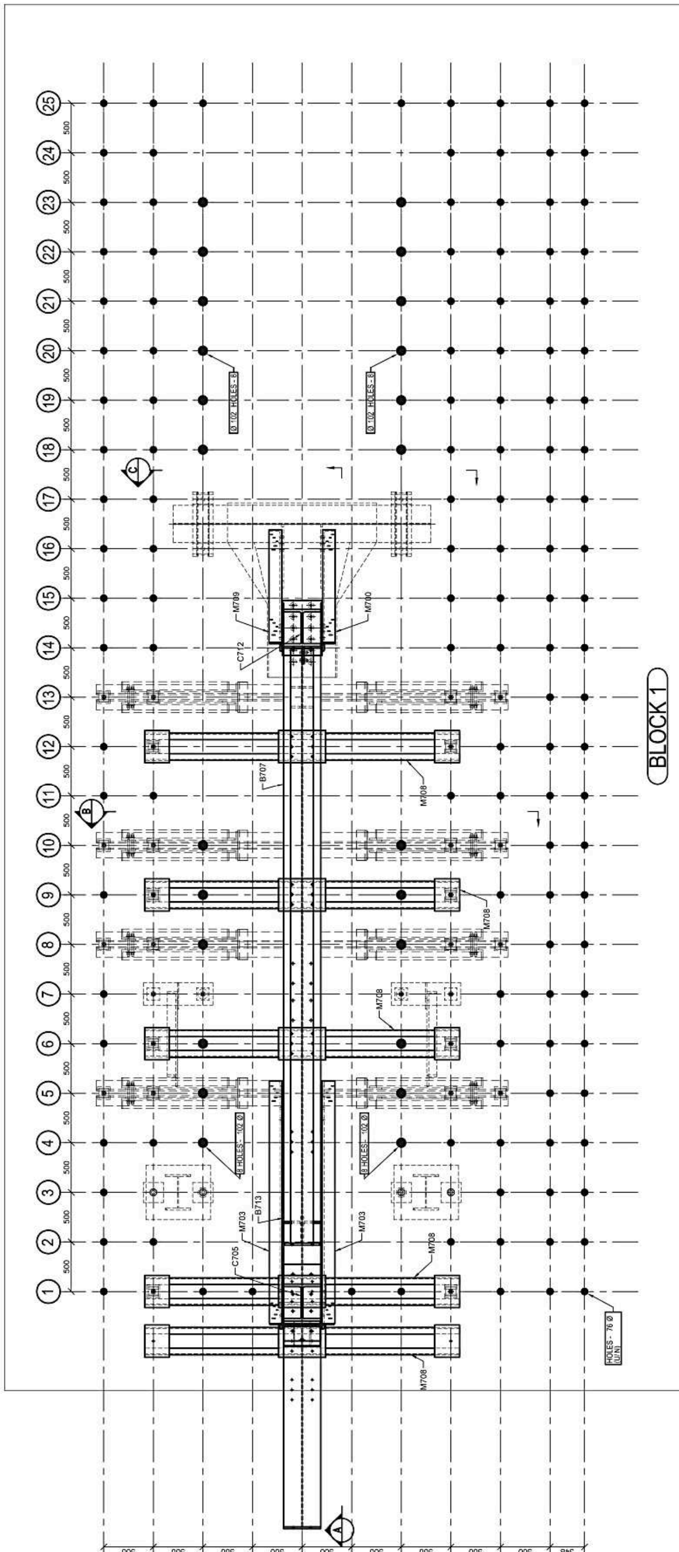

Figure C7–General arrangement used in Test #4

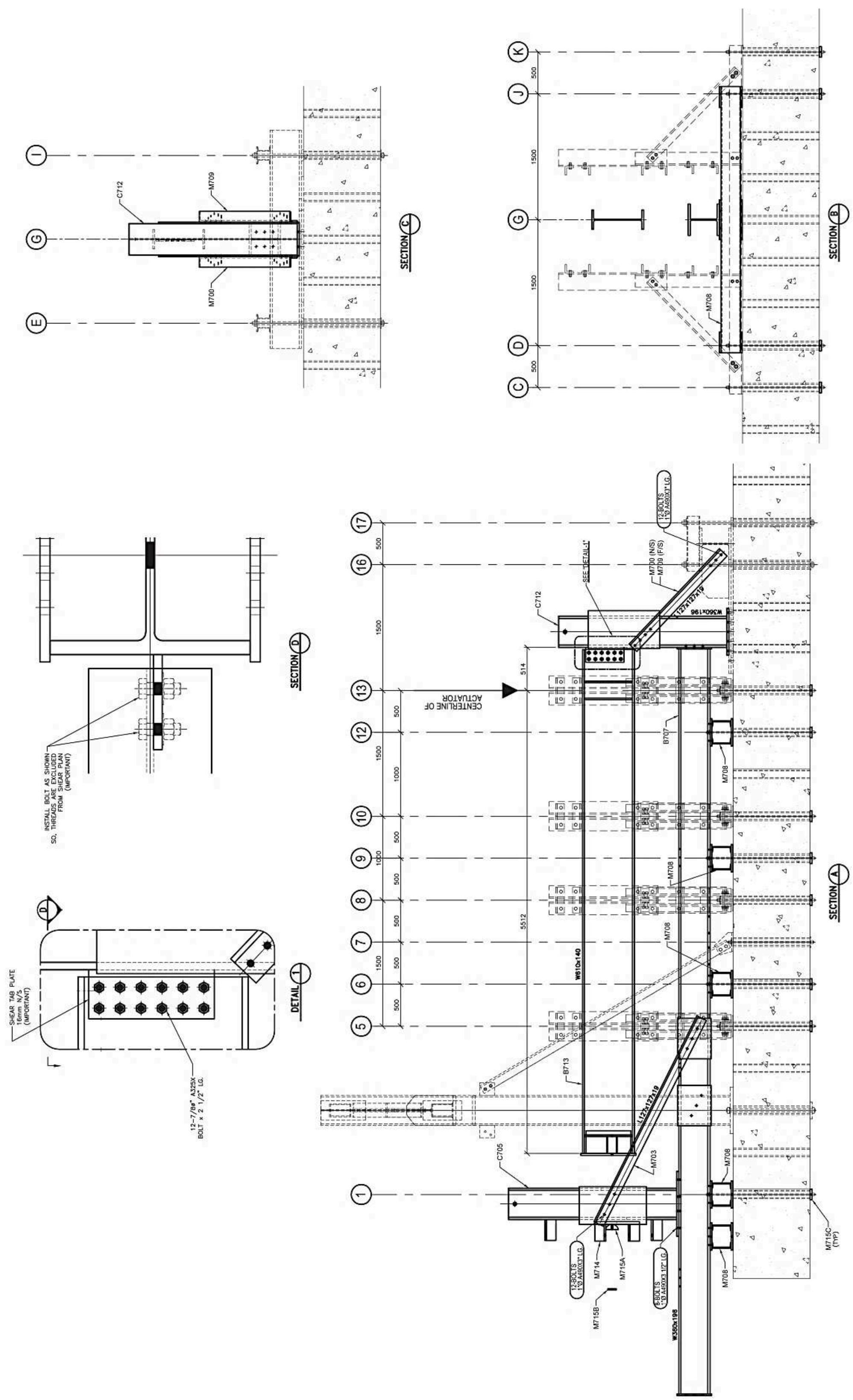

Figure C8–Erection details of Test #4

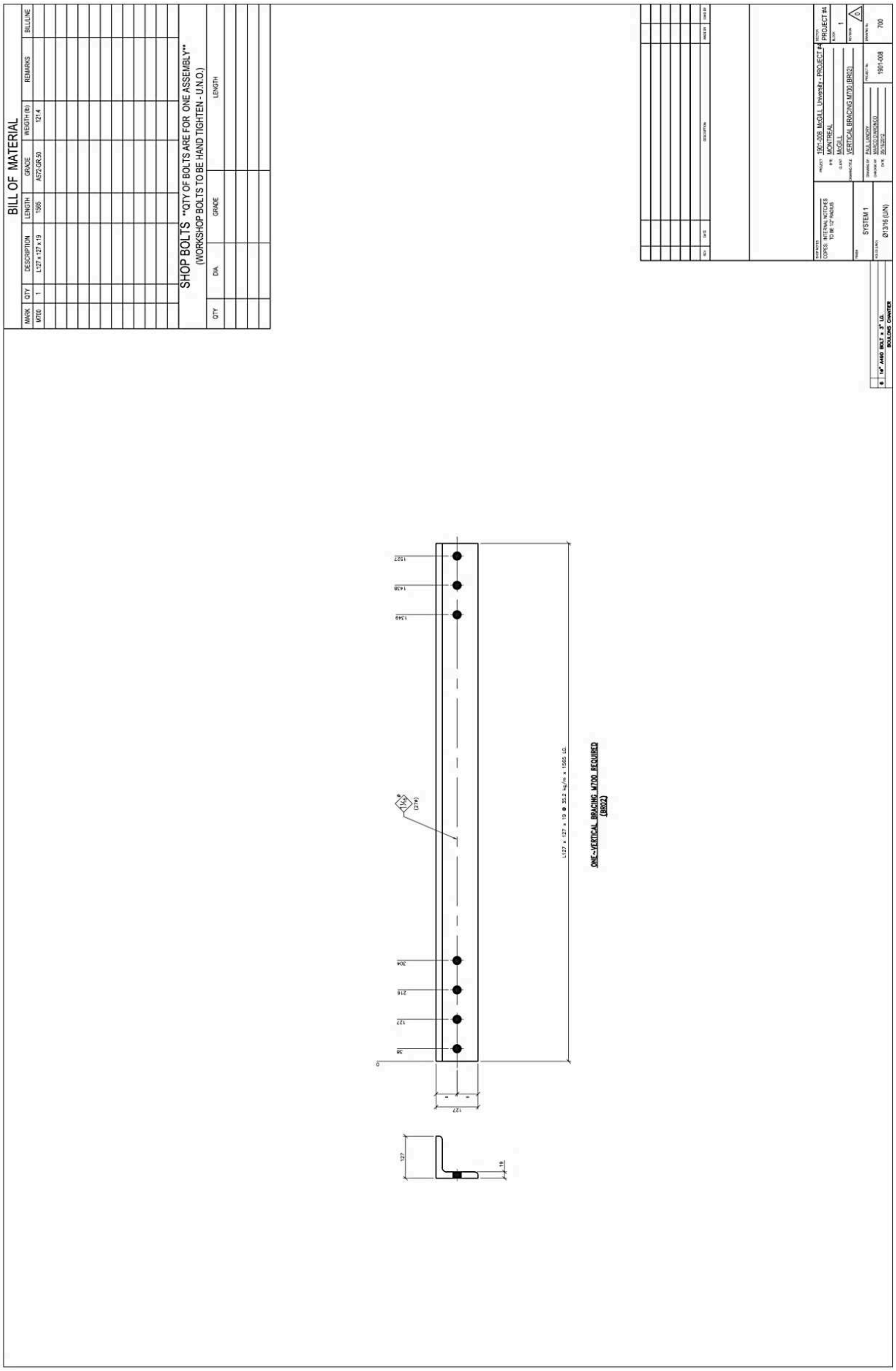

Figure C9−Shop drawing #700

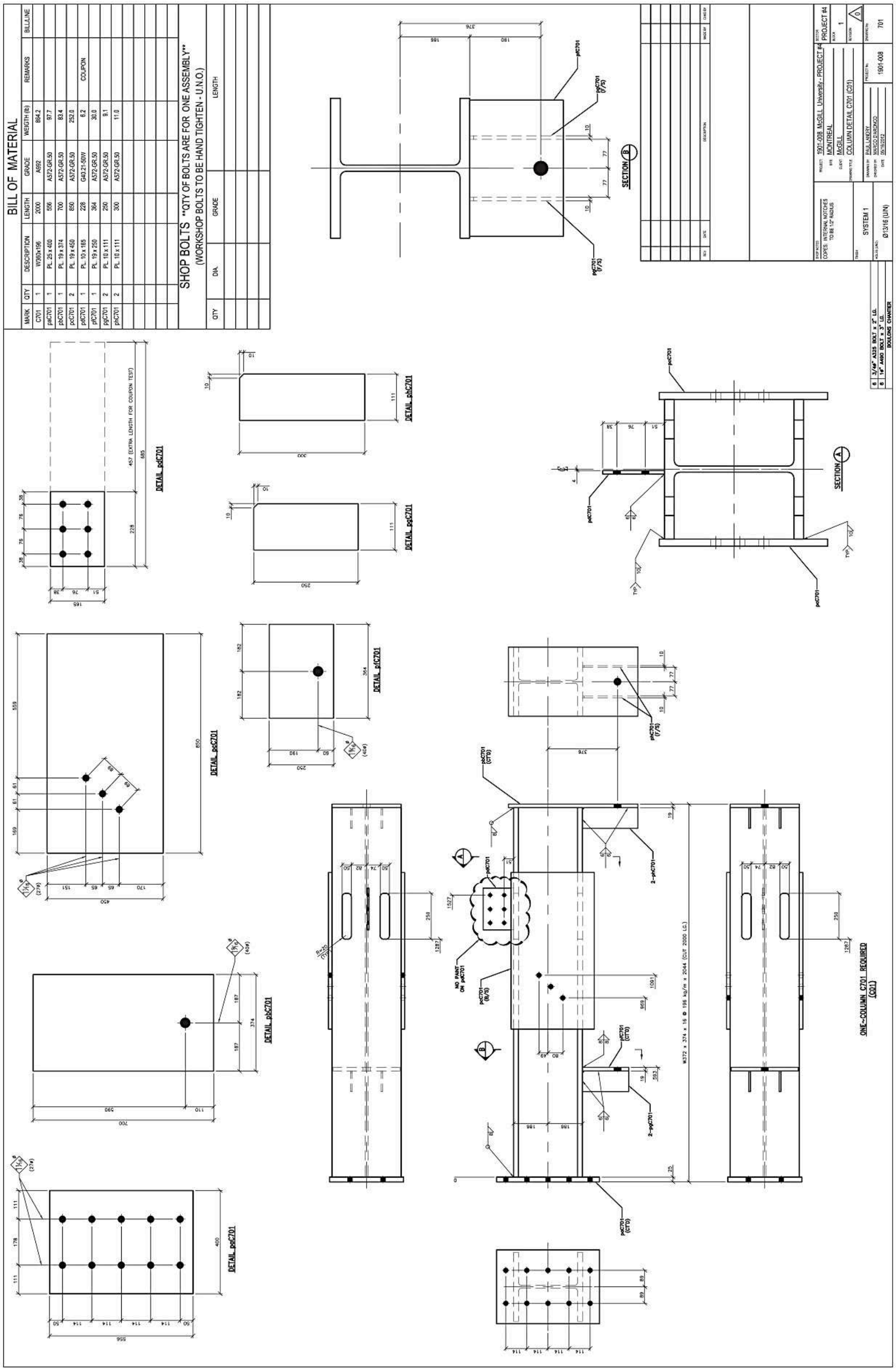

Figure C10–Shop drawing #701

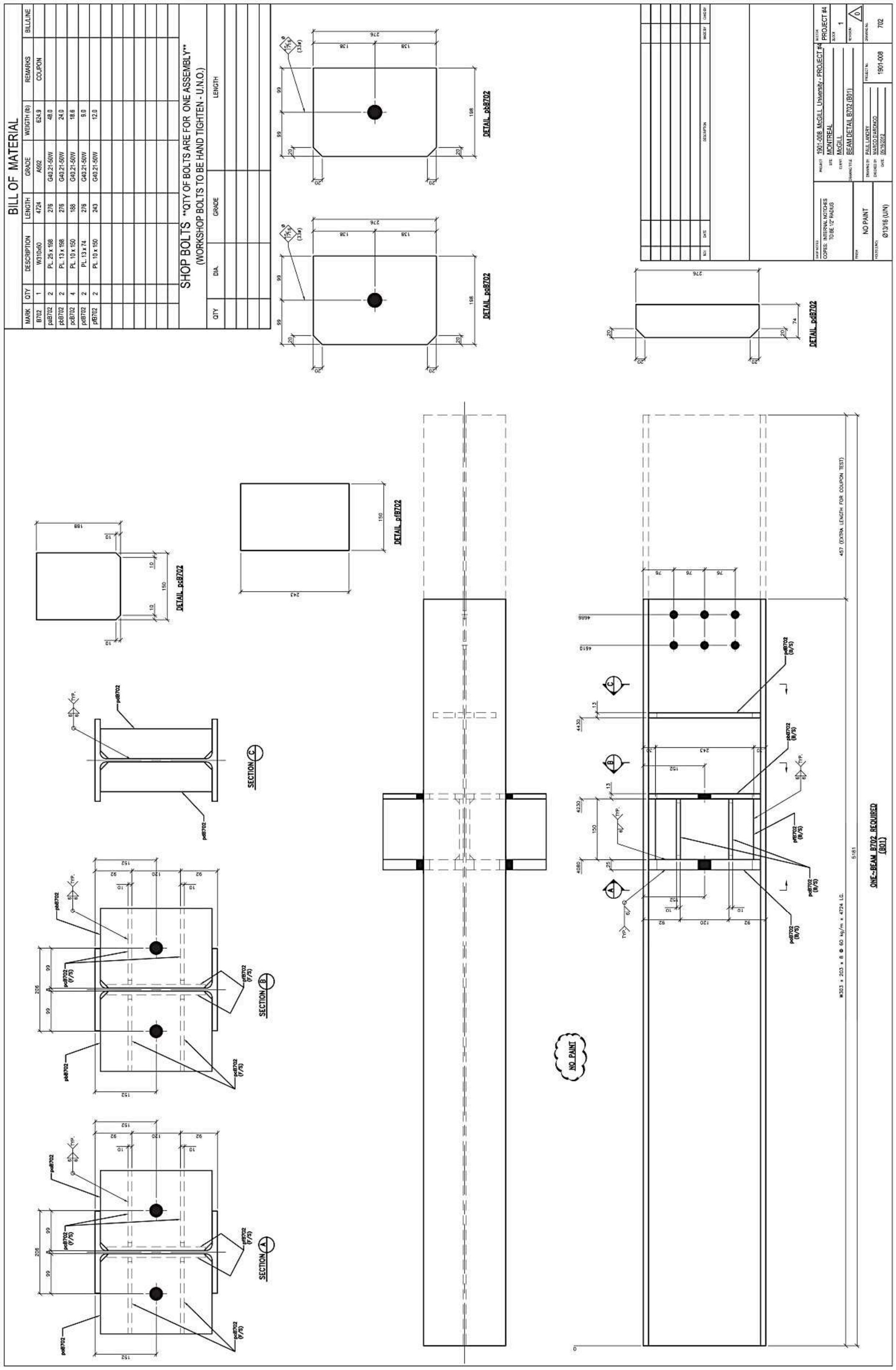

Figure C11–Shop drawing #702

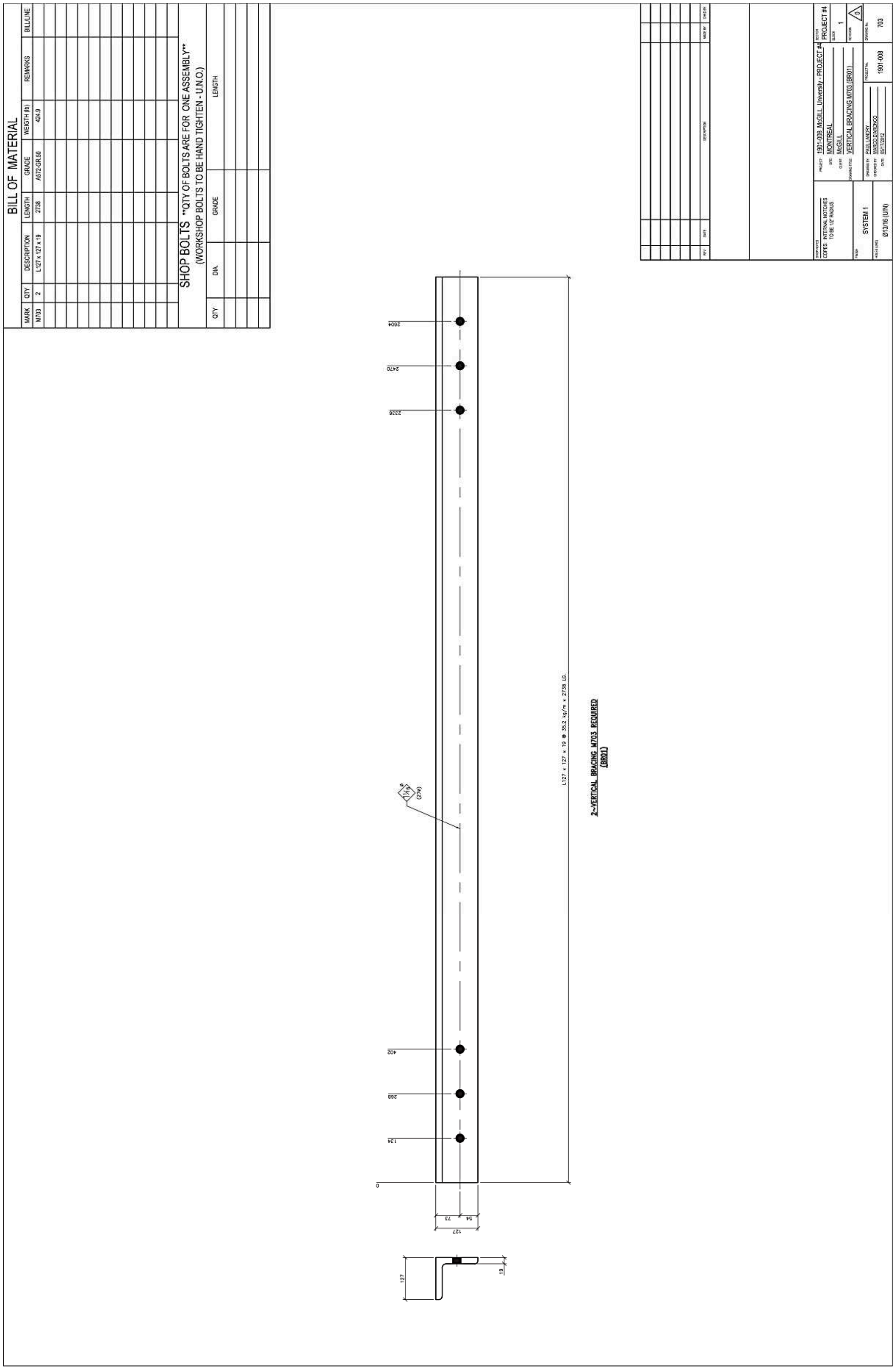

Figure C12−Shop drawing #703

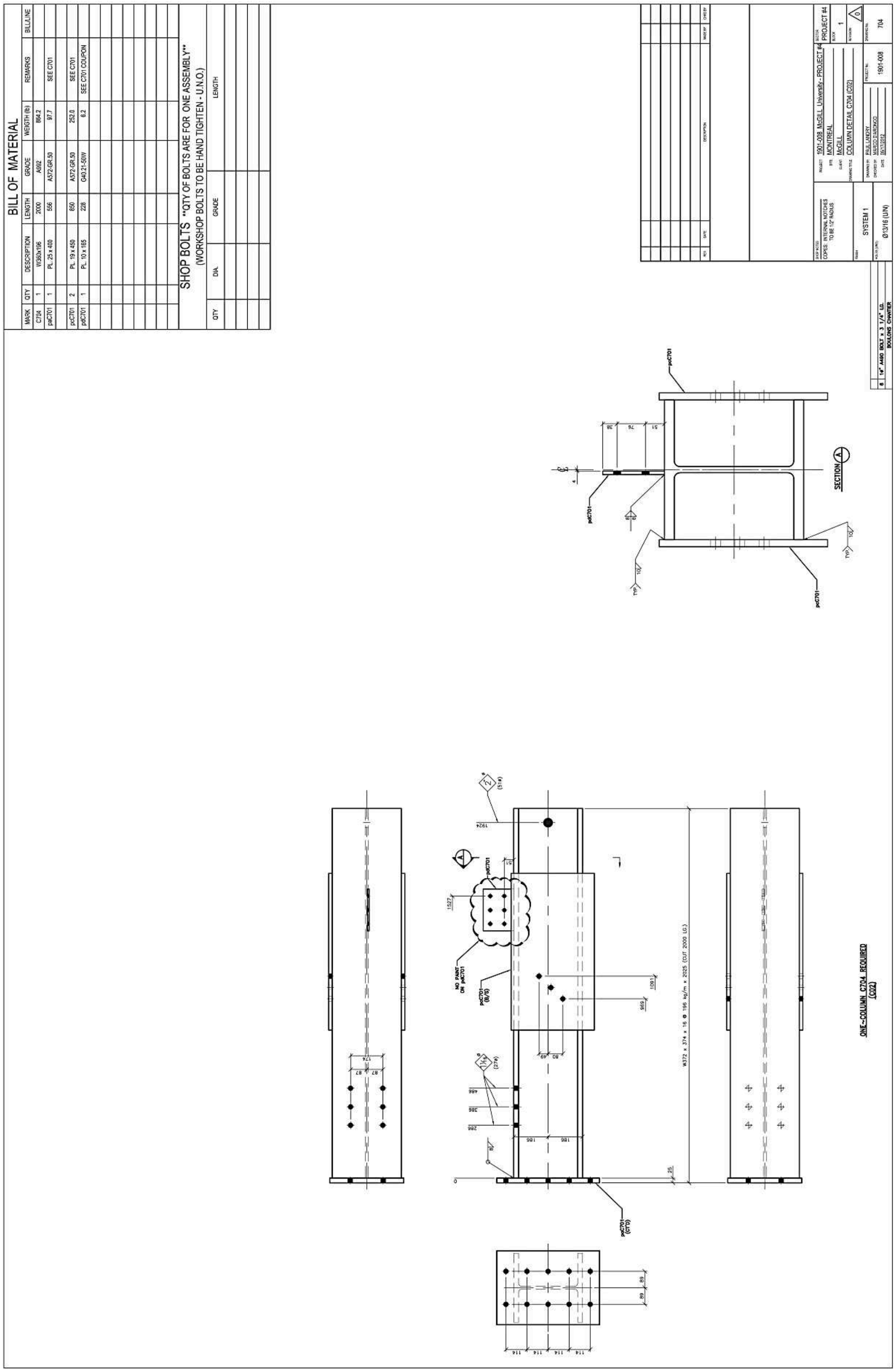

Figure C13−Shop drawing #704

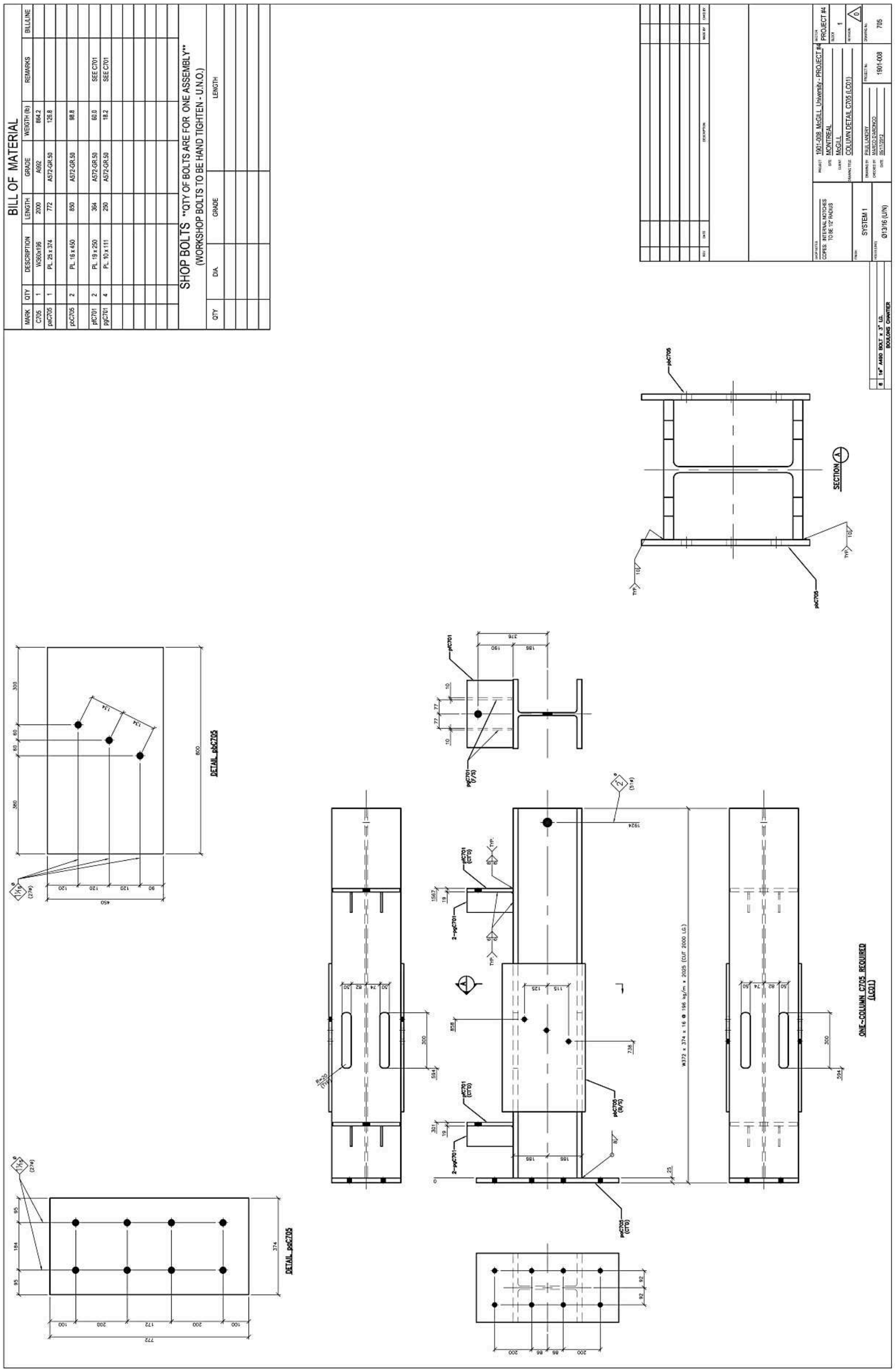

Figure C14–Shop drawing #705

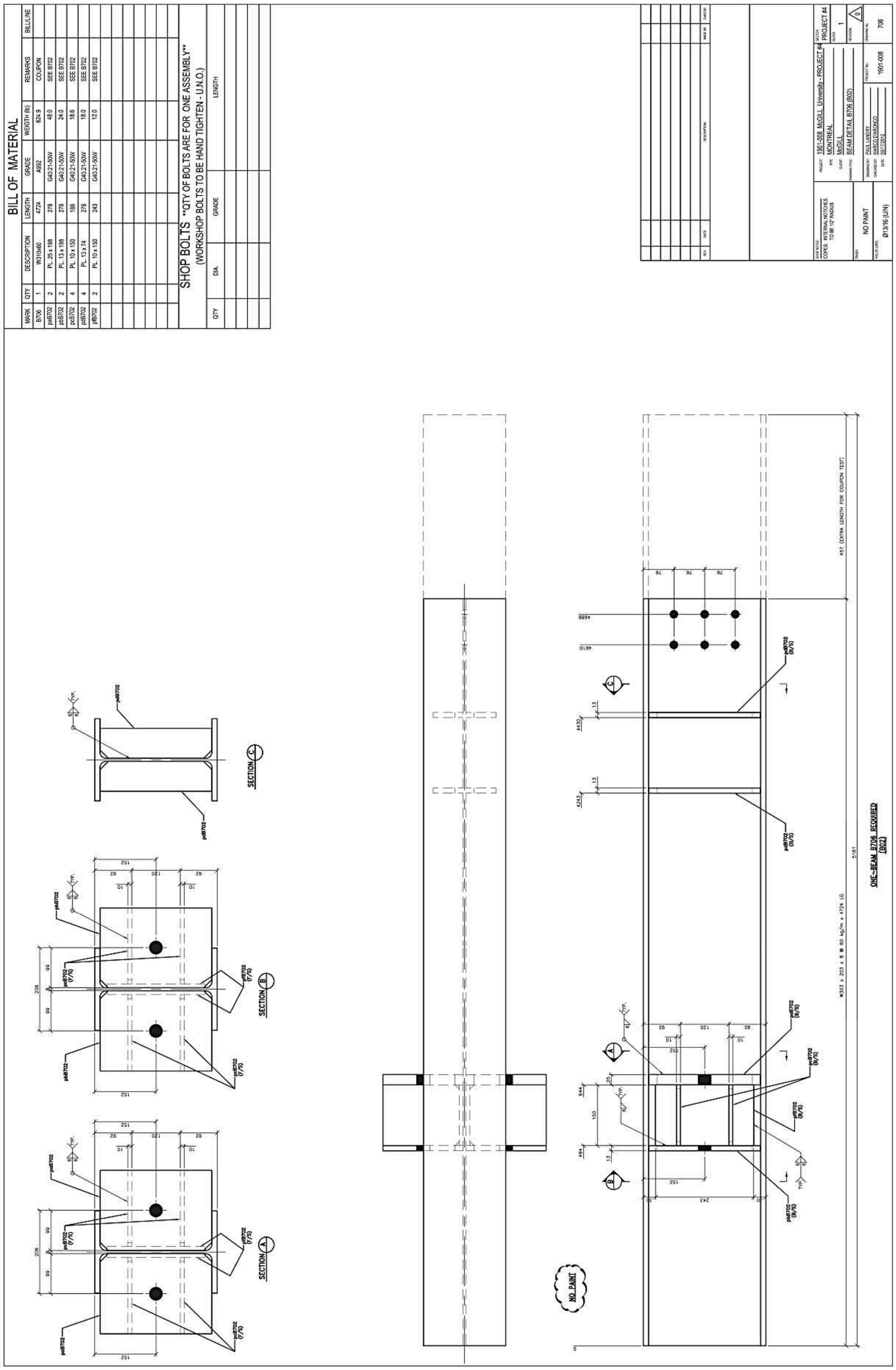

Figure C15−Shop drawing #706

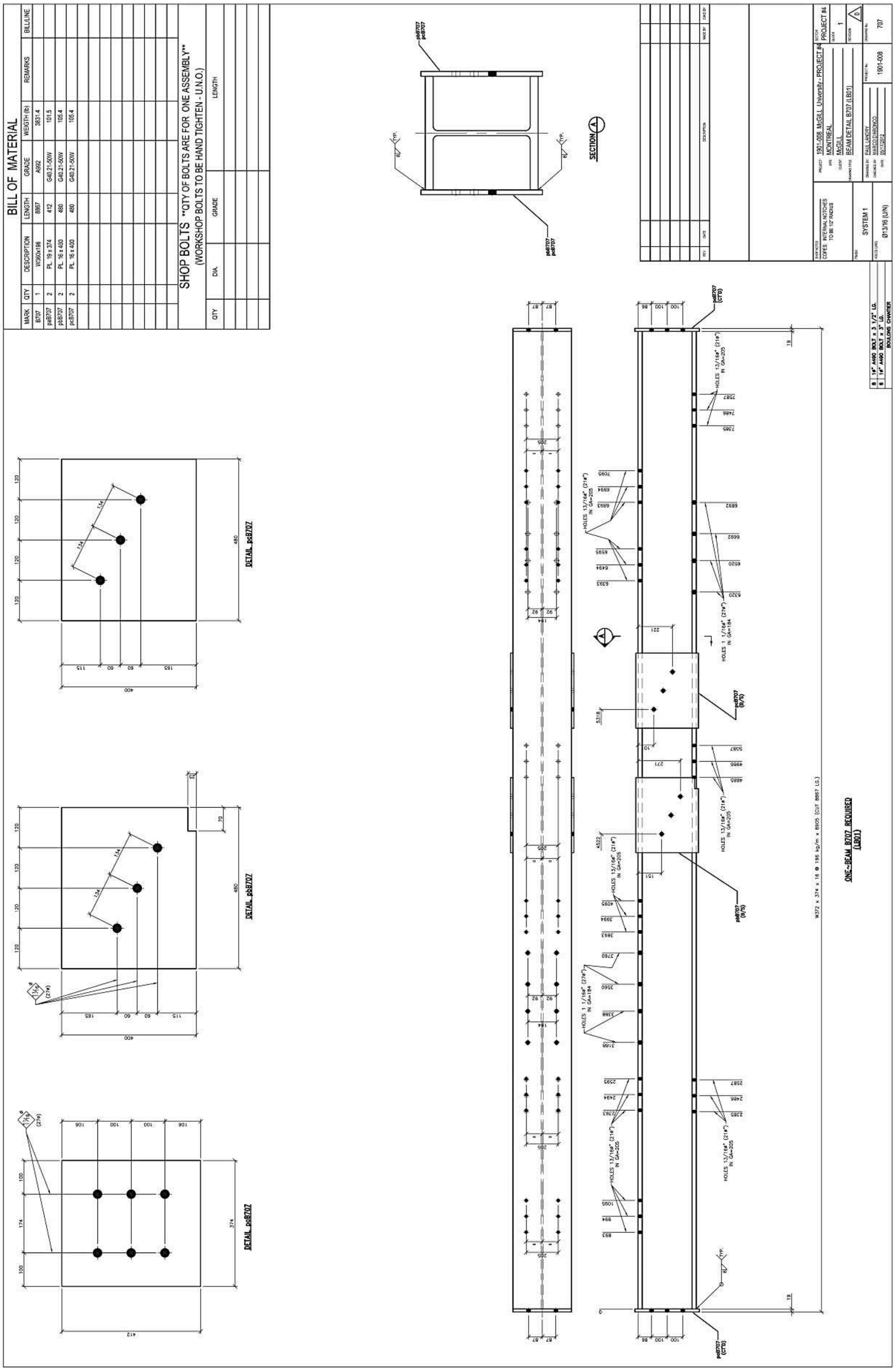

Figure C16–Shop drawing #707

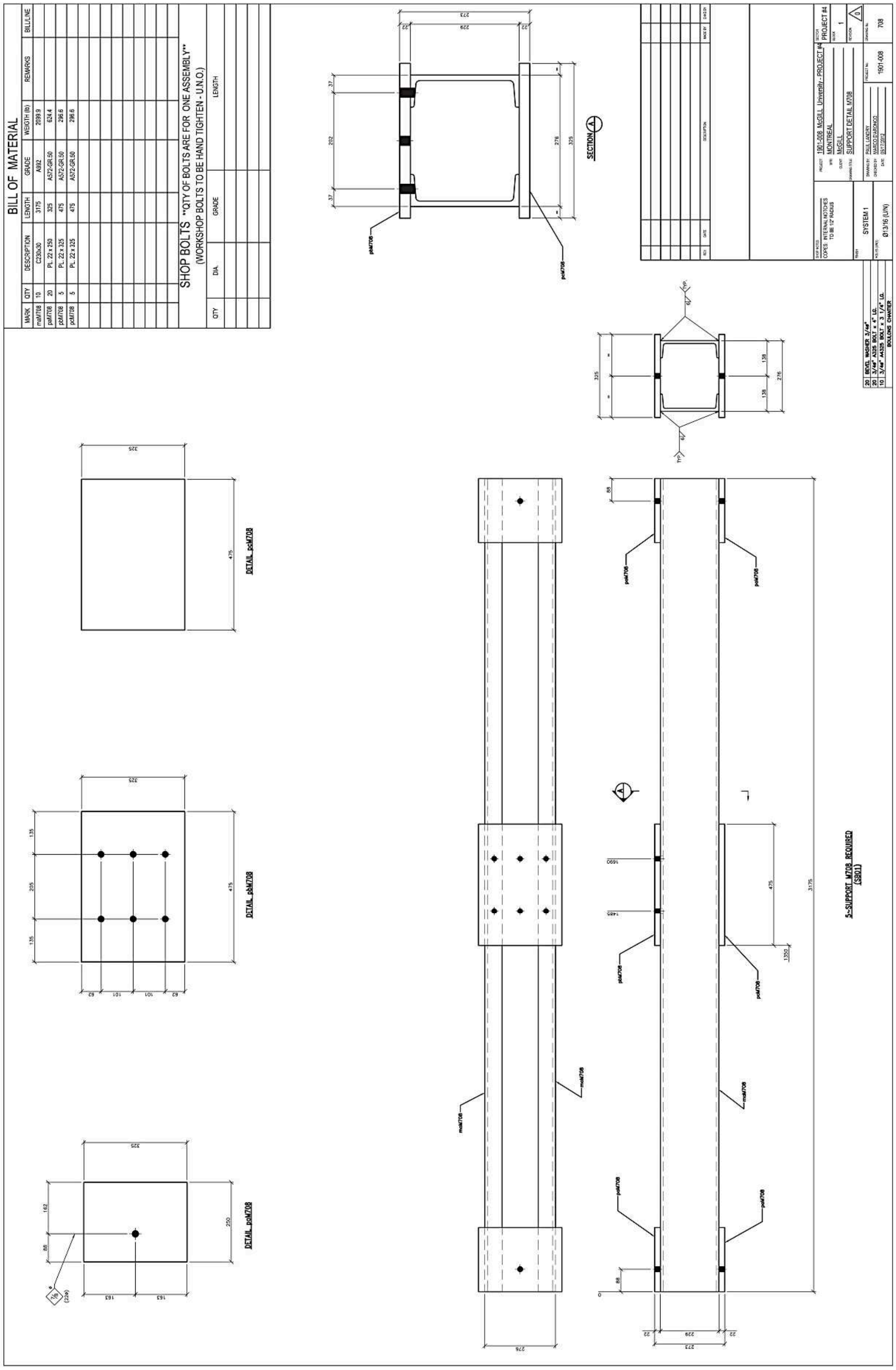

Figure C17−Shop drawing #708

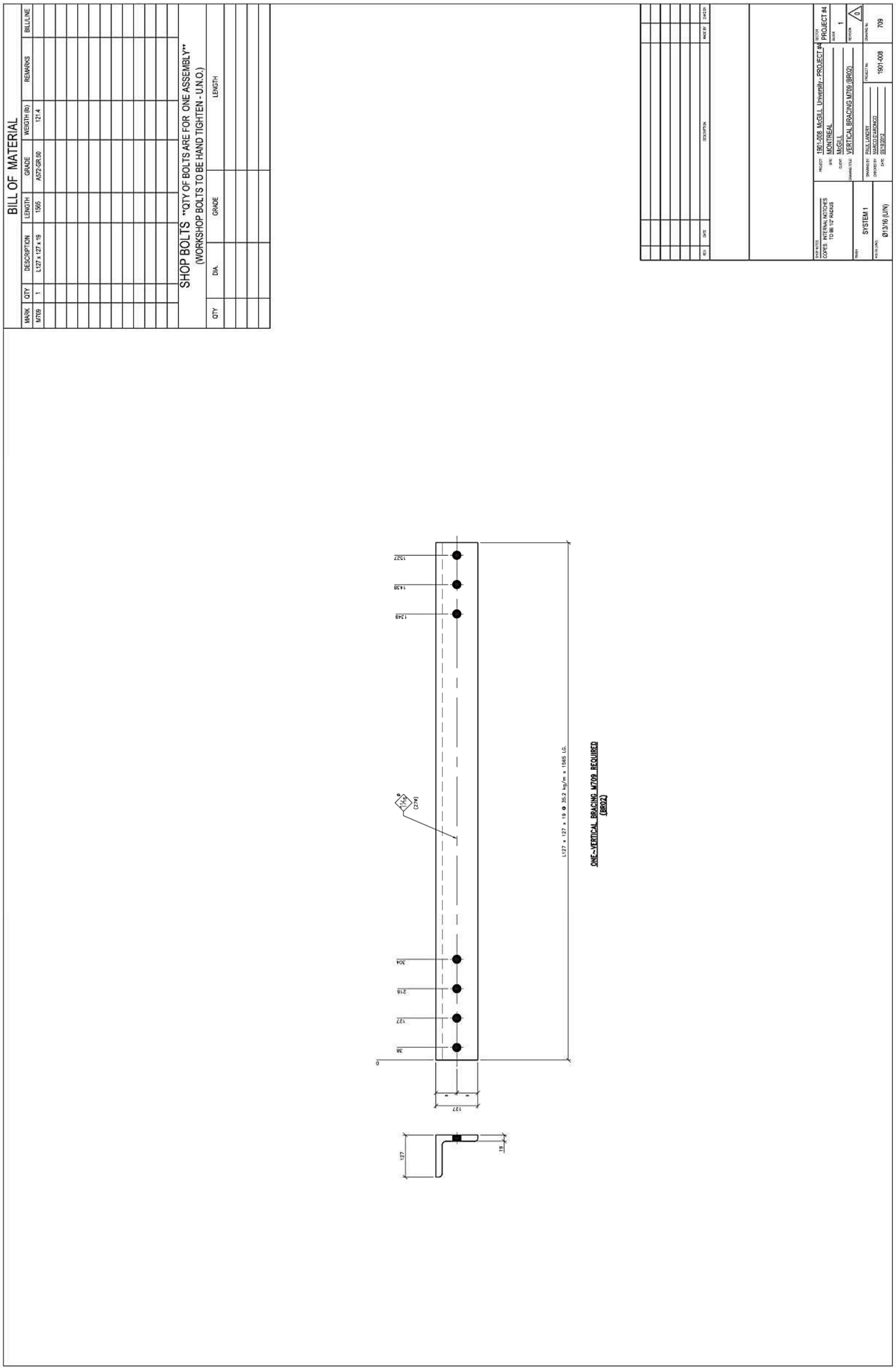

Figure C18−Shop drawing #709

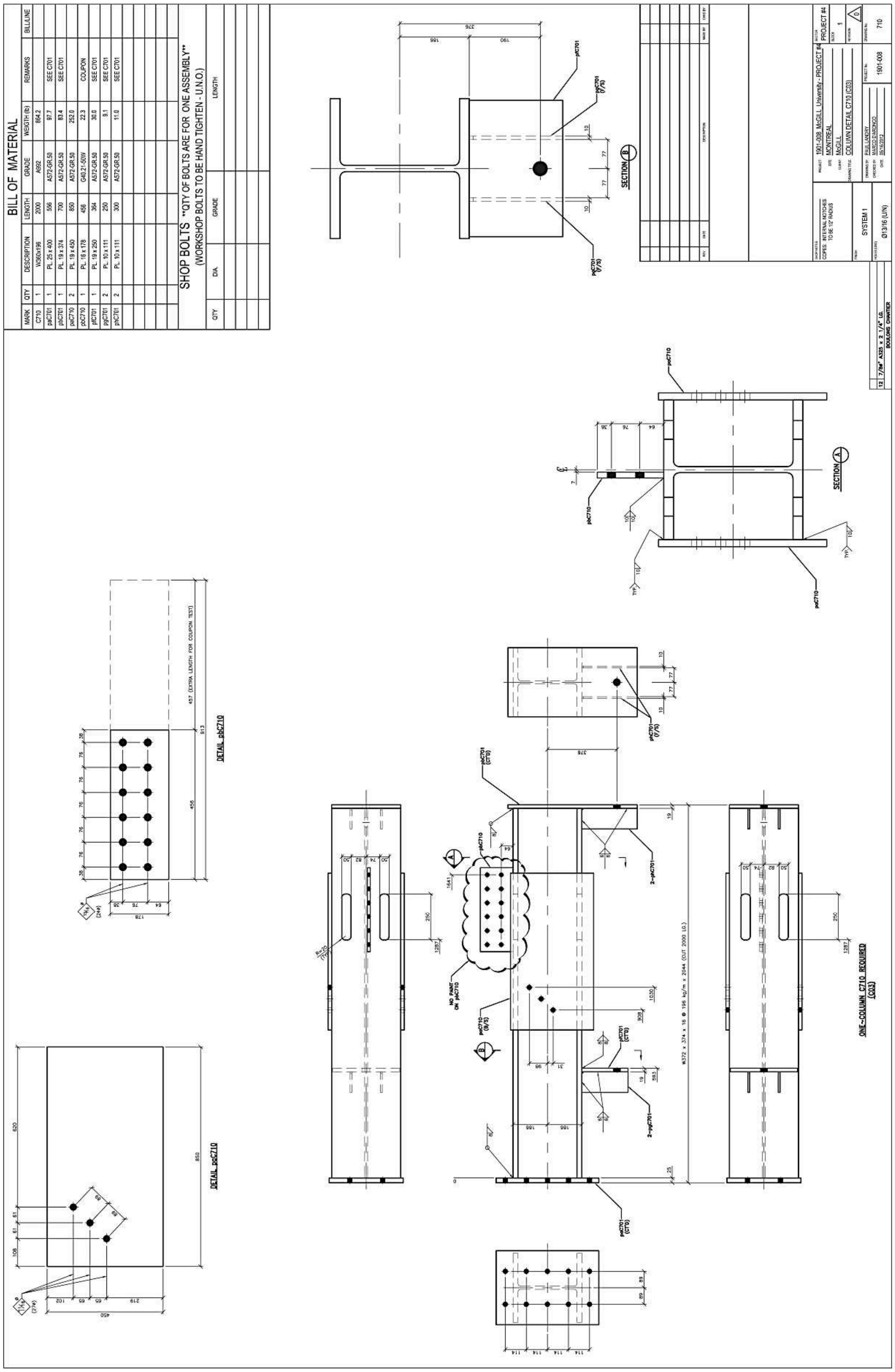

Figure C19–Shop drawing #710

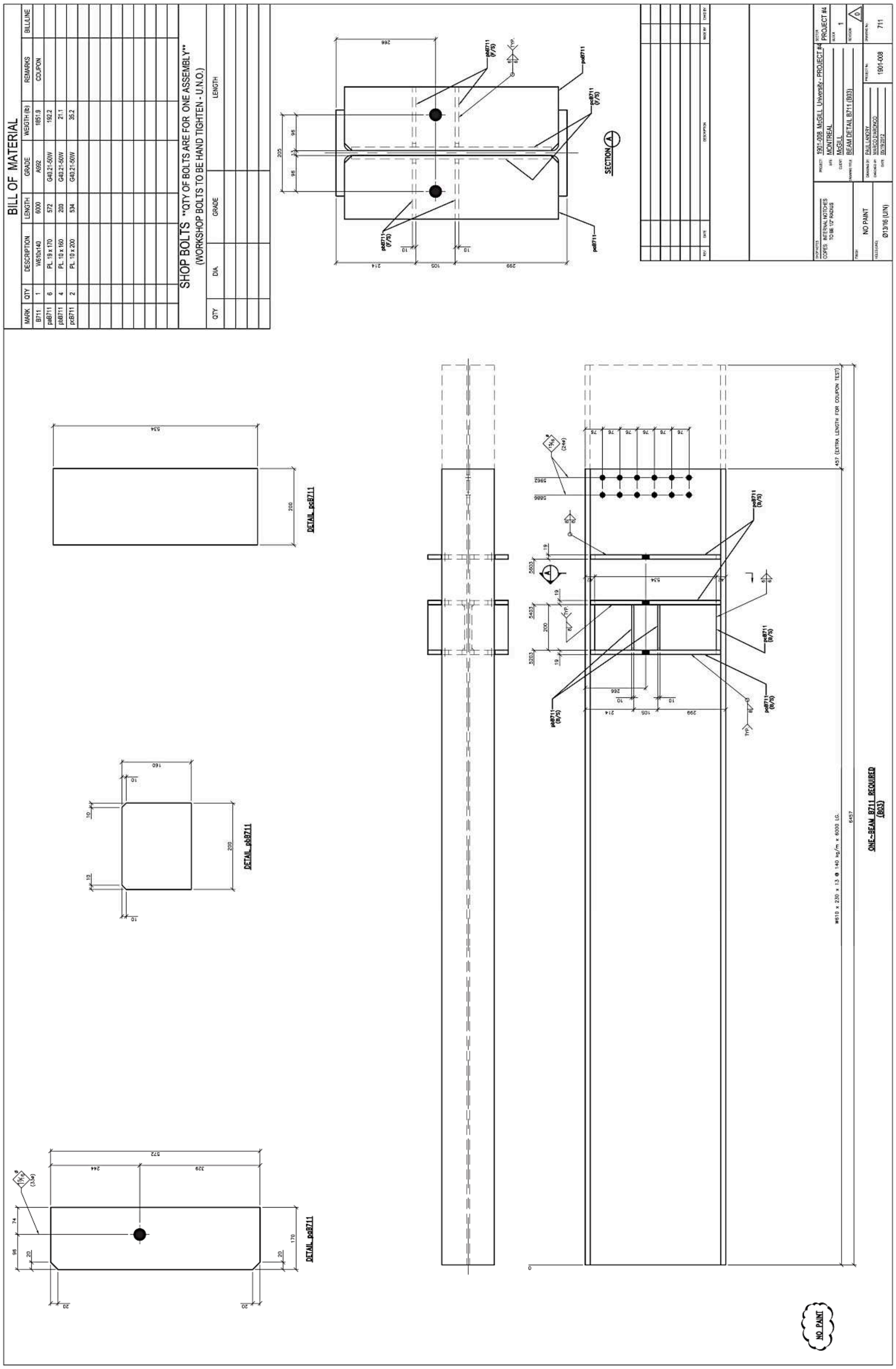

Figure C20−Shop drawing #711

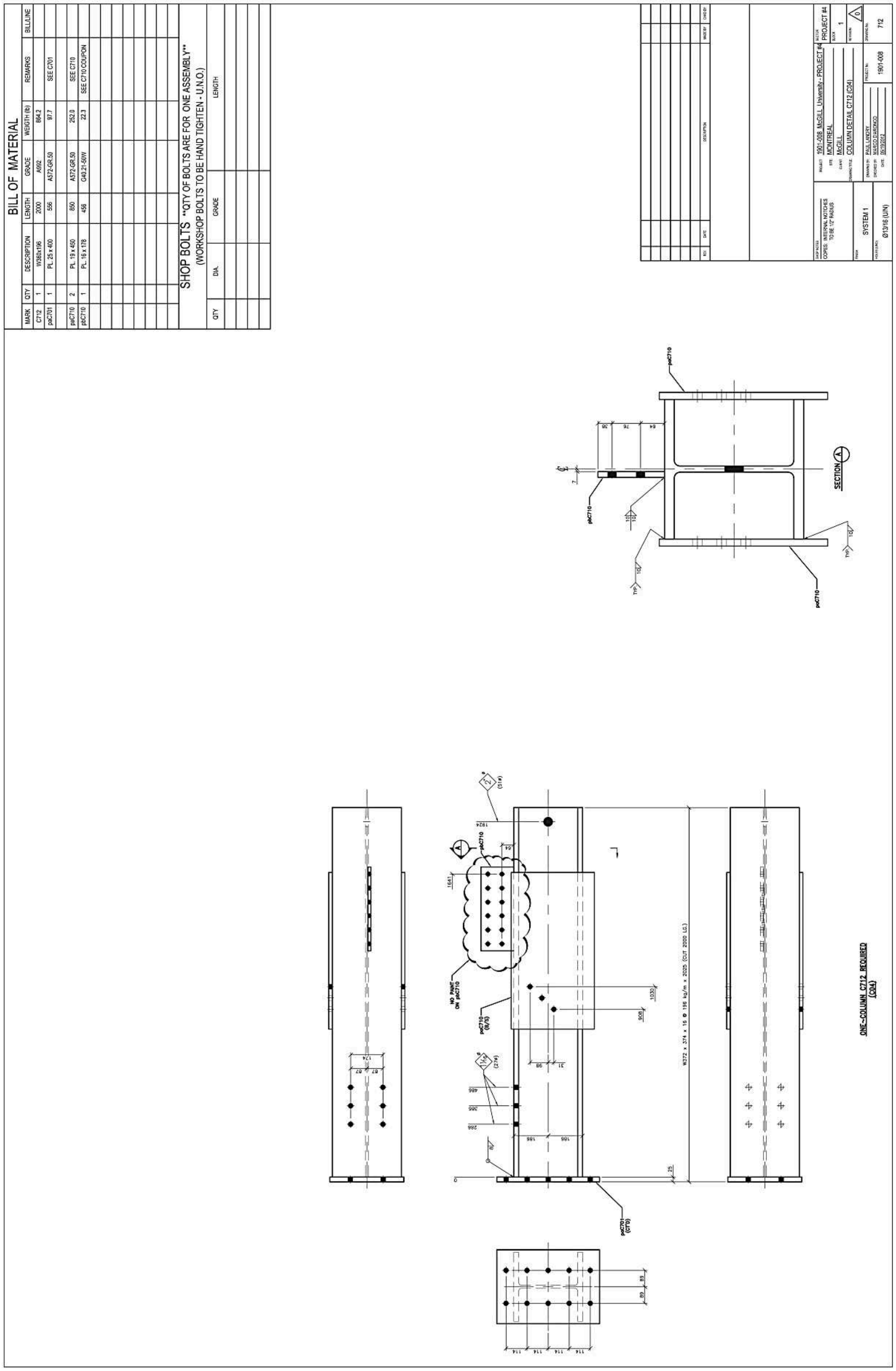

Figure C21–Shop drawing #712

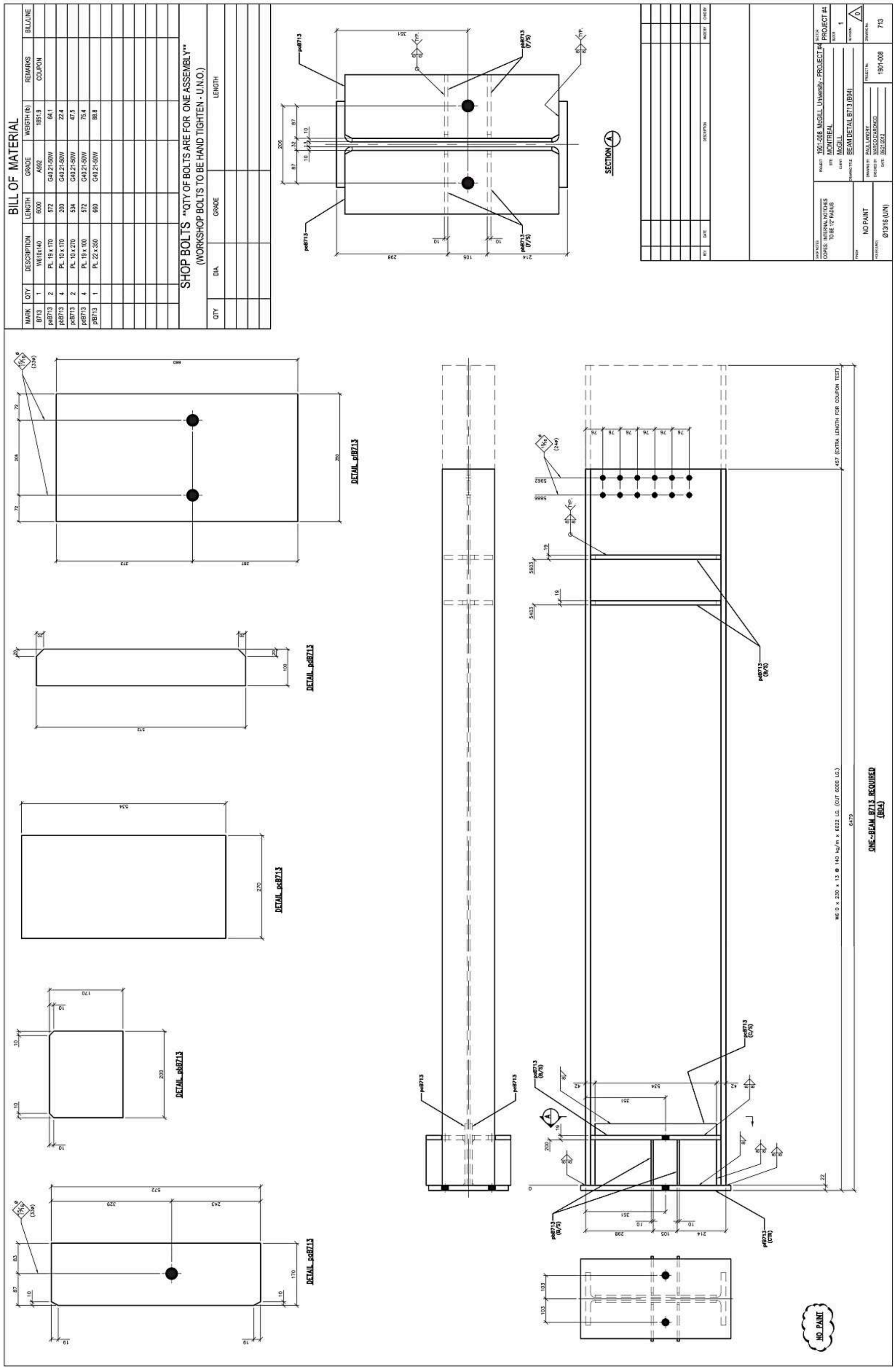

Figure C22−Shop drawing #713

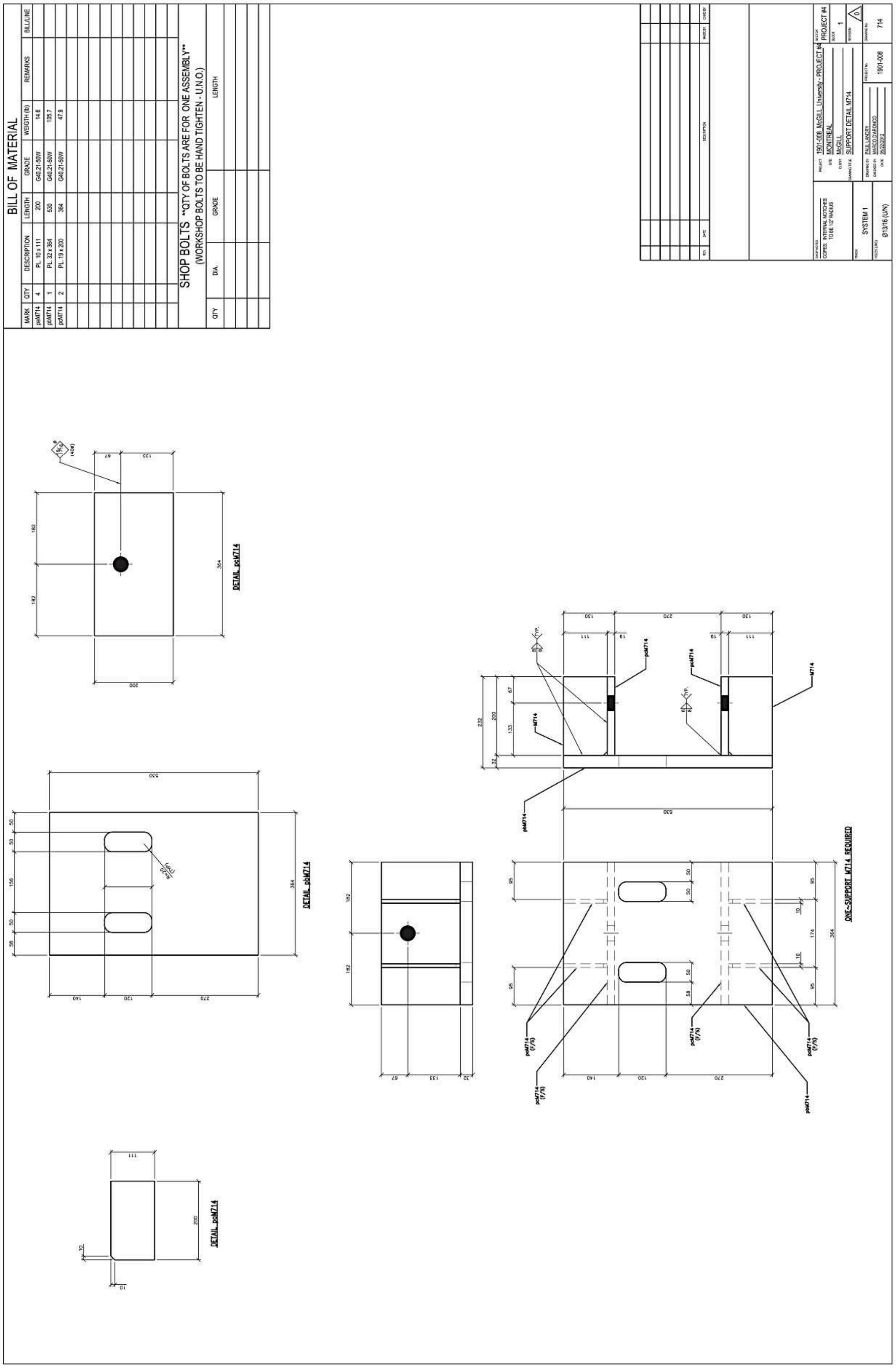

Figure C23−Shop drawing #714

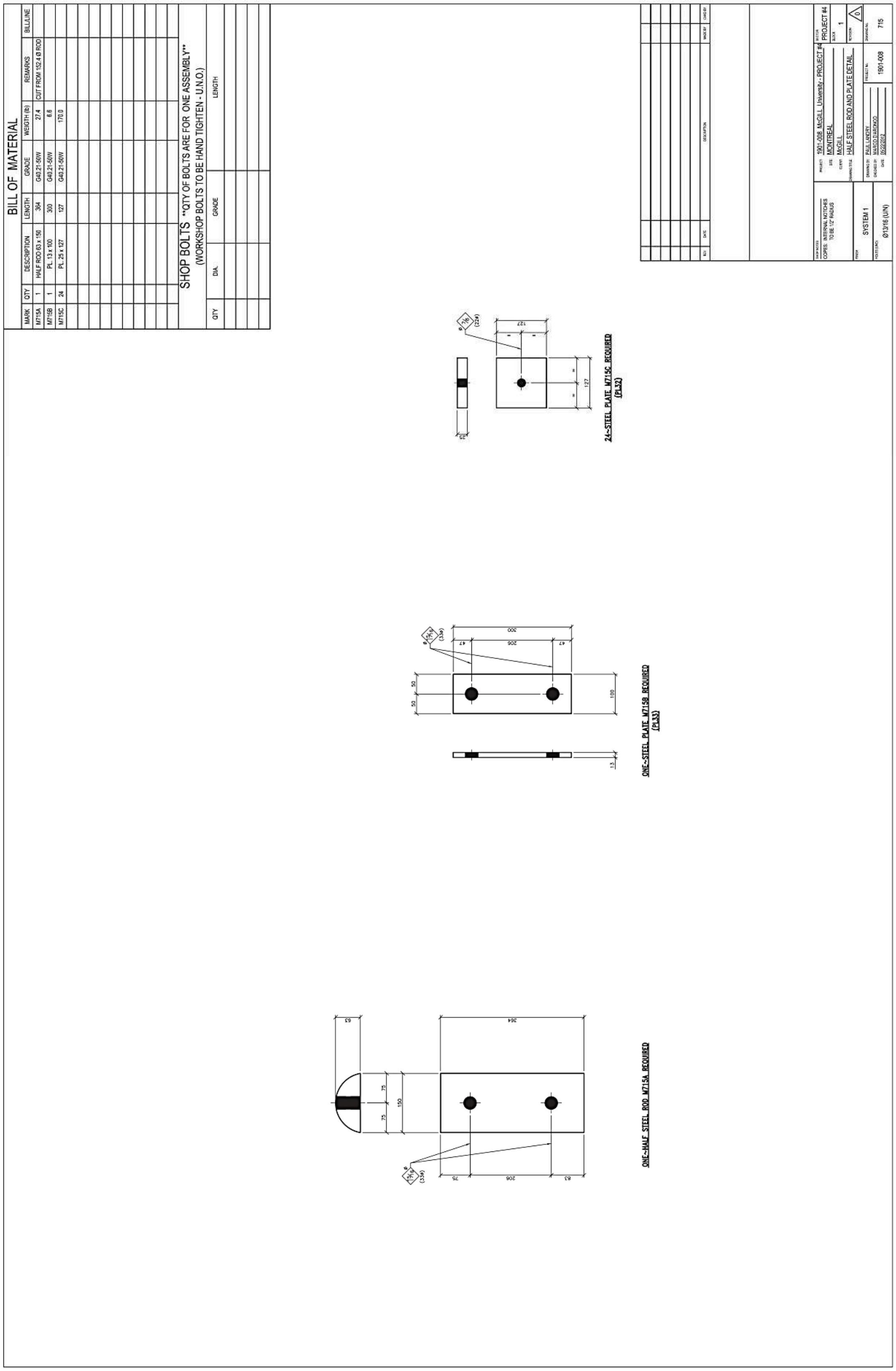

Figure C24−Shop drawing #715